UNDERSTANDING THE PATHOGENESIS OF AGE-RELATED MACULAR DEGENERATION

by Eunkyung An

M.S., August 2004, The George Washington University

B.A., December 2000, Sungshin Women's University

A Dissertation submitted to

The Faculty of
Columbian College of Arts and Sciences
of The George Washington University
in partial fulfillment of the requirements
for the degree of Doctor of Philosophy

January 31, 2010

Dissertation directed by

Yetrib Hathout
Assistant Professor of Integrative Systems Biology, of Pediatrics,
and of Biochemistry and Molecular Biology
and
Eric P Hoffman, Chairman of Integrative Systems Biology; Professor of Pediatrics
and of Biochemistry and Molecular Biology

The Columbian College of Arts and Sciences of The George Washington University certifies that Eunkyung An has passed the Final Examination for the degree of Doctor of Philosophy as of December 14, 2009. This is the final and approved form of the dissertation.

UNDERSTANDING THE PATHOGENESIS OF AGE-RELATED MACULAR DEGENERATION

Eunkyung An

Dissertation Research Committee:

Yetrib Hathout, Assistant Professor of Integrative Systems Biology, of Pediatrics, and of Biochemistry and Molecular Biology, Dissertation Co-Director

Eric P Hoffman, Chairman of Integrative Systems Biology; Professor of Pediatrics and of Biochemistry and Molecular Biology, Dissertation Co-Director

Anamaris M Colberg-Poley, Professor of Biochemistry and Molecular Biology and of Pediatrics, Committee Member

Mary C Rose, Professor of Integrative Systems Biology, of Pediatrics, and of Biochemistry and Molecular Biology, Committee Member

Copyright 2010 Eunkyung An
All rights reserved

D e d i c a t i o n

To my family whose love and support have been invaluable.

A c k n o w l e d g m e n t s

Wow! What a journey! My major life turning points such as marriage, having children, and entering parenthood all happened during this Ph.D program. I also remember tears and headaches from my comprehensive exam and presentations too. Yes, there were several points where I almost gave up this journey. To get though this wild but fun journey, I owe many people appreciation for their support, love, and devotion.

I would like to first thank my Mom. I know it challenged her to raise me and support me as a single mom. She always told me to choose the path that my heart wants. I don't know whether she understood me when I quit a good position from a trading company to be a student again, but she was always there when I needed her. She flew from Korea to help me out when I was burned out from trying to be a good mom, a good wife, and a good Ph.D. student. Thank you, Mom! Also, I would like thank my husband, Kyujin, for his devotion and endless support. When I was down for whatever reason, he encouraged me not to give up the program. And he also understood when I spent more time in the lab than home. I also thank my kids, Jeho and Eno, for being good sons. Without my family's support and devotion, I could not have finished the program.

Academically, I would like to first thank my mentor, Dr. Yetrib Hathout. He kindly and patiently guided me during this training with knowledge and understanding. Your explanations always made sense and were easy to understand! You are the greatest teacher and mentor. I also want to ask you for forgiveness because sometimes I was not a good

student as far as I remember; I was stubborn and selfish when we talked about this project and my graduation date. Thank you and sorry!

I also appreciate my co-mentor, Dr. Eric Hoffman, for his time and suggestions. Even with his unbelievably busy schedule, he was at every committee meeting with valuable suggestions. A Ph.D tends to be specialized to one certain area, but he is able to see the big picture for each project I hope to achieve one day.

I still remember when I cried in the office of Dr. Colberg-Poley. I tried to be strong during the meeting with her, but her sincere concern and encouragement touched the bottom of my heart. Thank you so much for the time you invested in me to help me pass the oral part of my comprehensive exam and to obtain the “Degree of Excellency”. Since that meeting with you, I see a Ph.D in biomedical science from a different angle. And I also appreciate you for serving as a reader!

Dr. Rose is one of the smartest P.I.s in the lung and epithelial cell meeting we have every month at the center. I always wanted her on my committee and I remember that I was afraid to ask her to be my committee member because she has multiple students to mentor. Even though you are busy with other students, thank you for serving as my committee member and being a great reader as well.

Dr. Donita Garland was my mentor for the masters program at the NIH, and now she is my dissertation committee member for my Ph.D program while she works at University of

Pennsylvania. Thank you so much for deciding to be a committee member and attending every committee meeting we had. I appreciate your time, your knowledge and passion about eye research.

Dr. Nagaraju is an immunology guru. He gave priceless suggestions on my study, especially on the TNF-alpha study and complement system. I also thank you for your time and effort as a committee member. I can feel your great affection toward research. I hope I can be like you one day.

I also would like to thank the girls in proteomics group. As we talked about, I feel you are my sisters; Kristy as a bitter sweet sister, Trina as a nice sister and Asako as a strict sister. You all have what I want to have characteristic-wise and wisdom-wise. Without you, the life at the lab wouldn't be fun and I don't think I could survive in the lab. Also I appreciate you for loving me even though I have a weird sense of humor! ☺ I also would like to thank Supti who did a lot of cell culture work for this project.

Oh! I can't forget Alan, Erica, and Chad. They gave me valuable direction on how to graduate without facing those deadlines in a hectic situation. Without your comments, I would run all over to meet those deadlines! I also thank Jenn for the friendship.

And foremost I thank Jesus Christ who has been a safe port in many storms. When I had any conflict at the lab, at home or even in myself, the Holy Spirit was always with me to keep from losing my mind.

A b s t r a c t o f D i s s e r t a t i o n

UNDERSTANDING THE PATHOGENESIS OF
AGE-RELATED MACULAR DEGENERATION

Age related macular degeneration (AMD) is the leading cause of central vision loss in the elderly population. The disease affects the macula and it can occur in “dry” or “wet” form. The dry AMD is the most prevalent form and is characterized by accumulation of extracellular deposits named "drusen" between the retinal pigment epithelium (RPE) and Bruch's membrane while the wet AMD is less common form and is characterized with growth of new blood vessels that breach the RPE monolayer and invade the photoreceptors. AMD is a complex disease in which age, genetic variants, and environmental factors are all considered to play a role. Although aging is known as a major risk factor for AMD, it has been shown that more than 75 % of AMD patients harbor certain genetic variations. Three major genetic risk factors have been identified to date and these include variant in the *complement factor H* (*CFH*) gene, in the promoter region of the *high temperature requirement protease 1* (*HTRA1*) gene and in the *Age-related maculopathy susceptibility 2* (*ARMS2)* gene. However it is not clear how these apparently unrelated genes lead to the same pathological features of AMD (e.g., drusen formation and choroidal neovascularization). The goal of this dissertation is to understand the downstream consequences of these polymorphisms on RPE cells and define molecular mechanisms of AMD pathogenesis. We hypothesized that AMD risk genotypes influence homeostasis of RPE secretome leading to progressive drusen formation and macular degeneration. To test this hypothesis: (i) we established primary RPE cell cultures from human autopsy eyes of donors with and without AMD risk genotypes, (ii) compared their secretome profiles using

stable isotope labeling by amino acid in cell culture (SILAC) strategy, and (iii) characterized key pathways linking the different risk genotypes to drusen formation and choroidal neovascularization. Our SILAC strategy readily facilitated high throughput screening for both detection and quantitation of RPE secreted proteins. In our first study of the RPE secretome, we found that RPE cells derived from AMD donors secrete elevated amounts of protein components found in drusen and these include complement components, amyloid, clusterin, fibronectin and TIPM-3 (Chapter 2). We also found that TNF-α, a pleiotropic cytokine, modulates secretion of specific proteins of RPE cells leading to dysregulation of the complement pathway and extracellular matrix remodeling (Chapter 3). Moreover, we found that RPE culture with *HTRA1/ARMS2* risk genotype secrete elevated amounts of HTRA1 and that HTRA1 cleaves key proteins involved in regulation of the complement pathway (e.g. clusterin, vitronectin and fibromodulin) and in amyloid deposition (clusterin, alpha 2 macroglobulin and ADAM9). We propose models where alteration of RPE extracellular environment due to genetic variants and external stimuli favors amyloid accumulation and complement deposition leading to progressive drusen buildup and ocular cell degeneration.

Table of Contents

Dedication iv

Acknowledgments v

Abstract of Dissertation viii

Table of Contents x

List of Figures xvi

List of Tables xx

List of Abbreviations xxi

Chapter 1: Introduction 1

1.1 Introduction to Age-related Macular Degeneration 1

1.2 AMD etiology and Risk factors 7

1.2.1 Aging 7

1.2.2 Genetic risk factors 8

1.2.2.1 Variants in the Complement factor H and Factor H like protein 1 are risk factors for developing AMD. 9

1.2.2.2 Variants in the ARMS2/HTRA1 loci are risks factors for developing AMD 11

1.2.3 Dietary and environmental factors 15

1.3 Drusen, the hallmark of AMD pathogenesis 16

1.4 RPE as potential source of drusen 18

1.5 Current treatments 20

1.6 Study of the cell secretome 22

1.7 Hypothesis and specific aims 26

Chapter 2: Secreted Proteome Profiling in Human RPE cell Cultures Derived from Donors with Age-related macular degeneration and Age matched Healthy Donors 28

2.1 Abstract 29

2.2 Introduction 30

2.3 Experimental Methods 32

2.3.1 Preparation of Primary RPE Cell Culture from Postmortem Autopsy Eyes 32

2.3.2 Screening RPE Cell Cultures for the Y402H CFH Variant 33

2.3.3 Stable Isotope Labeling by Amino Acids 34

2.3.4 Sample Preparation of Secreted Proteins 34

2.3.5 Nanoflow LC-MS/MS 35

2.3.6 Database Search 36

2.3.7 ZoomQuant Analysis 37

2.3.8 mRNA Isolation and Expression Profiling 37

2.3.9 Ingenuity Pathway Analysis 38

2.4 Results 39

2.4.1 EM Examination of Macular Biopsies 39

2.4.2 RPE Genotyping for the CFH Variant 42

2.4.3 Analysis of RPE Secreted Proteins 43

2.4.4 Secreted Protein Profiling in RPE Cells Prepared from AMD and Normal Age-Matched Healthy Donors 49

2.4.5 Network Analysis 57
2.5 Discussion 63
2.6 Conclusion 68
2.7 Acknowledgment 69

Chapter 3: Effect of TNF-α on Human ARPE-19 Secreted Proteins 70

3.1 Abstract 71
3.2 Introduction 73
3.3 Methods 76
3.3.1 SILAC and TNF-α treatment 76
3.3.2 Analysis of ARPE-19-secreted proteins 77
3.3.3 Preparation of microsomal fraction 77
3.3.4 Nanoflow LC-MS/MS 78
3.3.5 Database search 79
3.3.6 ZoomQuant analysis 80
3.3.7 Statistical analysis 80
3.3.8 Western blot analysis 81
3.4 Results 85
3.4.1 Effect of TNF-α on the viability of ARPE-19 cells 85
3.4.2 Effect of TNF-α on ARPE-19-secreted proteins 88
3.5 Discussion 99
3.5.1 Complement C3 100

3.5.2 Fibronectin and syndecan-4 101

3.5.3 Plasminogen activator inhibitor-1 106

3.5.4 Sulfhydryl oxidase 1 106

3.5.5 Trans-Golgi network protein 2 107

3.6 Acknowlegments 111

Chapter 4: Identification of Novel Substrates for the Serine Protease HTRA1 in the Human RPE Secretome 122

4.1 Abstract 123

4.2 Introduction 124

4.3 Materials and Methods 128

4.3.1 Establish Primary RPE cell culture from Postmortem Autopsy Eyes 128

4.3.2 Screening RPE cultures for AMD risk genotypes (HTRA1, ARMS2 and CFH) 129

4.3.3 Measurements of HTRA1 expression in RPE cells 130

A. qRT-PCR 130

B. Western Blot analysis 130

C. Targeted mass spectrometry quantification of RPE secreted HTRA1 131

4.3.4 Proteomics analysis of HTRA1 substrates 131

4.3.5 Liquid chromatography-tandem mass spectrometry 132

4.3.6 Database Search and Quantification 133

4.4 Results 134

4.4.1 Human primary RPE cell cultures and genotyping 134

4.4.2 Quantitative analyses of HTRA1 expression in genotyped RPE cells 136

4.4.3 Screening for HTRA1 substrate in RPE cell conditioned media 144

4.5 Discussion 151

4.5.1 HTRA1 cleaves proteins involved in complement cascade 151

4.5.2 HTRA1 cleaves proteins involved in the regulation of amyloid deposition. . 152

4.6 Acknowledgements 154

Chapter 5: Characterization of CFH and FHL-1 expression in genotyped human RPE cells and association with AMD 168

5.1 Introduction 169

5.2 Methods 173

5.2.1. Characterization of CFH and FHL-1 in the RPE secretome 173

5.2.2. Differential expression of wild type (T) and risk (C) allele in primary RPE cultures with heterozygous for the CFH variant 174

5.2.3. Detection of Y and H variants for the CFH and FHL-1 proteins in the secretome of RPE cells using western blot analysis 174

5.3 Results 175

5.3.1 Characterization of CFH and FHL-1 in RPE secretome 175

5.3.2 Antibody specific detection of Y and H variants of CFH and FGL-1 in the secretome of RPE heterozygous for the CFH risk allele 178

5.3.3 Differential allelic expression of CFH variants in RPE heterozygous for the CFH risk allele 178

5.4. Discussion 183

Chapter 6: Overall Discussion and Future Directions 185

6.1 Summary 185

6.2 Choice of biological model 185

6.3 Choice of techniques 186

6.4 Two models for AMD pathogenesis 187

6.4.1 Complement system model and AMD 188

6.4.2 HTRA1 model and AMD 195

6.4.2.1 HTRA1 cleaves protein involved in amyloid deposition 196

6.4.2.2 HTRA1 cleaves protein involved in complement pathway regulation. 196

6.4.2.3 Regulation of HTRA1 expression 199

6.4.3 Joint effects of HTRA1 pathway and complement pathway 202

6.5 Conclusions 202

6.6 Future directions 206

Chapter 7: References 208

List of Figures

Figure 1.1 Cross sectional representation of the human eye 3

Figure 1.2 AMD classifications..... 5

Figure 1.3 Locations of three SNPs in 10q26 as AMD genetic risk factors..... 13

Figure 1.4 MS-based quantitative proteomics with SILAC strategy 24

Figure 2.1 Electron micrographs of the cross section of the macula prepared from an (A) 81-, (B) 72-, and (C) 77-year old donors 40

Figure 2.2 Zoom scan as a tool to distinguish between contaminant and RPE originated protein 44

Figure 2.3 LTQ MS and MS/MS spectra of labeled and unlabeled peptide pairs of PEDF 51

Figure 2.4 Zoom MS scans of two peptides for PEDF..... 53

Figure 2.5 Differential expression of clusterin in RPE cell cultures prepared from AMD donors with the homozygous rare (CC) and heterozygous (CT) Y402-CFH genotype versus RPE cells prepared from age-matched healthy donors with the wild-type CFH genotype (TT)..... 59

Figure 2.6 Ingenuity pathway network of differentially secreted proteins detected in RPE cells derived from an AMD donor (with macular deposits and the homozygous rare Y402H-CFH genotype) versus RPE cells derived from an age-matched healthy donor (see data from Table 2.2)..... 61

Figure 3.1 Experimental design to study the effect of TNF-α on ARPE-19 secreted proteins 83

Figure 3.2 Cell viability in function of increased TNF-α concentration..... 86

Figure 3.3 Cellular localization of proteins identified in conditioned medium of ARPE-19 cells 90

Figure 3.4 Zoom scan mass spectra of labeled and unlabeled peptide pairs of complement C3 and syndecan-4 proteins 92

Figure 3.5 Bar graph for the 6 proteins whose secretion was found differentially altered in TNF-α-treated ARPE-19 cells 94

Figure 3.6 Effect of increasing concentrations of TNF-α on the secretion of Complement C3 by ARPE-19 cells 97

Figure 3.7 Sequence and cellular domains of human syndecan 4..... 104

Figure 3.8 Effect of TNF-α on the subcellular distribution of the TGON2..... 109

Figure 4.1 Schematic structure of full length human HTRA1 protein..... 125

Figure 4.2 Expression levels of HTRA1 mRNA and protein in human RPE cell cultures derived from donors with wild type and at risk genotype for the HTRA1 promoter region 138

Figure 4.3 Stable isotope labeled standard for absolute quantification of HTRA1 protein 140

Figure 4.4 Effect of the HTRA1 promoter genotype on HTRA1 expression in RPE culture 142

Figure 4.5 Differential SILAC strategy to screen for HTRA1 substrates in RPE conditioned medium 146

Figure 4.6 Clusterin, as a specific substrate for HTRA1 149

Figure 4. S1 Detection of clusterin degradation products in HTRA1 treated RPE conditioned medium 164

Figure 4. S2 No effect of HTRA1 on fibronectin 166

Figure 5.1 Schematic representations of a full length CFH and its truncated isoform FHL-1 171

Figure 5. 2 Characterization of RPE secreted CFH and FHL-1 176

Figure 5. 3 Specific detection of Y402 and H402 CFH/FHL-1 variants in conditioned media of human primary RPE cultures 179

Figure 5. 4 Specific allelic expression of CFH and FHL-1 in RPE cells wih heterozygous CFH risk genotype 181

Figure 6.1 Complement pathway and function of CFH 190

Figure 6.2 Cellular and molecular model for complement system and AMD pathogenesis 193

Figure 6.3 Cellular and molecular model for HTRA1 and AMD pathogenesis 197

Figure 6.4 Amyloid precursor protein and sites for enzymatic processing 200

Figure 6.5 Synergy between complement pathway and protease 204

List of Tables

Table 2.1 List of proteins identified in the conditioned media of human primary RPE cell cultures.....47

Table 2.2 Differential expression in AMD and age matched healthy donors.....55

Appendix 3.1 List of proteins found in the condition media of ARPE-19 cell cultures ...112

Appendix 3.2 Additional proteins identified by a single peptide pair in the conditioned medium of ARPE-19 cells 119

Table 4.1 Distribution of AMD risk genotypes among the established human primary RPE cell cultures (n=30).....135

Table 4. 2 List of potential HTRA1 substrates identified in the RPE conditioned medium ……...…148

Table 4.S1 Donor information: age, gender, AMD history, genotyping of SNPs for CFH, HTRA1/ARMS2, smoking history, cause of death and time of enucleation 155

Table 4.S2. List of extracellular proteins identified and quantified in HTRA1 treated and untreated RPE conditioned media 157

List of Abbreviations

2-DE	Two dimensional gel electrophoresis
Abeta	Amyloid beta
ABI	Applied Biosystems
ADAM9	Disintegrin and metalloproteinase domain-containing protein 9
AGE	Advanced glycation end product
AMD	Age-related macular degeneration
AP	Alternative pathway
APP	Amyloid precursor protein
AREDS	Age-related eye disease study
Arg	Arginine
ARMS2	Age-related maculopathy susceptibility 2
ARPE-19	A human retinal pigment epithelial cell line
ASE	Allele specific expression
ATCC	American Type Culture Collection
BACE	Beta-secretase
BP	Base pair(s)
BF	Complement factor b
C	Carbon
C1R	Complement c1r component
C1S	Complement c1s component

C2	Complement component 2
C3	Complement component 3
C3W	Hydrolyzed-C3
C3wBb	initial AP C3 convertase
C4	Complement component 4
C4bC2a	C3 convertase in CP and LP
C4BP	C4b binding protein
C5	Complement component 5
C6	Complement component 6
C7	Complement component 7
C8	Complement component 8
C9	Complement component 9
CFH	Complement factor H
CHAPS	3-[(3-cholamidopropyl)dimethylammonio]-1-propanesulfonate
CNV	Choroidal neovascularization
CP	Classical pathway
CpG	cytosine-guanine dinucleotide
CRP	C-reactive protein
Da	Dalton
Dlga	*Drosophila* disc large tumor suppressor
DMEM	Dulbecco's modified Eagle's medium
DTT	Dithiothreitol

ECM	Extracellular matrix
E. coli	*Escherichia coli*
EDTA	Ethylenediaminetetraacetic acid
EM	Electron microscopy
ER	Endoplasmic reticulum
F	Forward
F12	Ham's F12 medium
FACS	Fluorescence-activated cell sorting
FAD	Flavin adenine dinucleotide
FHL-1	Factor H like protein 1
FLSC	Fibrous long-spacing collagen
GAPDH	Glyceraldehyde-3-phosphate dehydrogenase
GRO	Growth-regulated protein
GWAS	Genome wide association studies
H	Histidine
h	Hour(s)
HTRA1	High temperature requirement protease 1
HTRA2	High temperature requirement protease 2
HTRA3	High temperature requirement protease 3
HTRA4	High temperature requirement protease 4
IgG	Immunoglobulin G
IgM	Immunoglobulin M
IPG strips	Immobilized pH gradient strips

I-κB	NF-κB Inhibitor
I-κB, α	I-κB, alpha protein
K	Lysine
kDa	KiloDalton
LC	Liquid chromatography
LD	Linkage Disequilibrium
LP	Lectin pathway
LRP	Low density lipoprotein receptor
LTQ	Linear ion trap quadropole
Lys	Lysine
MAC	Membrane attack complex
MCP-1	Monocyte chemotactic protein-1
MMP2	Matrix metalloproteinase-2
MMP9	Matrix metalloproteinase-9
M protein	A virulence factor that is produced by certain species of *Streptococcus*
mRNA	Messenger RNA
MS	Mass spectrometry
MS/MS	Tandem MS
MT	Mutant
N	Nitrogen
N/A	Not assigned
NCBInr	National Center for Biotechnology Information non redundent data base

ND	Not determined
NDRI	The National Disease Research Interchange
NEI	The National Eye Institute
NF-κB	Nuclear factor kappa-light-chain-enhancer of activated B-cells
NIH	The National Institutes of Health
PAGE	Polyacrylamide gel electrophoresis
PAI-1	Plasminogen activator inhibitor-1
PBS	Phosphate buffered saline
PCR	Polymerase chain reaction
PDT	Photodynamic therapy
PDZ	psd95, dlga, and zo-1
PEDF	Pigment epithelium derived factor protein
PIR	Protein information resources
PI	The isoelectric point
pM	10^{-12} molar
POS	Photoreceptor outer segment
PSD95	Post synaptic density protein
PVDF	Polyvinylidene fluoride
QSOX	Quiescin q6
qRT-PCR	Quantitative real-time PCR
R	Arginine
R	Reverse

RIPA	Radio immunoprecipitation assay
RNA	Ribonucleic acid
RPE	Retinal pigment epithelium
SDS	Sodium dodecyl sulfate
SILAC	Stable isotope labeling by amino acids in cell culture
SNP	Single nucleotide polymorphism
SPARC	Secreted protein acidic and rich in cysteine
TBST	Tris buffer containing salt and tween
TGON2	*Trans*-Golgi network protein-2
TIMP	Tissue inhibitor for metalloproteinase
TIMP-1	Tissue inhibitor for metalloproteinase-1
TLP	Thermal laser photocoagulation
TM	Transmembrane domain
TNFR	TNF-α receptor
TNF-α	Tumor necrosis factor alpha
TRAF	TNF receptor-associated factor
TrEMBL	Translations of European Molecular Biology Laboratory
Tyr	Tyrosine
UniProt	Universal protein resource
VEGF	Vascular endothelial growth factor
WT	Wild type allele
Xcorr	Cross correlation

XIC	Extracted ion chromatogram
Y	Tyrosine
zo-1	zonula occludens-1 protein
ΔCN	Delta cn

Chapter 1: Introduction

1.1 Introduction to Age-related Macular Degeneration

Age-related macular degeneration (AMD) is a leading cause of central vision loss in elderly population[1]. Its prevalence is increasing in developed countries due to longer life span and aging baby boomers. It is estimated that around 3 million individuals will develop AMD by the year 2020 in the United States[1]. AMD is a pathology that affects the macula, a 5 mm in diameter region located at the center of the retina and contains high density of cones connected to a complex network of neurons[2] (Figure1.1). This cellular network is supported by a layer of retinal pigment epithelium (RPE), which plays a major role in maintaining its integrity and function. The high density of cones in the macula makes this region a unique structure of the retina allowing high visual acuity by distinguishing fine details and colors. Unfortunately, this delicately orchestrated cellular network is vulnerable to aging, genetic and environmental risk factors often leading to compromised central vision.

There are generally two accepted subtypes of AMD based on fundoscopic examination of the retina (Figure 1.2 Top). The common dry AMD progresses slowly and accounts for more than 90% of AMD cases and the rare wet AMD involves a more rapid vision loss and accounts for less than 10% of all AMD cases. Clinically, the dry form of AMD is associated with the accumulation of deposits (drusen) between RPE monolayer and the Bruch's membrane, whereas the wet form is characterized by growth of new blood vessels (choroidal neovascularization (CNV)) breaching the RPE layer and damaging the retina (Figure 1.2 Bottom). It has been generally observed that patients with dry AMD

eventually develop the wet form, but very rarely do patients with no sign of dry form suddenly present with the wet form[3].

Figure 1.1 Cross sectional representation of the human eye

Going from outside to inside a human eye globe is composed of cornea, lens vitreous and retina. Retina, which covers more than 80% of the posterior of the eye, is composed of multilayers of cells. From the innermost to outermost, there are the ganglion cells, amacrine cells, bipolar cells, horizontal cells, photoreceptors, and RPE. The very center of the retina is defined as the macula, which is a region around 5 mm in diameter. When light of an image is absorbed by light-sensitive cells called photoreceptors, it is converted to electrical impulses by phototransduction and travels along the optic nerve to the brain. There are two kinds of photoreceptors: cones and rods. Cones are used to determine colors and image sharpness at bright light and rods are responsible for vision at dim light but do not have the ability to distinguish colors. While the central retina is dominated by cones, the peripheral retina is dominated by rods. Macula has the highest density of cones for high vision acuity. (Adapted from http://webvision.med.utah.edu)

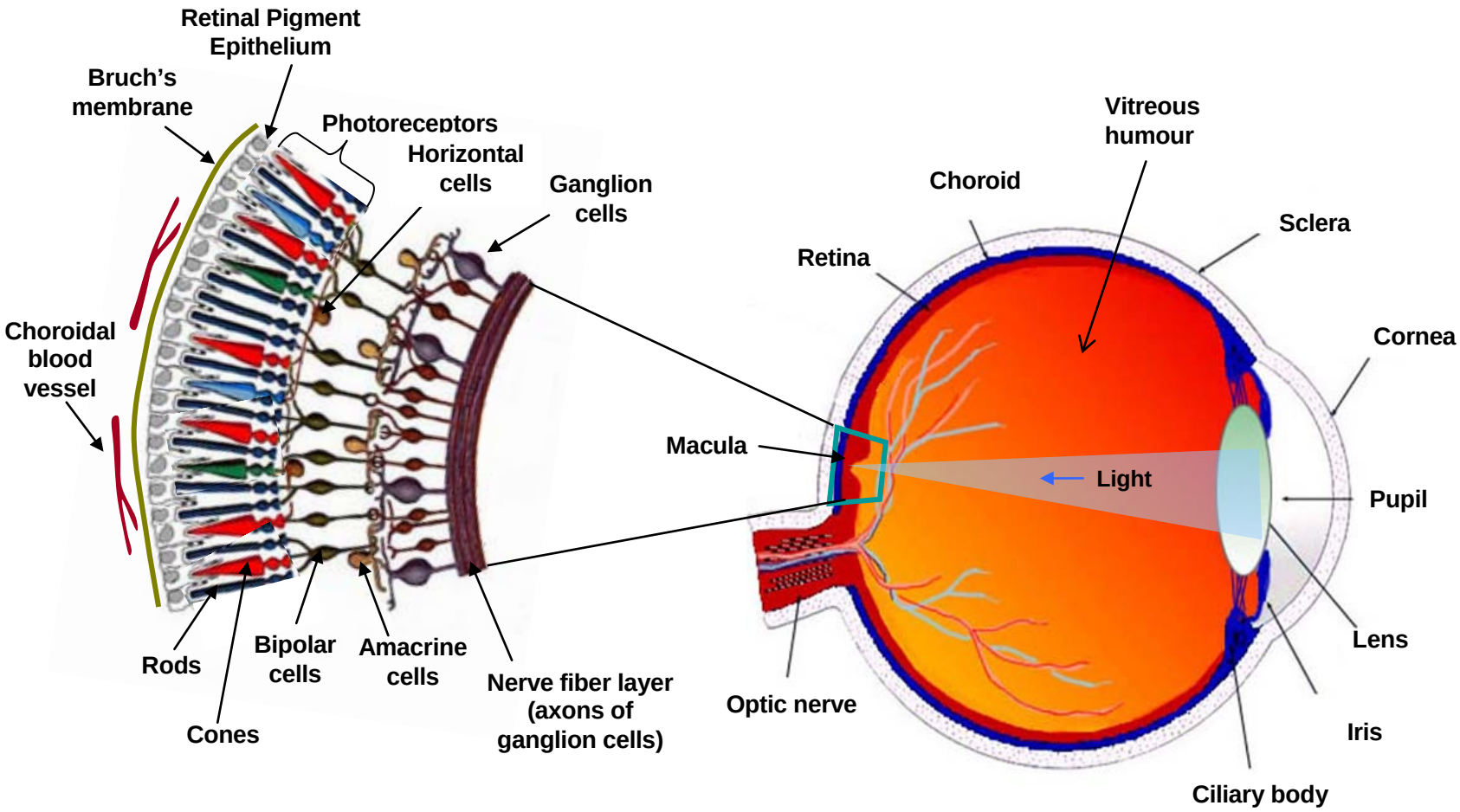
Retinal Pigment Epithelium
Bruch's membrane
Photoreceptors
Horizontal cells
Ganglion cells
Choroidal blood vessel
Rods
Cones
Bipolar cells
Amacrine cells
Nerve fiber layer (axons of ganglion cells)
Vitreous humour
Choroid
Sclera
Retina
Cornea
Macula
Light
Pupil
Lens
Optic nerve
Iris
Ciliary body

Figure 1.2 AMD classifications

Fundoscopic picture (top) and schematic representation (bottom) of normal retina (A), dry AMD (B) and wet AMD (C). While the macula of normal retinal looks clear in a fundoscopic picture, drusen (yellow pigmentation) and CNV are observed in dry AMD and wet AMD respectively.

(Adapted from http://webeye.ophth.uiowa.edu/dept/service/photo/cfundus.htm (for normal) and from http://www.eyesitemd.com/macular_degeneration.htm (for dry and wet)).

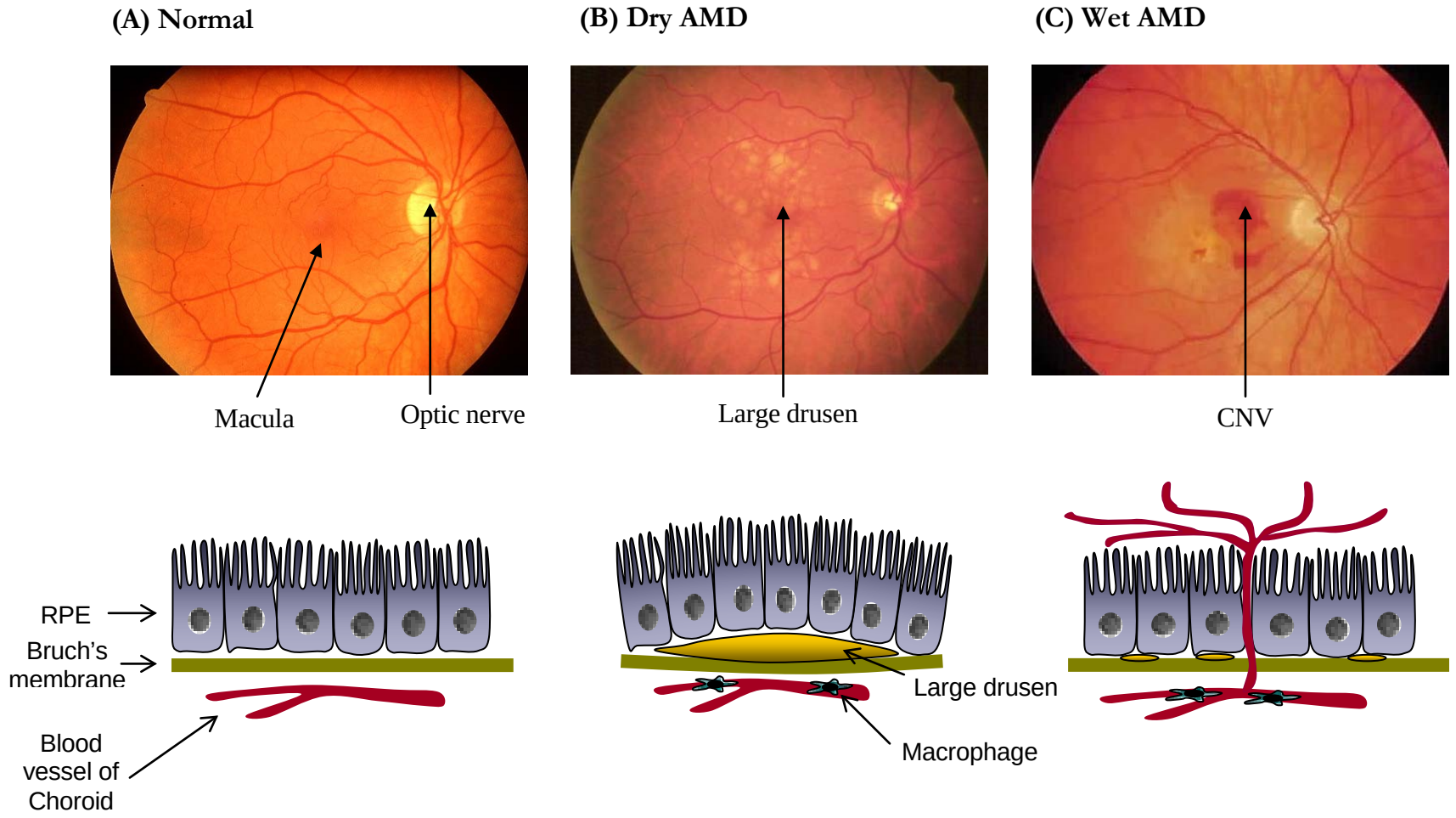
(A) Normal
(B) Dry AMD
(C) Wet AMD
Macula
Optic nerve
Large drusen
CNV
RPE
Bruch's membrane
Blood vessel of Choroid
Large drusen
Macrophage

1.2 AMD etiology and Risk factors

AMD is a complex and multifactorial disease involving a combination of risk factors including aging, genetic variants, dietary and environmental factors.

1.2.1 Aging

The average life span of humans in developed countries is increasing, mainly due to advances in public health[4]. Unfortunately, despite the benefits of a longer life span to "silver generation", there is increase in the incidence of age-related diseases such as Alzheimer's, Huntington's, Parkinson's, and AMD. AMD is late onset disease and strongly associated with age. Around 30% of individuals over the age of 75 years will develop some degree of AMD[1,5,6] and more than 1 in 10 individuals will have advanced AMD by their 80's[7]. Aging affects number of cells in the body resulting in progressive deterioration and failure of specific organs. In the context of vision, it has been shown that RPE cells accumulate a large number of brown-yellow pigments called lipofuscins with age[8,9]. It is hypothesized that lipofuscin accumulation in RPE cells may be due to decrease in the activity of lysosomal enzymes of the RPE cells[10,11]. Whether lipofuscins are associated with drusen formation outside RPE cells remains to be demonstrated[12-15]. However, it is more likely that homeostasis of RPE extracellular environment is also affected by ageing. Indeed, recent studies report accumulation of advanced glycation end products (AGEs) with age within RPE, Bruch's membrane, and subcellular deposits[16]. AGEs are formed by spontaneous non enzymatic reaction between proteins and carbohydrates. AGEs contribute to chronic inflammation by increasing vascular permeability and inducing the secretion of cytokines after binding to macrophages[17]. The formed products are usually degraded by

proteasomes in cells, then cleared. However, in the context of extracellualr matrix, which is more resistance to proteolysis, these AGEs might accumulate with age leading to progressive damage of the extracellular matrix (ECM) and increased inflammatory signaling. Indeed, several studies suggest exacerbating role of AGEs in AMD pathogenesis[16,18,19].

1.2.2 Genetic risk factors

Finding the causal genes for AMD has been hindered by several factors due to the fact that AMD is a late onset disease and family tree data are often not available. Hyman *et al*. (1983) was first to suggest that AMD is influenced by genetic factors using a case control study[20]. Additionally, monozygotic twin studies strongly support a genetic basis for AMD[21,22]. Development of high throughput gene sequencing methods and genome wide association studies (GWAS) screening of large cohorts of AMD patients and age matched controls made it possible to search for AMD genetic risk factors. Such studies started to reveal multiple loci for AMD including 1q31 and 10q26[23-32]. However, major advances in our understanding of AMD genetics did not occur until the last five years and I was very fortunate to witness major breakthroughs in the genetic studies of AMD during my thesis (2005-2009). This helped me not only in stratifying the samples collected for this study but also helped me redirect my aims and the overall scope of the project.

1.2.2.1 Variants in the Complement factor H and Factor H like protein 1 are risk factors for developing AMD.

In 2005, four laboratories working with independent cohorts of AMD and control cases demonstrated a strong association between a single nucleotide polymorphism (SNP) in the gene encoding for the complement factor H (CFH) and AMD[33-36]. This finding labeled AMD as a complement pathway driven disease. Activation of complement is divided into three pathways: the classical pathway (CP), the lectin pathway (LP), and the alternative pathway (AP). The CP is activated by antigen-antibody complexes and the LP by mannose-binding lectins to mannose groups of pathogens. The AP is constantly activated at a low level and ensures a rapid response to pathogens[37,38]. It has been suggested that the alternative pathway may represent up to 80 % of complement activation[38]. The *CFH* gene is located in chromosome 1 and encodes both full length CFH and truncated factor H like protein 1 (FHL-1). CFH is 140 kiloDalton (kDa) circulating glycoprotein mainly produced by the liver and it regulates AP by inactivating complement component 3b (C3b) and dissociating C3 convertase. Because of the strong association between CFH variant and AMD, it has been hypothesized that substitution of the tyrosine residue (Y) by the histidine residue (H) at position 402 might affect the binding of CFH to the cell surface, and thereby altering the inhibitory function of CFH on the complement alternative pathway. However, *in vitro* studies conducted with the full length CFH showed that substitution of Y by H did not affect the overall function of CFH, but reduced the binding affinity of the truncated FHL-1 to heparin[39,40]. This mutation also reduced the binding affinity of both CFH and FHL-1 to C-reactive protein (CRP) and A virulence factor that is

produced by certain species of *Streptococcus* (M protein) [40,41]. Whether this is relevant to AMD pathogenesis or not, remains to be investigated.

The identification of a strong association between the CFH variant and AMD prompted other investigators to screen for additional SNPs in genes encoding for components of the complement pathway. These targeted association studies led to the discovery of additional SNPs in the genes encoding for the *complement Factor B* (*BF*), *complement component 2* (*C2*), and *complement component 3* (*C3*)[42-46]. While some of these polymorphisms increased the risk of developing AMD (e.g. C3 and C2), others were found to be protective (e.g. BF and C2). These additional variants, taken together with the CFH variant, are additive and may account for nearly 75 % of AMD cases[42]. Also, no association between CFH variants and subtypes (dry and wet) of advanced AMD were found[43,47-49]. For example, Despriet *et al*. (2006) showed that H402 CFH variant is implicated in early AMD and in both subtypes of advanced AMD using 5681 individuals in the Rotterdam Eye Study[49]. Taken together, the complement system seems to play a major role in the development of AMD in both dry and wet form.

1.2.2.2 Variants in the ARMS2/HTRA1 loci are risks factors for developing AMD.

Independently from the complement pathway association studies, other major AMD genetic associations were found in 10q26 region in chromosome 10[23-32]. The 23Kb region was discovered almost at the same time as the CFH variant and harbors three important genes; *PLEKHA1, LOC387715,* and *PRSS11* encoding for the Pleckstrin homology domain-containing family 1 protein, a hypothetical protein later named age related maculapathy susceptibility 2 (ARMS2), and the high temperature requirement protease 1 (HTRA1) respectively[50-53]. Later studies refined this analysis and found a strong association between the rs10490924 SNP of the *LOC387715* (named ARMS2 thereafter) and the rs11200638 in the promoter region of the *HTRA1* gene. These two SNP2 are only 6096 base pairs (BP) apart and are in high linkage disequilibrium (LD) making it difficult to define the AMD causal gene. (Figure1.3)

Currently, there is an ongoing debate about the role of *ARMS2* and *HTRA1* polymorphisms in AMD. While original studies showed that risk variant in *HTRA1* results in increased expression of HTRA1 protein and that *HTRA1* might have a direct role in AMD pathogenesis[52,53], others suggested that the missense mutation in the *ARMS2* (e.g. A69S) is the causal variant possibly affecting the function of ARMS2 protein[54]. Further studies by Fritsche *et al*. (2008) complicated our understanding of the causal gene by showing that an insertion/deletion polymorphism in *ARMS2* (c.*372_815del443ins54), which is also in high LD with the *HTRA1* polymorhism, results in *ARMS2* messenger ribonucleic acid (mRNA) instability leading to its complete degradation[55]. Even though *ARMS2* has been cloned into *E. coli* (*Escherichia coli*) and shown to express a full length 11.3 kDa protein[56], the native cellular ARMS2 is still not well characterized. Recent studies

presented contradictory data about ARMS2 cellular localization; the earlier study suggests mitochondrial localization for ARSM2[54] while more recent studies suggest a cytosolic[57] or even extracellular localization[58].

On the other hand, *HTRA1* gene encodes a well characterized 50 kDa serine protease A1. HTRA1 is a member of the HTRA family that was initially reported in *E. coli* with a null mutant (MT) which was unable to grow at elevated temperature or failed to digest misfolded protein and named accordingly[59,60]. HTRA1 has been long considered to play a role in cell proliferation due to its down regulation in a number of tumor cells[61-63]. However, this same protein was found increased in a number of other diseases including arthritis[64,65], muscular dystrophy[66] and AMD[52]. *In vitro* studies have identified fibronectin and tubulin as potential HTRA1 substrates[64,67]. However, little is known about this protein in the context of ocular disease such as AMD and this will be addressed in Chapter 4.

To date, there are three major genetic risk factors associated with AMD, the HTRA1/ARMS2 loci and the CFH variant. The functions of these genes are apparently unrelated but lead to the possibility that AMD is a multifactorial disease involving different biological and biochemical pathways.

Figure 1.3 Locations of three SNPs in 10q26 as AMD genetic risk factors

The AMD associated variants at 10q26 overlap three genes; *PLEKHA1*, *ARMS2* and *HTRA1*. Later studies refined these to two SNPs (rs10490924 for *ARMS2* and rs11200638 for *HTRA1*) that are associated with AMD development, but these two SNPs are only 6 K base pair apart and are in high linkage disequlibrium which makes it difficult to define the causal gene. (EX:exon)

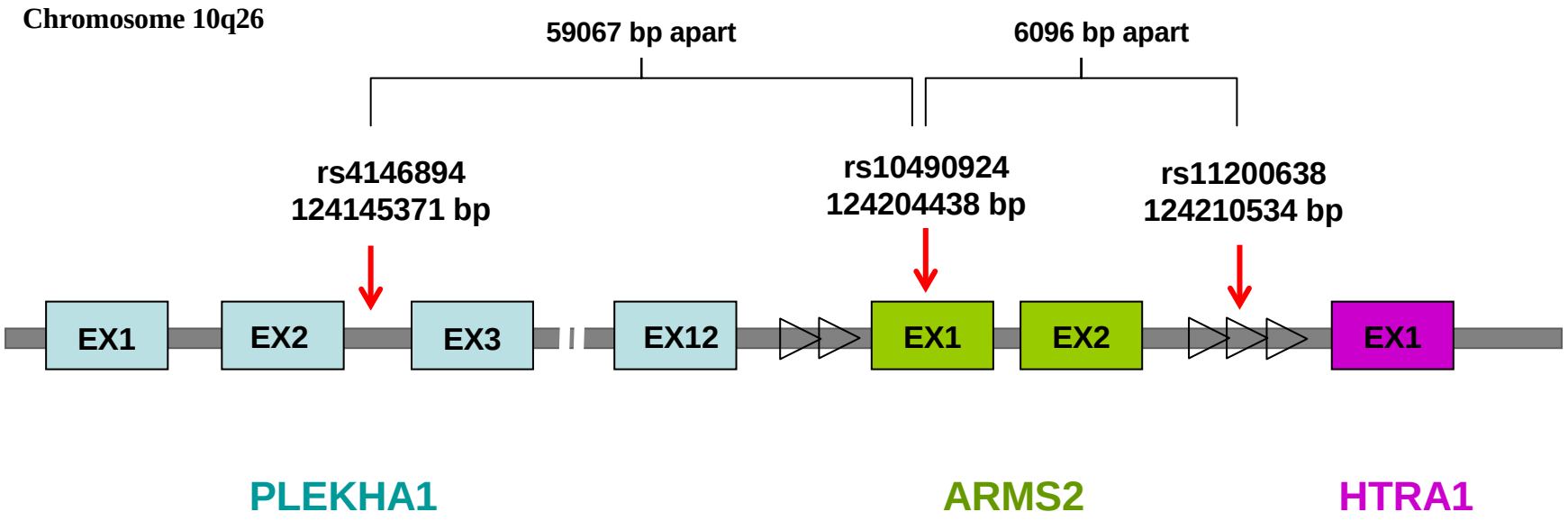
Chromosome 10q26
59067 bp apart
6096 bp apart
rs4146894
124145371 bp
rs10490924
124204438 bp
rs11200638
124210534 bp
EX1
EX2
EX3
EX12
EX1
EX2
EX1
PLEKHA1
ARMS2
HTRA1

1.2.3 Dietary and environmental factors

In addition to aging and genetic risk factors, diet and smoking can increase the risk of developing AMD. Even though high fat diet and exposure to light have been associated with risk of developing AMD[68-70], cigarette smoking was shown to be the strongest environmental risk factor. Thornton *et al*. (2005) reviewed 17 studies which investigated the effect of smoking and AMD and confirmed a strong association between smoking and AMD. Both forms of advanced AMD are more common in smokers than nonsmokers[71]. Smoking is a major source of oxidative stress and might increase the incidence and severity of AMD in genetically predisposed individuals. Indeed, recent studies by Schmidt *et al*. (2006) observe an increased prevalence of AMD among smokers harboring ARMS2[72] and others report similar combined effect between the CFH variant and smoking[49,73].

1.3 Drusen, the hallmark of AMD pathogenesis

Even though there are several risk factors for AMD, the common clinical feature associated with AMD is the formation of extracellular deposits called “drusen” that accumulate between the RPE and the Bruch’s membrane (Figure 1.2). All people accumulate some form of deposits in their retina with age. However, the increase in number and volume of these deposits is a strong indication of impending AMD. There are two clinically distinct categories of drusen; "hard" drusen with a discrete circular shape ranging between 63 μm and 125 μm, and soft drusen with a more diffuse shape and which are usually larger than 125 μm in diameter[74]. Small drusen are sometimes observed in healthy aging retina, but limited number of these small drusen are not associated with risk for developing AMD[5,75-77].

Histological examinations of cross sections of the macula from donors with clinically documented AMD and age matched healthy donors have increased our understanding of drusen subclasses and forms[78]. Additionally, electron microscopy (EM) has been an excellent tool to further characterize drusen texture and sizes[79]. Due to the apparent central role of drusen in AMD pathogenesis, there has been considerable effort to define their content and to develop models that may explain their formation. Drusen have been shown to contain a variety of components including members of the complement pathway[80,81], apo-lipoproteins[82], beta amyloids[83], and clusterin[84], as well as non-proteinaceous components such as lipids[85] carbohydrates[86] and cholesterol[87]. Overall, drusen contain a variety of molecules, yet they are very structured entities, thus making them intriguing and attractive subjects to investigate their cellular origin and what triggers

their formation. This has been partially addressed by our studies on the RPE secretome and its role in drusen formation.

1.4 RPE as potential source of drusen

RPE is a monolayer of cells situated between the neurosensory retina and the choroid (Figure 1.1) and functions as blood-retina barrier. The basal surface of RPE lies adjacent to Bruch's membrane and its apical surface along with a massive array of microvilli is in direct contact with the distal side of photoreceptors. Its main functions are to supply nutrients to the photoreceptors, isomerize all *trans*-retinol to 11-*cis* retinal (vision cycle) and dispose of shed photoreceptor outer segments (POS) by phagocytosis. POS are digested by lysosomes in the RPE cells; the oxidized or damaged proteins are degraded, but 11-*cis* retinal is converted from all *trans*-retinol and sent back to the photoreceptors where it can rebind to photoreceptor molecules (Rhodopsin for rods and iodopsin for cones) to absorb light.

It has long been hypothesized that RPE cells may play a primary role in drusen formation. Farkas *et al*. (1971) suggested that RPE ejects incompletely digested outer segment material into the ECM between the RPE basal lamina and Bruch's membrane leading to progressive build up of drusen deposits[88]. However, close examination of drusen structure and composition revealed that these entities are highly structured and contain mostly extracellular components and little intracellular components. Even though drusen composition has been partially characterized, their biogenesis and exact cellular source remain elusive. Because drusen are located just beneath the basal lamina of RPE cells, it strongly supports the main hypothesis of my dissertation "RPE secreted proteins might be directly involved in drusen formation and CNV in individuals with AMD risk genotypes". Indeed, RPE cells are known to secrete a variety of proteins such us growth factors[89], protease inhibitors[90,91], and proteins found in drusen[81,92-94]. Several pro-inflammatory and

anti-inflammatory components were also described to be secreted by RPE cells *in vitro* [95]. It has been demonstrated that RPE cells readily produce vascular endothelial growth factor (VEGF) *in vitro* and *in situ*[96] and are a source of this factor in diabetic retinas[97]. However, it is not understood how some individuals develop AMD in their early sixties while others are protected. We believe that both genetic and environmental risk factors influence protein expression and secretion of RPE leading to altered homeostasis of RPE extracellular milieu and build up of protein deposits.

1.5 Current treatments

Although dry AMD is more prevalent, therapeutic interventions have been focused on wet AMD, which comprises approximately 10 % of the AMD patients. Therapy for wet AMD has evolved from thermal laser photocoagulation (TLP) in the early to mid 1980s, to photodynamic therapy (PDT) in 2000 and most recently to inhibition of vascular growth factors. TLP results in scotoma, an area of vision loss, at the site of the treatment so it is limited to only around 13 % of patients with wet AMD (or 1.3 % of all AMD patients)[98]. PDT which uses intravenous infusion of Verteporfin, a photosensitizing drug, and laser also has some limitation. There is high rate of membrane recurrence, a risk of sudden permanent worsening of the vision and it is not recommended for patients with liver disease. A more recent therapy, anti-angiogenic treatment includes Pegaptanib sodium (Macugen®), Ranibizumab (Lucentis®), and Bevacizumab (Avastin®). Unfortunately, this anti-angiogenic treatment also has some limitations. These treatments need to be injected on average every month, and repeated intravitreal anti-VEGF therapy may lead to serious long term systemic adverse events such as thromboembolic events and death. For dry AMD, Age-related eye disease study (AREDS) suggests antioxidant and zinc supplementation which also has limitations such as increased death and risk of heart failure from Vitamin E[99], the risk of the developing lung cancer in smokers from β carotene[100-102], and genitourinary complication from Zinc[103]. Also it was shown not to be beneficial to people without AMD or bilateral AMD.

Overall, available treatments for AMD have resulted in a benefit to less than 50 % of patients with wet AMD, and therefore less than 5 % of all AMD patients and vision loss is not recovered with current treatments. Despite the fact that various animal models have

been developed displaying phenotypes of human AMD over the last 25 years, there is no exact animal model for AMD. A critical evaluation at the cellular and molecular levels of AMD may lead to better treatments for AMD.

1.6 Study of the cell secretome

The secretome or secretomics has recently emerged as a new term to describe the global study of proteins that are secreted by a cell, a tissue or an organism at any given time or under certain conditions[104]. Protein secretion is a well controlled and balanced process that is necessary for normal physiologic function. Chronic alterations or aberrant secretions of some proteins (such as in the case of RPE cells harboring AMD risk genotypes) could lead to pathologic condition. Thus, comprehensive analysis of secreted proteins in a given tissue under a given condition is an attractive approach to discovery of the underlying molecular mechanisms and defining new therapeutic targets.

Emerging methods in proteomics have greatly facilitated the global analysis of proteins in biological samples including tissues and culture media. Combinations of two dimensional gel electrophoresis (2-DE) and mass spectrometry (MS) have been widely used to characterize proteins secreted by cell cultures[105]. The technique relies on separation of secreted proteins by 2-DE followed by in-gel digestion of a protein spot (usually using trypsin as protease) and analysis of the resulting peptides by MS. This approach generates a highly specific peptide mass fingerprint that can be easily matched to a protein in the database using search engines such as Mascot (http://www.matrixscience.com). This approach was successfully used to identify some secreted proteins in hepatic[106], choroid plexus[107], and adipose[108] tissue cultures. While a 2-DE based approach can provide quick information about the protein content in the conditioned medium, several classes of protein (proteins with low amounts, extreme isoelectric point (pI) and extreme masses) may be overlooked, thus other approaches were needed for comprehensive analysis of the secretome. The shotgun approach in combination with multidimensional chromatographic

separations and MS is another strategy to separate and deconvolute complex protein mixtures for protein profiling. In this case, the complex protein mixture is first digested with a protease (usually trypsin) and the resulting peptides are analyzed by a combination of chromatographic methods and MS. Protein identification is performed by peptide sequencing using tandem mass spectrometry (MS/MS) and database searching. This method can easily be combined with stable isotope labeling for protein quantitation[109].

Stable isotope tags can be introduced to proteins via metabolic labeling using heavy amino acids[110], via enzymatic transfer of ^{18}O from water to peptides[111], or via chemical reaction using isotope-coded affinity tags[112]. In all methods, MS plays a crucial role for both protein identification and quantitation**.** We and others have found that stable isotope labeling by amino acids in cell culture (SILAC)[110] is the most promising strategy for accurate comparative proteomics when dealing with cell culture[113-122]. Because labeled and unlabeled cells can be mixed before protein extraction, variations that would result from sample processing and handling are extremely minimized. As shown in Figure 1.5, one set of cells (control cells) is grown in a medium in which some of the amino acids (usually Lysine(Lys) or Arginine (Arg) or both) are substituted by stable isotope labeled ones (in this case $^{13}C_6$-Arg and $^{13}C_6$, $^{15}N_2$-Lys). Fully labeled cells or their conditioned media can then be mixed at a 1:1 ratio with unlabeled cells or their conditioned media (experimental cells) for subsequent subcellular fractionation, protein processing and MS analysis.

Figure 1.4 MS-based quantitative proteomics with SILAC strategy

Control cells are grown in medium containing heavy $^{13}C_6$-Arg and $^{13}C_6$, $^{15}N_2$-Lys (red) while experimental cells are grown in medium containing light $^{12}C_6$-Arg and $^{12}C_6$,$^{14}N_2$ -Lys (green). After 6 to 7 cell doublings, all cellular proteins including secreted proteins are fully labeled with these amino acids. Cells including conditioned media are mixed at 1:1 and processed for subcellular fractionation and protein extraction. Samples containing labeled and unlabeled proteins are further separated by Sodium dodecyl sulfate (SDS)-Polyacrylamide gel electrophoresis (PAGE) and stained with Coomassie blue. Gel bands are sliced, digested by trypsin and the resulting peptides are analyzed by liquid chromatography (LC)-MS/MS. Base peak chromatogram shows LC profile of all peptides in a given band. The mass spectrometer performs an MS survey scan of eluting peptides. Heavy and light peptide pairs co-elute in the chromatogram but their masses are resolved by the MS. Zoom scan shows a pair of labeled (red) and unlabeled (green) peptides generated from the same protein in SILAC labeled and unlabeled sample, respectively. Individual peptides are then gated and further fragmented to provide MS/MS for sequencing and protein identification. Protein ratios in SILAC labeled versus unlabeled samples are determined from the intensity ratio of their corresponding heavy to light peptide pairs.

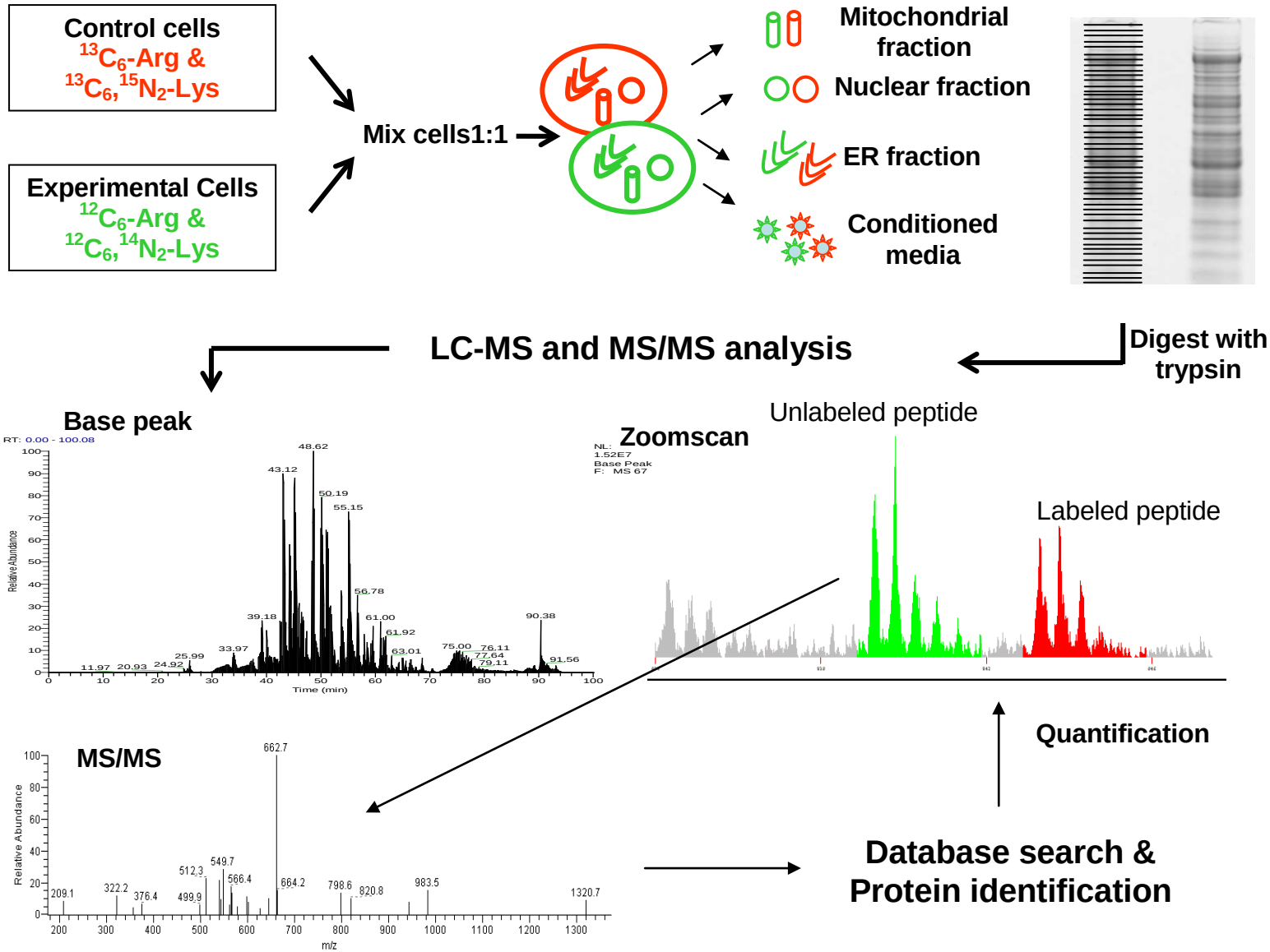
Control cells
$^{13}C_6$-Arg &
$^{13}C_6$,$^{15}N_2$-Lys
Experimental Cells
$^{12}C_6$-Arg &
$^{12}C_6$,$^{14}N_2$-Lys
Mix cells1:1
Mitochondrial fraction
Nuclear fraction
ER fraction
Conditioned media
LC-MS and MS/MS analysis
Digest with trypsin
Base peak
RT: 0.00 - 100.08
Relative Abundance
Time (min)
Zoomscan
Unlabeled peptide
Labeled peptide
MS/MS
m/z
Quantification
Database search &
Protein identification

1.7 Hypothesis and specific aims

As discussed in the introduction above, AMD is characterized by progressive degeneration of the macula attributed to abnormal accumulation of drusen deposits between the RPE and the Bruch's membrane that can be accompanied some times by CNV. Three strong genetic risk factors have been associated with this disease to date. The CFH polymorphism (Y402H-CFH) is responsible for 50% of AMD cases including both atrophic and exudative form[35] and the HTRA1/ARMS2 polymorphism is also responsible for more than 50% of AMD cases[52]. The risks from these loci are additive and may increase the risk of developing AMD to as much as 75%. While the genetics leading to AMD predisposition are becoming clear, the pathophysiology remains difficult to understand. We hypothesize that genetic risk factor with environmental risk factors will result in altered homeostasis of RPE extracellular environment leading to progressive drusen accumulation and/or CNV. These alterations are detectable using proteomics approaches and can be used to define key pathway(s) in AMD pathogenesis.

Aim 1: Quantitative analysis of secretome of human primary RPE cell cultures derived from AMD and age matched normal donor.

- **Sub-aim 1-A**: Establish human primary RPE cultures from human autopsy eyes of AMD (diagnosed by histological examinations of the macular and genotyped for the Y402H-CFH) and control donors.
- **Sub-aim 1-B**: Profile the RPE secretome using stable isotope labeling by amino acids in cell culture.

Aim 2: Tumor necrosis factor-alpha (TNF-α) induced changes in RPE secretome reveal molecular networks relevant to drusen formation and CNV

- **Sub-aim 2-A:** Optimize cell culture conditions to study the effect of TNF-α on APRE-19 cell line.
- **Sub-aim 2-B:** Optimize proteomics analysis method to study the effect of TNF- α on APRE-19 cell line.

Aim 3: Identification of novel HTRA1 substrates in the human RPE secretome

- **Sub-aim 3-A:** Stratification and characterization of RPE cultures by AMD risk genotypes (*CFH* and *HTRA1*) and clinical history of donors.
- **Sub-aim 3-B:** Define HTRA1 expression in RPE cell cultures with different HTRA1 promoter genotypes and identify potential HTRA1 substrate in the RPE conditioned medium.

Aim 4: Characterization of CFH and FHL-1 expression in genotyped human RPE cells and association with AMD.

Chapter 2: Secreted Proteome Profiling in Human RPE cell Cultures Derived from Donors with Age-related macular degeneration and Age matched Healthy Donors

It is essential to obtain homogeneous RPE cell cultures to study RPE secreted proteins. The goal of this chapter was to establish human primary RPE cultures from human autopsy eyes of AMD (diagnosed by histological examinations of the macular and genotyped for the Y402H-CFH) and control donors and profile the RPE secretome using stable isotope labeling by amino acids in cell culture.

This chapter was published in Journal of Proteome Research in 2006.
Journal of Proteome Research 5, 2599-610 (2006)

Eunkyung An[1, 2], Xiaoning Lu[1], Jessica Flippin[1], Joseph M Devaney[1], Brian Halligan[3] ,

Eric Hoffman[1], Karl Csaky[4], and Yetrib Hathout[1]

1. Research Center for Genetic Medicine, Children's National Medical Center, Washington, DC.
2. Program in Biochemistry and Molecular Genetics, Institute for Biomedical Sciences, The George Washington University, Washington, DC.
3. Bioinformatics, Human and Molecular Genetics Center, Medical College of Wisconsin, Milwaukee, Wisconsin.
4. National Eye institute, National Institutes of Health, Bethesda, Maryland

Correspondence should be addressed to:

Yetrib Hathout, Ph.D
Research Center for Genetic Medicine
Children's National Medical Center
111 Michigan Ave NW
Washington, DC 20010
yhathout@cnmcresearch.org
Telephone number: (202) 476-3136
Fax number: (202) 476-6014

2.1 Abstract

Age-related macular degeneration (AMD) is characterized by progressive loss of central vision, which is attributed to abnormal accumulation of macular deposits called “drusen” at the interface between the basal surface of the RPE and Bruch’s membrane. In the most severe cases, drusen deposits are accompanied by the growth of new blood vessels that breach the RPE layer and invade photoreceptors. In this study, we hypothesized that RPE secreted proteins are responsible for drusen formation and choroidal neovascularization. We used stable isotope labeling by amino acids in cell culture (SILAC) in combination with LC-MS/MS analysis and ZoomQuant quantification to assess differential protein secretion by RPE cell cultures prepared from human autopsy eyes of AMD donors (diagnosed by histological examinations of the macula and genotyped for the Y402H-CFH variant) and age-matched healthy control donors. In general, RPE cells were found to secrete a variety of extracellular matrix proteins, complement factors, and protease inhibitors that have been reported to be major constituents of drusen (hallmark deposits in AMD). Interestingly, RPE cells from AMD donors secreted 2 to 3-fold more galectin 3 binding protein, fibronectin, clusterin, matrix metalloproteinase-2 (MMP2) and pigment epithelium derived factor than RPE cells from age-matched healthy donors. Conversely, secreted protein acidic and rich in cysteine (SPARC) was found to be down regulated by 2-fold in AMD RPE cells versus healthy RPE cells. Ingenuity pathway analysis grouped these differentially secreted proteins into two groups; those involved in tissue development and angiogenesis and those involved in complement regulation and protein aggregation such as clusterin. Overall, these data strongly suggest that RPE cells are involved in the biogenesis of drusen and the pathology of AMD.

2.2 Introduction

Age-related macular degeneration (AMD) is a leading cause of blindness in the elderly population[7]. Currently, there is no effective cure for the disease due to a lack of therapeutic targets. AMD is characterized by proteinaceous deposits called "drusen" that accumulate between the RPE and Bruch's membrane[78,123,124]. An increase in the number and volume of these drusen is indicative of progressive AMD[2,125,126]. There are two forms of AMD: dry atrophic without neovascularization and wet with exudative neovascularization. The genetic predisposition to both forms has recently begun to be elucidated. Indeed, four independent groups have clearly demonstrated that a CFH polymorphism (Y402H) is strongly associated with the risk of developing AMD[33-36]. Additional recent studies have implicated gene variants of BF and complement 2, whose protein products are involved in the same pathway as CFH[42]. Although genetic factors of the disease are being unraveled, the pathophysiology remains difficult to understand. Specifically, the formation of the characteristic drusen and CNV in the retina is not well understood. It has been long hypothesized that RPE may play a primary role in the formation of drusen[88]. The RPE is composed of highly specialized and active phagocytic epithelial cells localized between the photoreceptors and choroids. These cells perform crucial functions in the eye, such as daily phagocytosis of fragments shed from rod and cone cells, processing and transport of nutrients, and recycling of visual pigments[127]. Unfortunately, these post-mitotic cells are vulnerable to aging effects and deteriorate with time, resulting in progressive degeneration.

In this study, we hypothesized that abnormal protein secretion by RPE cells might be involved in drusen and CNV formation in AMD patients, resulting in progressive

degeneration of the retina and loss of vision. RPE cells are known to secrete a variety of proteins such as growth factors[89]and protease inhibitors[91,128] and are a source of the VEGF involved in diabetic retinopathy [96,97]. Thus, profiling and cataloguing proteins secreted by RPE cells may provide insight into their role in AMD.

SILAC is becoming the method of choice for protein profiling when using cell culture systems [110,113]. Because labeled and unlabeled cells can be mixed before protein extraction, variations in protein ratios resulting from sample processing and handling are minimized. This method has been successfully used to accurately determine protein ratios between samples representing different biological states[114-116] and is suitable to study the phosphoproteome in cell culture systems[117-119] as well as protein-protein interactions[120,121]. More recently, SILAC was used to study and characterize secreted proteins in a pancreatic cancer cell line in search for potential pancreatic cancer biomarkers[122]. We implemented a similar strategy to examine differential protein secretion, “secretome profiling”, in primary human RPE cell cultures prepared from AMD donors and age matched healthy donors.

2.3 Experimental Methods

2.3.1 Preparation of Primary RPE Cell Culture from Postmortem Autopsy Eyes

Donor's eyes were received through Heartland Lions Eye Bank (eyes are collected within a few hours (4-6) after death and shipped in sterile physiologic solution). The average donor age was 65 years old and above, including both females and males. The anterior segment from each donor eye was removed by cutting around the iris and removing it along with the lens. A biopsy was then taken from the macula of each eye for histological examination by EM. RPE cells were harvested from the remaining tissue according to previously published procedures[129] with some modifications. Briefly, the vitrous and the retina were carefully peeled away from the RPE-choroid-sclera using fine forceps. Then the RPE-choroid was carefully separated from the sclera and placed face up in a small sterile Petri dish. Then, 0.1% dispase (Roche, Indianapolis, IN) prepared in Ca^{2+} and Mg^{2+}-free Hank's balanced salt solution was added to completely cover the tissue. After incubation at 37 °C for about 3 h with occasional shaking, the liquid was carefully aspirated and transferred to a sterile centrifuge tube. The suspension was then centrifuged at 300 x g for 5 min, and the cell pellet was resuspended gently in DMEM/F12 (Invitrogen, Carlsbad, CA) supplemented with 10% FBS (Invitrogen, Carlsbad, CA), 100 U/mL penicillin, and 100 μg/mL streptomycin. The suspended cells were then transferred to T25 culture flasks and placed in an incubator at 37 °C and 5% CO2 under humidified atmosphere. Growing cells were tested for their epithelial content using an established immunohistochemical staining for cytokeratins[130].

2.3.2 Screening RPE Cell Cultures for the Y402H CFH Variant

DNA was extracted from each of the RPE cultures obtained above and screened for the Y402H-CFH polymorphism (rs1061170). An allelic discrimination assay (TaqMan assay)[131] was used to detect homozygous MT rare allele (CC), heterozygous (CT) and wild type genotypes in *CFH* gene. The assay uses two TaqMan probes that differ at the polymorphic site, with one probe complementary to the wild-type allele and the other to the variant allele. The probes contained different fluorescent reporter dyes (VIC® and FAM™) to differentiate the amplification of each allele. A quencher dye is covalently linked to the wild-type or variant allele probes. When the probes are intact, fluorescence is quenched because of the physical proximity of the reporter and quencher dyes. During the polymerase chain reaction (PCR) annealing step, the TaqMan probes hybridize to the targeted polymorphic site. During the PCR extension phase, the reporter dye is cleaved by the nuclease activity of the Taq polymerase, leading to an increase in the characteristic fluorescence of the reporter dye. The signal generated by PCR amplification indicates the alleles that are present in the sample. Specific genotyping is determined by measuring the signal intensity of the two different reporter dyes after the PCR reaction.

An allele-specific PCR reaction was used for each single nucleotide polymorphism (SNP) including 20 ng genomic DNA, 900 nM forward (F) and reverse (R) PCR primers (F: 5'- CTTTATTTATTTATCATTGTTATGGTCCTTAGGAAAATGTTATTT- 3' and R: 5'- GGCAGGCAACGTCT-ATAGATTTACC-3'), 200 nM fluorescent allele discrimination probes (wild type allele (WT): VIC®-5'-TTTCTTCCATAATTTTG-3'; MT allele: VIC®-5'-TTTCTTCCATGATTTTG-3') and TaqMan Universal PCR Master Mix, No AmpErase UNG (Applied Biosystems, Foster City, CA) in a final volume of 10 μL.

The PCR was preformed at 95 °C for 10 min and 44 cycles of 15 s at 92 °C and 1 min at an annealing temperature of 60 °C. Reactions were performed using a MWG robot, and fluorescence ratios and allele calling measured using an ABI 7900 (Applied Biosystems, Foster City, CA)

2.3.3 Stable Isotope Labeling by Amino Acids

A suspension of RPE cells (about 150 000 cells) with the wild-type CFH genotype (TT-RPE) prepared from an eye of a healthy donor was incubated in custom-made DMEM/F12 medium without Arg nor Lys (Atlanta Biologicals, Lawrenceville, GA) to which the following were added: 10% FBS (Invitrogen, Carlsbad, CA), 100 U/mL each of penicillin and streptomycin, $^{13}C_6$-Arg (147.5 μg/mL), and $^{13}C_6$, $^{15}N_2$-Lys (91.25 μg/mL) (Cambridge Isotope Laboratories, Inc., Andover, MA). In parallel, the same amount of RPE cells were prepared from AMD donors with the homozygous rare CFH genotype (CC-RPE) and the heterozygous CFH genotype (CT-RPE) were grown in the same media containing unlabeled L-Arg and L-Lys instead of isotopically labeled ones. All RPE cells were sub-cultured to passage 4. After confluence, cells were washed five times with Phosphate buffered saline (PBS) to remove excess bovine serum proteins and then incubated in serum-free labeled and unlabeled media for a period of 18 h.

2.3.4 Sample Preparation of Secreted Proteins

Conditioned media from each of the labeled and unlabeled RPE cultures were collected in 15 mL tubes (BD Biosciences Falcon, San Jose, CA) and then filtered through a 0.22 μm nylon filter (Millipore, Bedford, MA). Any debris were pelleted by

centrifugation at 300x g at 300 x g, then at 1000 x g, and finally at 100000 x g then the supernatant was transferred to a new tube between each centrifugation. Aliquots (5 mL) from the conditioned medium of each RPE cell culture were taken and concentrated 100 times under vacuum centrifugation. The samples were then desalted against 10 mM Tris HCl, pH 7, using P6 Bio-Spin columns (Bio-Rad, Hercules, CA) and the protein content was determined using the Bio-Rad protein assay reagent following the manufacturer's instructions (Bio-Rad, Hercules, CA). Equal aliquots of labeled and unlabeled RPE secreted proteins were mixed together and then separated by SDS-PAGE. Coomassie-stained protein bands were digested with a gold grade trypsin (Promega, Madison, WI) and the resulting peptide solutions were passed through a 0.2 μm Polyvinylidene fluoride (PVDF) filter (0.22 μm pore size) prior to LC-MS/MS analysis.

2.3.5 Nanoflow LC-MS/MS

Nano-LC tandem mass spectrometry was performed on an LC-Packing system (DIONEX UltiMate Capillary/Nano LC System, Dionex Corp., Sunnyvale, CA) connected to a linear ion trap quadropole (LTQ) mass spectrometer (Thermo Electron Corporation, San Jose, CA). Each sample was injected via an autosampler and loaded onto a C18 trap column (300 μm x 1 mm, LC Packings) for 6 min at a flow rate of 10 μL/min. The sample was subsequently separated by a C18 reverse-phase column (75 μm x 15 cm, Vydac, Columbia, Maryland) at a flow rate of 300 nL/min. The mobile phases consisted of water with 0.1% formic acid (A) and 90% acetonitrile with 0.1% formic acid (B). A 90-min linear gradient from 5 to 50% B was typically employed. After LC separation, the sample was introduced into the mass spectrometer via a 10- μm silica tip (New Objective Inc.,

Ringoes, NJ) adapted to a nano-electrospray source (Thermo Electron Corporation, San Jose, CA). The spray voltage was set at 2.0 kV and the heated capillary at 160 °C. The LTQ was operated in data-dependent mode in which one cycle of experiments consisted of one full-MS survey and subsequently three sequential pairs of intercalated zoom scans and MS/MS experiments. The targeted ion counts in the ion trap during full-MS, zoom scan, and MS/MS were 30000, 3000, and 10000, respectively. The zoom scan events are of higher resolution and were used to determine the charge state of the ion as well as the ratio of labeled and unlabeled peptide pairs using the ZoomQuant software (see next section). Peptides were fragmented in the linear ion trap using collision-induced dissociation with the collision gas (helium) pressure set at 1.3 milliTorrs and the normalized collision energy value set at 35%.

2.3.6 Database Search

Protein searches were performed with the BioWorks 3.2 software (Thermo Electron Corp, San Jose, CA). Basically, each file was searched against the human National Center for Biotechnology Information non redundant data base (NCBInr) and the human SwissProt databases using the Sequest search engine set with the following possible protein modifications: 16 Dalton (Da) shift for oxidized Methionine and 6 and 8 Da shifts for stable isotope labeled Arg and Lys, respectively. The acceptance criteria for peptide identifications were set as follows: a DeltaCn (ΔCn) > 0.1, a variable threshold of Cross correlation (*Xcorr*) vs. charge state (*Xcorr*) 1.9 for z= 1, *Xcorr* = 2.5 for z = 2, and *Xcorr* = 3.5 for $z \geq 3$) and a peptide probability based score with a p value < 0.001. The rate of false positive identification was determined (using the same filtration criteria) by searching the

files against a reversed human NCBInr database. Using these stringent filtration criteria, the rate of false positive identification was less than 1.8%, thus increasing the confidence in the identified proteins.

2.3.7 ZoomQuant Analysis

To measure the intensity ratios of labeled and unlabeled peptide pairs, we used the ZoomQuant software developed by Halligan *et al*[132]. The generated Sequest output files were loaded into the Epitomize filter to generate a colon-delimited text file that contained the list of identified proteins, the sequence and atomic composition of the identified peptides with scan number, charge state, *Xcorr*, and mass data. This file was then loaded into the ZoomQuant software along with a file containing zoom scans that were extracted from the corresponding raw data file using a visual basic RawBitz script. Zoom scan information was then matched to the Sequest identified peptides, after which labeled and unlabeled pairs were detected based on their amino acid composition and theoretical masses. Ratios were determined from the peak areas of the isotope clusters of the labeled and unlabeled peptides.

2.3.8 mRNA Isolation and Expression Profiling

Total ribonucleic acid (RNA) was isolated from several RPE cell cultures: healthy donors with the wild-type CFH genotype (n =4), AMD donors with homozygous rare Y402H-CFH genotype (n =3), and AMD donors with heterozygous Y420H-CFH genotype (n = 3) using TRIZOL reagent (Invitrogen, Carlsbad, CA) and then cleaned up using a Qiagen Kit according to the manufacturer's protocol. Total RNA was then converted to

double biotinylated cRNAs and hybridized to separate Affymetrix Human U133 Plus 2.0 GeneChips. Procedures for cRNA preparation and GeneChip processing were performed as previously described[133,134].

2.3.9 Ingenuity Pathway Analysis

Differentially expressed proteins were evaluated by the Ingenuity computational pathway analysis software to identify possible global functions of the secreted protein pattern and association with the disease. The Ingenuity Pathway Analysis program uses a knowledge base derived from the literature to relate gene products to each other, based on their interaction and function. The knowledge base consists of a high quality expert-curated database containing 1.4 million biological findings consisting of more than 23,900 mammalian genes (10,300 for human, 5,200 for rat, and 8,400 for mouse) and millions of pathway interactions extracted from the literature. This knowledge database also integrates a broad range of systems biology including protein function, cellular localization, and small molecule and disease interrelationships. The Ingenuity Pathway Analysis suite identifies dynamically generated biological networks, global canonical pathways, and global functions. Basically, the relevant proteins with their fold change and corresponding "gi" accession number are uploaded as an Excel spreadsheet file into the Ingenuity software (http://www.ingenuity.com). Ingenuity then uses these proteins and their identifiers to navigate the curated literature database and extract an overlapping network between the candidate proteins. A score better than 2 is usually attributed to a valid network (the score represents the log probability that this network was found by random chance).

2.4 Results

2.4.1 EM Examination of Macular Biopsies

Examination of sections of the macula using EM is an effective way to determine and classify different histological AMD features[79]. Figure 2.1 shows a cross section of the macula from the eyes of 81 year old (A), 72 year old (B), and 77 year old (C) donors. The cross section of the retina is represented by three well-defined areas, namely the RPE, Bruch's membrane and the choroids (Figure 2.1A). Both the 72 year-old donor (Figure 2.1B) and the 77 year old donor (Figure 2.1C) retinal cross sections presented with deposits just beneath the basal lamina of the RPE whereas the retinal cross section of the 81 year-old donor appears free from deposits with the RPE cells perfectly aligned atop of Bruch's membrane (Figure 2.1A). The basal laminar deposits called fibrous long-spacing collagen (FLSC) seen in the retinal section from the 72 year old donor (Figure 2.1B) are accompanied by a thickening of Bruch's membrane which is believed to be consistent with the early stages of AMD[79]. An increase in the number and volume of these deposits is highly indicative of progressive AMD.

RPE cells were isolated from the retina of these autopsied eyes and resulted in growing colonies that could be propagated up to passage 12 before entering into a senescence phase. Thirty-five primary RPE cultures of 27 human subjects (RPE cultures were obtained from both the left and right eye of some subjects) were generated. Cultures were examined for their epithelial cell content using Fluorescent-activated cell sorting (FACS) analysis[116]. Only cell cultures with high epithelial content (equal to or greater than 80%) were kept for the study.

Figure 2.1 Electron micrographs of the cross section of the macula prepared from an (A) 81-, (B) 72-, and (C) 77-year old donors

The black arrows indicate the “FLSC” between the RPE and Bruch’s membrane seen in donor (B) or drusen particles seen in donor (C).

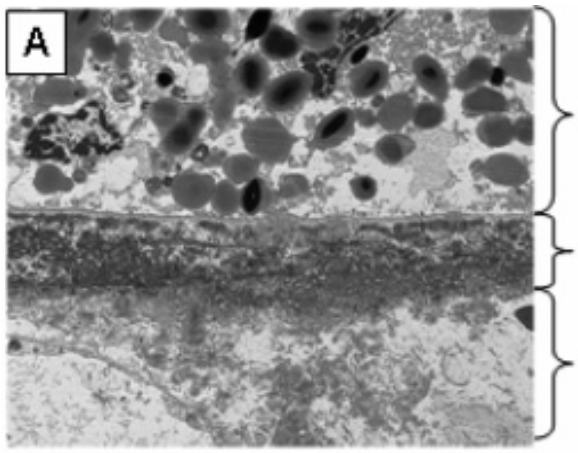

Retinal pigment Epithelium (RPE)

Bruch's membrane

Choroidal blood vessel

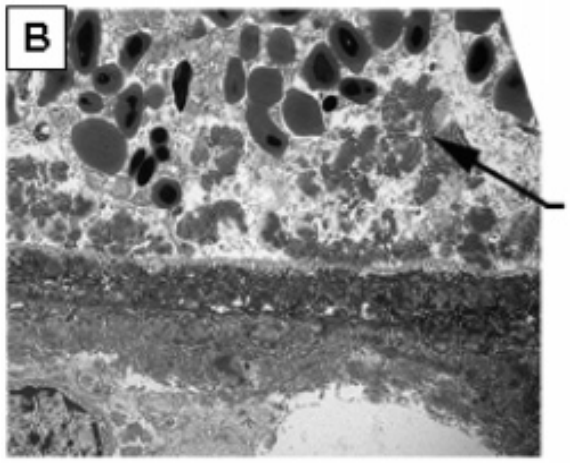

Basal laminar deposits

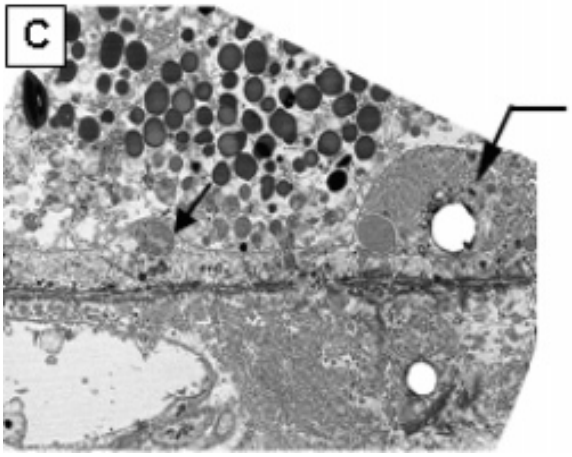

Drusen

2.4.2 RPE Genotyping for the CFH Variant

Each of the RPE cell cultures generated from AMD patients and normal donors were genotyped for the AMD-predisposing SNP (Y402H-CFH)[33-36] as described in the experimental methods. RPE cell cultures generated from the left and right eye of the same donor had the same genotype demonstrating the validity of our assay. Among the 35 genotyped RPE cell cultures, 14 were wild type (TT), 16 were heterozygote (CT), and only 5 harbored the homozygote rare CFH genotype (CC) associated with AMD. The EM histological examination did not always correlate with the CFH genotyping especially in the wild-type and heterozygous samples. Indeed, among the 14 RPE cell cultures with the wild type CFH genotype (TT-RPE), we were able to diagnose 5 with healthy macula (absence of any kind of deposit), 2 with basal laminar deposits (early stage AMD), and 3 with drusen deposits, whereas, the rest (4 RPE cultures) had inconclusive diagnoses.

Among the 16 RPE cell cultures with the heterozygous CFH genotype (CT-RPE) we were able to obtain conclusive diagnoses for 7 samples (3 with healthy macula, 2 with early stage AMD and 2 with large drusen deposits). Finally, 3 out of the 5 RPE cell cultures with the homozygous rare CFH genotype had large drusen deposits whereas 2 had completely healthy macula. These results are not surprising because not all individuals with clinically documented AMD have the CFH gene variant and conversely, not all individuals free of AMD are wild type at this locus. Similar findings were reported by Hageman *et al*.[35] in a study performed on a cohort of AMD cases (n = 404) and age matched controls (n = 131). Among the 404 AMD cases, only 146 were found to harbor the CC homozygous variant; whereas 183 harbored the heterozygous CT variant and 74 displayed the TT wild-type genotype. Among the 131 control cases, 16 were found to harbor the homozygous CC

genotype, 56 the heterozygous CT genotype, and 59 the TT wild-type genotype. These results suggest that AMD may be the result of more complex genetic factors acting in concert with environmental risk factors. Indeed, a recent genotyping study performed on a large cohort of AMD and control cases demonstrated that, aside from the CFH variant, there are additional SNPs that can protect or worsen one's risk of developing AMD[42]. Classification of any predisposing alleles may help define an individual's risk for AMD, whereas understanding the cellular and molecular mechanisms of the pathology (e.g., drusen formation and angiogenesis) may aid in defining therapeutic targets. In this study, we hypothesize that proteins secreted by the RPE are involved in drusen formation.

2.4.3 Analysis of RPE Secreted Proteins

The advantage of growing RPE cells in stable isotope labeled amino acid containing medium is that all cellular proteins are uniformly labeled with heavy isotope amino acids (e.g., $^{13}C_6$-Arg and $^{13}C_6$, $^{15}N_2$-Lys), making it easy to distinguish RPE secreted proteins from bovine serum contaminants. Indeed, several bovine proteins were still present in the culture medium even after washing the cells five times with PBS before incubating them in a serum-free conditioned medium (Figure 2.2B). Additionally, bovine serum proteins may be erroneously identified as their human homologues even after restricting protein database searches to human NCBInr fasta, thereby raising doubts as to the true origin of the identified protein. This problem was easily circumvented by using SILAC and by selecting only those proteins represented by labeled and unlabeled peptide pairs for further analysis (Figure 2.2C).

Figure 2.2 Zoom scan as a tool to distinguish between contaminant and RPE originated protein

A) is the base peak chromatogram showing the overall peak intensities and retention time of all the peptides detected in this gel slice. B) shows the zoom scan mass of two consecutive eluting peptides. The peptide with m/z 461 eluting at 26.6 min was detected as a singlet and belongs to bovine serum albumin as well as human albumin. The peptide eluting at 28.2 min was detected as a doublet peak at m/z 628.1 and 631.1, corresponding to the unlabeled and labeled peptide, respectively (C). This belongs to human RPE cells. Peptide sequences are shown on the top of each spectrum and were obtained by MS/MS analysis and database search. The labeled and unlabeled peptides are 6 Da apart and agree with one $^{13}C_6$- Arg residue in the peptide sequence.

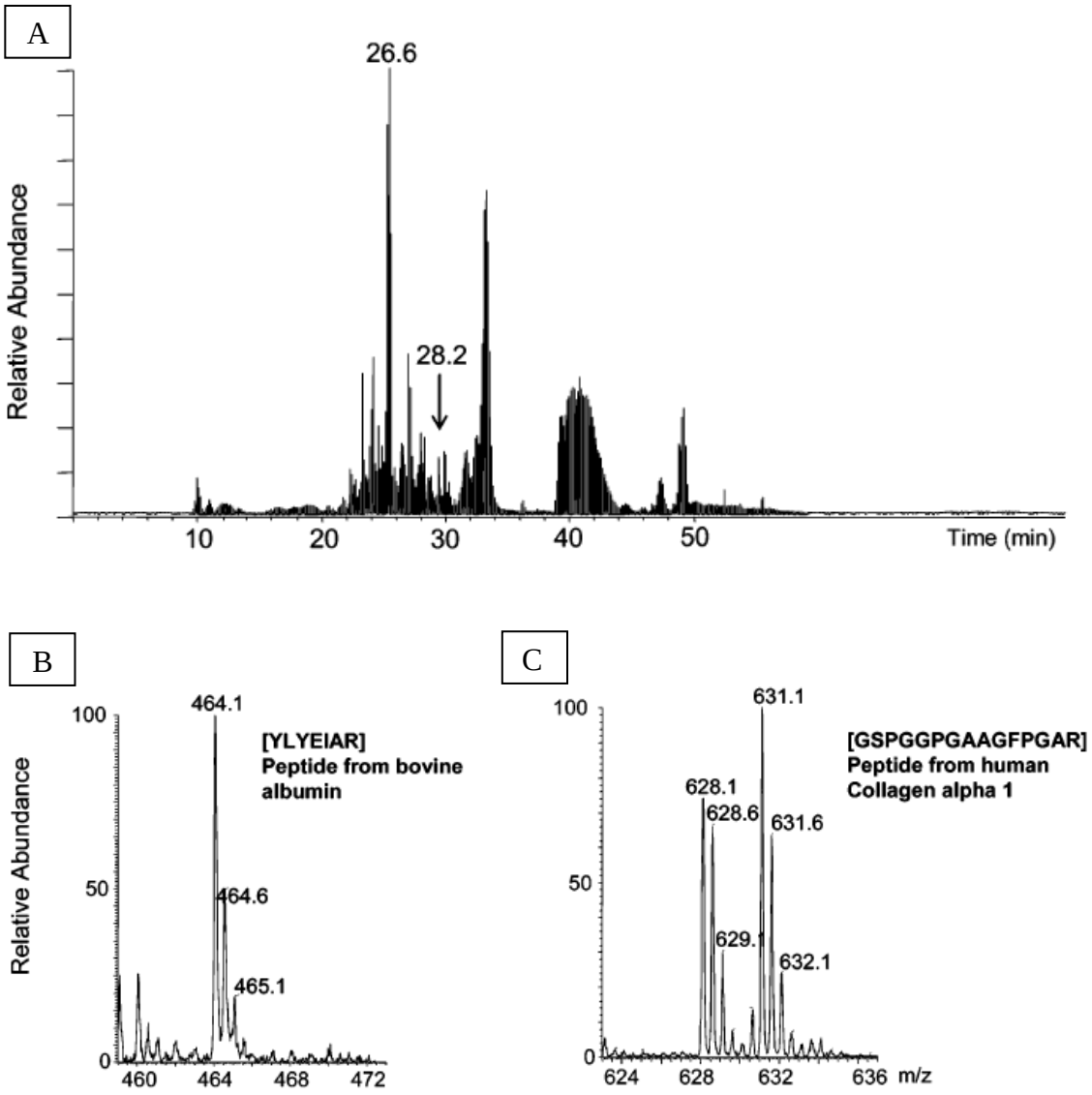
A
26.6
28.2
Relative Abundance
10
20
30
40
50
Time (min)
B
464.1
[YLYEIAR]
Peptide from bovine
albumin
464.6
465.1
100
50
0
460
464
468
472
C
631.1
628.1
628.6
631.6
629.1
632.1
[GSPGGPGAAGFPGAR]
Peptide from human
Collagen alpha 1
624
628
632
636
m/z

The detection of these peptide pairs was performed automatically by ZoomQuant software[132]. Basically, the software uses the peptide sequences generated by a Sequest database search, then calculates the theoretical mass of the peptide and looks for labeled and unlabeled peptide pairs based on Arg and Lys residue content. This procedure permits all single peptides generated from bovine proteins and/or other contaminants such as keratins to be filtered out. Only proteins represented by labeled and unlabeled peptide pairs are retained.

Table 2.1 summarizes all the 73 proteins that we have identified thus far in mixtures of conditioned media from labeled and unlabeled RPE cell cultures. Most of the reported peptides were identified with *X-corr* scores above 2.5 and 3.5, for the doubly and triply charged ions, respectively and a p value < 0.001 for peptide probability based score. The rate of false positive identification was less than 1.8% when a database search was performed against reversed fasta formats of human NCBInr and human SwissProt databases using the same filtration criteria. Although 13 out of the 73 proteins were represented by a single peptide, it was still possible to confidently identify these proteins based on the fact that both labeled and unlabeled peptides were detected and also by manually checking the corresponding MS/MS spectrum. Labeled and unlabeled peptide pairs readily validate each other, thus adding more confidence in the identification of these proteins.

Figure 2.3 A represents the mass spectrum obtained for pigment epithelium derived factor protein (PEDF) with peaks for unlabeled and labeled peptide pairs at m/z 607.66 and 611.66, respectively. The difference in mass between these doubly charged ions is 8 Da, suggesting that the peptide should contain one Lys residue (i.e., $^{13}C_6$, $^{15}N_2$-Lys).

Table 2.1 List of proteins identified in the conditioned media of human primary RPE cell cultures

Protein Name	Accession Number	Peptide Number	Secretion
Cell adhesion / connective tissue protein			
47 kDa heat shock protein precursor	123576	1	YES
Alpha 1 type I collagen preproprotein	22328092	1	YES
Alpha 2 type VI collagen isoform 2C2a precursor	17402879	2	YES
Alpha 2(I) collagen	2388555	3	YES
Basement membrane-specific heparin sulfate	24212664	6	YES
BIGH3	2996636	1	YES
Biglycan preproprotein	4502403	4	YES
Collagen alpha 1(I) precursor	115269	40	YES
Collagen alpha 1(III) precursor	4502951	35	YES
Collagen alpha 2(I) chain precursor	82654930	29	YES
Collagen alpha-1 (VI) chain precursor	13878903	10	YES
Fibulin-1 precursor	30581038	7	YES
Galectin 3 binding protein	5031863	9	YES
Fibronectin 1	34364820	49	YES
Immunoglobulin superfamily containing leucine	5031809	1	YES
Laminin, alpha 4 precursor	4504949	8	YES
Laminin, beta 1 precursor	4504951	10	YES
Laminin gamma-1 chain precursor	126369	11	YES
Migration stimulation factor	27227743	8	YES
Thrombospondin 1 precursor	40317626	6	YES
Thrombospondin 2 precursor	549136	4	YES
Complement regulator/immune response			
Clusterin precursor	116533	5	YES
Complement C1r component precursor	115204	4	YES
Complement C1s	6407558	3	YES
Complement C4-B	81175167	3	YES
Complement component 1 inhibitor precursor	15029894	7	YES
Complement factor B precursor	584908	4	YES
Complement factor H precursor	85681919	3	YES
Neuroleukin	189238	4	NO
Pentraxin- related gene	4506333	4	YES
Protease / protease inhibitor			
Carboxypeptidase A4	61743916	11	YES
Caspase 5	4757914	1	NO
Glia-derived nexin precursor	183064	6	YES
Matrix metalloproteinase 2 Preproprotein	11342666	2	YES
Plasminogen activator inhibitor type 1	24307907	8	YES

Procollagen C-endopeptidase enhancer	4505643	2	YES
The Mmp-inhibitory	6730224	2	YES
Catabolism			
Aldolase A	229674	5	NO
Alpha enolase	2661039	13	YES
Protein disulfide-isomerase	2135267	3	YES
Similar to triosephosphate isomerase 1	16877874	6	NO
Transketolase	4507521	1	NO
Cell organization and biogenesis			
ACTN4 protein	33874637	7	NO
Ezrin	119717	2	NO
Gelsolin isoform a	4504165	4	YES
Insulin-like growth factor binding protein 3	62243068	1	YES
Insulin-like growth factor binding protein 7	4504619	3	YES
Quiescin Q6	13325075	5	YES
TUBA6 protein	21619816	1	NO
Development			
Annexin 5	4502107	1	NO
Decorin isoform a preproprotein	4503271	2	YES
Decorin isoform b precursor	19743848	2	YES
Glutathione tranferase	4504183	2	NO
Pigment epithelium-derived factor	1144299	10	YES
Secreted protein, acidic, cysteine-rich	4507171	7	YES
Other functions			
14-3-3 gamma protein	5726310	2	NO
Alpha actinin	28723	11	NO
Alpha-fetoprotein precursor	4501989	3	YES
Beta-trace	410564	1	NO
CALU	49456627	12	YES
Extracellular matrix protein 1 isoform 1 precursor	4758236	2	YES
Follistatin-like 1 precursor	5901956	3	YES
Lumican	4505047	8	YES
Moesin/anaplastin lymphoma kinase fusion protein	14625824	2	NO
Mutant beta-actin	28336	8	NO
Nucleobindin 1 precursor	2506255	1	YES
Phosphoglycerate mutase processed protein	20530939	3	NO
Phosphopyruvate hydratase (Beta-enolase)	105934	3	NO
Muscle specific enolase	31167	3	NO
PRO1708	7959791	1	NO
Prostaglandin D2 synthase	32171249	2	YES
Tarsh protein	33667044	4	YES
Tyrosine 3-monooxygenase	30584583	1	NO

This was further confirmed by the MS/MS analysis of both labeled and unlabeled peptides (Figures 2.3B and 2.3C). Peaks representing the “y” ion series were all shifted by 8 Da in the MS/MS spectrum of the labeled peptide (Figure 2.3C) versus those of the unlabeled peptide (Figure 2.3B), whereas the “b” ion series remained unchanged.

2.4.4 Secreted Protein Profiling in RPE Cells Prepared from AMD and Normal Age-Matched Healthy Donors

To measure secreted protein levels in RPE cells from AMD versus normal donors, we analyzed 1:1 protein mixtures of conditioned media from fully labeled TT-RPE (wild-type control) cell cultures and from each of the unlabeled CT-RPE or CC-RPE cell cultures prepared from AMD donors with the homozygous rare and heterozygous Y402H-CFH genotypes, respectively. A control unlabeled TT-RPE was prepared from a different control donor and compared to the labeled TT-RPE. Because of the sequence homology between some human and bovine proteins, only peptide sequences unique to human proteins were used to determine protein ratios. Figure 2.4 shows an example for PEDF protein (87.5% sequence homology between human and bovine) where the ratio between labeled and unlabeled peptides is skewed when the same peptide sequence is shared between human and bovine proteins. Although the cells were carefully washed with PBS before incubation in serum-free media, there were still some bovine proteins present in the conditioned media. Because it is not possible to control the level of bovine protein contamination between samples, we decided to use only peptide sequences that are unique to human proteins for further analysis. Labeled and unlabeled peptide pairs unique to human proteins were thus detected, and their ratios were measured using ZoomQuant software.

The ZoomQuant script, which was previously designed to quantify peptide ratios generated from an ^{18}O proteolytic experiment[132], was slightly modified in the present study to accommodate data generated from a SILAC experiment using $^{13}C_6$-Arg and $^{13}C_6$, $^{15}N_2$-Lys as the labeling amino acids. Table 2.2 summarizes some of the secreted proteins for which ratios between normal and AMD RPE cells were obtained. In general, these ratios were close to 1 (mean average ratio = 1.26 ± 0.3) for most of the proteins when labeled TT-RPE cells (healthy control) were compared to unlabeled TT-RPE cells prepared from another healthy control donor. However, some of these same proteins were found differentially expressed when RPE cells of healthy controls with the wild-type genotype (TT-RPE) were compared to RPE cells of AMD donors with the heterozygous (CT-RPE) or homozygous rare (CC-RPE) Y402H-CFH genotype. Overall, CT-RPE and CC-RPE secreted at least 2-fold more clusterin, fibronectin, galectin 3 binding protein, lumican, PEDF, MMP2, tissue inhibitor for metalloproteinase-1 (TIMP-1), and complements C1r component (C1R) and complement C1s component (C1S) than the TT-RPE cells prepared from age-matched healthy donors. SPARC was found to be down regulated by almost 2-fold in AMD RPE cells when compared to healthy RPE cells. We used 1.6 as a significant cut off for fold change based on the mean average value obtained between two RPE cell cultures derived from two healthy donors (mean average ratio = 1.26 ± 0.3).

Figure 2.3 LTQ MS and MS/MS spectra of labeled and unlabeled peptide pairs of PEDF

(A) Top spectrum shows the zoom scan MS of labeled and unlabeled peptide pairs (m/z 607.66 and 611.66). These peaks correspond to a doubly charged ion species. Because the difference in m/z between labeled and unlabeled peptides is 4, this suggests that the peptide should contain a K (Lys) residue. Bottom two spectrums show MS/MS of both unlabeled peptide at m/z 607.66 (B) and labeled peptide at m/z 611.66 (C). The series of y ions are all shifted by 8 Da in the labeled versus unlabeled peptide, confirming the peptide sequence [ELLDTVTAPQK] for human PEDF.

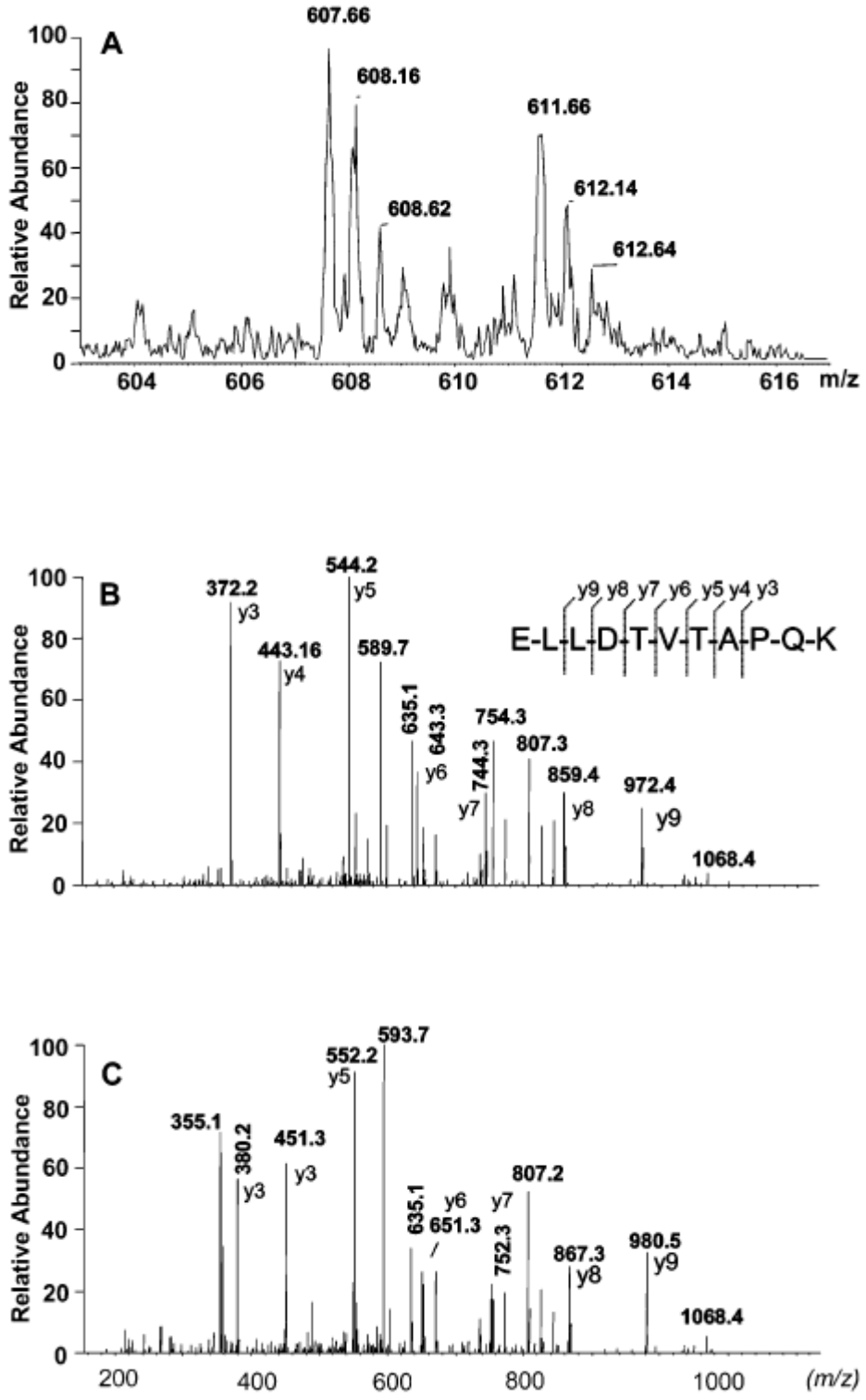
A
607.66
608.16
611.66
608.62
612.14
612.64
Relative Abundance
m/z
B
372.2
y3
544.2
y5
443.16
y4
589.7
635.1
643.3
y6
754.3
744.3
y7
807.3
859.4
y8
972.4
y9
1068.4
y9 y8 y7 y6 y5 y4 y3
E-L-L-D-T-V-T-A-P-Q-K
Relative Abundance
C
593.7
552.2
y5
355.1
380.2
y3
451.3
y3
807.2
635.1
y6
y7
651.3
752.3
867.3
y8
980.5
y9
1068.4
Relative Abundance
(m/z)

Figure 2.4 Zoom MS scans of two peptides for PEDF

The peptide on the top (LAAAVSNFGYDLYR) was found in both bovine and human PEDF whereas the peptide on the right (ELLDTVTAPQK) was unique to human PEDF. The ratio of the intensity of labeled to unlabeled peptides was decreased for the peptide in the left due the remaining bovine unlabeled PEDF present in the RPE conditioned medium.

LAAAVSNFGYDLYR

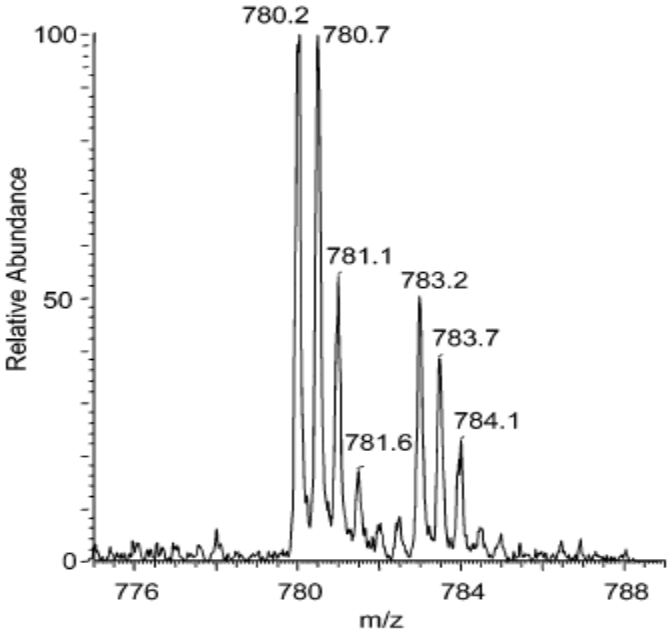

ELLDTVTAPQK

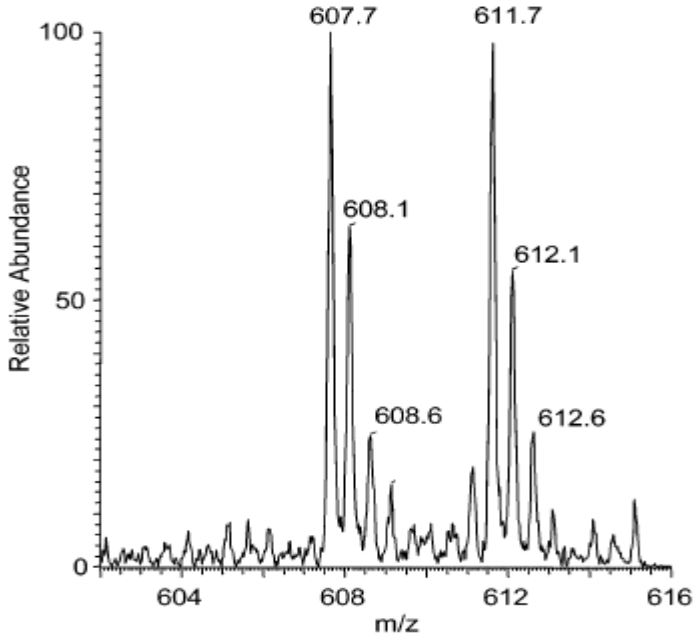

Table 2.2 Differential expression in AMD and age matched healthy donors

(Unlabeled control vs. labeled healthy donors) [a] Ratios were determined between labeled and unlabeled peptide pairs and the standard deviation was obtained based on the number of detected peptides per protein; these are included between parentheses. ND: not determined; TT: RPE cells from healthy control donors with the wild-type CFH genotype; CT: RPE cells from AMD donors with the heterozygous Y402H-CFH genotype; CC: RPE cells from AMD donors with the homozygous rare Y402H-CFH genotype.

Protein Name	Accession Number	Secretion	Ratio (Scan Numbers) [a] TT/TT	CT/TT	CC/TT
Cell adhesion / connective tissue protein					
Collagen alpha 1(I) precursor	115269	YES	1.51 ± 0.23 (09)	1.20 ± 0.37 (04)	1.56 ± 0.15 (06)
Collagen alpha 1(III) precursor	4502951	YES	0.98 ± 0.15 (22)	0.84 ± 0.08 (10)	1.51 ± 0.23 (27)
Collagen alpha 2(I) precursor	82654930	YES	1.53 ± 0.30 (10)	1.21 ± 0.10 (03)	1.71 ± 0.17 (16)
Galectin 3 binding protein	5031863	YES	1.05 ± 0.02 (02)	1.63 ± 0.15 (03)	2.22 ± 0.27 (11)
Fibronectin 1	34364820	YES	1.39 ± 0.17 (16)	2.02 ± 0.23 (13)	2.72 ± 0.35 (58)
Lumican	4505047	YES	1.58 ± 0.00 (01)	ND	3.45 ± 0.55 (04)
Migration stimulation factor	27227743	YES	1.36 ± 0.00 (01)	2.10 ± 0.09 (03)	2.71 ± 0.26 (05)
Complement regulator/immune response					
Clusterin precursor	116533	YES	0.92 ± 0.00 (01)	2.34 ± 0.30 (03)	3.23 ± 0.28 (02)
Complement C1r component precursor	115204	YES	ND	1.79 ± 0.00 (01)	2.20 ± 0.12 (02)
Complement C1s	6407558	YES	ND	1.61 ± 0.00 (01)	1.99 ± 0.27 (02)
Complement component 1 inhibitor precursor	15029894	YES	0.92 ± 0.00 (01)	1.54 ± 0.17 (02)	1.60 ± 0.20 (06)
Complement factor B precursor	584908	YES	NA	1.14 ± 0.00 (01)	1.54 ± 0.00 (01)
Complement factor H precursor	85681919	YES	2.16 ± 0.00 (01)	1.84 ± 0.38 (02)	3.29 ± 0.02 (02)
Protease / protease inhibitor					
Carboxypeptidase A4	61743916	YES	1.33 ± 0.00 (01)	0.98 ± 0.00 (01)	1.76 ± 0.31 (06)
Matrix metalloproteinase 2 preproprotein	11342666	YES	1.49 ± 0.00 (01)	ND	3.39 ± 0.47 (03)
Tissue Inhibitor of Metalloproteinase-1	6730224	YES	1.05 ± 0.18 (02)	1.25 ± 0.04 (02)	2.37 ± 0.12 (03)
Development					
Pigment epithelium-derived factor	1144299	YES	1.36 ± 0.00 (01)	2.14 ± 0.00 (01)	2.75 ± 0.10 (03)
Screted Protein, Acidic, Cystein-rich (Osteonectin)	4507171	YES	1.23 ± 0.06 (03)	0.59 ± 0.14 (02)	7.35 ± 0.00 (01)
Other functions					
Extracellular matrix protein 1 isoform 1 precursor	4758236	YES	ND	2.77 ± 0.00 (01)	ND

We further analyzed mRNA levels of this same set of differentially expressed proteins using a larger sample size of RPE cell cultures prepared from AMD donors with the homozygous rare (n = 3) and the heterozygous (n = 3) Y402H CFH genotype and from age-matched healthy donors (n = 4). The mRNA level for all the selected proteins remained unchanged between AMD RPE cells (CT-RPE and CC-RPE) and healthy TT-RPE cells except for clusterin, whose mRNA levels seem to reflect the trend observed at the protein level (Figure 2.5). The general poor correlation between mRNA and protein levels was previously reported in several systems[122,135,136] and might be due to differences in half-lives between mRNA and proteins.

2.4.5 Network Analysis

To analyze the overlapping network function between all the secreted proteins whose levels were found altered in AMD RPE cells versus normal RPE cells, we uploaded the set of proteins from Table 2.2 with their accession numbers and expression levels into the Ingenuity pathway analysis software. An overlapping network with a score of 35 (i.e., score > 2 is significant; it represents the log of the probability that the overlapping network was found by random chance) was obtained for 16 of the 19 uploaded proteins (Figure 2.6). Among the 19 uploaded proteins, 17 are known to be extracellular proteins whereas 2 (fibronectin and galectin 3 binding protein) are plasma membrane surface proteins, though these two proteins are also noted as secreted proteins in the SwissProt database. Upon examination, the most relevant function extracted from this overlapping network was related to tissue development and angiogenesis and included 9 proteins out of the 19 uploaded. Fibronectin, MMP2, PEDF, and SPARC were all found to be involved in the

remodeling of the ECM as well as regulating angiogenesis. Other proteins such as clusterin, BF, CFH, and C1R and C1S are involved in immunological as well as inflammatory diseases, whereas lumican, galectin 3 binding protein, and fibronectin proteins were found to be involved in cell adhesion and cellular matrix build up. Most of these secreted proteins were found to directly interact with each other such as MMP2 and its inhibitor Tissue inhibitor of metalloprotease (TIMP). Thus, the balance in the relative quantities of these proteins in the extracellular space might be crucial for maintaining tissue homeostasis at the interface between RPE and Bruch's membrane.

Figure 2.5 Differential expression of clusterin in RPE cell cultures prepared from AMD donors with the homozygous rare (CC) and heterozygous (CT) Y402-CFH genotype versus RPE cells prepared from age-matched healthy donors with the wild-type CFH genotype (TT)

The ratios are all normalized to a healthy RPE culture with the wild-type CFH genotype (TT). The top graph is for mRNA profiling and the measurements represent the average values obtained for 4 TT-RPE, 3 CT-RPE, and 3 CC-RPE cultures. The bottom graph is for ratios obtained at the protein level between pairwise comparisons of a CT-RPE, CC-RPE, and TT-RPE culture to another TT-RPE culture.

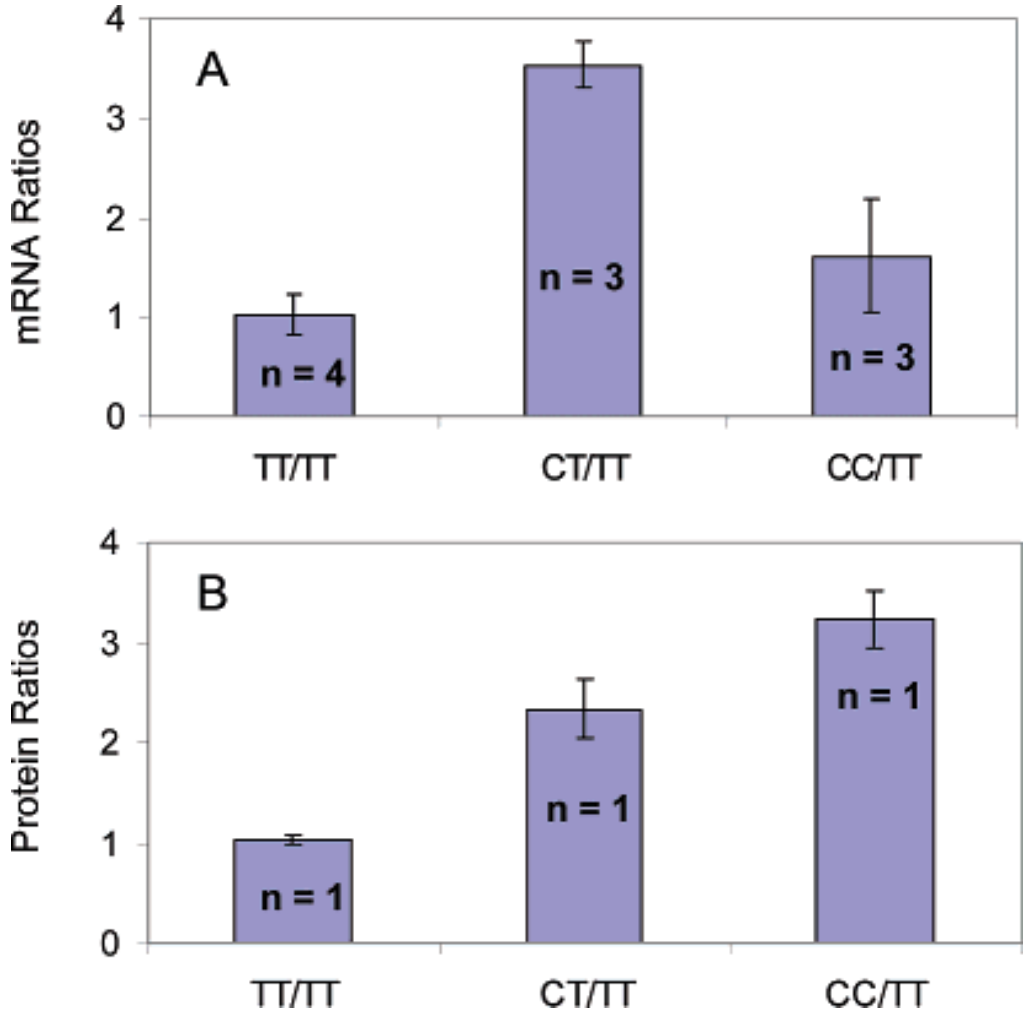
A
mRNA Ratios
4
3
2
1
0
n = 4
n = 3
n = 3
TT/TT
CT/TT
CC/TT
B
Protein Ratios
4
3
2
1
0
n = 1
n = 1
n = 1
TT/TT
CT/TT
CC/TT

Figure 2.6 Ingenuity pathway network of differentially secreted proteins detected in RPE cells derived from an AMD donor (with macular deposits and the homozygous rare Y402H-CFH genotype) versus RPE cells derived from an age-matched healthy donor (see data from Table 2.2)

Proteins with their gi number and corresponding fold change between the two cell cultures were uploaded into Ingenuity pathway analysis software (http://www.ingenuity.com). Proteins with a gray background were detected in the RPE conditioned media while other interacting proteins with a clear background were not detected in the conditioned media. BF: Complement Factor B, C1R: Complement C1r component precursor, C1S: Complement C1s, CFH: Complement Factor H, CLU: Clusterin, COL1A1: Collagen alpha 1(I) precursor, COL1A2: Collagen alpha 2(I) precursor, COL3A1: Collagen alpha 1(III) precursor, ECM1: Extracellular matrix protein 1 isoform 1 precursor, FN1: Hypothetical protein (Fibronectin 1), IGFBP5: Insulin-like growth factor binding protein 5, LGALS3BP: Galectin 3 binding protein, LUM: Lumican, MMP2: Matrix metalloproteinase 2 preproprotein, SERPINF1: Pigment epithelium-derived factor, SERPING1: Complement component 1 inhibitor precursor, SERPINH1: heat shock protein 47, SPARC: Secreted protein, acidic, cysteinerich, TIMP1: The Mmp-inhibitory, TNF: Tumor Necrosis Factor, VEGF: Vascular Endothelial Growth Factor, VTN: Vitronectin. The major interactions found between these proteins are indicated by different arrows.

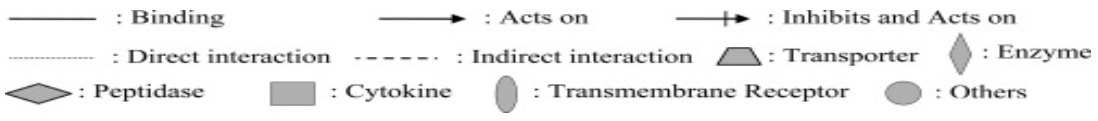

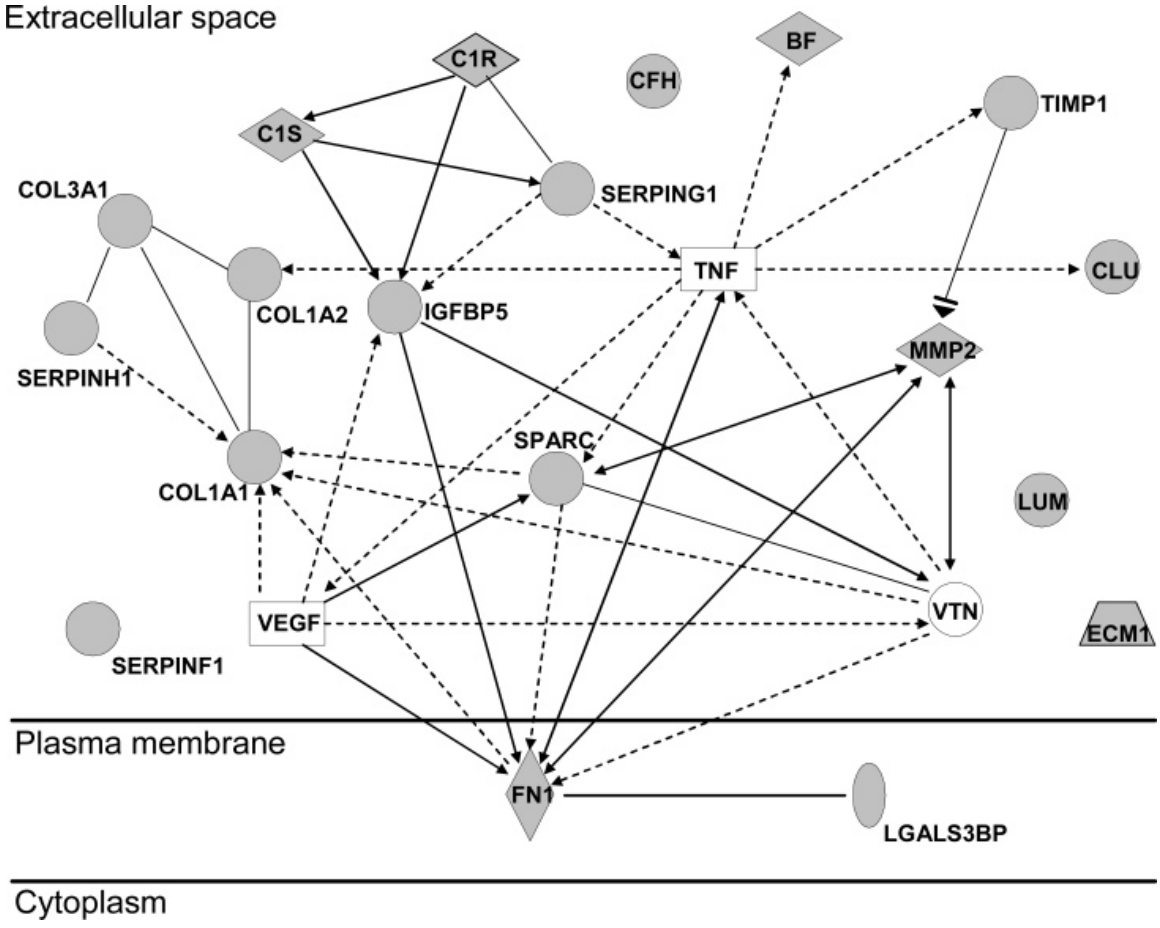
Extracellular space
C1R
BF
CFH
TIMP1
C1S
SERPING1
COL3A1
TNF
CLU
COL1A2
IGFBP5
SERPINH1
MMP2
SPARC
COL1A1
LUM
VTN
VEGF
ECM1
SERPINF1
Plasma membrane
FN1
LGALS3BP
Cytoplasm

2.5 Discussion

It has long been hypothesized that RPE cells might be involved in the biogenesis and formation of drusen[88]; however, only few studies have actually examined the direct relationship between RPE cells and drusen formation[93,137,138] using Quantitative real-time PCR (qRT-PCR) or immunostaining for the relevant proteins. In the present study, we investigated secreted proteins, the "secretome", of RPE cells using a SILAC-based strategy and examined their levels in AMD versus normal cells. In general, RPE cells were found to secrete a variety of connective tissue proteins, extracellular matrix proteins, complement factors, proteases, as well as protease inhibitors. Among the 73 proteins detected in the conditioned media, 53 were found to have a signal peptide for secretion according to the Swiss-Prot/ Translations of European Molecular Biology Laboratory (TrEMBL) database and/or by using the SignalP 3.0 predictor software http://www.cbs.dtu.dk/services/SignalP). The remaining 19 proteins corresponded to nonsecreted proteins, and this could have been the result of protein leakage or exocytosis vesicles in the conditioned media. Most importantly, some of the secreted proteins such as fibronectin, clusterin, complement factors, TIMP, and annexins are major components of drusen [35,81,139], and these were readily secreted by RPE cells. These findings clearly support the overall hypothesis that RPE cells might be directly involved in drusen formation. To our knowledge, this is the first evidence that RPE cells make and secrete their own CFH, the protein containing the Y402H variant that is strongly associated with the risk of developing AMD[33-36]. This local secretion of CFH by RPE cells could be highly relevant to AMD pathology. Indeed, CFH plays a critical role in protecting cells from complement attack as well as decreasing and limiting immune complex deposition as demonstrated in glomeruli of CFH-deficient

mice[128] which develop a renal disease that clinically resembles AMD. We hypothesize that the Y402H-CFH variant synthesized by RPE cells from AMD donors is dysfunctional and unable to efficiently clear the debris that accumulates between the basal lamina of RPE cells and Bruch's membrane to form drusen deposits. Unfortunately, because of the low abundance of this protein in the conditioned media, only 3 peptides were detected in this study, which did not allow for us to analyze whether the protein was mutated at position 402 in the RPE cells prepared from AMD donors with the homozygous Y402 CFH genotype. Further investigation using more samples is needed to obtain better sequence coverage for this protein and to determine its primary structure and potential activity.

The elevated secretion of clusterin seen in AMD versus normal RPE cells was significant both at the mRNA and protein levels. The exact function of clusterin is not well understood, but it is implicated in several functions such as response to cellular injury, lipid transport, apoptosis, and clearance of cellular debris caused by cell injury or death[140]. Recent reports show that clusterin is a major constituent of drusen collected from AMD donors and could be directly involved in their formation[81,84]. This protein was described to have a promiscuous binding property thus, it has been suggested that its accumulation at the RPE-Bruch's membrane inter-space could attract a myriad of molecules resulting in a nucleation site for drusen biogenesis[84]. More interestingly, clusterin was found to promote amyloid plaque formation in a mouse model of Alzheimer's disease[141] and drusen-like Alzheimer's aggregates do contain a large amount of α-amyloids[142,143], thus the elevated secretion of clusterin seen in the AMD donors could be directly involved in drusen biogenesis. Another interesting hypothesis that could directly link clusterin to immune complex mediated drusen formation is that clusterin functions as a complement regulatory

protein[144]. The increased secretion of clusterin by RPE cells of AMD donors could be a compensatory effect to correct for the low activity of the Y402H-CFH rare variant protein and this may result in even more debris accumulation given that clusterin attracts a variety of proteins. Overall, AMD RPE cells secreted more complement and complement factors than healthy RPE cells and this is in agreement with the large amount of complement detected in drusen[35].

Conversely, the 3-fold increase in MMP-2 secretion seen in AMD RPE cells versus healthy RPE cells correlates with previous studies, which showed that interphotoreceptor matrix, that is a unique ECM between photoreceptor and RPE, collected from AMD donor eyes contained 2-fold more MMP-2 than those collected from age-matched healthy control donor eyes[145]. Despite the fact that MMPs are not detected in drusen [146], their role in AMD pathology might reside in their indirect involvement in angiogenesis via their proteolytic activity and remodeling of the extracellular matrix[147]. Indeed, using a knockout mouse model, it has been shown that MMP-2 and MMP-9 deficient mice were more protected against laser induced CNV than wild-type mice expressing MMPs[147]. Thus, increased secretion of MMPs in the RPE cells of AMD donors could contribute to the risk of developing CNV. Nevertheless, this protein is tightly controlled by TIMP, which also showed a 2-fold increase in expression in AMD RPE cells versus healthy RPE cells. The ratio between MMP and TIMP might be involved in the regulation of angiogenesis. Unfortunately, we were not able to detect all isoforms of MMPs and their corresponding TIMPs to establish this overall balance in the conditioned media of AMD RPE cells versus healthy RPE cells. Angiogenesis is a complex tissue development event and involves several regulatory factors that need to be comprehensively measured and tested.

SPARC is another protein found in the conditioned media of RPE cells and might also be involved in angiogenesis. Because of the high homology found between human and bovine SPARC protein (i.e., 98.7% sequence homology) we could not detect any peptides that were unique to human SPARC to obtain more accurate protein ratios. Thus, all detected peptides for SPARC were used as an average to estimate the ratio for this protein across all samples (only peptides that were consistently detected across all the samples were used to estimate this ratio). Overall, SPARC protein expression was found to be down regulated in AMD RPE cells versus healthy RPE cells by 2- fold. SPARC, also known as osteonectin, has anti-adhesive properties and was recently reported to play a key role in the regulation of attachment-detachment of the RPE monolayer to Bruch's membrane [148]. Importantly, the decreased expression of SPARC in AMD donors could favor angiogenesis as this protein was found to have a potent inhibitory effect on angiogenesis[149,150]. Additionally, SPARC can also stimulate angiogenesis after proteolytic cleavage by MMPs[151,152]. Thus, the 3-fold increase in expression of MMP-2 in RPE cells of AMD versus healthy donors would favor angiogenesis by decreasing the amount of SPARC in the extracellular space while producing potent angiogenic SPARC peptides. This could explain the protective effect against laser-induced CNV seen in MMP-2 and MMP-9 deficient mice[147].

PEDF is another potent inhibitor of angiogenesis in the mammalian ocular compartment[153]. Surprisingly, the RPE prepared from AMD donors secreted more PEDF than the RPE from healthy controls. A slight increase was also observed at the mRNA level for RPE cells prepared from AMD donors with heterozygous CFH genotype (n = 3) versus RPE cells prepared from age-matched healthy controls (n = 4) (data not shown). This

intriguing increase in PEDF secretion (inhibitor of angiogenesis) in AMD cells was also reported by others in CNV-derived RPE cells[154] and could be the result of a compensatory effect to balance the angiogenic activity of VEGF, which might be present in the retinal extracellular environment. Indeed, angiogenesis is tightly controlled by the balance between PEDF and VEGF[155]. Unfortunately, we did not detect VEGF in this study and thus we could not determine the ratio between PEDF and VEGF. More specific experimental approaches might be needed to assess the overall amount of angiogenesis regulating factors in the conditioned media of RPE cells prepared from AMD and normal donors.

Other secreted proteins that were found to be increased in AMD RPE cells versus healthy RPE cells included galectin-3 binding protein, fibronectin, and lumican. Fibronectin and galectin-3 binding protein are known to promote integrin-mediated cell adhesion while lumican acts like collagen to form the extracellular matrix. The role of these proteins in AMD pathology and drusen biogenesis is not well understood. Nevertheless, fibronectin was previously reported to be more abundant in soft drusen, which are the hallmark of AMD pathology, than in nodular small drusen which are more ubiquitous retinal deposits[156,157]. Additionally, galectin-3 binding protein, also known as Human Mac-2 binding protein, was found to bind to a variety of extracellular proteins including fibronectin itself[158], and it may therefore be relevant to analyze drusen for the presence of galectin 3 binding protein in drusen in future investigations.

2.6 Conclusion

The survey of secreted proteins in RPE cells was greatly facilitated by the use of the SILAC strategy. Because secreted proteins are labeled with heavy stable isotope amino acids, they can be easily distinguished from bovine serum contaminants that may be present in the conditioned media. In our case, even after washing the cells twice with PBS before incubation in serum free media, we still detected several bovine serum proteins. Using this strategy in combination with SDS-PAGE, LC-MS/ MS, and ZoomQuant analysis, several specific RPE secreted proteins were identified, and their level of expression was determined between cells prepared from AMD donors and cells prepared from age-matched healthy control donors. Secreted proteins have many important cellular functions, and their global analysis (secretomics) could bring insight into their role in pathological conditions such as AMD as well as other diseases involving angiogenesis and protein aggregation. Although these are ex vitro studies, the generated data could be used to select important proteins and follow their occurrence and activity *in vivo*.

2.7 Acknowledgment

This work was supported by a philanthropic donation to Dr. Hathout and by the Parson's Foundation. Financial support to Dr. Karl Csaky was provided by the The National Institutes of Health (NIH)/ the National Eye Institute (NEI) intramural program. Eunkyung An thanks the Institute for Biomedical Sciences of George Washington University for their financial support. Eunkyung An is a predoctoral student in the Biochemistry and Molecular Genetics Program of the Institute for Biomedical Sciences at the George Washington University. This work is from a dissertation to be presented to the above program in partial fulfillment of the requirements for the Ph.D. degree. We also thank Dr. Kanneboyina Nagaraju for his advice and helpful discussion and Ms Stephanie Mitchell and Catherine Formolo for their help with manuscript editing.

Chapter 3: Effect of TNF-α on Human ARPE-19 Secreted Proteins

TNF- α was suggested to play an important role in regulation of differentially secreted proteins between RPE cells from AMD donor and normal donor in Chapter 2, and this supports role inflammation in AMD pathogenesis which has been suggested by other scientists. In this study, I used ARPE-19 cell as a model to see the effect of a non-lethal dose of TNF-α on RPE secretome which helps us understand AMD pathogenesis.

This chapter was published in Molecular Vision in 2008.
Molecular Vision **14**, 2292-303 (2008).

Eunkyung An[1,2], Heather Gordish-Dressman[1], Yetrib Hathout[1]

1. Research Center for Genetic Medicine, Children's National Medical Center, Washington, DC.

2. Program in Biochemistry and Molecular Genetics, Institute for Biomedical Sciences, The George Washington University, Washington, DC.

Correspondence should be addressed to:

Yetrib Hathout
Research Center for Genetic Medicine
Children's National Medical Center
111 Michigan Ave NW
Washington, DC 20010
yhathout@cnmcresearch.org
Telephone number: (202) 476-3136
Fax number: (202) 476-6014

3.1 Abstract

Purpose: To identify cytokine-induced changes in the secretome of human retinal pigment epithelial (RPE) cells and their potential implication in age-related macular degeneration pathogenesis.

Methods: Stable isotope labeling by amino in cell culture (SILAC) was used in combination with LC-MS/MS to measure differential protein secretion from tumor necrosis factor-α (TNF-α) treated ARPE-19 versus untreated ARPE-19 cells. Typically, one set of cells was subcultured in a medium in which Arg and Lys were replaced by $^{13}C_6$-Arg and $^{13}C_6$, $^{15}N_2$ -Lys while the other set of cells was grown in unlabeled medium. The fully labeled cells were then treated with TNF-α, while unlabeled cells were left untreated. Conditioned media from both treated and untreated cells were collected, mixed at 1:1 ratio, and processed for LC-MS/MS analysis. Labeled and unlabeled peptide pairs were identified and their intensities were used to determine protein ratios in TNF-α treated cells versus untreated cells. To validate the data, we performed a reverse experiment in which unlabeled cells were treated with TNF-α while labeled cells were kept untreated.

Results: A total of 146 proteins were identified as putatively secreted proteins in the conditioned medium of ARPE-19 cells and only six among these were differentially secreted following TNF-α treatment. Secretion of complement 3 and sulfhydryl oxidase-1 was increased by twofold, fibronectin by 1.7 fold, plasminogen activator inhibitor 1 by 1.9 fold and syndecan-4 by 4.35 fold while secretion of *trans*-Golgi network protein-2 was decreased by twofold.

Conclusions: TNF-α modulates secretion of specific proteins in ARPE-19 cells. These proteins are involved in pathways relevant to AMD pathogenesis (e.g., ECM remodeling, complement pathway, and angiogenesis).

3.2 Introduction

Age-related macular degeneration (AMD) is a leading cause of blindness in elderly individuals[7]. AMD is characterized by extracellular deposits (e.g., drusen) that accumulate beneath the RPE and along Bruch's membrane[78,123,124]. Previous studies have established a strong association between the Tyr402His variant in CFH (Y402H CFH) and the risk of developing AMD[33-36]. More recently, a variant in the promoter region of the gene encoding for the serine protease HTRA1 was found to be a second major risk factor for AMD [52,53,159]. However, the mechanisms by which these single point mutations contribute to AMD pathogenesis (e.g., drusen accumulation and CNV) are still not well understood. RPE cells have long been suspected to be a source for at least some of the material that accumulates in drusen[78,160]. Our study of the secretome of human primary RPE cultures clearly demonstrated that these cells can express and secrete several proteins found in drusen including CFH and complement components[161]. RPE are highly specialized epithelial cells that maintain integrity of the blood-retina barrier while performing vital functions such as phagocytosis of the outer segment of photoreceptor cells, recycling of visual pigment, and transport of nutrients to the photoreceptors[162]. Hence, RPE cells are continuously exposed to oxidative stress and proinflammatory stimuli that may disrupt their extracellular environment and challenge their local homeostasis. The presence of few small drusen in the macula of individuals over age 40 is normal and usually not harmful.

However, an increase in number and size of these deposits is a strong indication of a progressive AMD. Previous studies have shown that drusen attract macrophages to the sub-RPE space[157,163]. Activated macrophages are known to produce tumor necrosis

factor-α (TNF-α), a pleotropic cytokine, which has been shown to stimulate production of monocyte chemotactic protein (MCP-1) by RPE cells thus recruiting more macrophages to the vicinity of the sub-RPE space[164,165]. Chronic exposure of RPE cells to cytokine may alter their protein secretion pattern and increase the risk of complex deposition. However, RPE cells express both soluble and cell surface cytokine receptors as well as a variety of other factors, thus giving them some degree of control to modulate the effect of cytokines[166]. This regulation of the extracellular environment may be compromised in RPE cells carrying AMD genetic risk variants (e.g., the Y402H CFH and the HTRA1 promoter polymorphisms), leading to an accumulation of extracellular deposits. In this preliminary study we decided to examine the overall effect of TNF-α on the regulation of protein secretion by RPE cells and bring insight into cytokine-induced alterations and their role in AMD pathogenesis. We used ARPE-19 (A human retinal pigment epithelial cell line) as a model to optimize the conditions for future studies using human primary RPE cell culture. SILAC is a simple and accurate strategy for proteome profiling in cell culture systems[110]. Basically, one set of cells is grown in a medium where some of the amino acids, usually Arg as well as Lys, are labeled with stable isotopes (e.g., ^{13}Carbon (C) and/or ^{15}Nitrogen (N)), while the comparative sample is grown in medium containing unlabeled amino acids. This approach is the most systematic way to uniformly label all the proteins within the cell and obtain accurate protein ratios between two samples. Indeed, variations usually due to experimental handling are minimized in this case since labeled and unlabeled cells can be mixed before subcellular fractionation and protein extraction. For these reasons, the method has gained tremendous popularity and has been successfully implemented to study cell signaling[120,167-169], phosphoproteomics[119,170,171],

and cell-secreted proteins[122,161,172]. In this study, we implemented the SILAC strategy to define differential protein secretion in ARPE-19 exposed to a non-lethal dose of TNF-α. Analysis of these proteins should bring insight into the response of RPE cells to cytokines and eventual implication in AMD pathogenesis.

3.3 Methods

3.3.1 SILAC and TNF-α treatment

ARPE-19 was purchased from the American Type Culture Collection (ATCC; Manassas, VA). The cells were routinely maintained in DMEM/ F12 containing 10% FBS (ATCC), 100 U/ml of penicillin, 100 μg/ml of streptomycin (Invitrogen, Gibco, Carlsbad, CA), and 1 mM of sodium pyruvate (Sigma Aldrich, St. Louis, MO). To study the effect of TNF-α on ARPE-19 secreted proteins, we performed differential SILAC and used mass spectroscopy to measure the ratios of individual secreted proteins in TNF-α treated ARPE-19 and untreated ARPE-19 cells (Figure 3.1). One set of ARPE-19 cells were subcultured in DMEM/ F12 (Atlanta Biologicals, Lawrenceville, GA) custom-made medium where Arg and Lys were replaced by $^{13}C_6$-Arg and $^{13}C_6$, $^{15}N_2$ -Lys. After at least 12 cell doublings (roughly four passages), cellular proteins were uniformly labeled with these stable isotope-containing amino acids. In parallel, the same numbers of cells were grown in DMEM/F12 unlabeled medium. Ten days after confluence, both labeled and unlabeled cells were washed 6 times with sterile PBS (Invitrogen, Carlsbad, CA) before incubating them in serum-free medium containing stable isotope-labeled amino acids for labeled cells and regular amino acids for unlabeled cells. The metabolically labeled cells were treated with 10 ng/ml TNF-α (a nonlethal dose), while unlabeled cells were kept untreated. After 24 h incubation, conditioned media of both treated and untreated cells were collected, mixed at 1:1 ratio and analyzed, as described below. To validate the data, we performed a reverse experiment in which unlabeled cells were treated with TNF-α while labeled cells were kept untreated.

3.3.2 Analysis of ARPE-19-secreted proteins

Conditioned media from TNF-α-treated and untreated ARPE-19 cells were collected and filtered through 0.2 μm polyethersulfone syringe filter (Corning Inc., Corning, NY) to remove floating cells and debris. Filtered media from treated and untreated cells were then mixed at 1:1 ratio (v/v) and concentrated to dryness using centrifugal filtration (Millipore Corporation, Billerica, MA) followed by vacuum centrifugation. The resultant residue was then dissolved in 6 μl of Laemmli buffer containing 50 mM Dithiothreitol (DTT) and further fractionated by SDS–PAGE using 10% Tris HCl pre-cast criterion gels (Bio-Rad, Hercules, CA). The gel was then stained with Bio-Safe Coommassie (Bio-Rad) and each lane was excised into 36 to 43 bands. Each band was then in-gel digested using trypsin (Promega, Madison, WI), and the resultant peptides were extracted and analyzed by nano-LC MS/ MS, as described in the next section.

3.3.3 Preparation of microsomal fraction

After collection of conditioned media, treated and untreated cells were washed with PBS, dissociated in 0.05% trypsin-Ethylenediaminetetraacetic acid (EDTA) solution (Invitrogen) and transferred into previously weighed Eppendorf tube. Cells were pelleted by centrifugation at 300x g then washed with 2 volumes of PBS solution and 100 mM NaCl. Treated and untreated cells were then mixed at 1:1 ratio (w/w) and resuspended in 1.5 ml of Tris-EDTA mix buffer that contained 10 mM Tris HCl pH 7.4, 1 mM EDTA, 2.5 M sucrose (Sigma Aldrich), and 1 protease inhibitor tablet (Pierce, Rockford, IL) per 10

ml. The cells were then mechanically lysed by passing them 15 times through a 1 ml syringe with a 23 gauge needle. The cell lysis was pelleted by centrifugation for 10 min at 4,000x g at 4 °C, and the supernatant containing the microsomal fraction was transferred to a clean 1.5 ml Eppendorf tube and further centrifuged at 13,000x g for 20 min to obtain the microsomal pellet. The microsomal pellet was then resuspended in protein extraction buffer containing 7 M urea, 2 M thiourea, 2% 3-[(3-cholamidopropyl)dimethylammonio]-1-propanesulfonate (CHAPS) (w/v), and 50 mM DTT. Protein concentration of each fraction was determined by Bio-Rad protein assay (Bio-Rad). Aliquots of 50 μg were separated on SDS–PAGE. Gel bands were excised, digested with trypsin, and the resultant peptides analyzed by LC-MS/MS as described in the next section.

3.3.4 Nanoflow LC-MS/MS

Nano-LC tandem mass spectrometry was performed on an LC-packing system (Dionex Ultimate Capillary/Nano LC system, Dionex Corp., Sunnyvale, CA) connected to a LTQ instrument (Thermo Fisher Scientific, San Jose, CA). Each sample was injected via an auto-sampler and loaded onto a C18 trap column (5 μm, 300 μm i.d. x 5 mm; Dionex LC-Packings, Sunnyvale, CA) and washed with water containing 0.1% trifluoroacetic acid for 6 min at a flow rate of 10 μl/min. The sample was subsequently separated by a C18 reverse-phase column (3.5 μm, 100 μm x 15 cm, Agilent, Santa Clara, CA) at a flow rate of 200 nl/min. The mobile phases consisted of water with 0.1% formic acid (A) and 90% acetonitrile with 0.1% formic acid (B). A linear gradient from 5 to 65% of solvent B was employed over a period of 100 min to separate peptide mixture. Eluted peptides were introduced into the mass spectrometer via a 10 μm silica tip (New

Objective Inc., Ringoes, NJ) adapted to a nano-electrospray source (Thermo Fisher Scientific Inc., Waltham, MA). The spray voltage was set at 1.7 kV and the heated capillary at 180 °C. LTQ was operated in the data-dependent mode in which each cycle consisted of one full-MS survey and subsequently three sequential pairs of intercalated zoom scans and MS/MS events. The targeted ions count in the mass spectrometer trap was 30,000 for full-MS scans, 3,000 for zoom scans, and 10,000 for MS/MS scans. Peptides were fragmented in the linear ion trap using collision-induced dissociation with the collision gas (helium) pressure set at 1.3 ml and the normalized collision energy value set at 35%. The zoom scan events, of higher resolution, were used to determine the charge state of each ion as well as the ratio of labeled to unlabeled peptide pairs using the ZoomQuant software developed by Halligan *et al*. [132].

3.3.5 Database search

Protein identification was performed by searching the 17,806 human protein sequences in the SwissProt database (UniProtKB/Swiss-Prot release 54.6 of December 2007) using Bioworks 3.3 (Thermo Fisher Scientific, San Jose, CA) and indexed with assumptions for enzymatic tryptic hydrolysis with the possibility of two missed cleavages and the following modifications: 16 Da shift for oxidized Met, 6 and 8 Da shifts for incorporation of stable isotope labeled Arg and Lys, respectively. Stringent filtering criteria were used for database search and peptide identifications: DeltaCn (ΔCn) > 0.1, a variable threshold of *Xcorr* versus charge state (*Xcorr*=1.9 for z=1, *Xcorr*=2.5 for z=2, and *Xcorr*=3.5 for z=3), peptide probability-based score with a p value <0.001, and more

than 2 different peptides per protein. A reverse database search using the same criteria gave a false positive rate of 0%, thus increasing confidence in protein identification.

3.3.6 ZoomQuant analysis

For quantitative analysis we used ZoomQuant Software [132]. In this case proteins were identified using BioWorks 3.1 software that is compatible with ZoomQuant software to generate Sequest output files and extract zoom scans from the mass spectrometry raw data. Each peptide was manually validated by examining zoom scans to verify the labeled and unlabeled pairs. Identified peptides were required to have a matched peptide partner 6 Da greater for Arg terminating peptides, 8 Da greater for Lys containing peptides, and other proper combinations for missed cleavage peptides. Because manually checking zoom scan with pairs of labeled and unlabeled peaks is itself stringent, filtration based on the *X corr* was lowered in this case, to increase proteome coverage (e.g., $X\ corr \geq 1.8$ for doubly charged ions and $X\ corr \geq 2.5$ for triply charged ions).

3.3.7 Statistical analysis

To check the significance of differentially expressed proteins in TNF-α treated cells versus non-treated cells, a *t*-tests for equal variances was performed using the Sidak method[173]. Basically, an average ratio was calculated from the total scans of labeled and unlabeled peptide pairs detected for a given protein. These averaged ratios were then compared in the control pairs versus TNF-α treated cells and untreated cells in both the

forward and reverse SILAC experiment. The obtained p values were then adjusted for the three way multiple comparisons using the Sidak method.

3.3.8 Western blot analysis

To validate proteome profiling data, we cultured ARPE-19 cells in 10 cm dishes (Corning Inc. Life Sciences, Lowell, MA) to 100% confluence. Cells were washed 6 times with PBS to remove any residual FBS proteins, and treated with various TNF-α concentrations (0.25 to 20 ng/ml) in serum free media for 24 h. Conditioned media were collected and filtered though 0.2 μm Polyethersulfone syringe filter (Corning Inc.). To check NF-κB activation, we collected cell pellets, washed them with PBS, and lysed with 100 μl of Radio immunoprecipitation assay (RIPA) buffer (Sigma Aldrich, St. Louis, MO) buffer. Protein extracts were separated by SDS–PAGE on a 4 to 15% Tris HCl gradient gel (BioRad) under reducing conditions then transferred to a nitrocellulose membrane (Amersham Biosciences, Piscataway, NJ) for western blot analysis. Nonspecific binding was blocked with 5% milk (BioRad Laboratories Inc., Hercules, CA), and the membrane was incubated overnight with goat polyclonal antibody against human C3 (Complement Technology, Tyler, TX), rabbit polyclonal antibody against human IκB-α (Cell Signaling, Danvers, MA) or mouse monoclonal antibody against human vinculin (Sigma) in 2.5% milk. The next day, the membrane was rinsed with Tris buffer containing salt and Tween (TBST) and incubated with antigoat antibody (Jackson Lab, West Grove, PA) for C3, and antirabbit Immunoglobulin G (IgG) (BioRad) for IκB-α or antimouse antibody (GE Healthcare, Buckinghamshire, England) for vinculin. All

secondary antibodies were conjugated with horseradish peroxidase, and immunoblots were visualized by chemiluminescence (Amersham Biosciences Inc., Piscataway, NJ)

Figure 3.1 Experimental design to study the effect of TNF-α on ARPE-19 secreted proteins

ARPE-19 cells were grown in medium where Lys and Arg were replaced by $^{13}C_6$, $^{15}N_2$ -Lys, and $^{13}C_6$-Arg. In parallel, ARPE-19 cells were cultured in medium with normal Lys and Arg. After cells were fully labeled with heavy and light amino acids, 10 ng/ml of TNF-α was added into each flask of labeled cells and unlabeled cells and incubated for 24 h in serum-free medium while the other remaining flasks were incubated in the same serumfree medium without TNF-α. **A**: For the control experiment, conditioned medium from labeled cells (e.g., untreated) was mixed at a 1:1 ratio with conditioned medium from unlabeled cells (e.g., untreated). **B**: To check the effect of TNF-α on ARPE-19 secreted proteins, we mixed the conditioned medium from labeled cells (e.g., treated with TNF-α) at a 1:1 ratio with conditioned medium from unlabeled cells (untreated). **C**: To validate the data, we performed a reverse experiment in which conditioned medium of labeled cell (e.g., untreated) was mixed at a 1:1 ratio with unlabeled cells (e.g., treated with TNF-α). Sample pairs were then processed as described in the method for subsequent LC-MS analysis and determination of protein ratios.

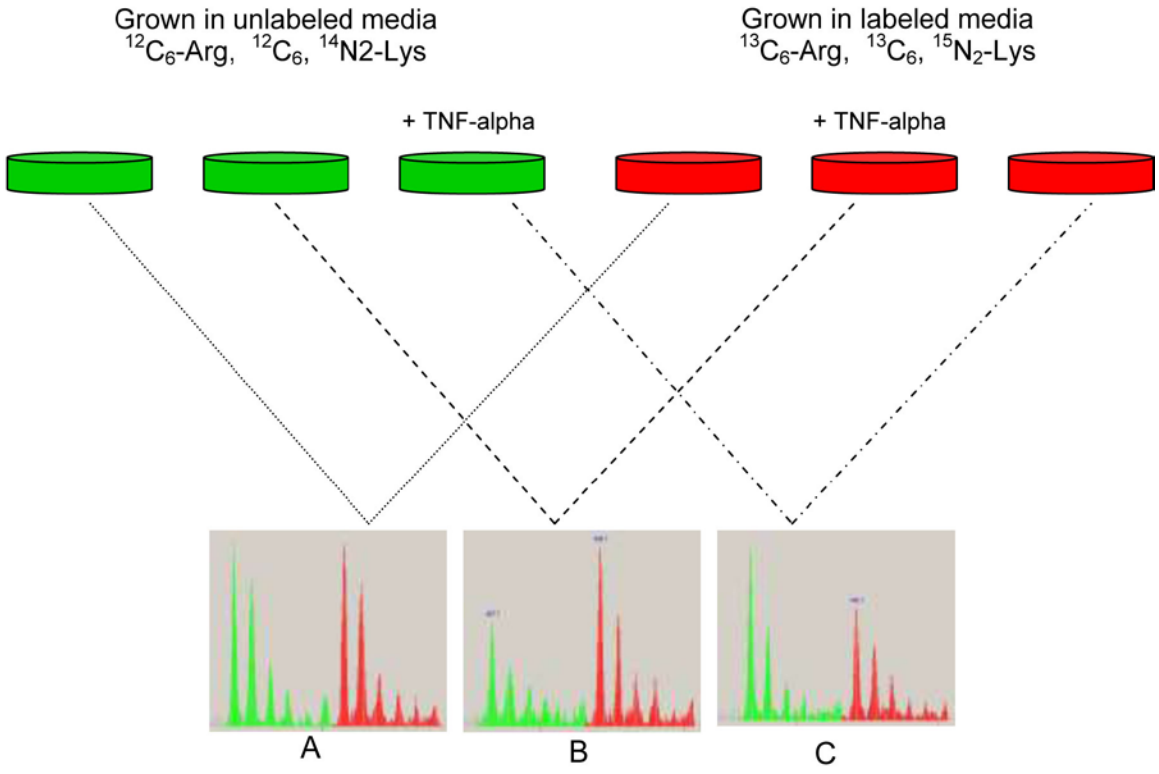
Grown in unlabeled media
$^{12}C_6$-Arg, $^{12}C_6$, $^{14}N2$-Lys
Grown in labeled media
$^{13}C_6$-Arg, $^{13}C_6$, $^{15}N_2$-Lys
+ TNF-alpha
+ TNF-alpha
A
B
C

3.4 Results

3.4.1 Effect of TNF-α on the viability of ARPE-19 cells

To ensure minimum cell death and minimum release of intracellular proteins into the condition medium of TNF-α-treated ARPE-19 cells, we monitored cell viability after incubating them for 24 h with different concentrations of TNF-α using trypan blue exclusion. Figure 3.2 shows the percent of viable cells after 24 h incubation with different TNF-α concentrations. TNF-α concentration up to 30 ng/ml (1.72 pM (10^{-12} molar)) produced only a small percent of cell death (e.g., <10% compared to untreated cells). These data are in agreement with a previous study where it has been shown that RPE cells are more resistant to TNF-α-induced apoptosis than other cell type[174]. We have thus chosen 10 ng/ml as the optimal concentration to study the effect of TNF-α on ARPE-19-secreted proteins. This concentration resulted in minimum cell death (<5%) and detectable cell response.

Figure 3.2 Cell viability in function of increased TNF-α concentration

Both viable and dead cells were counted using a hemocytometer. A percent of viable cells to the total cells was then calculated for each culture flask. Error bars represent standard deviations obtained from triplicate experiment for each dose of TNF-α used. To assess the number of cell death in the control group we have chosen not to normalize the values to 0 ng/ml of TNF-α.

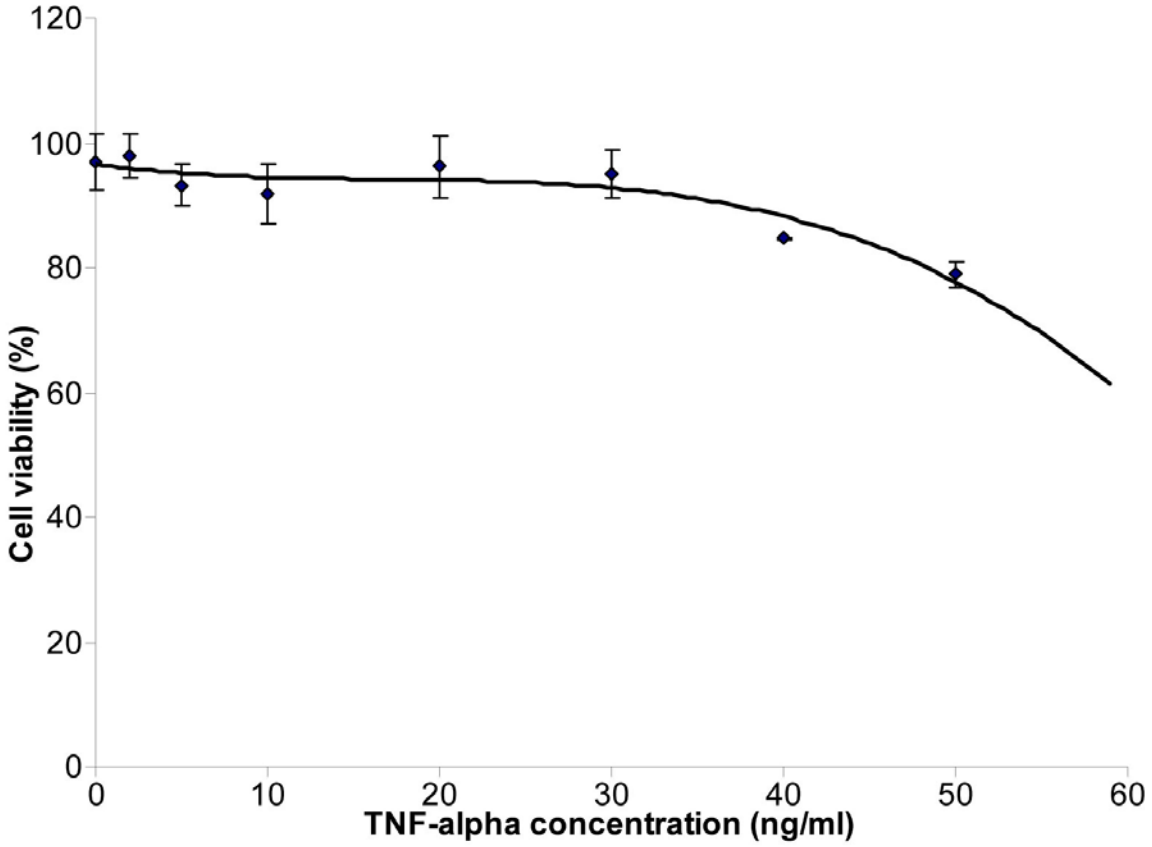
120
100
80
60
40
20
0
Cell viability (%)
0
10
20
30
40
50
60
TNF-alpha concentration (ng/ml)

3.4.2 Effect of TNF-α on ARPE-19-secreted proteins

One of the advantages of using the SILAC strategy is that all cellular proteins, including secreted proteins, are uniformly labeled with the stable isotope-labeled amino acids (e.g., $^{13}C_6$-Arg, $^{13}C_6$, $^{15}N_2$-Lys). Thus, in a 1:1 mixture of conditioned media collected from labeled and unlabeled cells, most of the peptides generated from cellular proteins would be detected as pairs of labeled and unlabeled peaks, while peptides from residual bovine serum proteins and contaminant proteins, such as keratin, would be detected as single peaks. In this study, a total of 221 proteins were identified in the conditioned medium of ARPE-19 cells, but only 146 proteins were of RPE cell origin; these are listed in Appendix 3.1 with their accession number, peptide count, subcellular localization, and function. The cellular localization of these proteins as well as their function was deduced from their annotations in the Universal protein resource (UniProt) database using the Protein Information Resources (PIR) tool. As shown in Figure 3.3A, 76 (52%) of these 146 proteins were found to be putatively secreted, 6 (4%) were of microsomal origin, 52 (36%) were of cytosolic origin, and the remaining 12 (8%) were unassigned. While the number of identified cytosolic proteins was high, their actual relative quantities estimated from spectral count were low compared to the secreted proteins (Figure 3.3B). All proteins in Appendix 3.1 were identified with at least two different peptides and validated by detection of labeled and unlabeled peptide pairs. Additional proteins that were identified by a single peptide pair in the conditioned medium of ARPE-19 cells are reported in Appendix 3.2. Even though each of these proteins was represented by a single peptide sequence, their identity was still validated by detection and sequencing of both labeled and unlabeled peptide pair. Detection of only

one representative peptide for each of these proteins suggests that they might be present in very low abundance in ARPE-19 conditioned medium. Zoom scan spectra of labeled and unlabeled peptide pairs were used to determine secreted protein ratios in TNF-α-treated cells versus untreated cells. Figure 3.4 shows example spectra of labeled and unlabeled peptide pairs of complement C3 and syndecan-4 whose secretion was significantly altered by TNF-α treatment.

This differential secretion was clearly maintained in both forward and reverse SILAC experiments thus validating the data. Among the 146 proteins reported in Appendix 3.1, only 6 were found to be altered in their concentrations after TNF-α treatment (Figure 3.5).

Figure 3.3 Cellular localization of proteins identified in conditioned medium of ARPE-19 cells

Panel A shows a pie chart depicting the subcellular distribution of the proteins identified in the conditioned medium of ARPE-19 cells. Panel B shows a bar graph plot representing the abundance of each class of proteins based on the spectral count of the total peptides detected. Other classes of proteins with no known subcellular localization and no known function was annotated as (N/ A) meaning not assigned.

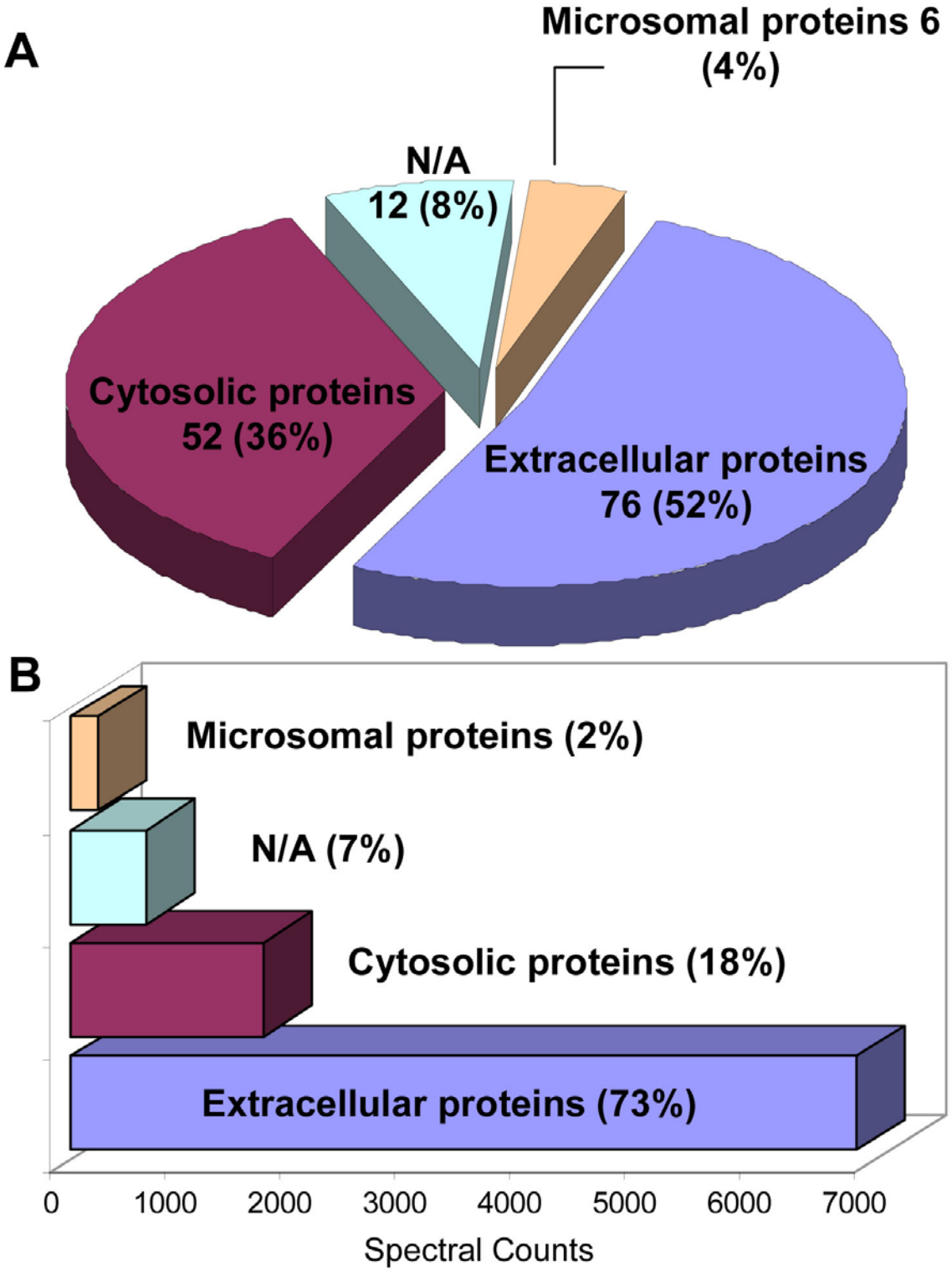
A
Microsomal proteins 6
(4%)
N/A
12 (8%)
Cytosolic proteins
52 (36%)
Extracellular proteins
76 (52%)
B
Microsomal proteins (2%)
N/A (7%)
Cytosolic proteins (18%)
Extracellular proteins (73%)
0
1000
2000
3000
4000
5000
6000
7000
Spectral Counts

Figure 3.4 Zoom scan mass spectra of labeled and unlabeled peptide pairs of complement C3 and syndecan-4 proteins

Panels A and D show the mass spectra and the relative intensity of labeled and unlabeled peptide pairs detected for complement C3 (A) and for syndecan-4 (D) in TNF-α-treated ARPE-19 cells versus untreated cells. In this case labeled cells were treated with TNF-α (+TNF-α) while unlabeled cells remained untreated (-TNF-α). Panels B and E show the mass spectra obtained for these same set of peptides in the reverse experiment where unlabeled cells were treated with TNF-α (+TNF-α) while labeled cells remained untreated (-TNF-α). Panel C shows the tandem mass spectrum and the fragment ions obtained for the doubly-charged ion m/z=645.2 and confirming the peptide sequence [SGSDEVQVGQQR] of complement C3 protein. Panel F shows the tandem mass spectrum and the fragment ions obtained for the doubly-charged ions m/z=579.3 and confirming the peptide sequence [AGSGSQVPTEPK] of syndecan-4 protein.

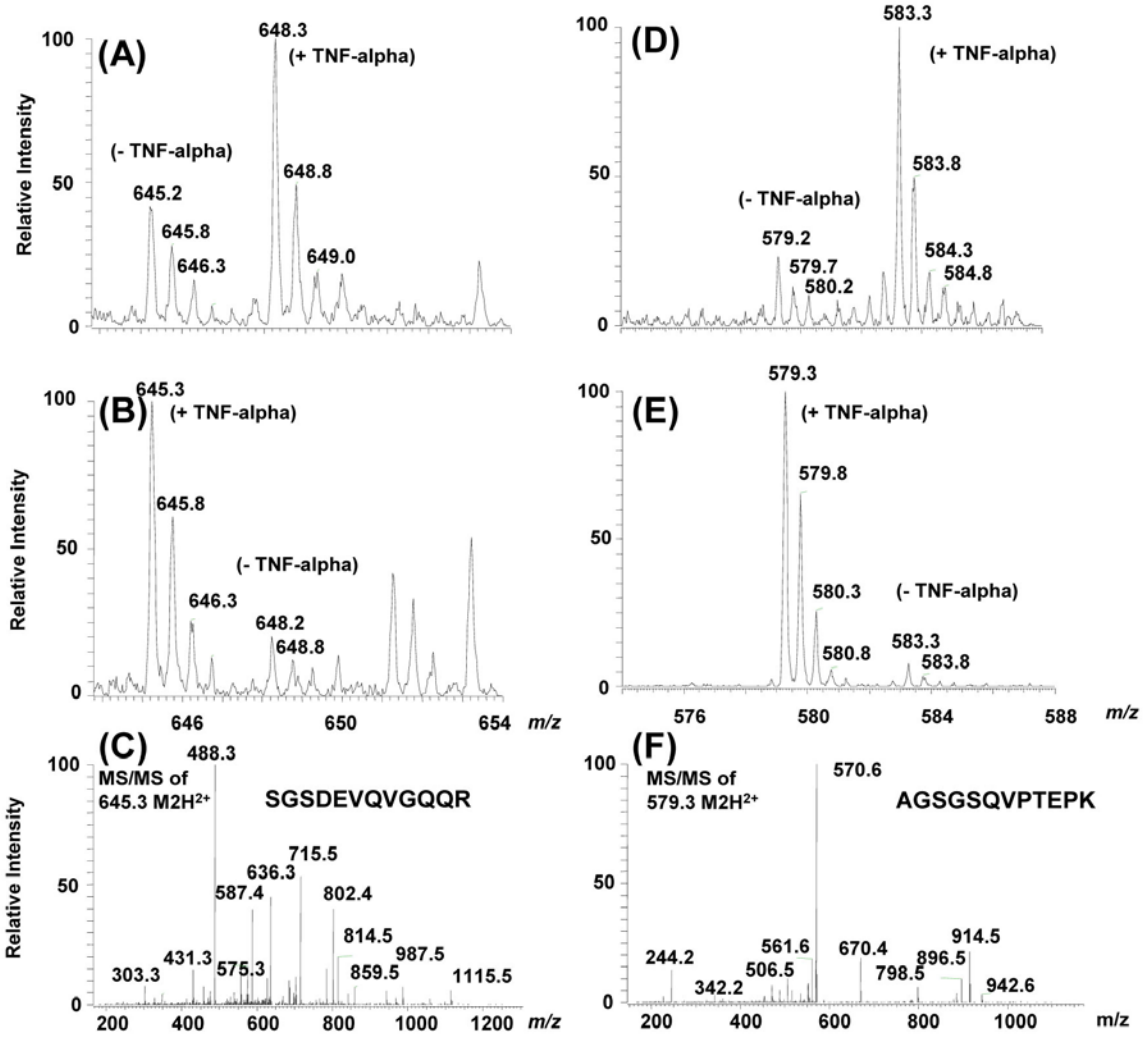
(A)
648.3
(+ TNF-alpha)
(- TNF-alpha)
645.2
645.8
646.3
648.8
649.0
(D)
583.3
(+ TNF-alpha)
583.8
(- TNF-alpha)
579.2
579.7
580.2
584.3
584.8
(B)
645.3
(+ TNF-alpha)
645.8
(- TNF-alpha)
646.3
648.2
648.8
(E)
579.3
(+ TNF-alpha)
579.8
580.3
(- TNF-alpha)
580.8
583.3
583.8
(C)
MS/MS of
645.3 M2H2+
SGSDEVQVGQQR
488.3
715.5
636.3
587.4
802.4
814.5
987.5
431.3
303.3
575.3
859.5
1115.5
(F)
MS/MS of
579.3 M2H2+
AGSGSQVPTEPK
570.6
561.6
670.4
914.5
244.2
506.5
896.5
798.5
342.2
942.6
Relative Intensity
m/z

Figure 3.5 Bar graph for the 6 proteins whose secretion was found differentially altered in TNF-α-treated ARPE-19 cells

Blue bars indicate ratios in control versus control cells (both labeled and unlabeled cells were untreated). Purple bars indicate ratios in TNF- α-treated cells versus untreated cells and in this case SILAC labeled cells were treated with TNF-α while unlabeled cells were kept untreated. Yellow bars indicate ratios in TNF-α-treated cells versus untreated cells and in this case unlabeled cells were treated with TNF-α while SILAC-labeled cells were kept untreated. Numbers inside of bars represent the total MS scans of labeled and unlabeled peptide pairs detected for each protein. The error bars represent the standard deviation between ratios of these individual scans. The p-values were obtained using three pair-wise *t*-tests (Sidak method) where all ratios for a given protein in control versus control were compared to ratios obtained in TNF-α treated versus untreated cells in both the reverse and forward experiments and these values are as follow (* represents p-value less than 1.00E-05, and ** represents p-value less than 0.001).

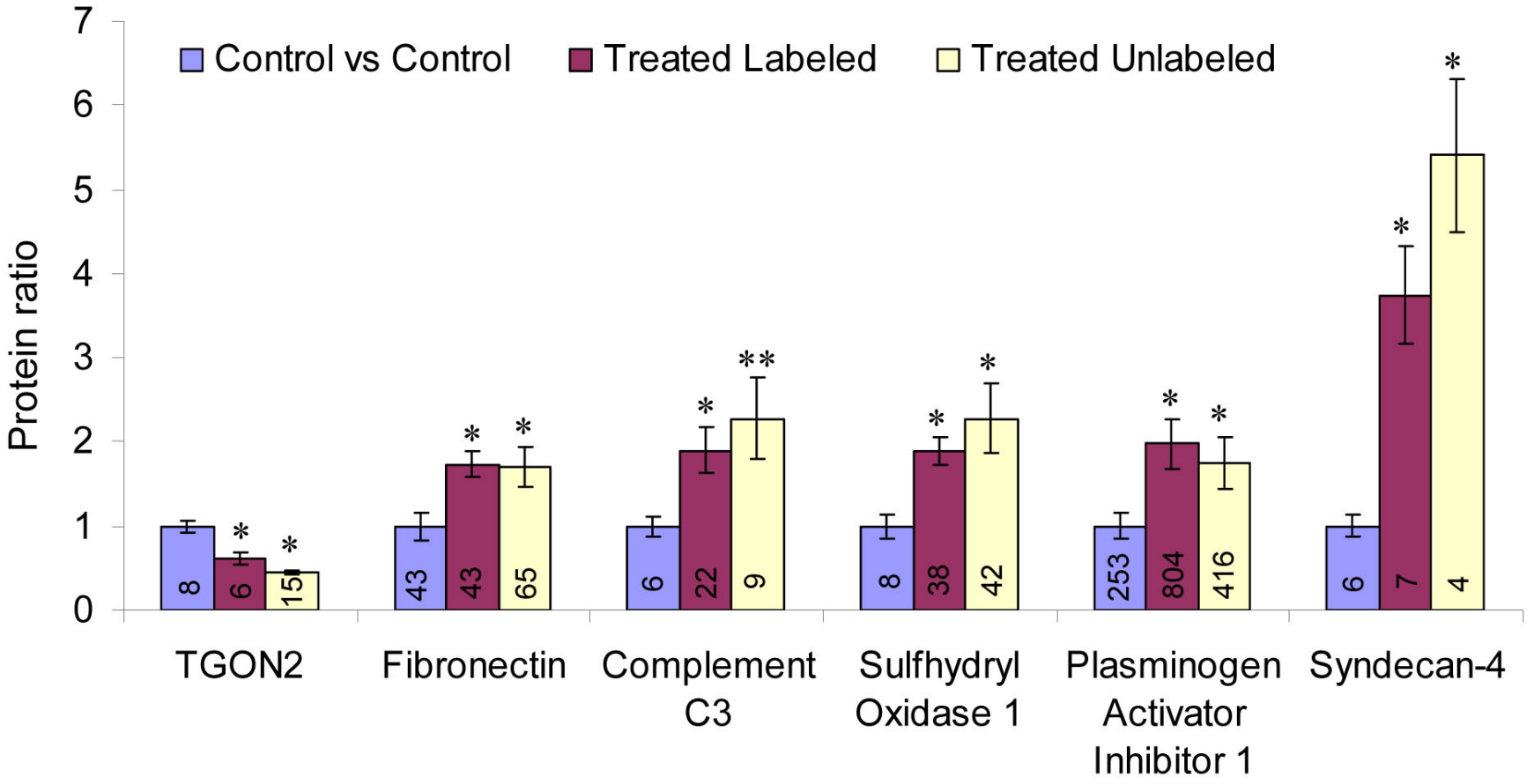
Control vs Control
Treated Labeled
Treated Unlabeled
Protein ratio
0
1
2
3
4
5
6
7
8
6
15
43
43
65
6
22
9
8
38
42
253
804
416
6
7
4
*
**
TGON2
Fibronectin
Complement C3
Sulfhydryl Oxidase 1
Plasminogen Activator Inhibitor 1
Syndecan-4

Trans-Golgi network protein-2 (TGON2) was the only protein whose secretion was decreased (by a factor of 2±0.01) in TNF-α treated cells versus untreated cells while the other 5 proteins, complement C3, fibronectin, sulfhydryl oxidase 1, plasminogen activator inhibitor 1 and syndercan-4 were increased by a factor of 2.03±0.42, 1.70±0.12, 2.04±0.26, 1.92±0.16, 4.35±0.54, respectively. Because of the importance of the complement pathway in AMD, secretion of C3 was further investigated in ARPE-19 cells treated with different doses of TNF-α. Vinculin, whose abundance remained unchanged between TNF-α treated and untreated cells, was used as a loading control for data normalization while I-κB,α (NF-κB Inhibitor, alpha protein) degradation was used to monitor the TNF-α induced NF-κB pathway. As shown in Figure 3.6, the secretion of C3 was increased with TNF-α in dose dependent manner while I-κB significantly decreased, indicating activation of the NF-κB pathway. This experiment was repeated three times, yielding same trend of C3 expression as a function of TNF-α concentration.

Figure 3.6 Effect of increasing concentrations of TNF-α on the secretion of Complement C3 by ARPE-19 cells

Cells were treated with increasing concentrations of TNF-α ranging from 0 to 20 ng/ml for 24 h in serum-free media. Conditioned media were collected, and the levels of each protein were evaluated by western blot analysis. Panel A shows western blot against complement C3; both C3-α and C3-β subunits are detected. Panel B shows western blot against cytosolic I-κB, α revealing activation of NF-κB signaling pathway. C: western blot against vinculin, a housekeeping protein whose level remained unchanged following TNF-α treatment. Panel D shows bar graphs of the relative expression of complement C3 to vinculin expression in function of different TNF-α concentration. Standard deviations were obtained from 3 replicate experiments with p-values <0.05 *.

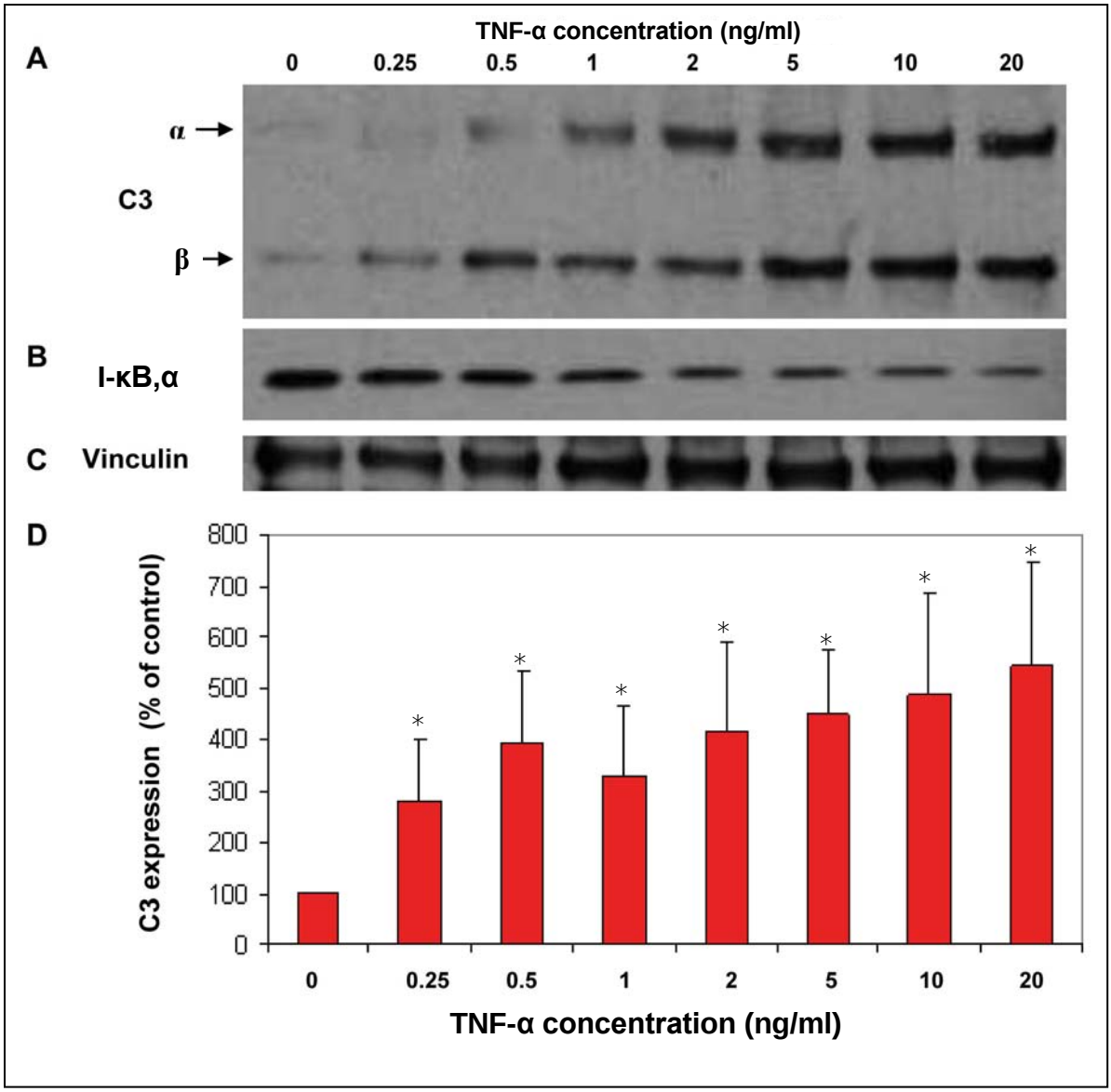
TNF-α concentration (ng/ml)
A
0
0.25
0.5
1
2
5
10
20
α
C3
β
B
I-κB,α
C
Vinculin
D
C3 expression (% of control)
800
700
600
500
400
300
200
100
0
*
TNF-α concentration (ng/ml)

3.5 Discussion

Human ARPE-19 cells secrete a variety of proteins that are involved in regulation and maintenance of the extracellular matrix, complement pathway, as well as immune and inflammatory responses. Only six proteins among the total identified proteins in ARPE-19 condition medium were found altered in their quantities following 24 h treatment with TNF- α. This response indicates that ARPE-19 cells possess a cell surface receptor for TNF-α that acts on specific gene expression via activation of the NF-κB pathway [166,175]. Indeed, this pathway was further confirmed by the observation of a TNF-α dose-dependent decrease of I-κB,α, whose binding is known to prevent translocation of the transcription factor NF-κB to nucleus[176]. The promoter regions of the genes encoding for complement C3, plasminogen activator inhibitor, and syndercan-4 have a binding site for NF-κB as judged from the literature and as determined by TFSEARCH algorithm using 1,000 bp downstream of the promoter region. Therefore, these genes are potential targets for response to TNF-α treatment. Interestingly, the three other proteins altered by TNF-α (e.g., TGON2, fibronectin, and sulfhydryl oxidase 1) do not have any known binding site for NF-κB in the promoter region of their corresponding genes indicating that the regulation of these proteins by TNF-α may occur via alternative pathways or involves intermediate proteins.

Previous studies have shown that TNF-α also induces secretion of a variety of chemokines (e.g., interleukin-8, growth-regulated protein (GRO), MCP-1, and cytokines (endothelin-1) in RPE cells[177-179]. Most of these studies used an immunoassay based assay or mRNA expression assays that amplify the signal of these molecules and facilitate their detection. In the present study, we were not able to detect these

components using our proteomic approach. This is most likely due to their inherent limited amount and their short half life. Additionally, these proteins are generally of low molecular mass (<10 kDa) and may generate only a few tryptic peptides to be detected by mass spectrometry. This shows the limitation of the proteomic approach in detecting this class of proteins and prompt for additional strategies to increase proteome coverage in the future. Nevertheless, proteomics studies allow simultaneous detection and quantification of several proteins that otherwise would have been overlooked in hypothesis-driven studies. Using a proteomics approach, we identified additional proteins whose secretion from ARPE-19 cells was influenced by TNF-α.

3.5.1 Complement C3

The secretion of this protein was significantly induced by TNF-α in ARPE-19 cells. This result is in agreement with previous studies where it has been shown that cytokines regulate C3 production in different cell types including human intestinal epithelial cell line, Caco-2[180] as well as rat glomerular endothelial cells[181]. The production of C3 in interleukin-1-treated intestinal cells was abolished by NF-κB inhibitors[180], indicating that C3 is a target gene for NF-κB transcription factor. It is most likely that a similar pathway is involved in TNF-α-treated ARPE-19. However, to the best of our knowledge, this is the first time that TNF-α has been shown to induce C3 secretion in human RPE cells. Local secretion of C3 by RPE cells could be detrimental in individuals carrying Y402H CFH variant since CFH is the physiologic inhibitor of C3 activation and protects cells from autologous injuries by complement C3[37]. Additionally, it has been shown that monocytes, which are a major source of TNF-α, are attracted by

sub-RPE deposits[80]. Therefore, in individuals with compromised CFH activity due to the Y402H mutation, this could generate a positive-feedback loop whereby the newly attracted mononcytes generate a chronic exposure of RPE cells to cytokines. In turn, this leads to increased secretion of C3 by these cells, leading to progressive immune complex deposition and autologous complementmediated RPE injury. This hypothesis remains however to be verified in a model system using primary RPE cells with mutated and wild type CFH.

3.5.2 Fibronectin and syndecan-4

Secretion of fibronectin and syndecan-4 was significantly induced in TNF-α-treated ARPE-19 cells. Syndecan-4, especially, was threefold to fivefold more abundant in the conditioned medium of TNF-α-treated cells versus untreated cells. These two proteins are major constituents of the ECM and play a crucial role in cell adhesion and connectivity. While fibronectin is an extracellular protein that adheres to the cell surface to maintain their integrity and shape, syndecan-4 is a single pass transmembrane protein composed of an extracellular domain “ectodomain” bearing four heparin sulfate chains, a transmembrane domain (TM), and a short C terminal cytoplasmic domain. Even though treatment of ARPE-19 with TNF-α resulted in a significant increase of fibronectin secretion neither the literature nor software prediction supports the involvement of the NF-κB pathway in this process, suggesting that this protein might be indirectly upregulated. Indeed, fibronectin was identified in SDS–PAGE around 100 to 250 kDa indicating that the protein was fragmented. Upregulation of fibronectin fragments might be due to proteases involved in ECM degradation such as the serine protease HTRA1[64].

Interestingly, mutation in the promoter region of the gene encoding for HTRA1 was recently found to be strongly associated with AMD pathology[52,53,159]. Nevertheless, the exact mechanism(s) by which this single point mutation leads to drusen formation and macular degeneration remains to be further investigated. Although the molecular mass of syndecan-4 core protein is around 21 kDa, this protein was detected at around 250 kDa in our SDS–PAGE. This abnormal SDS–PAGE migration is most probably due to the O-linked glycosaminglycan chains. This hypothesis is in agreement with previous studies where it has been shown that intact syndecan migrates at higher molecular mass in the gel than does heparinase-treated syndecan[182]. All the peptides identifying this protein in our study belonged to the ectodomain sequence (Figure 3.7) suggesting that the N terminal part of the protein is shed into the conditioned medium of TNF-α treated ARPE-19 cells. Previous study has shown that TNF-α induces the overall expression of syndecan-4 in endothelial cells via NF-κB activation[183]. Other studies have shown that syndecan-4 shedding is mediated by matrix metalloproteinase-9 (MMP9) and is dependent of NF-κB signaling[184]. In our proteomic profiling data we did detect 2 peptides for MMP9 and these were found to be more abundant in TNF-α-treated than untreated cells (data not shown). Unfortunately, due to the inherent low amount of this protein in the conditioned medium of ARPE-19, we were not able to detect these same peptides in our reverse experiment. What remains to be examined is whether the increased amount of syndecan-4 seen in the conditioned medium of TNF-α-treated ARPE-19 cells was due to induction of its expression via NF- κB activation or to the increased shedding of its ectodomain. In either case, shedding of this from the surface of ARPE-19 cells exposed to TNF-α could be a

protective mechanism against TNF-α cytotoxicity, and this may explain the resistance of these cells to TNF-α-induced apoptosis[174].

Indeed, it has been documented that the TNF-α signaling pathway synergizes with the binding of matricellular protein Cysteine-rich protein 61 to syndecan-4 ectodomain and triggers a cascade leading to apoptosis[184]. Nevertheless, the contribution of this shedding to AMD pathogenesis remains to be carefully examined even though some studies demonstrated that drusen contained some glycosaminoglycan and heparan sulfate-conjugated proteoglycans[185,186]. Also, at present it is uncertain whether CFH, an important factor in AMD pathology, binds to heparan sulfate of syndecans and whether shedding of syndecan will make cell more vulnerable to increased complement C3 secretion. More studies on the interactions between cell surface proteoglycan and CFH (both the H402 variant and the wild type) are needed.

Figure 3.7 Sequence and cellular domains of human syndecan 4

The sequence from amino acid 1 to 18 represents the signal peptide and is usually cleaved out in the endoplasmic reticulum (ER) before the protein is trafficked to the cell surface. Sequence from 19 to 45 represents the extracellular domain of the protein. Sequence from 146 to 170 represents the TM and the sequence from 171 to 198 represents the C terminal cytoplasmic domain. Gray highlights tryptic peptides that were detected and identified by LC-MS/MS analysis. Note that all the detected peptides belonged to the extracellular domain of the protein suggesting that syndecan 4 sheds its ectodomain into the condition medium in response to TNF-α treatment.

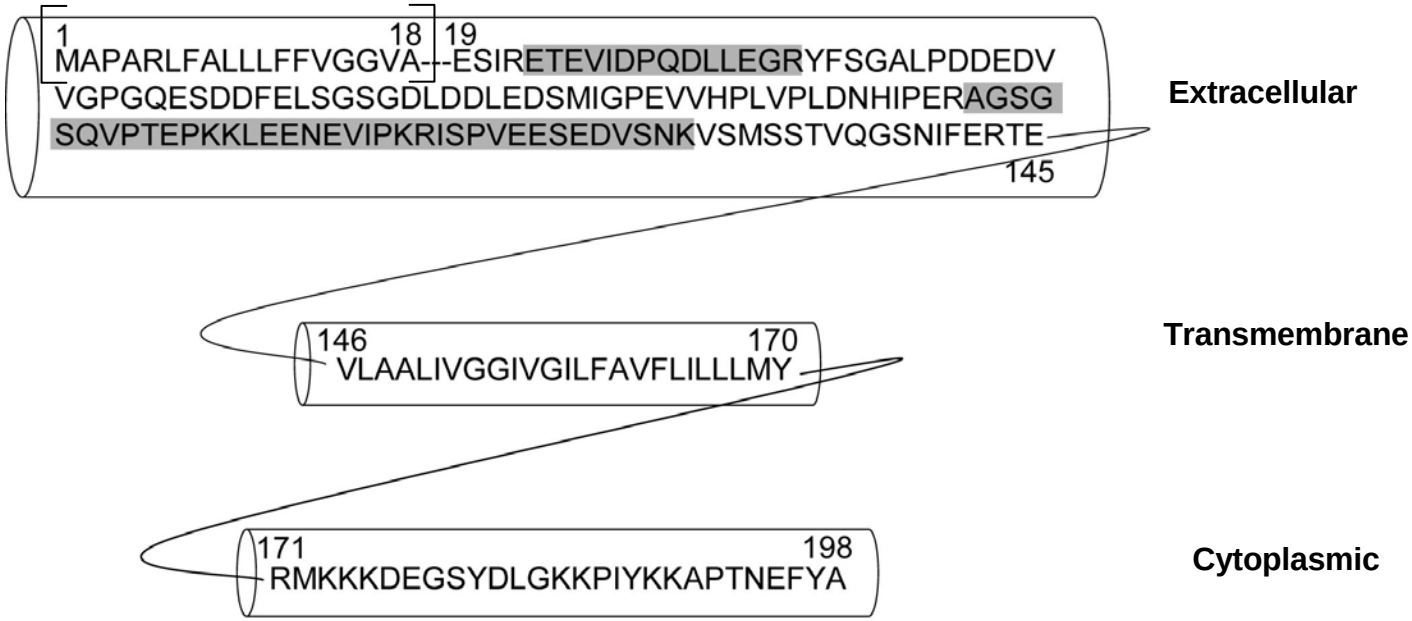
1
18
19
MAPARLFALLLFFVGGVA---ESIRETEVIDPQDLLEGRYFSGALPDDEDV
VGPGQESDDFELSGSGDLDDLEDSMIGPEVVHPLVPLDNHIPERAGSG
SQVPTEPKKLEENEVIPKRISPVEESEDVSNKVSMSSTVQGSNIFERTE
145
146
170
VLAALIVGGIVGILFAVFLILLLMY
171
198
RMKKKDEGSYDLGKKPIYKKAPTNEFYA
Extracellular
Transmembrane
Cytoplasmic

3.5.3 Plasminogen activator inhibitor-1

Based on the spectral count of total peptides generated per protein, plasminogen activator inhibitor-1 (PAI-1) appears as one of the highly abundant proteins in the conditioned medium of ARPE-19 cells (29 peptides and 1474 spectral count were detected for this protein even under basal conditions). The secretion of PAI-1 was further increased by two fold in TNF-α-treated ARPE-19 cells versus untreated cells. Previous studies have shown that TNF- α readily induces PAI-1 in different cell types[187-190]. PAI-1 is a physiologic inhibitor of plasminogen activator and plays an important role in the regulation of the extracellular matrix. Its expression is increased in several fibrotic diseases and regulated by various cytokines, growth factors, and chemical/ physical agents[191]. RPE cells secrete both urokinase plasminogen activator and its inhibitor PAI-1[192] and the balance between these two components likely plays a crucial role in maintaining the extracellular environment of RPE cells including regulation of angiogenesis[193-196]. Interestingly, PAI-1 was found to be more abundant in the serum of patients with early or advanced AMD than of healthy individuals, suggesting its potential implication in AMD pathogenesis[197].

3.5.4 Sulfhydryl oxidase 1

A protein also known as quiescin Q6 (QSOX), sulfhydryl oxidase 1 has two known isoforms generated by alternative splicing. Isoform 1, a single pass membrane protein, can be found in the ER and Golgi apparatus while isoform 2, missing the C terminal domain of isoform 1, is mainly found in the extracellular space[198]. All the 17 peptides identified for this protein in our study belonged to isoform 2, consistent with a

secreted form. In other words, we did not detect any peptide sequence belonging to the C terminal domain of isoform 1. QSOX protein utilizes a thioredoxin domain and a small flavin adenine dinucleotide (FAD)-binding domain to form disulfide bonds in proteins and peptides especially in proteins destined for secretion[198]. QSOX is typically found in the cell along the secretory machinery and in the extracellular space. However, little is known about the secreted form and its significance. Whether this secreted form has a role in disulfide bond formation of proteins in the extracellular space or is merely carried along with proteins during their secretion remain to be determined. Nevertheless and to the best of our knowledge, this is the first demonstration that TNF-α induces secretion of QSOX in human RPE cells despite the lack of a binding site for activated NF-κB promoter region of its gene. It is believed that this protein may play a crucial role in ECM remodeling[199] which might be relevant in diseases involving ECM deposition such as AMD, Alzheimer and fibrosis.

3.5.5 *Trans*-Golgi network protein 2

TGON2 was the only protein that was found to be decreased in the conditioned medium of TNF-α-treated versus untreated ARPE-19 cells. While TGON2 was decreased in the extracellular space of treated cells, its amount was actually increased in the microsomal fraction of this same set of cells (Figure 3.8), indicating that the changes were due to retention of this protein rather than inhibition of its expression. Indeed, TGON2 is involved in regulating membrane traffic to and from the *trans*-Golgi network. RPE cells express both TNF receptor-associated factor-1 and 2 (TRAF-1 and TRAF-2) at their surface[175]. The decreased amount of TGON2 at the surface of TNF-α- treated cells

could be associated with the internalization of TNF-α/ TNF-α receptor (TNFR) complex to modulate TNF-α signaling[200,201] Indeed, it has been shown that TNFR can be localized both at the cell surface and to the Golgi apparatus of endothelial cells, and that TNF-α binding modulates its trafficking[202].

Overall, this study showed that TNF-α modulated the RPE secretion of a variety of proteins that play a major role in ECM remodeling, complement network and angiogenesis which might be relevant to AMD pathogenesis. Although preliminary, this study demonstrated that TNF-α induced secretion of specific proteins in ARPE-19 cells. Even though these cells are not an ideal RPE model in respect to primary cultures, they were used as proof of principle to demonstrate that several secreted proteins can be qualitatively and quantitatively monitored in TNF-α-treated versus untreated cells. These proteins set may serve as a catalog for future targeted studies that use human primary RPE cells or human retinal cross-sections.

Figure 3.8 Effect of TNF-α on the subcellular distribution of the TGON2

TGON2 was found to decrease in the extracellular space and increase in the microsomal fraction in TNF-α-treated ARPE-19 cells (dark bars) when compared to untreated ARPE-19 cells (clear bars). This strongly suggests that TNF-α influences TGON2 trafficking in ARPE-19 cells.

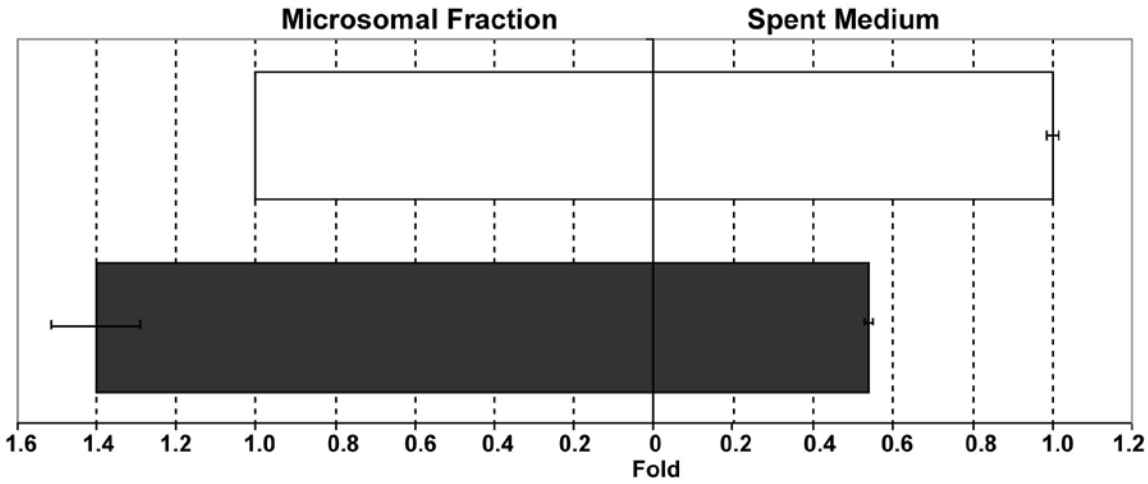
Microsomal Fraction
Spent Medium
1.6
1.4
1.2
1.0
0.8
0.6
0.4
0.2
0
0.2
0.4
0.6
0.8
1.0
1.2
Fold

3.6 Acknowlegments

This work was supported by NIH/NEI grant 5R21EY016723–02. Eunkyung An is a predoctoral student in the Biochemistry and Molecular Genetics program of the Institute for Biomedical Sciences at the George Washington University. This work is from a dissertation to be presented to the above program in partial fulfillment of the requirements for the Ph.D degree. We thank Dr. Kristy Brown for her help with mass spectrometry maintenance and Dr. Zhangzhi Hu for Bioinformatics support.

Appendix 3.1 List of proteins found in the condition media of ARPE-19 cell cultures

Serum free condition media were collected from 24 h ARPE-19 cell cultures. The protein content in these media were concentrated and separated by SDS–PAGE. Gel bands where excised, digested with trypsin and the resulting peptides analyzed by LC-MS/MS as described in the method. UniProt ID column shows accession number for each identified protein. Peptide count column shows the number of tryptic peptides detected and identified for each protein. The last column indicates the subcellular localization of each protein. Each of these proteins were identified by at least two peptides and validated by detection of both labeled and unlabeled peptide pairs.

UniProt ID	Protein Name	Peptide Count	Cellular location
Cell adhesion/ connective tissue proteins			
P98160	Basement membrane-specific heparan sulfate proteoglycan core protein	56	Extracelluar space
P55287	Cadherin-11	2	Extracelluar space
P19022	Cadherin-2	19	Membrane
P20908	Collagen alpha-1(V) chain	8	Extracellular space
P12107	Collagen alpha-1(XI) chain	9	Extracellular space
P39060	Collagen alpha-1(XVIII) chain	5	Extracellular space
P05997	Collagen alpha-2(V) chain	2	Extracellular space
Q14574	Desmocollin-3	4	Membrane
Q14126	Desmoglein-2	11	Membrane
Q14118	Dystroglycan	2	Extracelluar space
P35555	Fibrillin-1	6	Extracellular space
P02751	Fibronectin	36	Extracellular space
Q12841	Follistatin-related protein 1	5	Extracellular space
P35052	Glypican-1	9	Extracellular space
P05362	Intercellular adhesion molecule 1	5	Membrane
Q16363	Laminin subunit alpha-4	16	Extracellular space
O15230	Laminin subunit alpha-5	8	Extracellular space
P07942	Laminin subunit beta-1	13	Extracellular space
P11047	Laminin subunit gamma-1	14	Extracellular space
Q9Y4K0	Lysyl oxidase homolog 2	4	Extracellular space
Q15262	Receptor-type tyrosine-protein phosphatase kappa	7	Membrane
P34741	Syndecan-2	2	Membrane
P31431	Syndecan-4	5	Membrane
P07996	Thrombospondin-1	22	Extracellular space
P35442	Thrombospondin-2	2	N/A
Q15582	Transforming growth factor-beta-induced protein ig-h3	12	Extracellular space
Complement regulator/Immune response			
O75882	Attractin	6	Extracellular space
P61769	Beta-2-microglobulin	4	Extracellular space

Appendix 3.1 (continued)

UniProt ID	Protein Name	Peptide Count	Cellular location
P00736	Complement C1r subcomponent	8	Extracellular space
P09871	Complement C1s subcomponent	5	N/A
P01024	Complement C3	11	Extracellular space
P81605	Dermcidin	3	Extracellular space
P02794	Ferritin heavy chain	3	Cytoplasm
P02792	Ferritin light chain	4	Cytoplasm
P06744	Glucose-6-phosphate isomerase	14	Cytoplasm
P61626	Lysozyme C	2	Extracellular space
P09603	Macrophage colony-stimulating factor 1	3	Extracellular space
P20962	Parathymosin	2	Nucleus
P26022	Pentraxin-related protein PTX3	9	Extracellular space
P05155	Plasma protease C1 inhibitor	10	Extracellular space
P06454	Prothymosin alpha	4	Nucleus
O75326	Semaphorin-7A	5	Membrane
Development			
Q6UX71	Plexin domain-containing protein 2	3	Membrane
P09486	SPARC	8	Extracellular space
Protease /Peptidase / Inhibitor			
Q13443	ADAM 9	2	Extracellular space
P05067	Amyloid beta A4 protein	3	Extracellular space
Q06481	Amyloid-like protein 2	2	Membrane
P13497	Bone morphogenetic protein 1	4	N/A
Q9UI42	Carboxypeptidase A4	9	Extracellular space
P09668	Cathepsin H	7	lysosome
Q9UBR2	Cathepsin Z	3	lysosome
P14780	Matrix metalloproteinase-9	2	Extracellular space
P01033	Metalloproteinase inhibitor 1	2	Extracellular space
P16035	Metalloproteinase inhibitor 2	3	Extracellular space
P30086	Phosphatidylethanolamine-binding protein 1	3	Cytoplasm
P36955	Pigment epithelium-derived factor	8	Extracellular space

Appendix 3.1 (continued)

UniProt ID	Protein Name	Peptide Count	Cellular location
P05121	Plasminogen activator inhibitor 1	29	Extracellular space
P25787	Proteasome subunit alpha type-2	5	Cytoplasm
P25788	Proteasome subunit alpha type-3	2	Cytoplasm
P28066	Proteasome subunit alpha type-5	2	Cytoplasm
P60900	Proteasome subunit alpha type-6	5	Cytoplasm
O14818	Proteasome subunit alpha type-7	2	Cytoplasm
P20618	Proteasome subunit beta type-1	3	Cytoplasm
P49721	Proteasome subunit beta type-2	3	Cytoplasm
P49720	Proteasome subunit beta type-3	3	Cytoplasm
P28074	Proteasome subunit beta type-5	7	Cytoplasm
P28072	Proteasome subunit beta type-6	4	Cytoplasm
Q9Y6L7	Tolloid-like protein 2	2	Extracellular space
P01034	Cystatin-C precursor	2	Extracellular space
P12955	Xaa-Pro dipeptidase	2	N/A
Signal transduction			
P31946	14-3-3 protein beta/alpha	6	Cytoplasm
P62258	14-3-3 protein epsilon	9	Cytoplasm
P61981	14-3-3 protein gamma	3	Cytoplasm
P63104	14-3-3 protein zeta/delta	6	Cytoplasm
P07355	Annexin A2	14	Extracellular space
P12429	Annexin A3	2	Cytoplasm
P08758	Annexin A5	3	Cytoplasm
O94985	Calsyntenin-1	12	Membrane
Q9H4D0	Calsyntenin-2	7	Membrane
Q13740	CD166 antigen	6	Membrane
Q9UNN8	Endothelial protein C receptor	3	Membrane
Q16610	Extracellular matrix protein 1	3	Extracellular space
P09382	Galectin-1	4	Cytoplasm
Q08380	Galectin-3-binding protein	15	Extracellular space
O94760	N(G),N(G)-dimethylarginine dimethylaminohydrolase 1	2	N/A

Appendix 3.1 (continued)

UniProt ID	Protein Name	Peptide Count	Cellular location
P30101	Protein disulfide-isomerase A3	6	ER
Q99497	Protein DJ-1	6	Cytoplasm
P10599	Thioredoxin	2	Cytoplasm
Q16881	Thioredoxin reductase 1, cytoplasmic	7	Cytoplasm
Q13308	Tyrosine-protein kinase-like 7	3	Membrane
Q6EMK4	Vasorin	6	Extracellular space
Catabolism			
P15121	Aldose reductase	2	Cytoplasm
P06733	Alpha-enolase	12	Cytoplasm
Q05524	Alpha-enolase, lung specific	5	Cytoplasm
P13929	Beta-enolase	2	Cytoplasm
O00462	Beta-mannosidase	9	lysosome
P43251	Biotinidase	2	Extracellular space
Q13822	Ectonucleotide pyrophosphatase/phosphodiesterase family member 2	9	Extracellular space
P09104	Gamma-enolase	5	Cytoplasm
Q92820	Gamma-glutamyl hydrolase	5	Extracellular space
P00338	L-lactate dehydrogenase A chain	6	Cytoplasm
P40925	Malate dehydrogenase, cytoplasmic	7	Cytoplasm
P40926	Malate dehydrogenase, mitochondrial	4	Mitochondria
P15586	N-acetylglucosamine-6-sulfatase	2	Lysosome
P00558	Phosphoglycerate kinase 1	15	Cytoplasm
P18669	Phosphoglycerate mutase 1	3	Cytoplasm
P15259	Phosphoglycerate mutase 2	2	N/A
P07237	Protein disulfide-isomerase	4	Extracellular space
P29401	Transketolase	13	N/A
P60174	Triosephosphate isomerase	14	N/A
P62988	Ubiquitin	5	Cytoplasm
Cell organization and biogenesis			
P63313	Thymosin beta-10	2	Cytoplasm
P68133	Actin, alpha skeletal muscle	16	Cytoplasm

Appendix 3.1 (continued)

UniProt ID	Protein Name	Peptide Count	Cellular location
P60709	Actin, cytoplasmic 1	4	Cytoplasm
O00468	Agrin	26	Extracellular space
P12814	Alpha-actinin-1	12	Cytoplasm
O43707	Alpha-actinin-4	17	Cytoplasm
P27797	Calreticulin	6	Extracellular space
Q14019	Coactosin-like protein	5	Cytoplasm
P24592	Insulin-like growth factor-binding protein 6	2	Extracellular space
Q16270	Insulin-like growth factor-binding protein 7	8	Extracellular space
P62937	Peptidyl-prolyl cis-trans isomerase A	5	Cytoplasm
P23284	Peptidyl-prolyl cis-trans isomerase B	9	ER
P07737	Profilin-1	5	N/A
O60361	Putative nucleoside diphosphate kinase	2	N/A
P35241	Radixin	3	Membrane
O00391	Sulfhydryl oxidase 1	17	Extracellular space
P00441	Superoxide dismutase	3	Extracellular space
P62328	Thymosin beta-4	3	Cytoplasm
O43493	*Trans*-Golgi network integral membrane protein 2	4	Membrane
P06753	Tropomyosin alpha-3 chain	4	Cytoplasm
P67936	Tropomyosin alpha-4 chain	6	Cytoplasm
Q12907	Vesicular integral-membrane protein VIP36	2	Membrane
P08670	Vimentin	10	Cytoplasm
Other functions			
P62158	Calmodulin (CaM)	4	Membrane
P99999	Cytochrome C	3	Mitochondria
Q96FE7	Phosphoinositide-3-kinase-interacting protein 1	2	Membrane
Q8N0Y7	Probable phosphoglycerate mutase 4	2	N/A
Q07954	Prolow-density lipoprotein receptor-related protein 1	7	Membrane
P41222	Prostaglandin-H2 D-isomerase precursor	2	Extracellular space
P00491	Purine nucleoside phosphorylase	2	N/A
Q99969	Retinoic acid receptor responder protein 2	4	Extracellular space

Appendix 3.1 (continued)

UniProt ID	Protein Name	Peptide Count	Cellular location
O75368	SH3 domain-binding glutamic acid-rich-like protein	4	Cytoplasm
Q9H299	SH3 domain-binding glutamic acid-rich-like protein 3	2	Cytoplasm
P37837	Transaldolase	4	Cytoplasm
Q969H8	Uncharacterized protein C19orf10 precursor	3	Extracellular space

Appendix 3.2 Additional proteins identified by a single peptide pair in the conditioned medium of ARPE-19 cells

Additional proteins detected in the conditioned media of ARPE-19 cell cultures were represented by a single tryptic peptide. The identity of this single peptide was validated by the presence of its labeled homolog peptide. UniProt ID column indicates the accession number of each of these proteins. Peptide count column indicates the number of peptides identified for each of these proteins. The Scan count column indicates the number of times this peptide was detected and analyzed by the mass spectrometer. The higher the number the more abundant is the peptide. The last column indicates the subcellular location of each of these proteins.

Uniprot ID	Protein name	Peptide Count	Scan Count	Subcellular location
P62857	40S ribosomal protein S28	1	1	Cytoplasm
P08253	72 kDa type IV collagenase	1	2	Secreted
P11021	78 kDa glucose-regulated protein	1	5	ER, Melanosome
Q9HBZ2	Aryl hydrocarbon receptor nuclear translocator 2	1	1	Nucleus
Q15121	Astrocytic phosphoprotein PEA-15	1	1	Cytoplasm
Q6Y288	Beta-1,3-glucosyltransferase	1	4	ER
P07686	Beta-hexosaminidase beta chain	1	1	Lysosome
P07711	Cathepsin L1	1	1	Lysosome
P00450	Ceruloplasmin	1	4	Secreted
Q76M96	Coiled-coil domain-containing protein 80	1	2	Secreted
P04080	Cystatin-B	1	1	Cytoplasm, Nucleus
P30046	D-dopachrome decarboxylase	1	1	Cytoplasm
Q02487	Desmocollin-2	1	7	Cell membrane
O95633	Follistatin-related protein 3	1	2	Secreted, Nucleus
P09211	Glutathione S-transferase P	1	5	Cytoplasm
Q9Y5Z4	Heme-binding protein 2	1	1	Cytoplasm
P22626	Heterogeneous nuclear ribonucleoproteins A2/B1	1	1	Nucleus
Q8NHP8	HUMAN LAMA-like protein 2	1	1	Lysosome
Q14767	Latent-transforming growth factor beta-binding protein 2	1	1	Secreted
Q86YC3	Leucine-rich repeat-containing protein 33	1	3	Membrane
P30740	Leukocyte elastase inhibitor	1	33	Cytoplasm
P26038	Moesin	1	3	Membrane, Cytoplasm
P58546	Myotrophin	1	4	Cytoplasm
P20933	N(4)-(beta-N-acetylglucosaminyl)-L-asparaginase	1	5	Lysosome
P05408	Neuroendocrine protein 7B2	1	2	Secreted
P11464	Pregnancy-specific beta-1-glycoprotein 1	1	1	Secreted
Q9BUQ8	Probable ATP-dependent RNA helicase DDX23	1	4	Nucleus
O00469	Procollagen-lysine,2-oxoglutarate 5-dioxygenase 2	1	1	Rough ER
P25786	Proteasome subunit alpha type 1	1	2	Cytoplasm, Nucleus
P25789	Proteasome subunit alpha type 4	1	11	Cytoplasm, Nucleus
P28070	Proteasome subunit beta type 4	1	2	Cytoplasm, Nucleus

Appendix 3.2 (continued)

Uniprot ID	Protein name	Peptide Count	Scan Count	Subcellular location
O60888	Protein CutA	1	8	membrane
Q92520	Protein FAM3C	1	3	Secreted
P06703	Protein S100-A6	1	14	Cytoplasm, Nucleus
P61457	Pterin-4-alpha-carbinolamine dehydratase	1	2	Cytoplasm, Nucleus
O95084	Serine protease 23	1	1	Secreted
O75830	Serpin I2	1	25	Secreted
P61956	Small ubiquitin-related modifier 2	1	9	Nucleus
P18827	Syndecan-1 precursor	1	2	Membrane
O60347	TBC1 domain family member 12	1	1	N/A
Q08629	Testican-1	1	1	Secreted
O75347	Tubulin-specific chaperone A	1	1	Cytoplasm
P30530	Tyrosine-protein kinase receptor UFO	1	5	Membrane

Chapter 4: Identification of Novel Substrates for the Serine Protease HTRA1 in the Human RPE Secretome

A SNP in promoter region of HTRA1 has been identified as genetic risk factor for AMD. In this chapter, the status of HTRA1 expression in RPE cells was examined and potential HTRA1 substrates were screened to understand its role in AMD pathology.

This chapter has been submitted as a manuscript for publication.

Eunkyung An[1,2], Supti Sen[1], Sung Kyu Park[3], Heather Gordish-Dressman[1], Kristy J. Brown[1] and Yetrib Hathout[1].

1. Research Center for Genetic Medicine, Children's National Medical Center, Washington, DC.
2. Program in Biochemistry and Molecular Genetics, Institute for Biomedical Sciences, The George Washington University, Washington, DC.
3. Department of Cell Biology, The Scripps Research Institute, 10550 North Torrey Pines Road, SR11, La Jolla, CA.

Correspondence should be addressed to:

Yetrib Hathout
Research Center for Genetic Medicine
Children's National Medical Center
111 Michigan Ave NW
Washington, DC 20010
yhathout@cnmcresearch.org
Telephone number: (202) 476-3136
Fax number: (202) 476-6014

4.1 Abstract

Purpose: To define a role of the serine protease HTRA1 in Age-related Macular Degeneration (AMD) by evaluating its expression in primary RPE cells derived from donors with wild type or *HTRA1* promoter risk variant and by identifying potential HTRA1 substrates in the RPE extracellular milieu.

Methods: Primary RPE cell cultures were established from human autopsy eyes and screened for *CFH, ARMS2* and *HTRA1* risk genotypes using TaqMan assay. HTRA1 expression in genotyped RPE cells was determined using real time PCR and quantitative proteomics. Potential HTRA1 substrates were identified by incubating RPE conditioned media with or without human recombinant HTRA1. Selectively cleaved proteins were quantified using differential stable isotope labeling by amino acids in cell culture strategy.

Results: *HTRA1* mRNA levels were 3 fold higher in primary RPE cells homozygous for the *HTRA1* promoter risk allele than in RPE cells with the wild type allele. This translated into a 2-fold increase in HTRA1 levels in RPE secretome with the risk genotype. A total of 196 extracellular proteins were identified in the RPE secretome and only 5 were found selectively cleaved by the human recombinant HTRA1. These include fibromodulin with 90% cleavage, clusterin (50%), ADAM9 (54%), vitronectin (54%) and alpha 2 macroglobulin (55%).

Conclusions: Recombinant HTRA1 cleaves RPE secreted proteins involved in regulation of the complement pathway (clusterin, vitronectin and fibromodulin) and of amyloid deposition (clusterin, alpha 2 macroglobulin and ADAM9). These findings suggest a potential link between HTRA1, complement regulation and amyloid deposition in AMD pathogenesis.

4.2 Introduction

Major advances in our understanding of age related macular degeneration (AMD) genetics have occurred over the last few years[33-36,50-54]. Three strong genetic loci predisposing to AMD have been identified to date, the CFH variant (rs1061170, CFH Y402H), the *HTRA1* promoter variant (rs11200638, - 512 G>A) and the *ARMS2* variant (rs10490924, A69S)[33-36,50-54]. However, it is not clear how these functionally unrelated genes lead to the predominant pathological features in AMD[203] (e.g., drusen formation and/or CNV). Additionally, the HTRA1 and ARMS2 polymorphisms are in high LD making it difficult to pinpoint the causal gene[50-53]. While the original studies showed that an *HTRA1* promoter variant results in increased expression of HTRA1 protein[52,53], later studies have challenged these findings and suggested that an *ARMS2* variant is the causal factor[54,55]. In this study, we sought to examine the status of HTRA1 expression and define its potential substrates in the context of the extracellular milieu of RPE cell, which approach may provide insights into the role of HTRA1 in AMD pathogenesis.

HTRA1 is member of the high temperature requirement A family of serine proteases compromising three other members: High temperature requirement protease 2 (HTRA2), High temperature requirement protease 3 (HTRA3) and High temperature requirement protease 4 (HTRA4). The exact role of these different types of HTRAs is not well understood. However, all seem to exhibit a non specific protease activity. HTRA1 is a 50 kDa secreted protein composed of signal peptide, an insulin growth factor binding domain, a Kazal like protease inhibitor domain, a conserved serine protease domain and a PDZ domain (Figure 4.1). HTRA1 is expressed in a variety of tissue and organs with the highest levels in placenta and mature epidermis[204].

Figure 4.1 Schematic structure of full length human HTRA1 protein

Boxes represent protein domains and numbers indicate amino acid position.

SP: signal peptide domain (1-22) cleaved in mature secreted protein; IGFBP: insulin growth factor binding protein domain (33-100); Kazal-like: Kazal like domain has similar structure as Kazal type serine protease inhibitors. This domain may be responsible for inhibition of auto cleavage of HTRA1(101-155). Serine protease domain: contains histidine, aspartate, and serine (HDS) as catalytic triad (204-364); PDZ: Post synaptic density protein (PDS95), *Drosophila* disc large tumor suppressor (Dlga), and zonula occludens-1 protein (zo-1) domain) (365-467) recognizes a broad range of hydrophobic polypeptides of HTRA1 substrate.

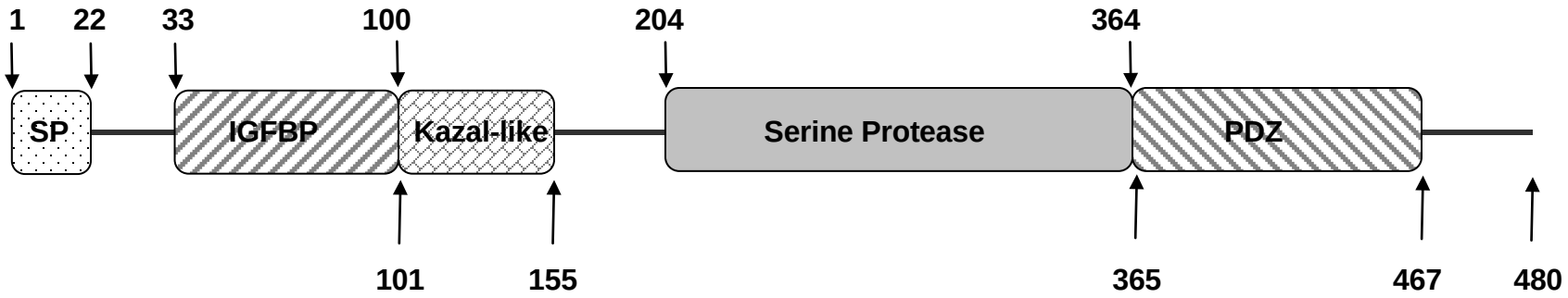
1
22
33
100
204
364
SP
IGFBP
Kazal-like
Serine Protease
PDZ
101
155
365
467
480

Altered expression of this protein has been associated with a number of pathological conditions including AMD[52,205]. While low levels of HTRA1 are reported in many cancer lines and tumors[61-63,206], high levels of HTRA1 are reported in rheumatoid arthritis[64], osteoarthritis[64,207,208], Alzheimer's disease[209] and Duchenne muscular dystrophy[66]. Moreover, a single nucleotide polymorphism (SNP) in the promoter region of *HTRA1* was recently identified as a major genetic risk factor for AMD[52,53] with odd ratios similar or even greater than those reported for CFH[52]. *In vitro* studies have shown that HTRA1 is involved in the degradation of number of proteins including tubulins[67], insulin growth factor binding protein-5[210], amyloid precursor[209], fibronectin[64] and aggrecan[211]. However, little is known about the expression of this protein and its substrate specificity in the context of RPE extracellular environment.

4.3 Materials and Methods

4.3.1 Establish Primary RPE cell culture from Postmortem Autopsy Eyes

Eye globes or poles of Caucasian donors were received through the National Disease Research Interchange (NDRI, Philadelphia, PA). Donors included both male and female with and without clinical history of AMD. Donors with diabetes or other known ocular disease were excluded from this study. Eye globes were obtained on average 9 hours (h) after death and delivered to our laboratory in less than 24 h. Serology tests were performed by NDRI of each donor to exclude samples with potential infectious diseases. Primary RPE cell cultures were prepared according to Engelmann and Valtink[212] with slight modifications. Briefly, the anterior segment from each donor eye was removed by cutting around the iris. The eye cup was opened flat by five incisions along the sclera. One cm^2 of central retinal region was excised for this experiment. Neurosensory retina was removed from the excised piece with forceps and the RPE/choroid layer was separated from sclera and washed gently with PBS containing penicillin (100 U/mL) and streptomycin (100 µg/mL). The RPE/choroid was then incubated in 0.5 mg/ml of collagenase mixture IA + IV (1:1) for 5 h. The suspension containing RPE cells was carefully transferred to a sterile centrifuge tube and pelleted by centrifugation at 100 X g for 5 min. The cell pellet was resuspended in DMEM/F12 supplemented with 10 % FBS, 100 U/mL penicillin, and 100 µg/mL streptomycin and was seeded on 0.1 % gelatin coated plate. Growing cultures were tested for their epithelial cell content using an established immunochemical staining for cytokeratin 18[116,161,213]. All these cultures were frozen at the second passage for subsequent studies.

4.3.2 Screening RPE cultures for AMD risk genotypes (HTRA1, ARMS2 and CFH)

DNA was extracted from each of the RPE cultures and screened for *HTRA1*, *ARMS2* and *CFH* gene variants using allele discrimination TaqMan assay[26]. Allele specific PCR reaction for each SNP was performed with 30 ng of genomic DNA, 900 nM of forward and reverse PCR primers and 200 nM of fluorescent VIC® and FAM™ allele discrimination probes in a final volume of 8 µL. The PCR reaction was performed at 95 °C for 11 min and 44 cycles of 15 s at 92 °C and 1 min at an annealing temperature of 60 °C. Reactions were performed using a MWG robot, and fluorescence ratios and allele calling measured using an ABI 7900 (Applied Biosystem, Foster City, CA).

For the *HTRA1* variant (rs11200638; -512 G>A), the following forward and reverse primers (F: 5'-CTGCCAGCTCCGCGGACGCT-3', R: 5' CCCCGCGGTCAGGGTCCC-G-3') and the following fluorescent allele discrimination probes (WT-VIC®-5'-TCGTCCG-GCCGCA-3'; MT-FAM™-5'-TCGTCCAGCCGCA-3') were used. The following forward and reverse PCR primers (F: 5'-CTTATTTATTTATCATTGTTATG-GTCCTTAGGAA-AATGTTATTT-3' and R: 5'-GGCAGGCAACGTCTATAGATTTA-CC-3') and the following fluorescent allele discrimination probes (WT: VIC®-5'-TTTCTTCCATAATTT-TG-3'; MT-FAM™-5'-TTTCTTCCATGATTTTG-3') were used to screen for the CFH variant (rs1061170; 1227 T>C). For *ARSM2* variant (rs10490924; 270 G>T,) pre-designed primers and probes (Assay ID C__29934973_20, Applied Biosystems, Foster City, CA) were used.

4.3.3 Measurements of HTRA1 expression in RPE cells

A. qRT-PCR: To quantify *HTRA1* expression at the mRNA level, total RNA was extracted from RPE cultures with wild type genotype GG (n = 11), heterozygous risk allele GA (n = 7) and homozygous risk allele AA (n = 3) for the *HTRA1* promoter region using TRIzol (Invitrogen, Carlsbad, CA) according to the manufacturer's instructions. Each extracted RNA sample was treated with DNAse-I and cDNA was synthesized using SuperScript III first-Strand Synthesis kit (Invitrogen, Carlsbad, CA) with oligo dT primer. qRT-PCR was performed on ABI 7900 with 20X *HTRA1* primers and probe (Assay ID Hs01016151_m1, Applied Biosystems, Foster City, CA) and 20 X Glyceraldehyde-3-phosphate dehydrogenase (GAPDH) primers and probe for the control. Relative quantification was performed using the comparative threshold (CT) method after determining the CT values for reference (*GAPDH*) and target (*HTRA1*) genes in each sample sets according to the $2^{-\Delta\Delta Ct}$ method ($\Delta\Delta$CT, delta-delta CT)[214] as described by the manufacturer (ABI; User Bulletin 2).

B. Western Blot analysis: To quantify HTRA1 expression at the protein level, RPE cells with heterozygous or homozygous risk alleles, as well as RPE cells with the wild type genotype, for *HTRA1* promoter region were cultured in 10 cm dishes. After confluence, cultures were washed 6 times with sterile PBS and incubated with serum free medium for another 24 h. Conditioned media were collected, filtered though 0.2 µm Polyethersulfone syringe filter (Corning Inc, Corning, NY) and assayed for protein concentration using Bradford assay (Pierce, Rockford, IL). Equal amounts of proteins (10 µg) from each sample were concentrated by vacuum centrifugation and resuspended in 14 µL of 50% Laemmli buffer (Bio-Rad, Hercules, CA). Proteins were separated by SDS-PAGE under

reducing condition and transferred to nitrocellulose membrane (Amersham Biosciences, Piscataway, NJ) for western blot analysis. Nonspecific binding sites were blocked with 5 % milk (BioRad, Hercules, CA) and membrane was incubated overnight with rabbit polyclonal antibody against human HTRA1 (1:1K, Abcam, Cambridge, MA) in 2.5 % milk. Next day, the membrane was rinsed with Tris buffer containing salt and Tween and incubated with goat anti-rabbit IgG (1:3K, BioRad, Hercules, CA) conjugated with horseradish peroxidase. Immunoblots were visualized by chemiluminescence (Amersham Biosciences, Piscataway, NJ), and Ponceau red was used to control for protein loading.

C. Targeted mass spectrometry quantification of RPE secreted HTRA1: The concentration of stable isotope labeled HTRA1 protein was determined by mass spectrometry after spiking conditioned medium of SILAC labeled RPE cells grown in the presence of $^{13}C_6$-Arg, $^{13}C_6$,$^{15}N_2$-Lys with known amounts of human recombinant HTRA1. The stock of stable isotope labeled HTRA1 was then used as a standard to spike conditioned media collected from RPE cultures with wild type, heterozygous or homozygous genotype for the *HTRA1* promoter risk allele. Spiked samples were resolved on SDS-PAGE and the bands in the 50K region were excised and in gel-digested with trypsin. Resulting peptides were extracted and analyzed by LC-MS/MS as described below.

4.3.4 Proteomics analysis of HTRA1 substrates

Potential HTRA1 substrates were identified in the conditioned media of RPE cells using differential SILAC where one set of cells are grown in $^{13}C_6$-Arg, $^{13}C_6$, $^{15}N_2$-Lys containing medium while the other set are grown in regular medium containing $^{12}C_6$-Arg, $^{12}C_6$,$^{14}N_2$-Lys[161]. Aliquots of unlabeled conditioned medium containing 50 µg total proteins

were concentrated 4 times to reduce the volume using vacuum centrifugation, then incubated with human recombinant HTRA1 (Invitek, Berlin, Germany) at 37 °C for 4 h (enzyme to total proteins ratio, 1:100, w/w) and for 20 h (enzyme to total proteins ratio, 1:200, w/w) while similar aliquots of SILAC labeled medium were left untreated. To validate the data, a reverse experiment was performed where SILAC labeled samples were treated with HTRA1 while unlabeled sample were kept untreated [215]. Treated and untreated sample pairs were then mixed at 1:1 and further concentrated using 30 kDa cut off filter (Millipore Corporation, Billerica, MA) and processed for SDS-PAGE and mass spectrometry analysis. After staining the gel with Bio-Safe Coomassie (Bio-Rad, Hercules, CA), each lane was sliced into 65 bands and each band was in gel digested with trypsin and the resulting peptides analyzed by LC-MS/MS as described below. To validate the proteomic results, human recombinant clusterin (R&D Systems, Minneapolis, MN) and human purified CFH, C3b and C3 (Complement Technology, Tyler, TX) were incubated with HTRA1 for 6 h (enzyme to recombinant protein ratio, 1:25).

4.3.5 Liquid chromatography-tandem mass spectrometry

LC-MS/MS was performed on a nano HPLC system (NanoLC 2D, Eksignet, Dublin, CA) connected to a hybrid LTQ/Orbitrap instrument (Thermo Fisher Scientific, San Jose, CA). Eluting peptides were introduced into the mass spectrometer via a 10 μm silica tip (New Objective Inc., Ringoes, NJ) adapted to a nano-electrospray source (Thermo Fisher Scientific Inc, Waltham, MA). The spray voltage was set at 1.3 kV and the heated capillary at 180 °C. The LTQ/Orbitrap was operated in data-dependent mode in which one cycle of experiments consisted of one full-MS survey followed by three sequential pairs of

intercalated MS/MS experiments. The targeted ion counts in the ion trap during full-MS, and MS/MS were 30,000 and 10,000, respectively. MS measurements were performed with the Orbitrap at 60,000 resolution and accuracy better than 5 ppm. Peptides were fragmented in the linear ion trap using collision-induced dissociation with the collision gas (helium) pressure set at 1.3 milliTorrs and the normalized collision energy value set at 35%.

4.3.6 Database Search and Quantification

Protein identification was performed using Bioworks 3.3 software package equipped with Sequest search engine against human SwissProt database (UniProtKB/Swiss-Prot release 15.4 of June 2009) indexed with assumptions for fully enzymatic tryptic cleavage with two missed cleavages and the following possible protein modifications: 16 Da shift for oxidized Met and 6 and 8 Da shifts for stable isotope labeled Arg and Lys, respectively. The search result was filtered with DTASelect using the following acceptance criteria: DeltaCn (ΔCn) > 0.08, a variable threshold of *Xcorr vs* charge state (*Xcorr* $\geq$ 1.8 for z = 1, *Xcorr* $\geq$ 2.5 for z = 2, and *Xcorr* $\geq$ 3.5 for z = 3, and *XCorr* $\geq$ 4.5 for z = 4). MS spectra for each identified peptide were extracted from raw data using Raw_Xtractor. Census, a proteomics quantification software, was used to generate extracted ion chromatogram (XIC) for each peptide and measure protein ratios in SILAC labeled versus unlabeled samples. Data were checked for validity by spectral visualization [216].

4.4 Results

4.4.1 Human primary RPE cell cultures and genotyping

We have collected autopsy eyes from 34 donors and established 30 primary RPE cultures. Donor's mean age is 65 years, and average time from death to enucleation is 9 h. Cells were sub-cultured to validate their epithelial origin and to screen for AMD associated SNPs (*CFH*, *HTRA1* and *ARMS2*), as described in the Methods. Detailed information about the gender, age, clinical history and genotype of each donor are reported in the supplemental Table 4.S1. The overall genotype distribution of the 30 established RPE cultures is shown in Table 1. Only 8 of the donors were found to harbor the wild type genotype for CFH, HTRA1 and ARMS2. The remaining 22 donors were heterozygotes and/or homozygotes for at least one of the three candidate genes. *HTRA1* and *ARMS2* variants were found to be in complete LD in our small sample pool and this is in agreement with a previous study[57]. Seven of the donors had a clinical history of AMD; as indicated in parentheses under each group in Table 1. Interestingly, six out of the seven clinically documented AMD donors harbored at least one of the at-risk gene variants. The single donor carrying a diagnosis of AMD but without any currently identified risk allele was reported to smoke 2 packs of cigarettes per day for 40 years.

Table 4.1 Distribution of AMD risk genotypes among the established human primary RPE cell cultures (n=30)

		HTRA1/ARMS2		
		GG/GG[a]	GA/GT[b]	AA/TT[c]
CFH	TT[a]	8 (1)	3	1
	TC[b]	4 (1)	8 (2)	2 (1)
	CC[c]	1	2 (1)	1 (1)

[a]wild type [b]heterozygote [c]homozygote risk.

4.4.2 Quantitative analyses of HTRA1 expression in genotyped RPE cells

To examine the effect of *HTRA1* promoter polymorphism on the expression levels of HTRA1, we selected 21 actively growing RPE cultures including 11 with wild type genotype GG, 7 with heterozygous genotype GA, and 3 with homozygous genotype AA for the risk allele in promoter region of the *HTRA1* gene. HTRA1 expression was examined in these cells both at the mRNA and protein levels. The HTRA1 mRNA levels were 3 fold and 1.5 fold higher in primary RPE cultures with homozygous risk allele and heterozygous risk allele for the HTRA1 promoter, respectively, than in primary RPE cultures with wild type homozygous genotype (Figure 4.2A). This was further confirmed by western blot analysis of HTRA1 protein in the conditioned medium collected from RPE cultures with different *HTRA1* promoter genotypes (Figure 4. 2B).

To further validate our western blot analysis we performed absolute quantitative analysis of the HTRA1 protein in RPE secretome using stable isotope labeled HTRA1 as a standard and mass spectrometry. We first determined the concentration of HTRA1 secreted by SILAC labeled RPE cells grown in $^{13}C_6$-Arg, $^{13}C_6$, $^{15}N_2$-Lys by spiking their conditioned medium with 200 ng/mL of recombinant unlabeled HTRA1 (Figure 4.3). The average intensity ratio of unlabeled and labeled peptide pairs from the recombinant HTRA1 and the RPE secreted HTRA1 respectively was found equal to 0.1 ± 0.01 and was used to calculate the amount of RPE secreted HTRA1. This RPE cell culture secreted about 20 ± 1.49 ng/mL of HTRA1 (Fig. 3D). Having validated the approach, a known amount of the established stable isotope labeled HTRA1 standard was spiked into the conditioned media collected from unlabeled primary RPE cultures with different genotypes for the *HTRA1* promoter risk allele. HTRA1 levels were about two times elevated in RPE cells with

homozygous genotype for the *HTRA1* promoter risk allele (44 ± 1.13 ng/mL) and in RPE cells with heterozygous genotype for the *HTRA1* prompter risk allele (44 ± 13.34 ng/mL) than in RPE cells with wild type genotype for the *HTRA1* promoter (24 ± 3.55 ng/mL) (Figure 4.4).

Figure 4.2 Expression levels of HTRA1 mRNA and protein in human RPE cell cultures derived from donors with wild type and at risk genotype for the HTRA1 promoter region

A) qRT-PCR of *HTRA1* mRNA levels in primary RPE cultures. Samples were prepared from RPE cultures with wild type (n = 11), heterozygote (n = 7) and homozygote (n = 3) genotype for the *HTRA1* promoter risk allele (G is the wild type allele and A is the risk allele). Total RNA was isolated from cultured RPE cells as described in the methods. cDNA was prepared by reverse transcription using SuperScript III first-strand Synthesis kit. qRT- PCR was performed using forward and reverse primers recognizing exons 6 and 7 of the *HTRA1* gene. *HTRA1* mRNA transcript levels were measured using an ABI 7900HT system according to manufacturer's instructions. All values were normalized to wild type GG genotype. B). Western blot analysis of HTRA1 protein levels in the conditioned media of RPE cultures. RPE cells with wild type genotype GG (n =3), at risk heterozygous genotype AG (n = 3) and at risk homozygous genotype AA (n = 3) were grown in serum containing medium. After confluence, the medium was replaced with serum free medium for 24 h. Media were collected, equal amounts of proteins (10 μg) from each sample were concentrated and resolved by SDS-PAGE for western blot analysis. HTRA1 band intensities were normalized to total loaded proteins. Error bars represent standard error between 3 replicate samples.

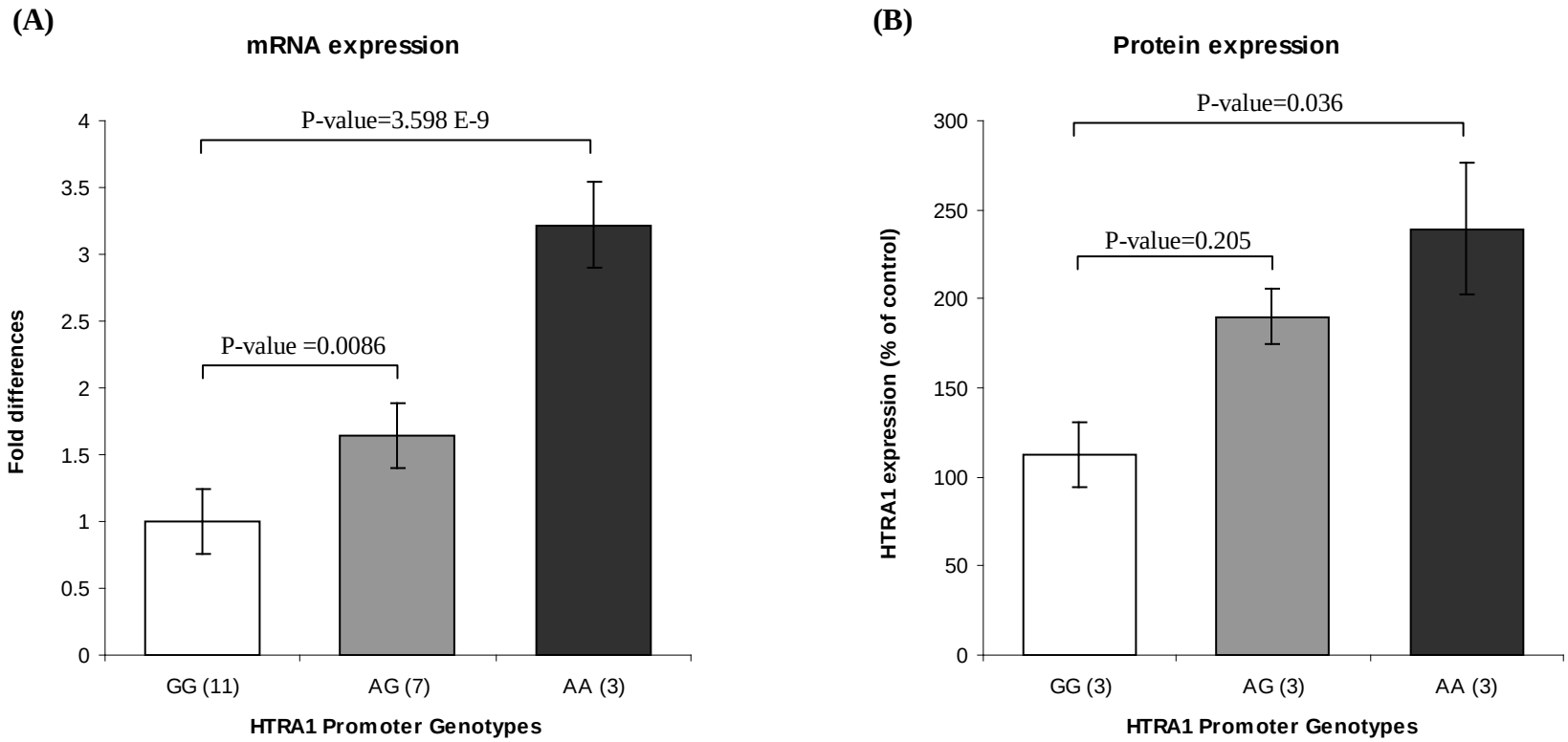
(A)
mRNA expression
P-value=3.598 E-9
P-value =0.0086
Fold differences
4
3.5
3
2.5
2
1.5
1
0.5
0
GG (11)
AG (7)
AA (3)
HTRA1 Promoter Genotypes
(B)
Protein expression
P-value=0.036
P-value=0.205
HTRA1 expression (% of control)
300
250
200
150
100
50
0
GG (3)
AG (3)
AA (3)
HTRA1 Promoter Genotypes

Figure 4.3 Stable isotope labeled standard for absolute quantification of HTRA1 protein

Conditioned medium collected from a fully labeled RPE culture grown in medium containing $^{13}C_6$-Arg and $^{13}C_6$, $^{15}N_2$-Lys was spiked with human recombinant unlabeled HTRA1 at a final concentration of 200 ng/mL. Samples were run on SDS-PAGE, bands were sliced, digested by trypsin and the resulting peptides analyzed by LC-MS/MS. (A) SDS-PAGE of total secreted proteins collected from a 24 h RPE culture grown in SILAC labeled serum free medium. As expected HTRA1 protein was identified with six different peptides around 50K in boxed area. (B) Example of a mass spectrum for the YNFIADVVEK peptide of HTRA1. This peptide was detected as a pair of unlabeled (599.31 *m/z*) and labeled peptide (603.31 *m/z*) both as doubly charged ions. Both these peptides were sequenced and their mass difference of 8 Da (4 Da for the doubly charged ions) agrees with a Lys residue at the C terminal. (C) Intensity ratio of heavy to light peak was determined from extracted ion chromatogram (XIC) for unlabeled and labeled peptide pairs using Census software and reflects the ratio of endogenous RPE HTRA1 to the recombinant HTRA1. (D) A total of six peptide pairs were detected for HTRA1 and the ratios between unlabeled and labeled peptide pairs was measured. Since the amount of recombinant HTRA1 added to the conditioned medium is known, it allowed us to calculate that 10 cm culture dish containing 3 x 10^6 RPE cells secrete about 20 ± 1.49 ng/mL of HTRA1 in 20 h.

(A)

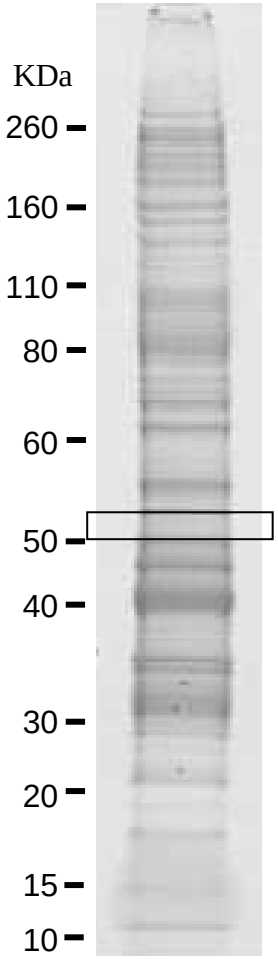

(B)

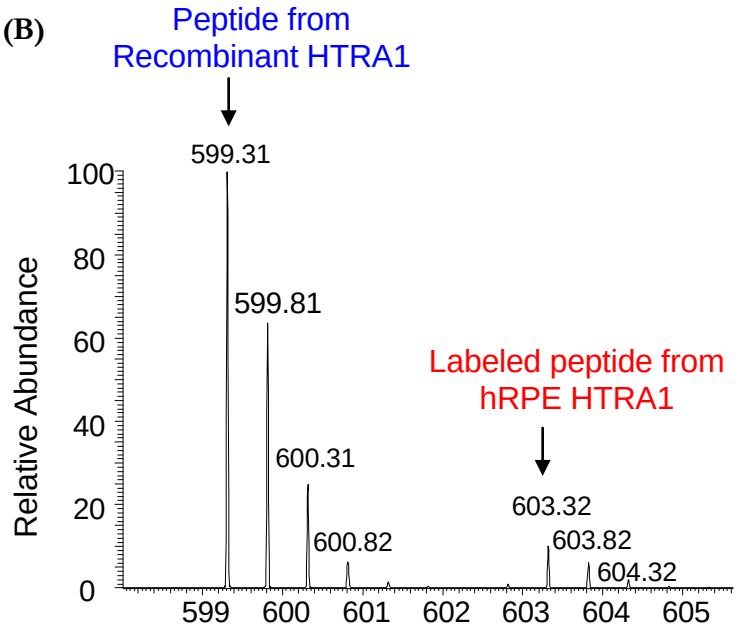

(C)

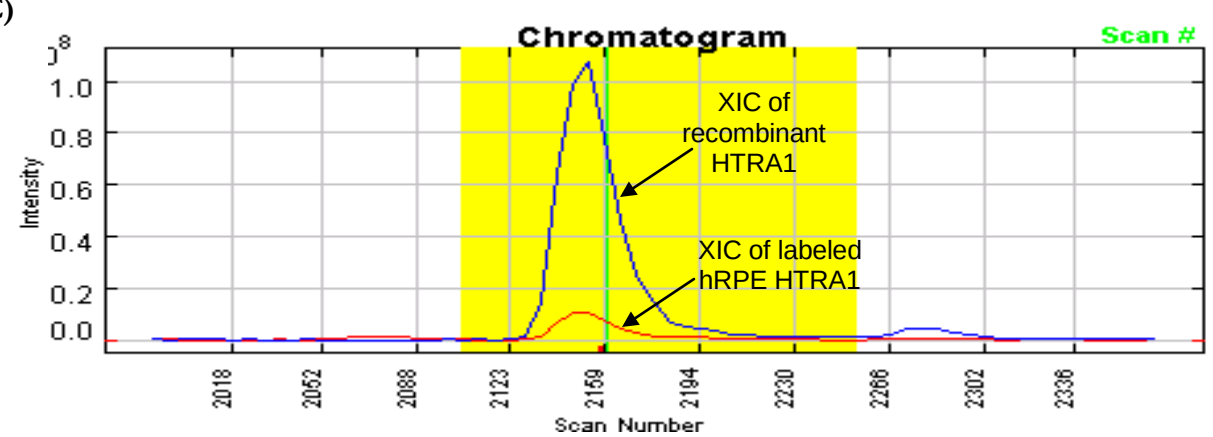

(D)

Peptides	Ratio (L/U)
LPVLLLGR	0.09
IAPAVVHIELFR	0.09
LHRPPVIVLQR	0.09
KFLTESHDR	0.10
YNFIADVVEK	0.10
VTAGISFAIPSDK	0.10
	0.10 ± 0.01

Figure 4.4 Effect of the HTRA1 promoter genotype on HTRA1 expression in RPE culture

Stable isotope labeled HTRA1 (20 ng/mL) was used as a standard to spike conditioned media collected from fully confluent RPE cultures with homozygous wild type genotype GG (n = 5), heterozygous at risk genotype GA (n = 3), and homozygous at risk genotype AA (n = 2) for the *HTRA1* promoter. The quantities of secreted HTRA1 were calculated from intensity ratios of light and heavy peptide pairs detected from the unlabeled RPE secreted HTRA1 and the stable isotope labeled HTRA1 standard. Error bars represent standard deviation between replicate samples used for each genotype.

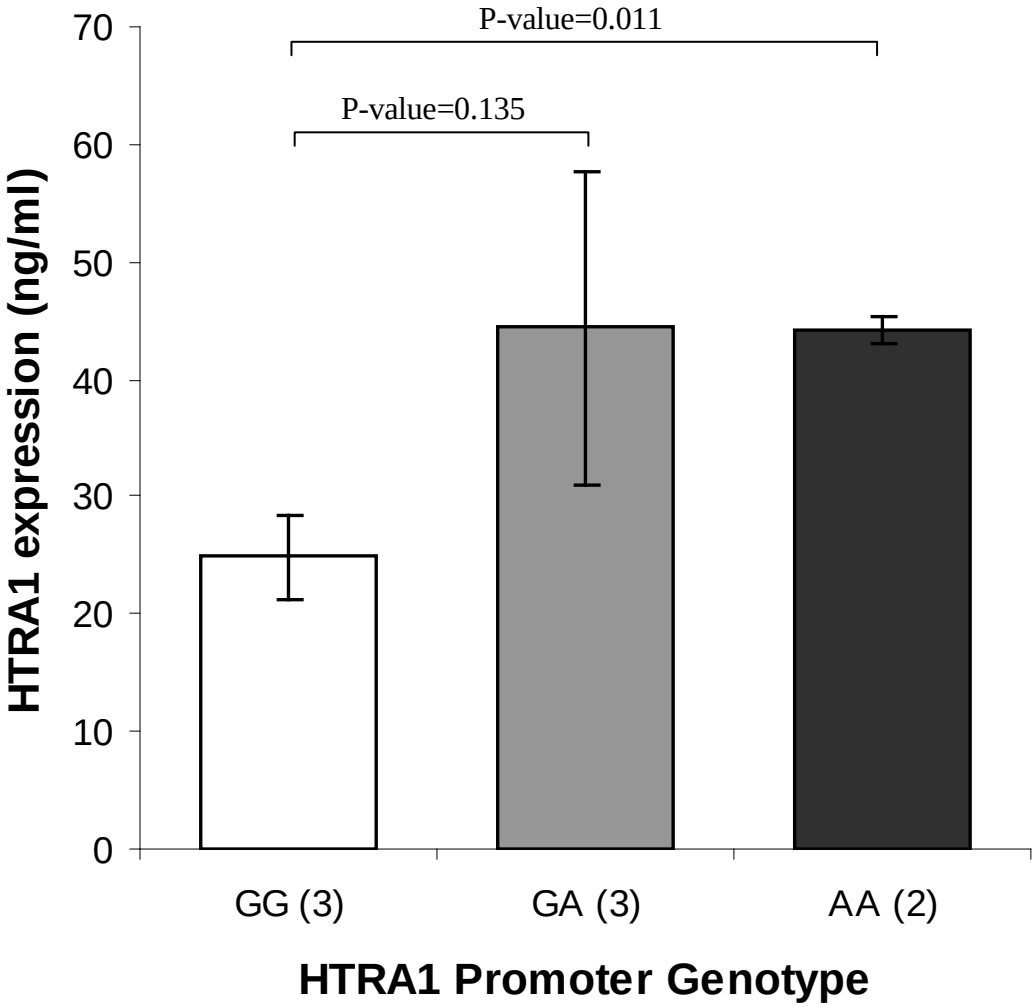
P-value=0.011
P-value=0.135
70
60
50
40
30
20
10
0
HTRA1 expression (ng/ml)
GG (3)
GA (3)
AA (2)
HTRA1 Promoter Genotype

4.4.3 Screening for HTRA1 substrate in RPE cell conditioned media

Differential SILAC strategy[110] in combination with SDS-PAGE and LC-MS/MS allowed both detection and quantification of proteins that were selectively cleaved by the recombinant HTRA1. A total of 196 extracellular proteins were identified and quantified in the primary RPE conditioned media (supplemental Table 4.S2). However, only 5 of these 196 proteins were found to be selectively cleaved by HTRA1. This approach is exemplified for clusterin protein (Figure 4.5). The clusterin ratio between SILAC labeled and unlabeled sample remained at 1:1 when both samples were untreated, but decreased to 0.5 in HTRA1 treated versus untreated samples, demonstrating that HTRA1 degraded clusterin under the experimental conditions employed. Specific degradation of clusterin was further confirmed by the detection of clusterin peptides in lower bands (~ 35 Da) in HTRA1 treated samples versus untreated samples (see supplemental Figure 4.S1).

The five proteins that were degraded by HTRA1 -- fibromodulin, alpha 2 macroglobulin, vitronectin, ADAM9, and clusterin -- are reported in Table 4.2 with their accession number and their ratios in HTRA1 treated versus untreated samples. Fibromodulin was the most affected protein since its levels deceased by 70% and by > 90% after treatment with HTRA1 for 4 h and 20 h, respectively. Similarly clusterin, vitronectin and alpha-2 macroglobulin were decreased by more than 50% after 20 h treatment with HTRA1. The increased degradation of alpha-2 macroglobulin in 4 h versus 20 h incubation with HTRA1 is not understood and needs further examination.

To evaluate whether HTRA1 cleaved clusterin, a major component of drusen and a regulator of the complement pathway, we verified its degradation using purified recombinant proteins for HTRA1, as well as for CFH, C3 and C3b, components of the

complement pathway. Figure 4.6 shows SDS-PAGE migration pattern of these four human purified proteins incubated with or without HTRA1. Two µg of each protein were incubated with 0.08 µg (0.4 pM) of recombinant HTRA1 for 6 h at 37 °C. While clusterin was significantly degraded by HTRA1 (> 50% degradation), CFH, C3 and C3b remained intact, clearly demonstrating that clusterin is a specific substrate for HTRA1.

Figure 4.5 Differential SILAC strategy to screen for HTRA1 substrates in RPE conditioned medium

Top figure: SILAC labeled or unlabeled conditioned media were incubated with (+) or without (-) HTRA1 (500 ng) for 20 h at 37°C. Treated and untreated conditioned media were then mixed at 1:1 ratio and processed for SDS-PAGE and LC-MS/MS as described in the Methods. Clusterin was identified by 15 labeled and unlabeled peptide pairs in the RPE secretome. Bottom figure shows mass spectra for one of the clusterin peptide detected as pair of SILAC labeled and unlabeled peptide. The intensity ratio of these peaks was equal to 1 when both samples were untreated with HTRA1 (left panel), but dropped to 0.5 in treated versus untreated sample pairs (center and right panel). This clearly indicates that clusterin was degraded by HTRA1.

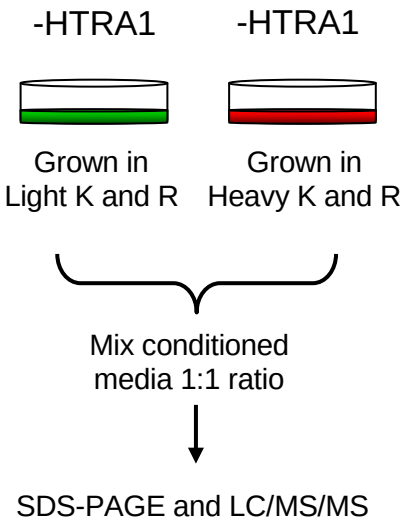
-HTRA1
-HTRA1
Grown in
Light K and R
Grown in
Heavy K and R
Mix conditioned
media 1:1 ratio
SDS-PAGE and LC/MS/MS

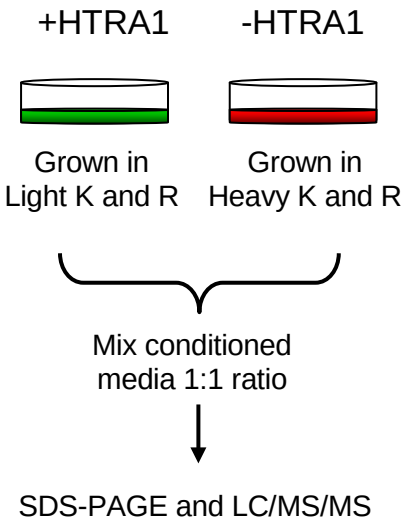
+HTRA1
-HTRA1
Grown in
Light K and R
Grown in
Heavy K and R
Mix conditioned
media 1:1 ratio
SDS-PAGE and LC/MS/MS

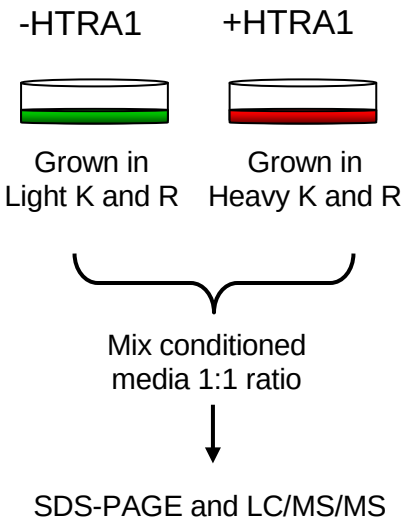
-HTRA1
+HTRA1
Grown in
Light K and R
Grown in
Heavy K and R
Mix conditioned
media 1:1 ratio
SDS-PAGE and LC/MS/MS

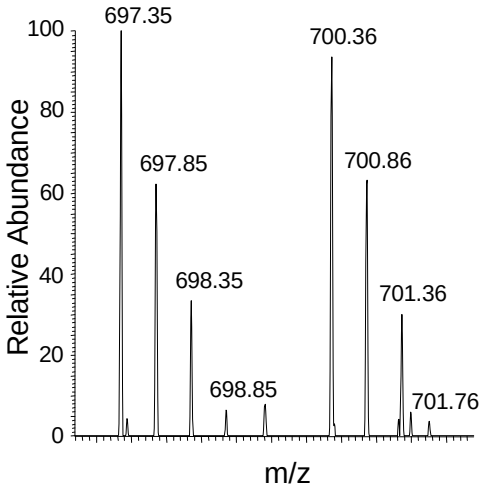
Relative Abundance
m/z
697.35
697.85
698.35
698.85
700.36
700.86
701.36
701.76

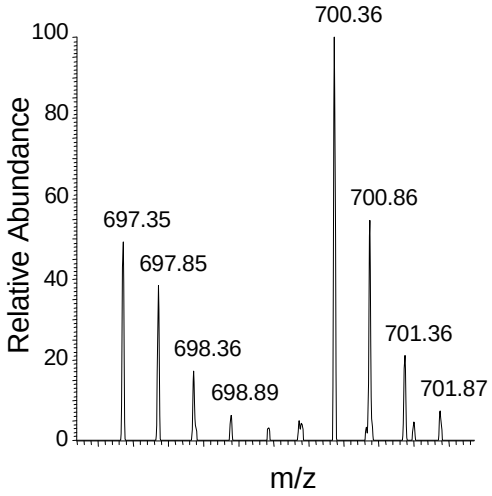
Relative Abundance
m/z
697.35
697.85
698.36
698.89
700.36
700.86
701.36
701.87

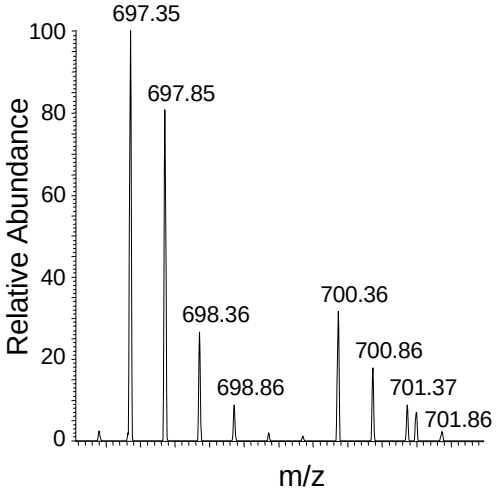
Relative Abundance
m/z
697.35
697.85
698.36
698.86
700.36
700.86
701.37
701.86

Table 4. 2 List of potential HTRA1 substrates identified in the RPE conditioned medium

Protein name	Accession #	Control (-)HTRA1/(-)HTRA1	4 h (+)HTRA1/(-)HTRA1	20 h (+)HTRA1/(-)HTRA1
Fibromodulin	Q06828	1.13 ± 0.15	0.32 ± 0.01	0.13 ± 0.00
Alpha-2-macroglobulin	P01023	0.90 ± 0.02	0.16 ± 0.00	0.45 ± 0.00
Vitronectin	P04004	1.06 ± 0.42	1.07 ± 0.10	0.46 ± 0.05
ADAM9	Q13443	0.97 ± 0.07	1.01 ± 0.10	0.46 ± 0.11
Clusterin	P10909	1.00 ± 0.08	0.81 ± 0.00	0.48 ± 0.09

ADAM 9: Disintegrin and metalloproteinase domain-containing protein 9

Figure 4.6 Clusterin, as a specific substrate for HTRA1

Shotgun proteome profiling analysis suggested that clusterin is selectively cleaved by HTRA1. To validate this finding 4 recombinant proteins regulator of the complement pathway including human recombinant clusterin, purified human CFH, C3 and C3b were incubated with human recombinant HTRA1. Each protein (2 µg) was incubated with (+) and without (-) recombinant HTRA1 (0.08 µg) for 6 h at 37 °C (enzyme to protein ratio, 1:25, w/w) in 4 µl solution of 50 mM Tris-HCl, pH 7.5, 150 mM NaCl, 5 mM $CaCl_2$. Samples separation was performed on 4-12 % precast gel and visualized with Coommassie blue. While clusterin was significantly degraded by HTRA1 (> 50% degradation) other proteins CFH, C3 and C3b remained intact. First two lines represent HTRA1 alone after 0 and 6 h incubation at 37°C in the same buffer. Arrows denotes HTRA1 itself and * indicates HTRA1 cleaved products.

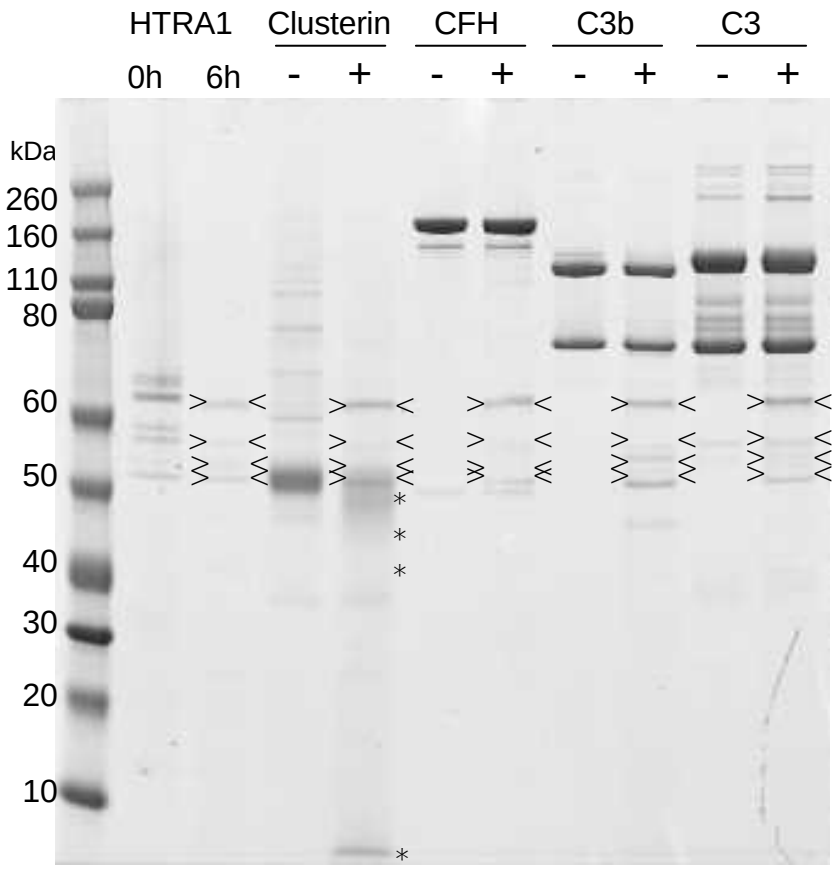
HTRA1
Clusterin
CFH
C3b
C3
0h
6h
-
+
-
+
-
+
-
+
kDa
260
160
110
80
60
50
40
30
20
10

4.5 Discussion

HTRA1 expression was significantly increased in RPE secretome harboring the homozygous genotype for the *HTRA1* promoter risk allele than in RPE cells with wild type genotype. This agrees with the study by Yang *et al*., which shows that *HTRA1* mRNA levels were three times higher in lymphocytes collected from AMD donors than those collected from age matched control donors[52]. Others have demonstrated a similar increase in the HTRA1 mRNA levels in the macular region of autopsy eyes collected from AMD donors with at risk HTRA1 promoter genotype[205].

Local secretion of HTRA1 by RPE cells prompted us to screen for potential substrates in the context of RPE extracellular milieu. Our SILAC strategy readily facilitated high throughput screening for such substrates among several hundred proteins. The HTRA1-cleaved proteins included fibromodulin, clusterin, alpha-2 macroglobulin, ADAM9, vitronectin (Table 4.2) and to some extent TGF-beta (Table S2). Interestingly, fibronectin which has been reported to be a substrate for HTRA1 in arthritis tissues[64] was not affected by HTRA1 treatment in the context of RPE extracellular milieu (see supplement Figure 4.S2).

4.5.1 HTRA1 cleaves proteins involved in complement cascade.

Vitronectin and clusterin are thought to act as fluid phase regulators of the complement pathway by inhibiting the terminal complex formation[217,218]. Additionally, fibromodulin, which was selectively degraded by HTRA1, is also reported to be involved in the regulation complement pathway by inhibiting the alternative pathway by directly binding to CFH[219]. The binding affinity of fibromodulin to the CFH is higher in the case of

Y402 over H402 variant[220]. Degradation of these complement pathway regulators by HTRA1 clearly supports a link between HTRA1 and the complement pathway in AMD pathogenesis. However, further protein-protein interaction studies are needed to confirm this network.

4.5.2 HTRA1 cleaves proteins involved in the regulation of amyloid deposition.

Other interesting proteins that were found selectively cleaved by HTRA1 in the context of RPE extracellular milieu are those involved in the regulation of amyloid deposition. Indeed, both alpha-2 macroglobulin and ADAM9 are involved in processing of amyloid precursor protein. While ADAM9 cleaves the amyloid precursor at the amyloid beta (Abeta) domain and releases a neuroprotective extodomain[221,222], alpha 2 macroglobulin was recently reported to inhibit amyloid fibrils formation[223] probably via sequestering the beta amyloid polypeptide[224]. Moreover, a recent study shows that *ADAM9* knockout leads to retinal degeneration in mice[225] supporting our hypothesis that levels of ADAM9 might be decreased in the presence of high levels of HTRA1 and thus leading to amyloid accumulation in the sub RPE extracellular space. Clusterin was also reported to be a protective chaperone protein against amyloid deposition[226,227] and its degradation by HTRA1 might also contribute to uncontrolled amyloid deposition. The fact that HTRA1 cleaves these proteins strongly supports the indirect implication of HTRA1 in drusen formation. Indeed, amyloid, which is readily secreted by RPE cells (see Supplemental Table 4.S2), is a major component in drusen[143,228] and may be more likely to accumulate in the case where HTRA1 expression is increased (Figure 6.3).

Although preliminary, these data strongly suggest a role for HTRA1 in AMD pathogenesis and link it to both the complement pathway and to amyloid deposition. We suggest that increased expression of HTRA1 in RPE cells with risk genotype will directly affect factors involved in the regulation of complement pathway (e.g. clusterin, vitronectin and fibromodulin) as well as factors involved in regulation of amyloid deposition (clusterin, alpha 2 macroglobulin, ADAM9). However, these pathways remain to be directly verified in human autopsied eyes and/or in AMD animal models when they become available.

4.6 Acknowledgements

We thank all the donors and their families. We also thank Dr. Kristy Brown for her help with mass spectrometry analysis, Drs. Eric P Hoffman and Joseph M Devaney for help with genetic analyses, and Drs. Mary Rose and Anamaris M Colberg-Poley for help with manuscript editing. This research was supported by NIH/NEI grant R21EY016723, and a NEI ARRA administrative supplement R21EY016723-02S109 and partially by the NICHD/NIH core grant 5R24HD050846. Eunkyung An is a predoctoral student in the Biochemistry and Molecular Genetics Program of the Institute for Biomedical Sciences at the George Washington University. This work is from a dissertation to be presented to the above program in partial fulfillment of the requirements for the Ph.D. degree.

Table 4.S1 Donor information: age, gender, AMD history, genotyping of SNPs for CFH, HTRA1/ARMS2, smoking history, cause of death and time of enucleation

Donor	Age	Gender	AMD	SNP		Smoking	Cause of Death	Enucleation
				CFH	HTRA1/ ARMS2			
1	76	M	Normal	TT	AA/TT	N/D	Parkinson's Disease	6
3	57	F	Normal	TC	AA/TT	1ppd for 45 years	Lung cancer with Mets	10
4	78	F	Normal	TT	GG/GG	No	unknown	10
5	81	F	Normal	TT	GA/GT	N/D	Subarachnoidal bleed	4
6	72	M	Normal	TC	GA/GT	quit in 1993	Chronic obstructive pulmonary disease	12
7	61	F	Normal	CC	GG/GG	1 ppd for 40 years	Probable Myocardial infarction	10
8	48	F	Normal	TT	GG/GG	No	Congestive Heart Failure	14
9	68	F	AMD	TT	GG/GG	2 ppd for 40 years	Stroke	3
10	80	M	Normal	CC	GA/GT	quit in 1984	Acute Myocardial infarction	9.4
11	66	F	Normal	TC	GA/CT	quit in 1998	Amyotrophic lateral sclerosis	9.5
12	74	M	Normal	TT	GG/GG	quit in 1980	Myocardial infarction	7.5
13	65	F	Normal	TC	GA/GT	1 ppd duration unknown	Respiratory Arrest	6
14	82	M	AMD	TC	GA/GT	1 ppd for 40 years	Cardial related	12
15	11	M	Normal	TT	GAGT	No	Multiple Trauma	8.5
16	69	M	Normal	TC	GG/GG	1 ppd, quit 1982	Acute Myocardial infarction	13
17	81	M	AMD	CC	AA/TT	N/D	Cardial arrest	10.5
18	59	F	Normal	TT	GG/GG	No	Respiratory Failure	1
19	80	F	AMD	TC	GG/GG	No	GI bleed	9
20	68	F	Normal	TT	GG/GG	No	Chronic obstructive pulmonary disease	8
23	17	M	Normal	TC	GG/GG	N/D	Motor vehicle accident	9
24	75	F	Normal	TC	GAGT	N/D	Respiratory Arrest	4
25	50	M	Normal	TT	GG/GG	No	Myocardial infarction	17
26	62	F	Normal	TC	GA/GT	No	Cardiac arrest	30
27	70	M	Normal	TT	GAGT	2 ppd for 35 years	Probable Myocardial infarction	8
29	62	F	Normal	TC	GA/GT	No	Myocardial infarction	9

30	59	M	Normal	TT	GG/GG	2 ppd for 40 years	Respiratory Failure	6
31	49	M	Normal	TC	GG/GG	a few packs per week	Probable Myocardial infarction	9.5
32	75	F	AMD	TC	AA/TT	No	Pancreatic Cancer	7
33	77	F	AMD	CC	GA/GT	No	throat cancer	5
34	81	M	AMD	TC	GA/GT	Quit in 1970	Cardiocingentic schock	3

[a]A total of 34 autopsy eyes were collected. 30 RPE cell cultures were established.
[b](M = male, F = female, N/D = not determined, ppd = pack per day)

Table 4.S2. List of extracellular proteins identified and quantified in HTRA1 treated and untreated RPE conditioned media

Accession	Protein names	Peptide #	Control (-)/(-)	HTRA1 Treatment		Localization
				4h (+)/(-)	20h (+)/(-)	
Q8NCC3	1-O-acylceramide synthase	3	0.83 ± 0.00	1.17 ± 0.16	1.02 ± 0.36	Secreted
P08253	72 kDa type IV collagenase	13	0.89 ± 0.05	1.03 ± 0.12	1.05 ± 0.06	Secreted
Q8IUX7	Adipocyte enhancer-binding protein 1	13	0.81 ± 0.00	1.29 ± 0.19	1.03 ± 0.05	Secreted
O00468	Agrin	14	0.83 ± 0.09	1.07 ± 0.18	1.02 ± 0.19	Secreted
P01011	Alpha-1-antichymotrypsin	14	1.11 ± 0.08	1.13 ± 0.21	0.98 ± 0.02	Secreted
P01023	Alpha-2-macroglobulin - around 160K	5	0.90 ± 0.02	0.16 ± 0.00	0.45 ± 0.00	Secreted
P01023 *	Alpha-2-macroglobulin - around 60K	6	ND	4.42 ± 0.00	ND	Secreted
P06733	Alpha-enolase	25	1.14 ± 0.10	1.01 ± 0.05	0.70 ± 0.05	Membrane
Q9H4A4	Aminopeptidase B	8	1.09 ± 0.32	0.97 ± 0.11	0.82 ± 0.00	Secreted
P05067	Amyloid beta A4 protein	19	0.82 ± 0.10	1.07 ± 0.14	1.03 ± 0.22	Membrane
P07355	Annexin A2	17	0.77 ± 0.00	1.12 ± 0.18	1.12 ± 0.33	Secreted
Q8NCW5	Apolipoprotein A-I-binding protein	3	1.23 ± 0.48	1.05 ± 0.14	1.11 ± 0.03	Secreted
O75882	Attractin	11	0.90 ± 0.15	1.05 ± 0.03	0.92 ± 0.07	Secreted
P98160	Basement membrane-specific heparan sulfate proteoglycan core protein	27	1.07 ± 0.09	1.06 ± 0.07	1.04 ± 0.05	Secreted
P61769	Beta-2-microglobulin [Cleaved into: Beta-2-microglobulin form pI 5.3]	10	0.98 ± 0.14	1.06 ± 0.04	1.07 ± 0.05	Secreted
P21810	Biglycan	13	0.99 ± 0.10	0.98 ± 0.05	0.93 ± 0.05	Secreted
P43251	Biotinidase	3	0.99 ± 0.08	1.10 ± 0.07	0.90 ± 0.22	Secreted
P13497	Bone morphogenetic protein 1	3	0.86 ± 0.18	1.16 ± 0.31	ND	Secreted
P80723	Brain acid soluble protein 1	9	1.17 ± 0.11	1.03 ± 0.24	1.14 ± 0.28	Membrane
P55287	Cadherin-11	12	1.10 ± 0.08	1.00 ± 0.01	1.04 ± 0.02	Membrane
P55290	Cadherin-13	5	1.05 ± 0.11	1.05 ± 0.16	1.05 ± 0.04	Membrane
P19022	Cadherin-2	12	0.92 ± 0.04	1.06 ± 0.18	1.06 ± 0.29	Membrane
P55285	Cadherin-6	7	0.92 ± 0.23	1.05 ± 0.00	0.93 ± 0.06	Membrane
P27797	Calreticulin	24	1.07 ± 0.05	1.08 ± 0.11	1.00 ± 0.04	Secreted
O94985	Calsyntenin-1	29	0.91 ± 0.03	1.04 ± 0.16	1.03 ± 0.11	Membrane
Q9H4D0	Calsyntenin-2	23	0.87 ± 0.07	1.04 ± 0.16	0.99 ± 0.09	Membrane

O43852	Calumenin	31	1.23 ± 0.10	1.08 ± 0.24	1.09 ± 0.32	Secreted
Q9UI42	Carboxypeptidase A4	22	1.04 ± 0.10	1.04 ± 0.03	1.02 ± 0.00	Secreted
P16870	Carboxypeptidase E	4	0.89 ± 0.11	0.97 ± 0.29	0.94 ± 0.01	Secreted
P49747	Cartilage oligomeric matrix protein	5	0.97 ± 0.03	1.07 ± 0.03	1.01 ± 0.04	Secreted
P13500	C-C motif chemokine 2	5	1.13 ± 0.08	1.06 ± 0.15	1.16 ± 0.20	Secreted
P48509	CD151 antigen	1	1.15 ± 0.00	1.33 ± 0.00	1.14 ± 0.00	Membrane
Q13740	CD166 antigen	4	1.07 ± 0.12	1.19 ± 0.27	1.04 ± 0.03	Membrane
Q8NFZ8	Cell adhesion molecule 4	5	0.97 ± 0.04	ND	1.02 ± 0.23	Membrane
P00450	Ceruloplasmin	11	1.17 ± 0.13	1.05 ± 0.20	0.98 ± 0.14	Secreted
P36222	Chitinase-3-like protein 1	18	1.38 ± 0.09	1.08 ± 0.42	1.04 ± 0.34	Secreted
O00299	Chloride intracellular channel protein 1	3	1.03 ± 0.06	0.73 ± 0.00	0.51 ± 0.07	Membrane
Q9Y696	Chloride intracellular channel protein 4	5	0.98 ± 0.10	0.81 ± 0.04	0.83 ± 0.15	Membrane
P10909	Clusterin	15	1.00 ± 0.08	0.81 ± 0.00	0.48 ± 0.09	Secreted
Q76M96	Coiled-coil domain-containing protein 80	20	0.70 ± 0.09	1.07 ± 0.19	1.06 ± 0.04	Secreted
P02452	Collagen alpha-1	55	1.06 ± 0.11	1.11 ± 0.13	1.03 ± 0.08	Secreted
P02458	Collagen alpha-1	5	1.30 ± 0.29	1.28 ± 0.00	1.06 ± 0.31	Secreted
P02461	Collagen alpha-1	46	1.27 ± 0.13	1.10 ± 0.30	1.07 ± 0.30	Secreted
P02462	Collagen alpha-1	6	0.91 ± 0.10	1.05 ± 0.11	1.09 ± 0.01	Secreted
P12107	Collagen alpha-1	10	1.05 ± 0.03	1.11 ± 0.23	1.07 ± 0.01	Secreted
P12109	Collagen alpha-1	35	1.12 ± 0.06	1.03 ± 0.13	1.03 ± 0.21	Secreted
P20908	Collagen alpha-1	21	1.10 ± 0.17	1.07 ± 0.05	1.07 ± 0.08	Secreted
P39059	Collagen alpha-1	9	1.20 ± 0.09	0.99 ± 0.24	0.88 ± 0.29	Secreted
Q99715	Collagen alpha-1	32	0.97 ± 0.16	1.08 ± 0.00	0.99 ± 0.09	Secreted
P05997	Collagen alpha-2	32	1.08 ± 0.08	1.07 ± 0.13	0.99 ± 0.18	Secreted
P08123	Collagen alpha-2	95	1.05 ± 0.10	1.06 ± 0.02	1.05 ± 0.03	Secreted
P08572	Collagen alpha-2	16	0.87 ± 0.13	1.21 ± 0.05	1.19 ± 0.03	Secreted
P12110	Collagen alpha-2	16	1.10 ± 0.13	1.04 ± 0.07	0.95 ± 0.16	Secreted
P12111	Collagen alpha-3	23	0.63 ± 0.09	1.05 ± 0.44	1.18 ± 0.20	Secreted
Q9BXJ0	Complement C1q tumor necrosis factor-related protein 5	3	0.90 ± 0.04	0.98 ± 0.19	1.06 ± 0.14	Secreted
P00736	Complement C1r subcomponent	12	1.11 ± 0.04	1.05 ± 0.09	1.05 ± 0.19	Secreted

P09871	Complement C1s subcomponent	22	1.08 ± 0.03	1.04 ± 0.05	1.04 ± 0.07	Secreted
P01024	Complement C3	43	0.95 ± 0.10	1.06 ± 0.26	1.11 ± 0.24	Secreted
P0C0L4	Complement C4-A	24	1.29 ± 0.34	1.13 ± 0.28	1.04 ± 0.21	Secreted
P00751	Complement factor B	17	1.37 ± 0.06	1.03 ± 0.33	1.07 ± 0.34	Secreted
P08603	Complement factor H	20	0.98 ± 0.10	1.08 ± 0.08	1.02 ± 0.09	Secreted
Q9UBG0	C-type mannose receptor 2	6	1.10 ± 0.17	1.05 ± 0.05	1.04 ± 0.04	Membrane
P01034	Cystatin-C	7	0.98 ± 0.04	1.01 ± 0.02	1.05 ± 0.03	Secreted
Q15828	Cystatin-M	3	1.00 ± 0.04	1.03 ± 0.16	1.00 ± 0.20	Secreted
P01036	Cystatin-S	3	1.24 ± 0.02	1.21 ± 0.07	1.04 ± 0.17	Secreted
P01037	Cystatin-SN	3	0.90 ± 0.00	1.03 ± 0.12	1.12 ± 0.09	Secreted
P07585	Decorin	12	1.03 ± 0.19	0.97 ± 0.10	0.97 ± 0.22	Secreted
Q9UBP4	Dickkopf-related protein 3	7	0.89 ± 0.04	1.09 ± 0.07	0.86 ± 0.07	Secreted
P27487	Dipeptidyl peptidase 4	27	1.08 ± 0.10	1.07 ± 0.09	0.99 ± 0.02	Secreted
Q96PD2	Discoidin, CUB and LCCL domain-containing protein 2	4	0.93 ± 0.07	ND	1.16 ± 0.22	Membrane
Q13443	Disintegrin and metalloproteinase domain-containing protein 9	2	0.97 ± 0.07	1.01 ± 0.10	0.46 ± 0.11	Membrane
Q13822	Ectonucleotide pyrophosphatase/phosphodiesterase family member 2	37	1.00 ± 0.07	1.06 ± 0.08	1.00 ± 0.17	Secreted
Q12805	EGF-containing fibulin-like extracellular matrix protein 1	9	0.92 ± 0.04	1.02 ± 0.03	1.09 ± 0.04	Secreted
O95967	EGF-containing fibulin-like extracellular matrix protein 2	4	0.96 ± 0.16	1.04 ± 0.12	1.16 ± 0.44	Secreted
O43854	EGF-like repeat and discoidin I-like domain-containing protein 3	6	0.96 ± 0.17	1.09 ± 0.19	1.14 ± 0.03	Secreted
Q9Y6C2	EMILIN-1	18	0.98 ± 0.05	1.04 ± 0.04	1.09 ± 0.01	Secreted
Q9HCU0	Endosialin	2	0.94 ± 0.16	1.27 ± 0.00	1.20 ± 0.07	Membrane
Q9NQ30	Endothelial cell-specific molecule 1	3	0.95 ± 0.10	1.12 ± 0.07	0.99 ± 0.31	Secreted
P61916	Epididymal secretory protein E1	4	1.03 ± 0.04	ND	1.04 ± 0.01	Secreted
Q16610	Extracellular matrix protein 1	9	1.01 ± 0.22	1.10 ± 0.20	0.96 ± 0.13	Secreted
P15311	Ezrin	30	1.03 ± 0.10	1.04 ± 0.02	1.05 ± 0.02	Membrane
Q16658	Fascin	8	0.98 ± 0.12	0.97 ± 0.15	0.40 ± 0.04	Membrane
P35555	Fibrillin-1	11	0.81 ± 0.03	0.93 ± 0.34	1.00 ± 0.16	Secreted
Q06828	Fibromodulin	5	1.13 ± 0.15	0.32 ± 0.01	0.13 ± 0.00	Secreted
P02751	Fibronectin	71	1.05 ± 0.07	1.09 ± 0.03	1.13 ± 0.01	Secreted
P23142	Fibulin-1	19	1.31 ± 0.00	1.03 ± 0.42	0.88 ± 0.11	Secreted

Q14315	Filamin-C	62	0.95 ± 0.09	1.00 ± 0.00	0.97 ± 0.12	Membrane
P19883	Follistatin	3	0.84 ± 0.13	1.01 ± 0.12	1.05 ± 0.11	Secreted
Q12841	Follistatin-related protein 1	7	0.98 ± 0.02	1.07 ± 0.08	1.02 ± 0.08	Secreted
P09382	Galectin-1	8	0.99 ± 0.03	0.94 ± 0.03	1.08 ± 0.05	Secreted
Q08380	Galectin-3-binding protein	23	0.98 ± 0.05	1.05 ± 0.08	0.99 ± 0.11	Secreted
P09104	Gamma-enolase	8	1.14 ± 0.11	0.98 ± 0.07	0.88 ± 0.07	Membrane
Q92820	Gamma-glutamyl hydrolase	4	1.03 ± 0.00	1.15 ± 0.36	1.03 ± 0.06	Secreted
P06396	Gelsolin	34	1.06 ± 0.07	1.02 ± 0.12	1.04 ± 0.22	Secreted
P07093	Glia-derived nexin	36	0.99 ± 0.10	0.93 ± 0.06	0.87 ± 0.20	Secreted
P06744	Glucose-6-phosphate isomerase	29	1.09 ± 0.05	1.06 ± 0.08	0.98 ± 0.03	Secreted
P22352	Glutathione peroxidase 3	5	1.33 ± 0.20	1.07 ± 0.38	0.98 ± 0.21	Secreted
P06737	Glycogen phosphorylase, liver form	18	1.05 ± 0.23	0.98 ± 0.02	0.81 ± 0.18	Membrane
P35052	Glypican-1 [Cleaved into: Secreted glypican-1]	8	1.13 ± 0.14	1.15 ± 0.15	1.08 ± 0.15	Secreted
P28799	Granulins	3	0.83 ± 0.10	0.73 ± 0.00	1.17 ± 0.39	Secreted
Q14393	Growth arrest-specific protein 6	5	0.85 ± 0.10	1.02 ± 0.29	1.08 ± 0.22	Secreted
Q9UBI6	Guanine nucleotide-binding protein G	2	0.94 ± 0.07	0.98 ± 0.04	0.75 ± 0.10	Membrane
P10915	Hyaluronan and proteoglycan link protein 1	5	0.93 ± 0.06	1.09 ± 0.35	1.11 ± 0.29	Secreted
O14498	Immunoglobulin superfamily containing leucine-rich repeat protein	6	0.95 ± 0.04	0.97 ± 0.00	0.97 ± 0.06	Secreted
P18065	Insulin-like growth factor-binding protein 2	7	1.02 ± 0.04	1.21 ± 0.06	1.04 ± 0.04	Secreted
P17936	Insulin-like growth factor-binding protein 3	10	0.61 ± 0.04	1.33 ± 0.33	1.16 ± 0.20	Secreted
P22692	Insulin-like growth factor-binding protein 4	2	1.19 ± 0.00	ND	1.07 ± 0.19	Secreted
P24593	Insulin-like growth factor-binding protein 5	13	1.15 ± 0.07	1.12 ± 0.22	1.04 ± 0.20	Secreted
P24592	Insulin-like growth factor-binding protein 6	3	1.13 ± 0.01	1.07 ± 0.07	1.05 ± 0.03	Secreted
Q16270	Insulin-like growth factor-binding protein 7	19	1.02 ± 0.04	1.04 ± 0.06	1.03 ± 0.01	Secreted
P26006	Integrin alpha-3	3	0.98 ± 0.01	1.08 ± 0.04	1.13 ± 0.14	Membrane
P05556	Integrin beta-1	7	1.00 ± 0.06	1.07 ± 0.20	0.98 ± 0.10	Membrane
P05231	Interleukin-6	5	0.78 ± 0.04	1.11 ± 0.48	1.05 ± 0.36	Secreted
P03956	Interstitial collagenase	8	0.66 ± 0.04	1.05 ± 0.52	0.99 ± 0.55	Secreted
Q08431	Lactadherin	7	1.17 ± 0.10	1.11 ± 0.01	1.06 ± 0.15	Membrane
P24043	Laminin subunit alpha-2	5	0.73 ± 0.00	0.99 ± 0.24	1.36 ± 0.08	Secreted

Q16363	Laminin subunit alpha-4	37	0.95 ± 0.10	1.02 ± 0.07	1.05 ± 0.10	Secreted
O15230	Laminin subunit alpha-5	28	0.92 ± 0.09	1.08 ± 0.05	1.03 ± 0.09	Secreted
P07942	Laminin subunit beta-1	44	0.99 ± 0.06	1.05 ± 0.00	1.04 ± 0.02	Secreted
P55268	Laminin subunit beta-2	28	0.95 ± 0.10	1.00 ± 0.04	1.01 ± 0.07	Secreted
P11047	Laminin subunit gamma-1	40	0.97 ± 0.07	1.06 ± 0.03	1.04 ± 0.07	Secreted
Q14767	Latent-transforming growth factor beta-binding protein 2 - around 250K	16	0.63 ± 0.08	1.39 ± 0.40	0.98 ± 0.01	Secreted
Q14767 *	Latent-transforming growth factor beta-binding protein 2 - around 200K	4	ND	ND	3.47 ± 0.64	Secreted
P51884	Lumican	10	1.12 ± 0.11	1.05 ± 0.17	1.06 ± 0.22	Secreted
P11279	Lysosome-associated membrane glycoprotein 1	2	0.97 ± 0.10	1.01 ± 0.08	1.01 ± 0.22	Membrane
P13473	Lysosome-associated membrane glycoprotein 2 - around 50 K	1	0.74 ± 0.00	1.06 ± 0.06	ND	Membrane
P13473 *	Lysosome-associated membrane glycoprotein 2 - around 37K	1	ND	1.12 ± 0.17	1.28 ± 0.00	Membrane
Q9Y4K0	Lysyl oxidase homolog 2	9	0.72 ± 0.13	1.12 ± 0.46	1.07 ± 0.49	Secreted
Q9UM22	Mammalian ependymin-related protein 1	4	1.00 ± 0.11	ND	1.00 ± 0.04	Secreted
P08493	Matrix Gla protein	3	0.97 ± 0.02	1.39 ± 0.07	0.80 ± 0.05	Secreted
P01033	Metalloproteinase inhibitor 1	6	1.00 ± 0.02	0.98 ± 0.17	1.03 ± 0.09	Secreted
P16035	Metalloproteinase inhibitor 2	8	0.97 ± 0.02	1.02 ± 0.09	1.06 ± 0.01	Secreted
P26038	Moesin	55	1.01 ± 0.10	1.04 ± 0.03	1.03 ± 0.04	Membrane
P29966	Myristoylated alanine-rich C-kinase substrate	7	1.03 ± 0.10	1.11 ± 0.09	1.12 ± 0.02	Membrane
Q92859	Neogenin	5	0.75 ± 0.18	ND	1.10 ± 0.31	Membrane
P14543	Nidogen-1	15	1.13 ± 0.17	1.11 ± 0.26	1.02 ± 0.23	Secreted
Q14112	Nidogen-2	7	1.10 ± 0.28	1.04 ± 0.04	1.10 ± 0.06	Secreted
Q02818	Nucleobindin-1	26	1.00 ± 0.08	1.09 ± 0.03	0.99 ± 0.01	Secreted
P80303	Nucleobindin-2	7	0.99 ± 0.23	0.91 ± 0.04	1.03 ± 0.17	Secreted
Q9NRN5	Olfactomedin-like protein 3	4	0.89 ± 0.06	0.97 ± 0.09	0.93 ± 0.18	Secreted
Q13219	Pappalysin-1	13	1.02 ± 0.09	1.01 ± 0.06	1.03 ± 0.02	Secreted
P26022	Pentraxin-related protein PTX3	17	0.91 ± 0.03	1.03 ± 0.08	1.05 ± 0.00	Secreted
Q6UXB8	Peptidase inhibitor 16	7	1.08 ± 0.06	1.05 ± 0.22	1.01 ± 0.10	Secreted
Q92626	Peroxidasin homolog	20	0.86 ± 0.04	1.04 ± 0.15	1.09 ± 0.21	Secreted
Q15124	Phosphoglucomutase-like protein 5	10	0.82 ± 0.04	0.74 ± 0.15	1.29 ± 0.05	Membrane
Q96FE7	Phosphoinositide-3-kinase-interacting protein 1	2	1.02 ± 0.23	ND	0.96 ± 0.16	Membrane

P55058	Phospholipid transfer protein	5	0.99 ± 0.03	0.93 ± 0.00	1.10 ± 0.08	Secreted
P36955	Pigment epithelium-derived factor	10	1.17 ± 0.11	1.06 ± 0.14	1.02 ± 0.14	Secreted
Q9BTY2	Plasma alpha-L-fucosidase	3	0.96 ± 0.30	1.07 ± 0.12	0.72 ± 0.00	Secreted
Q9Y646	Plasma glutamate carboxypeptidase	4	0.99 ± 0.08	1.09 ± 0.00	0.82 ± 0.19	Secreted
P05155	Plasma protease C1 inhibitor	25	1.25 ± 0.10	1.02 ± 0.20	1.03 ± 0.23	Secreted
P05121	Plasminogen activator inhibitor 1	41	0.87 ± 0.05	1.04 ± 0.27	1.05 ± 0.21	Secreted
Q6UX71	Plexin domain-containing protein 2	5	0.90 ± 0.07	0.89 ± 0.32	1.07 ± 0.26	Membrane
P15151	Poliovirus receptor	5	0.91 ± 0.07	1.07 ± 0.34	1.05 ± 0.03	Secreted
Q10471	Polypeptide N-acetylgalactosaminyltransferase 2	13	0.95 ± 0.06	1.03 ± 0.09	1.09 ± 0.09	Secreted
Q7Z7M9	Polypeptide N-acetylgalactosaminyltransferase 5	8	0.76 ± 0.13	1.05 ± 0.12	1.05 ± 0.16	Membrane
Q07954	Prolow-density lipoprotein receptor-related protein 1	35	0.95 ± 0.14	1.05 ± 0.01	0.96 ± 0.06	Membrane
P41222	Prostaglandin-H2 D-isomerase	7	0.95 ± 0.02	1.05 ± 0.18	1.01 ± 0.17	Secreted
P55145	Protein ARMET	3	1.17 ± 0.03	1.23 ± 0.04	1.09 ± 0.07	Secreted
P07237	Protein disulfide-isomerase	40	1.11 ± 0.05	1.02 ± 0.07	1.02 ± 0.08	Secreted
Q92520	Protein FAM3C	6	1.11 ± 0.11	1.04 ± 0.17	1.06 ± 0.03	Secreted
P28300	Protein-lysine 6-oxidase	2	0.63 ± 0.10	0.96 ± 0.00	1.12 ± 0.01	Secreted
Q92954	Proteoglycan 4	12	0.94 ± 0.04	1.20 ± 0.06	1.09 ± 0.23	Secreted
P50395	Rab GDP dissociation inhibitor beta	17	1.04 ± 0.15	1.03 ± 0.10	0.99 ± 0.08	Membrane
P35241	Radixin	21	1.20 ± 0.43	ND	1.09 ± 0.07	Membrane
P62491	Ras-related protein Rab-11A	2	0.98 ± 0.04	1.09 ± 0.00	1.04 ± 0.06	Membrane
A1L4H1	Scavenger receptor cysteine-rich domain-containing protein LOC284297	5	0.73 ± 0.10	1.17 ± 0.00	1.40 ± 0.14	Secreted
P13521	Secretogranin-2	9	0.57 ± 0.09	1.17 ± 0.48	0.73 ± 0.13	Secreted
Q13228	Selenium-binding protein 1	3	1.18 ± 0.00	0.00 ± 0.00	0.87 ± 0.05	Membrane
O75326	Semaphorin-7A	8	0.91 ± 0.05	1.04 ± 0.22	1.08 ± 0.27	Membrane
Q12884	Seprase	6	0.86 ± 0.19	1.07 ± 0.13	0.93 ± 0.16	Membrane
P10124	Serglycin	6	0.98 ± 0.05	0.94 ± 0.01	0.98 ± 0.03	Secreted
Q92743	Serine protease HTRA1	18	0.95 ± 0.00	8.55 ± 11.83	12.3 ± 17.4	Secreted
O75094	Slit homolog 3 protein	2	0.84 ± 0.11	ND	1.21 ± 0.16	Secreted
P09486	SPARC	16	0.96 ± 0.03	1.05 ± 0.11	1.04 ± 0.13	Secreted
Q01082	Spectrin beta chain, brain 1	26	0.90 ± 0.09	1.03 ± 0.14	1.14 ± 0.23	Membrane

P52823	Stanniocalcin-1	3	0.80 ± 0.03	1.35 ± 0.00	1.15 ± 0.24	Secreted
O76061	Stanniocalcin-2	6	0.93 ± 0.05	1.06 ± 0.08	1.13 ± 0.02	Secreted
O00391	Sulfhydryl oxidase 1	29	0.88 ± 0.05	1.01 ± 0.11	1.05 ± 0.04	Secreted
Q99536	Synaptic vesicle membrane protein VAT-1 homolog	4	1.02 ± 0.50	0.89 ± 0.06	0.83 ± 0.31	Membrane
P31431	Syndecan-4	5	1.14 ± 0.09	1.07 ± 0.11	0.93 ± 0.08	Membrane
Q9Y490	Talin-1	15	0.95 ± 0.13	0.74 ± 0.14	0.21 ± 0.04	Membrane
Q08629	Testican-1	7	0.72 ± 0.16	1.15 ± 0.48	0.91 ± 0.14	Secreted
P07996	Thrombospondin-1	35	0.77 ± 0.06	1.07 ± 0.34	0.98 ± 0.19	Secreted
P35442	Thrombospondin-2	15	0.85 ± 0.08	1.04 ± 0.16	0.96 ± 0.07	Secreted
P49746	Thrombospondin-3	13	0.86 ± 0.07	1.05 ± 0.19	0.93 ± 0.14	Secreted
P00750	Tissue-type plasminogen activator	2	0.77 ± 0.00	1.01 ± 0.14	1.06 ± 0.02	Secreted
P61812	Transforming growth factor beta-2	5	0.87 ± 0.00	1.12 ± 0.18	1.02 ± 0.15	Secreted
Q15582	Transforming growth factor-beta-induced protein ig-h3	24	0.79 ± 0.06	1.38 ± 0.26	1.15 ± 0.03	Secreted
P37802	Transgelin-2	8	0.87 ± 0.04	1.02 ± 0.14	0.72 ± 0.00	Membrane
O00300	Tumor necrosis factor receptor superfamily member 11B	3	1.12 ± 0.14	0.93 ± 0.05	1.03 ± 0.12	Secreted
P30530	Tyrosine-protein kinase receptor UFO	3	0.99 ± 0.15	0.72 ± 0.19	0.91 ± 0.04	Membrane
P78324	Tyrosine-protein phosphatase non-receptor type substrate 1	4	0.97 ± 0.05	1.15 ± 0.15	1.30 ± 0.13	Membrane
Q969H8	UPF0556 protein C19orf10	7	1.04 ± 0.09	1.01 ± 0.17	1.04 ± 0.04	Secreted
P19320	Vascular cell adhesion protein 1	9	1.24 ± 0.35	1.01 ± 0.18	0.95 ± 0.16	Membrane
Q6EMK4	Vasorin	9	1.03 ± 0.08	1.04 ± 0.04	1.06 ± 0.05	Secreted
P13611	Versican core protein	27	0.88 ± 0.06	1.11 ± 0.15	1.03 ± 0.21	Secreted
P07225	Vitamin K-dependent protein S	7	0.77 ± 0.03	1.02 ± 0.26	1.06 ± 0.20	Secreted
P04004	Vitronectin	4	1.06 ± 0.42	1.07 ± 0.10	0.46 ± 0.05	Secreted

* Proteins detected as cleavage fragments

ND: not determined

Figure 4. S1 Detection of clusterin degradation products in HTRA1 treated RPE conditioned medium

(A) Show SDS-PAGE of SILAC labeled and unlabeled RPE secreted protein mixture pairs in both HTRA1 (500 ng) untreated (-) and treated samples (+). Clusterin was identified by unique peptides around 45K and 35K in the SDS-PAGE, (B) Shows mass spectra of labeled and unlabeled peptide pair detected for clusterin in the 45 kDa upper band. Ratio of these peptide pairs were 1:1 when both labeled and unlabeled samples were kept untreated but dropped to about 0.5 in HTRA1 treated samples versus non treated samples. (C) Shows mass spectra of another labeled and unlabeled clusterin peptide detected in lower band (~ 35 KDa) however this time the peptide was intense only in HTRA1 treated samples suggesting a degradation product of clusterin by recombinant HTRA1. Small amounts of this same peptide marked with circle was still detected in untreated sample (-HTRA1) and those could be a result of activity of RPE secreted HTRA1.

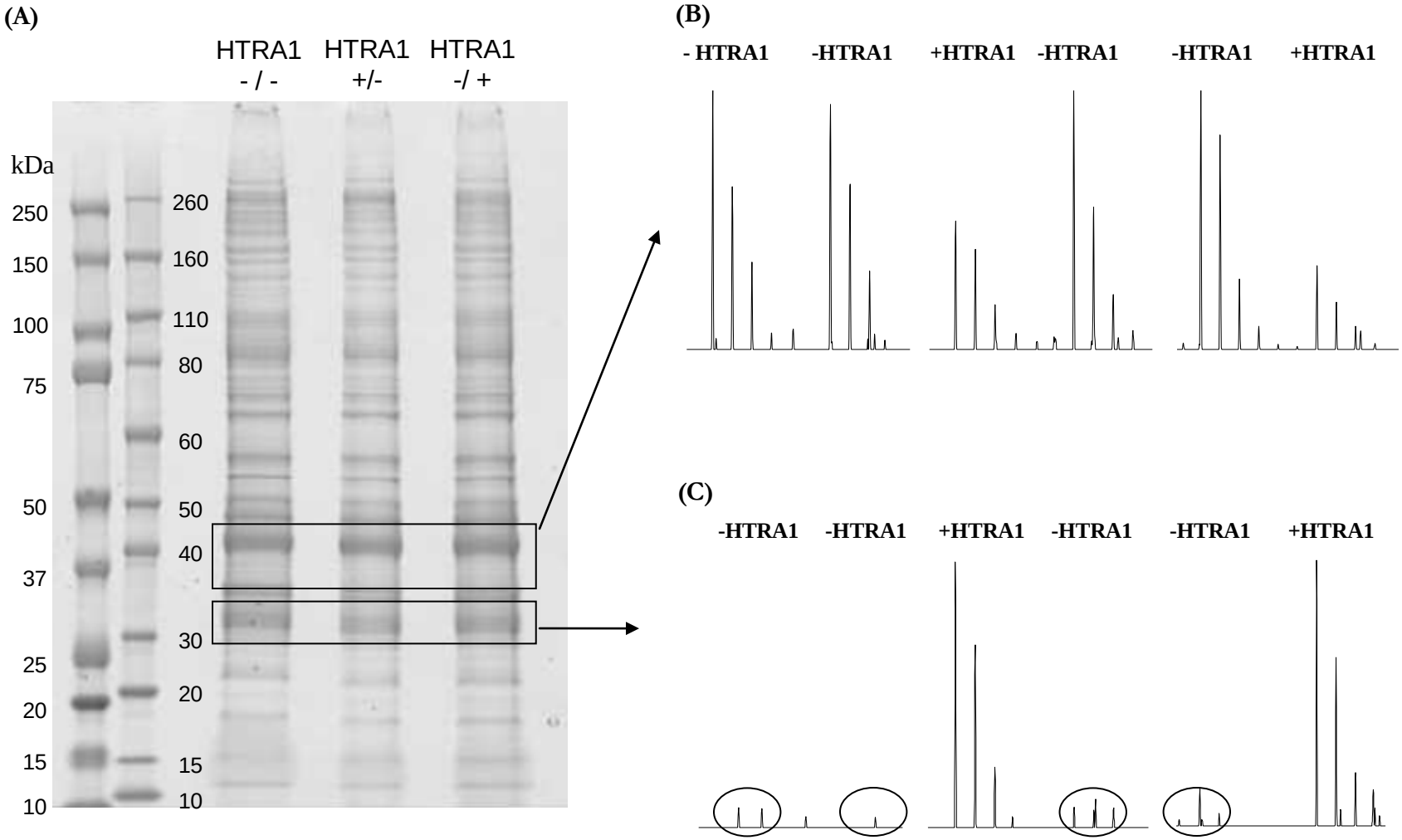
(A)
HTRA1 - / -
HTRA1 +/-
HTRA1 -/ +
kDa
250
150
100
75
50
37
25
20
15
10
260
160
110
80
60
50
40
30
20
15
10
(B)
- HTRA1
-HTRA1
+HTRA1
-HTRA1
-HTRA1
+HTRA1
(C)
-HTRA1
-HTRA1
+HTRA1
-HTRA1
-HTRA1
+HTRA1

Figure 4. S2 No effect of HTRA1 on fibronectin

Spectra show pairs of SILAC labeled and unlabeled peptides detected for fibronectin protein in HTRA1 (500 ng) treated (+) versus untreated (-) RPE conditioned medium. (A) Mass spectra when both SILAC labeled and unlabeled samples were untreated. (B) Mass spectra when unlabeled sample was treated while SILAC labeled sample was kept untreated. (C) Mass spectra of a reverse experiment when unlabeled sample was untreated while labeled sample was treated. Both 4 hours and 20 hours incubation with HTRA1 did not affect the ratios of fibronectin in HTRA treated sample versus untreated sample.

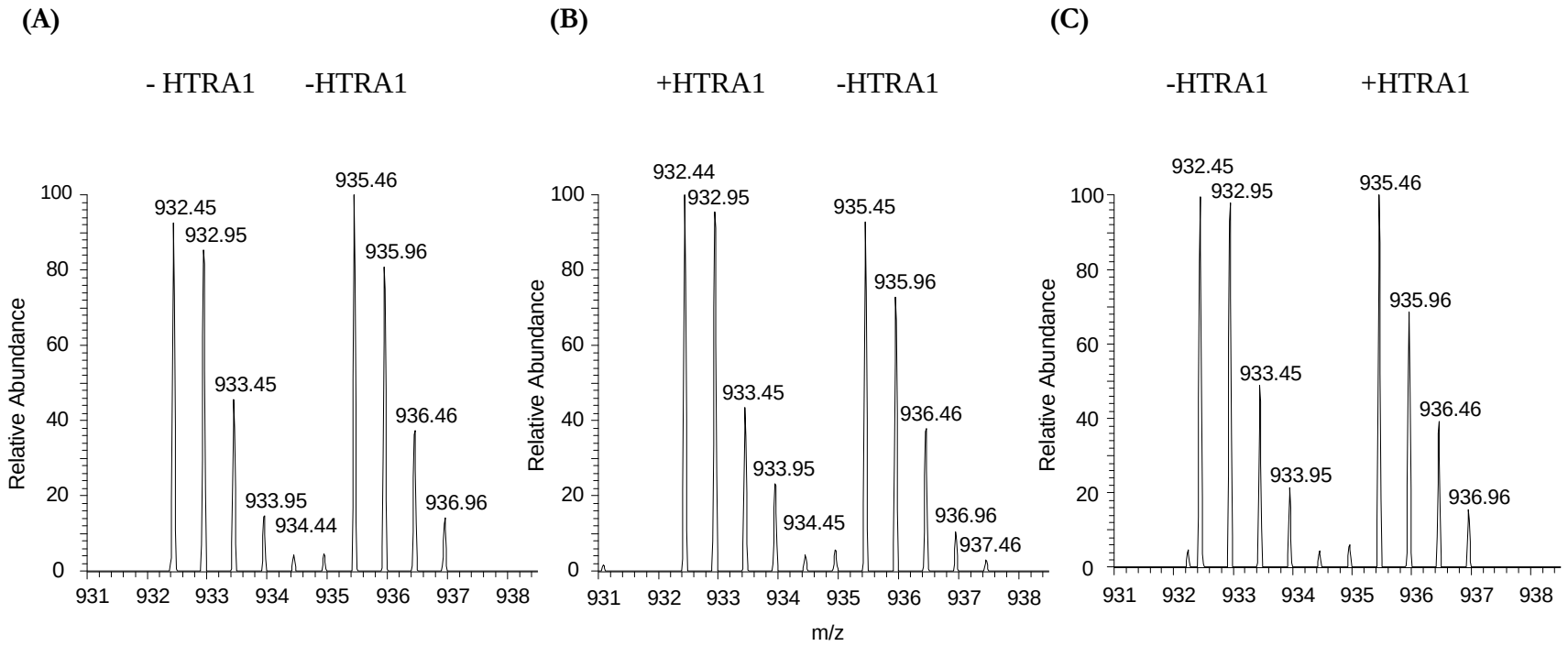
(A)
- HTRA1
-HTRA1
(B)
+HTRA1
-HTRA1
(C)
-HTRA1
+HTRA1
Relative Abundance
m/z
932.45
932.95
933.45
933.95
934.44
935.46
935.96
936.46
936.96
932.44
934.45
935.45
937.46

Chapter 5: Characterization of CFH and FHL-1 expression in genotyped human RPE cells and association with AMD

More than 50% of established RPE cultures from AMD donors harbors heterozygote alleles for *CFH* (Table 4.1), which prompted us to evaluate whether these wild type and risk alleles are expressed differently at mRNA and protein level. Moreover, we examined the effect of genotype on the expression and secretion of two known isoforms encoded by the *CFH* gene (e.g., CFH and FHL-1).

Eunkyung An[1,2], Heather Gordish-Dressman[1], Hui Sun [3], and Yetrib Hathout[1].

1. Research Center for Genetic Medicine, Children's National Medical Center, Washington, DC.
2. Program in Biochemistry and Molecular Genetics, Institute for Biomedical Sciences, The George Washington University, Washington, DC.
3. Department of Physiology and Jules Stein Eye Institute, David Geffen School of Medicine at UCLA, LA

Correspondence should be addressed to:

Yetrib Hathout
Research Center for Genetic Medicine
Children's National Medical Center
111 Michigan Ave NW
Washington, DC 20010
yhathout@cnmcresearch.org
Telephone number: (202) 476-3136
Fax number: (202) 476-6014

5.1 Introduction

A SNP in the coding region of *CFH* (rs1061170, 1277 C>T, CFH Y402H) has been identified as a major genetic risk factor for developing AMD[33-36]. CFH is an important regulator of the alternative complement pathway. CFH inhibits alternative complement activation on cell surfaces by acting as a cofactor of factor I-mediated C3b cleavage and by dissociating C3 convertase[229]. This has placed the complement system at center stage in AMD pathogenesis. The *CFH* gene is located in chromosome 1 and a missense mutation at exon 9 leads the substitution of a Y by an H residue at position 402 (e.g., CFH Y402H) increases the risk of developing AMD by more than 50%. The *CFH* gene encodes for two proteins (Figure 5.1), a full length CFH protein which is composed of 20 sushi domains and a truncated isoform FHL-1 which is composed of the same first 7 domains with 5 additional amino acids (VSFTL) at the C terminus[230]. A typical sushi domain has around 50-60 amino acids residue and contains 2 disulfide bonds[231]. Sushi domain is a common motif in protein-protein interaction, and it is also known as short consensus repeats[232]. The missense mutation is located in sushi domain 7 and affects both isoforms. *In vitro* studies suggest domain 7 as a binding site for heparin, CRP, and the streptococcal M protein[40,41] (Figure 5.1). While the missense mutation does not affect the expression levels of CFH or FHL-1 in serum[40,233], the binding affinity of both isoforms to CRP and M protein are reduced[39,40]. However, the two isoforms differ in their binding affinity to heparin. While binding of CFH to heparin does not change, it is reduced in the case of FHL-1[39,40]. However, no studies have investigated the expression and the status of CFH and FHL-1 in the context of RPE extracellular milieu. Four out of 8 clinically documented AMD donors were heterozygotes for the CFH Y402H variant (see our established collection of primary

RPE culture Table 4.1). This prompted us to evaluate differential allelic expression of wild type and risk allele in primary RPE cultures with heterozygous for the CFH variants.

Figure 5.1 Schematic representations of a full length CFH and its truncated isoform FHL-1

The *CFH* gene in chromosome 1 encodes full length CFH with 20 sushi domains and a truncated FHL-1 with 7 domains and an additional 5 amino acids at the C-terminus. The SNP located in exon 9 of the *CFH* gene causes a tyrosine (Y) to histidine (H) substitution at position 402 in both the full length CFH and FHL-1 isoform. Binding sites for C3b, heparin, CRP, and M protein are indicated at the bottom of the figure. CFH has 8 N-glycosylated sites while FHL-1 has no glycosylation sites. (Each blue circle represents one sushi domain, and the curved lines on the sushi domains 9, 12-15 and 17-18 of CFH represent a N-linked glycosylation.)

Chromosome 1

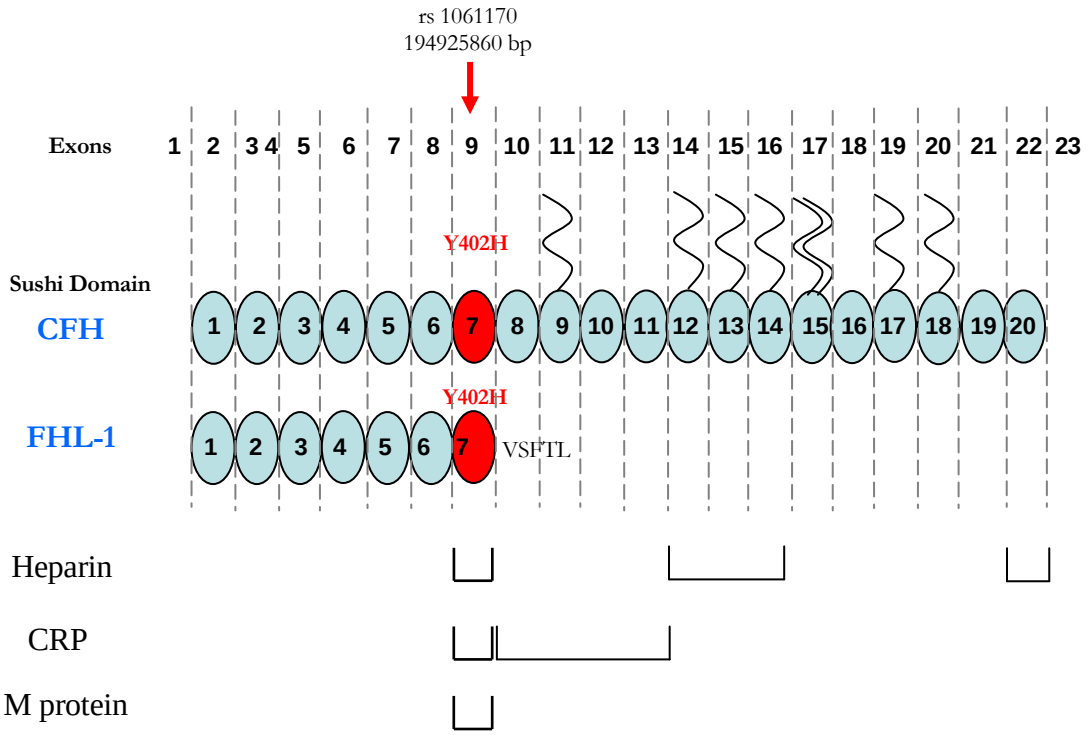

5.2 Methods

5.2.1. Characterization of CFH and FHL-1 in the RPE secretome

Conditioned medium from a primary RPE culture was collected and concentrated using centrifugal filtration (Millipore Corporation, Billerica, MA). Protein content was determined using the Bio-Rad protein assay reagent following the manufacturer's instructions (Bio-Rad, Hercules, CA). Aliquots containing 80 μg and 35 μg of total secreted proteins were used for 2-DE/ MS analysis and for 2-DE /western blot analysis respectively. Samples were desalted using Bio-Spin columns (Bio-Rad, Hercules, CA). Each sample was dried by centrifugation under reduced pressure then 180 μL of rehydration buffer containing 7 M Urea, 2 M Thiourea, 2% CHAPS, 50 mM DTT and carrier ampholytes were added to the dry sample to solubilize and denature the proteins. Electrophoresis in the first dimension was performed on 11 cm Immobilized pH gradient (IPG) strips (pH 3–10) in an electrofocusing chamber (Bio-Rad, Hercules, CA). The second-dimension of electrophoresis was performed on 10 % Criterion Tris-HCl precast gels (Bio-Rad, Hercules, CA). In the 80 μg sample, protein spots were visualized by Bio-Safe Coomassie stain (Bio-Rad, Hercules, CA) in the 2-DE. Each spot was excised, in gel digested by trypsin and the resulting peptides analyzed using LTQ/Orbitrap as described in Method of Chapter 4. In parallel, the 2-DE with 35 μg secreted proteins was used for detection of CFH and FHL-1 using goat polyclonal antibody against human CFH (1:1K, Complement Technology, Tyler, TX) for primary antibody and anti-goat IgG (1:5K, R&D Systems, Minneapolis, MN) for secondary antibody.

5.2.2. Differential expression of wild type (T) and risk (C) allele in primary RPE cultures with heterozygous for the CFH variant

To determine relative expression between wild type (T) and risk (C) allele in 12 donors heterozygous for the CFH variant, we used an allele specific expression (ASE) strategy [234]. Genomic DNA and total RNA were isolated from RPE cultures and cDNA was generated as described in Chapter 4. An allele specific qRT-PCR reaction was performed for the wild type and the risk allele probes using 50 ng of cDNA at 95 °C for 11 min and 44 cycles of 15 s at 92 °C and 1 min at an annealing temperature of 60 °C. Genomic DNA (20ng) was used as a reference and for background substraction. Relative quantification of each allele was obtained using the comparative threshold (CT) method after determining the CT values for reference (genomic DNA) and target (*cDNA*) in each sample sets according to the $2^{-\Delta\Delta Ct}$ method as described in Chapter 4.

5.2.3. Detection of Y and H variants for the CFH and FHL-1 proteins in the secretome of RPE cells using western blot analysis

Relative expression between Y and H variants for the CFH and FHL-1 proteins was determined in the secretomes collected from 7 RPE cell cultures heterozygous for the CFH/FHL-1 variant. Anti-CFH, anti-Y402 CFH and anti-H402 CFH were a gift from Dr. Sun Hui, UCLA[40] and were used to detect Y and H variants in both CFH and FHL-1 proteins secreted by RPE cells (1:300). Goat anti-rabbit Immunoglobulin M (IgM) and IgG (1:3K, SouthernBiotech, Birmingham, AL) were used as secondary antibodies. RPE secretome from donors with homozygote wild type allele TT (n =3) and homozygote risk allele CC (n = 3) were used as controls.

5.3 Results

5.3.1 Characterization of CFH and FHL-1 in RPE secretome

A representative 2-DE of primary RPE secretome is shown Figure 5.2 A. A total of 261 protein spots were excised and identified by M/S analysis as described in the Methods. CFH was detected as multiple spots with the expected molecular mass (e.g. 150 kDa) for a full length glycosylated protein. The pI for these different CFH spots ranged from 3.5 to 7 is probably reflecting different glycosylation states of the secreted CFH. On the other hand, FHL-1 was identified as one single spot around 45 kDa and a pI of 6.6 in agreement with the PI of theoretical unglycosylated form of the protein. These data were further validated by western blot analysis of a 2-DE separated RPE secretome (Figure 5.2 B). The CFH antibody detected both full length CFH and its trucncated isoform FHL-1. Again, CFH was detected as multiple spots with patterns similar to those identified by MS in Figure 5.2 A, while FHL-1 was represented by a single spot similar to one defined for FHL-1 in Figure 5.2A. These data all together confirm local secretion of both CFH and FHL-1 by RPE cells.

Figure 5. 2 Characterization of RPE secreted CFH and FHL-1

(A) Representative 2-DE of RPE secretome. Total secreted proteins (80 µg) were concentrated from conditioned medium of a 24 h RPE culture and processed for 2-DE and mass spectrometry as described in the Methods section. The gel was stained with Bio Safe Commassie blue and each spot was excised digested by trypsin. The resulting peptides were analyzed by LC-MS/MS. A total of 260 proteins were identified (Data not shown). Spots corresponding to CFH and FHL-1 are indicated by blue circle. (B) A representative western blot of 2-DE anlysis of the RPE secererome. An aliquot containing 35 µg of total RPE secreted proteins was separated by 2-DE and transferred to PVDF membrane for western blot using goat polyclonal antibody against human CFH and anti goat IgG as secondary antibody. Spots, detected by western blot, were similar to those detected by mass spectrometry analysis. Some impurities were detected around 75 kDa and they are presumably due to non specific reactions of the polyclonal antibody.

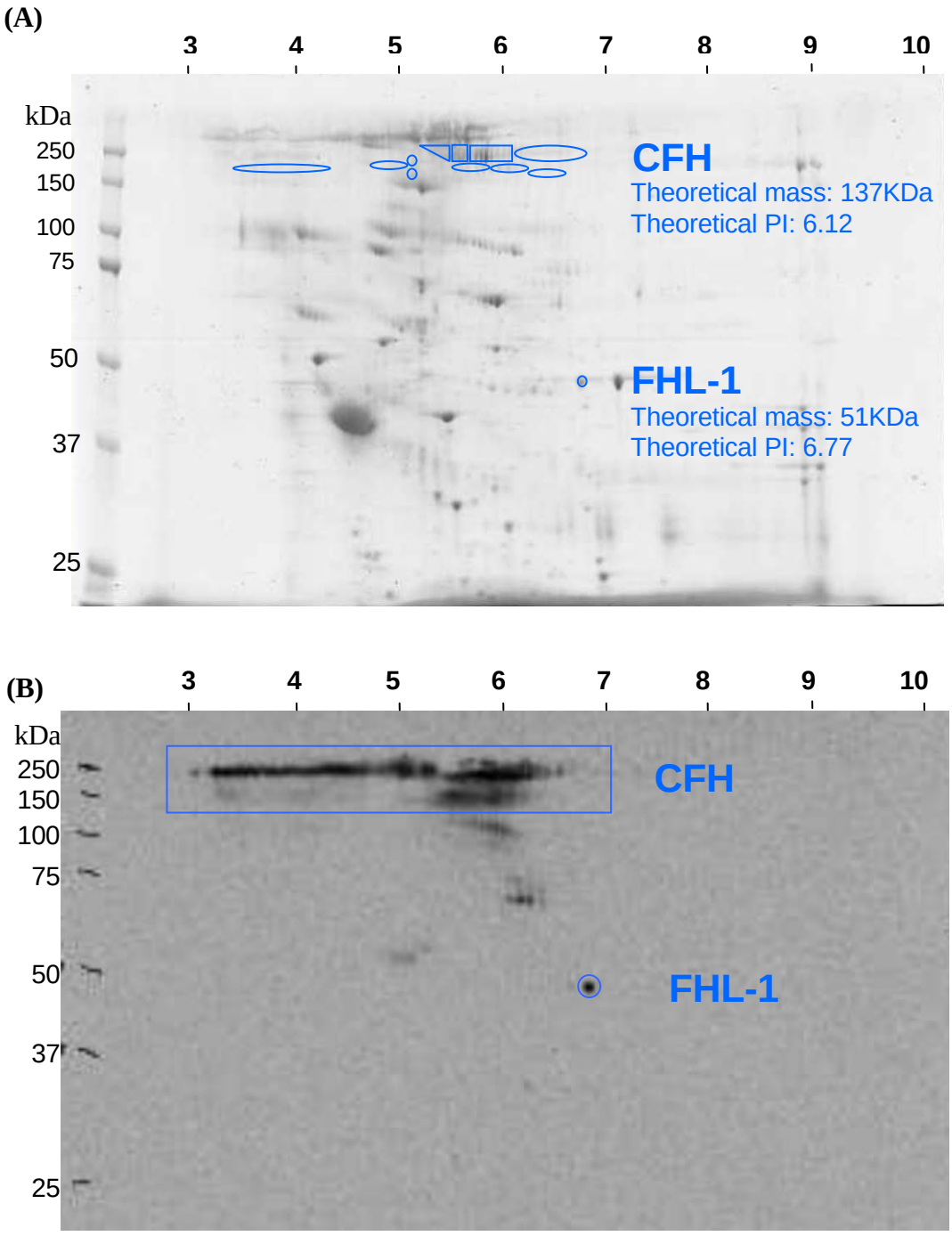
(A)
3
4
5
6
7
8
9
10
kDa
250
150
100
75
50
37
25
CFH
Theoretical mass: 137KDa
Theoretical PI: 6.12
FHL-1
Theoretical mass: 51KDa
Theoretical PI: 6.77
(B)
3
4
5
6
7
8
9
10
kDa
250
150
100
75
50
37
25
CFH
FHL-1

5.3.2 Antibody specific detection of Y and H variants of CFH and FGL-1 in the secretome of RPE heterozygous for the CFH risk allele

As shown in Figure 5.3, western blot analysis using Y specific and H specific CFH antibody detected both isoforms (e.g., CFH around 150 kDa and FHL-1 around 45 kDa) in the RPE secretome, which is consistent with our 2-DE data above. As expected RPE cells homozygous for CFH wild type allele secreted only the Y402 forms of the CFH and FHL-1 and while RPE cells homozygous for the CFH risk allele secreted only the H402 forms of the CFH and FHL-1 protein and RPE cells heterozygous for the CFH risk allele secreted both the Y402 and H402 forms of the CFH and FHL-1 (Figure 5.3).

5.3.3 Differential allelic expression of CFH variants in RPE heterozygous for the CFH risk allele

Total mRNA was extracted from 12 RPE cultures with heterozygous for the CFH risk allele and allele specific cDNA was amplified and quantified. No difference was found in expression between the wild type (T) and risk (C) allele at mRNA level for the CFH (Figure 5.4 A). At the protein level there was no difference in the levels of the Y and H variants in the CFH secretion (Figure 5.4 B). However, there was a significant decrease, by almost two fold, in the secretion of the at-risk H variant versus the wild type Y variant for the FHL-1 protein (Figure 5.4 C).

Figure 5. 3 Specific detection of Y402 and H402 CFH/FHL-1 variants in conditioned media of human primary RPE cultures

CFH and FHL-1 were detected in the conditioned medium of RPE cell cultures with homozygous wild type genotype T/T (n =3), heterozygous risk allele C/T (n = 7) and homozygous risk allele C/C (n = 3) for the *CFH* gene. A rabbit polyclonal antibody was used against human CFH (Top). A specific monoclonal antibody was used against the Y402 variant (Middle). A specific monoclonal antibody was used against the H402 variant (Bottom). As expected both CFH and FHL-1 were detected around 150 kDa and 50 kDa respectively. Y specific antibody detected only the Y402 variants and not the H402 variants while the H specific antibody detected only the H402 variants and not the Y402 variants.

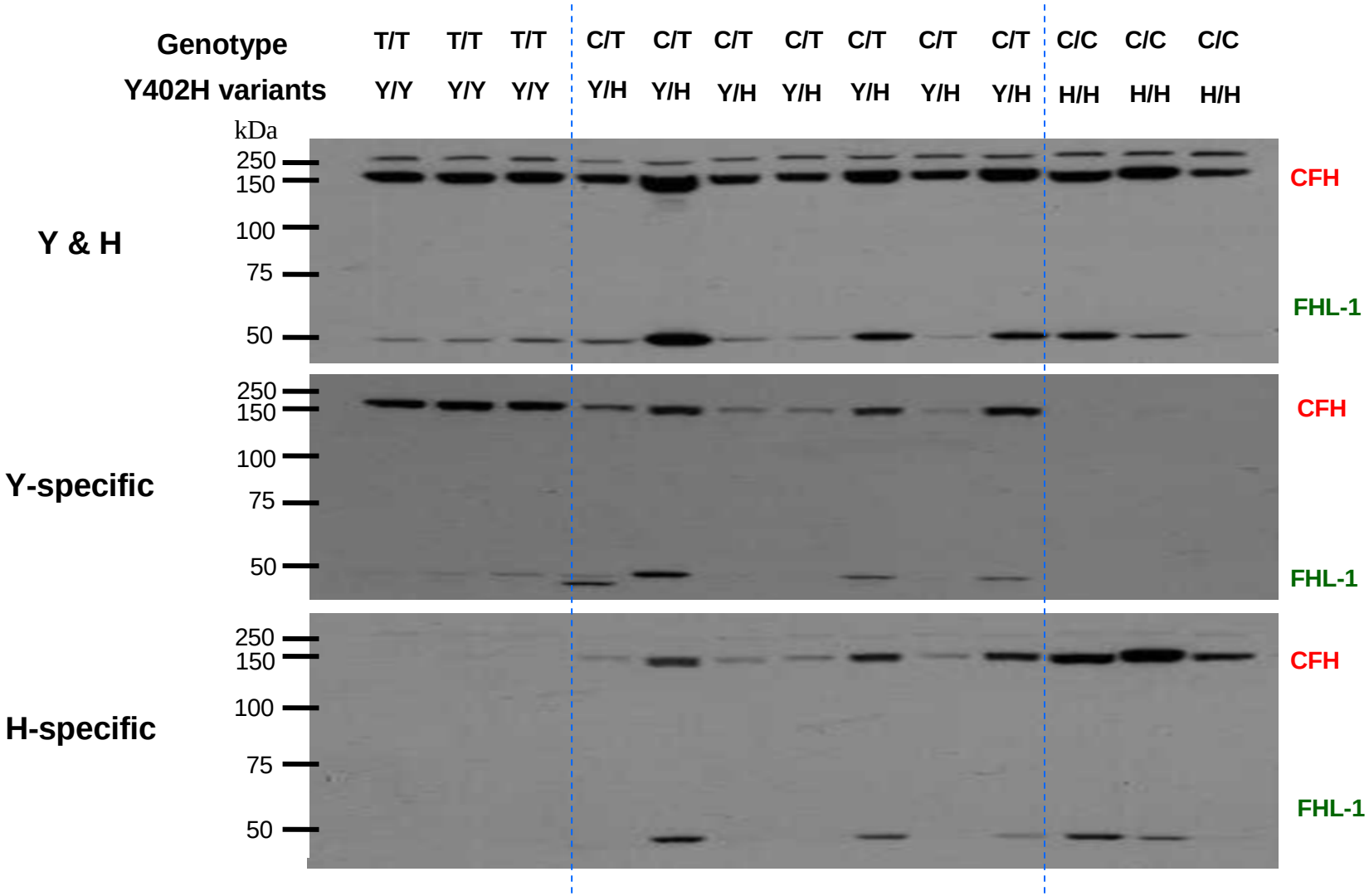
Genotype
T/T T/T T/T C/T C/T C/T C/T C/T C/T C/T C/C C/C C/C
Y402H variants
Y/Y Y/Y Y/Y Y/H Y/H Y/H Y/H Y/H Y/H Y/H H/H H/H H/H
kDa
Y & H
250
150
100
75
50
CFH
FHL-1
Y-specific
250
150
100
75
50
CFH
FHL-1
H-specific
250
150
100
75
50
CFH
FHL-1

Figure 5. 4 Specific allelic expression of CFH and FHL-1 in RPE cells wih heterozygous CFH risk genotype

Total mRNA was extracted from 12 RPE cultures with heterozygous risk genotype for the *CFH* gene and reverse transcribed with CFH primers recognizing either the wild type (T) or the at-risk (C) genotype. Differential expression was measured using TaqMan assay. The values were normalized to those of the wild type T genotype (A). A differential level in secretions of the Y402 and H402 variants of CFH was determined from the western blot band intensities obtained in figure 5.3 (B). Similarly differential secretion of Y402 and H402 variants of FHL-1 was determined from the western blot band intensities obtained in figure 5.3 (C). While there is no difference between wild type and at-risk allele in (A) and (B), there is almost two fold decrease in the secretion of risk H variant than wild type Y variant for the FHL-1 protein (C). Values are normalized to the Y402 variant and error bar represents standard deviation.

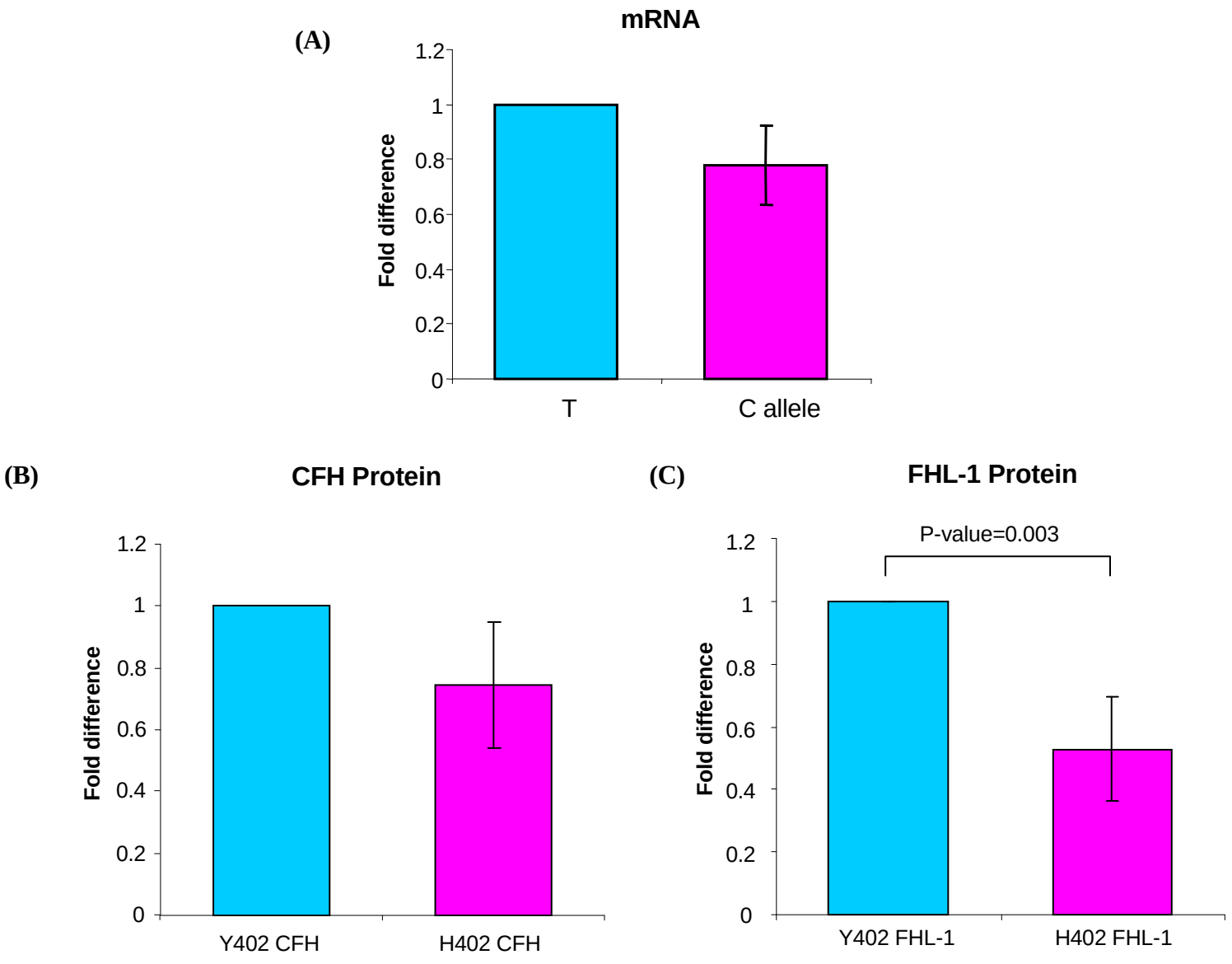
(A)
mRNA
Fold difference
1.2
1
0.8
0.6
0.4
0.2
0
T
C allele
(B)
CFH Protein
Fold difference
1.2
1
0.8
0.6
0.4
0.2
0
Y402 CFH
H402 CFH
(C)
FHL-1 Protein
P-value=0.003
Fold difference
1.2
1
0.8
0.6
0.4
0.2
0
Y402 FHL-1
H402 FHL-1

5.4. Discussion

A SNP in the *CFH* gene (rs1061170, 1277 C>T) causes a missense mutation at the amino acid position 402 (sushi domain 7) in both CFH and the truncated isoform FHL-1. Because domain 7 is suggested to participate in binding to heparin, CRP and M protein[40,41], it has been hypothesized that the AMD-associated SNP in the *CFH* gene may affect interactions of the *CFH* gene product with its ligands. The full length CFH has five heparin binding domains, five CRP binding domain, and one M protein binding domain. Several *in vitro* studies have shown that the Y402H variant does not affect the binding affinity of the full length CFH to heparin[39,40], but does reduce the binding affinity for the FHL-1[39]. This indicates a potential role of the FHL-1 but not full length CFH, in AMD pathogenesis.

Interestingly, FHL-1 to CFH ratio (1:3.5) was higher by almost 3 fold in RPE extracellular milieu (Figure 5.3) compared to circulating FHL-1/CFH ratio (less than 1:10)[229]. This strongly supports potential role of the truncated isoform in the context of RPE extracellular environment. FHL-1 has a number of activities similar to those of the CFH, including inhibition of the alternative complement pathway and binding to heparin and cell surface[235,236]. Because FHL-1 is shorter and has less ligand binding sites than CFH (see Figure 5.1), the polymorphism in the *CFH* gene may render FHL-1 more vulnerable to the effects of Y402H missense mutation. Although FHL-1 and CFH are encoded by a single gene, regulated by the same gene promoter and initiate transcription at the same start site, their transcripts are differently regulated most probably at the posttranscriptional level. It is more likely that FHL-1 to CFH ratio is dictated by tissue specificity, genetics and environmental factors.

In conclusion our data and the *in vitro* binding assay studies[39,40] strongly support the role of FHL-1 and to less extent the full length CFH in AMD pathogenesis. FHL-1 H402 variant might fail to bind to RPE cell surface and inhibit C3 activation leading to exacerbated alternative pathway activation and immune complex deposition. However, further investigations are required to determine whether Y402H missense mutation really affects the binding of FHL-1 to RPE cell surface.

Chapter 6: Overall Discussion and Future Directions

6.1 Summary

AMD is a complex multifactorial disease accompanied by progressive structural and/or physiological changes occurring in the macula (e.g., drusen formation accompanied or not with CNV). Better knowledge of the molecular mechanisms leading to these changes is required to define therapeutic targets. Using integrated genomics and proteomics approaches we have established two working models for AMD pathogenesis that might explain drusen formation and CNV. Our models are built upon genomics and proteomics data obtained on primary RPE cell cultures derived from human autopsy eyes. Toward this end, we have developed a robust workflow where primary RPE cell cultures are established from freshly collected human autopsy eyes and screened for AMD risk genotypes for subsequent proteome profiling.

6.2 Choice of biological model

Various animal models displaying phenotypes of human AMD have been developed using either genetic manipulations[237-254]or laser induced CNV[255,256] in both mouse and rat. However, only primates have a macula similar to that of human[257,258], and these are often very costly and hard to maintain as a colony to perform experiments because of the age related onset of the disease. Therefore, human autopsy eyes, collected from donors with and without AMD, are the closest and most adequate biological model to study AMD pathogenesis. Immunohistological and electron microscopy studies of retinal cross section prepared from autopsy eyes of AMD and normal donors greatly advanced our

understanding of the clinical feature of AMD[78,79,259,260]. Additionally, human autopsy eyes have been widely used to establish primary RPE cell cultures and study their function and role in vision[261-263]. Given that the only cell type adjacent to drusen deposits are RPE cells, it is widely felt that RPE cells have a major role in their formation. A primary function of RPE cells is to phagocytose POS and transport nutrients from the blood to the photoreceptor[264]. RPE cells and photoreceptors are very dependent on each other and mutation in genes that are expressed in RPE or photoreceptor can lead to retinal degeneration. In this study we have chosen to use RPE cell culture to create a model for AMD pathogenesis (e.g., drusen formation and CNV) by integrating genomics and proteome profiling data and by identifying altered pathways in RPE derived from donors with AMD versus RPE derived from age-matched healthy donors.

6.3 Choice of techniques

With advances in genomics, proteomics, and bioinformatics, a wealth of information can now be collected and integrated to better understand the underlying molecular mechanisms of a disease or a condition. In this dissertation, we have used these technologies to advance our understanding of AMD pathogenesis. While genomics is a mature technology and can provide large data sets in timely manner, proteomics is still in its evolving state and requires specialized instrumentation and computational tools. Established primary RPE cultures were screened for all currently known AMD risk genotypes using our standardized TaqMan assay. Our developed SILAC strategy greatly facilitated high throughput analysis of the secretome of primary RPE cells and provided us with key pathways that might explain drusen formation and CNV.

6.4 Two models for AMD pathogenesis

Three strong genetic loci disposing to AMD--the *CFH* (rs1061770, CFH Y402H), the *HTRA1* (rs11200638, -512 G>A) and the *ARMS2* (rs10490924, A69S)--have been identified and are now validated in multiple studies with different cohorts and group ethnicity[23-36] . The fact that HTRA1 and ARMS2 variants are in high LD, it makes difficult to pinpoint the causal gene at this time. CFH and HTRA1/ARMS2 variants are found to be associated with both dry and wet forms, and show similar association in most ethnic groups studied, except those of Asian decent where the wet form of AMD is most prevalent[265-270]. The question remains how these apparently unrelated genes lead to the same pathological features (drusen formation and CNV) of AMD.

Our integrated genomic and proteomic data obtained on genotyped RPE cell cultures derived from human autopsy eyes have begun to shed light on the relationships between RPE secreted proteins and AMD pathogenesis (Chapter 2-4). Indeed, we show that RPE cells derived from AMD donors with CFH H402 variant secrete elevated amounts of protein components found in drusen than RPE cells derived from age matched donors with wild type CFH Y402 (Chapter 2). We also found that RPE secretome is altered by TNF-α suggesting a potential role of cytokine in AMD pathogenesis (Chapter 3). Moreover, in Chapter 4, we demonstrated that RPE cells with *HTRA1/ARMS2* risk genotype secrete elevated amounts of the serine protease HTRA1, which cleaves key proteins involved in regulation of the complement pathway (e.g., clusterin, vitronectin and fibromodulin) and in amyloid deposition (e.g.,clusterin, alpha 2 macroglobulin and ADAM9), thus linking HTRA1 risk variant pathway to CFH risk variant pathway. With these *in vitro* data, we propose two different but additive models that might explain AMD

pathogenesis *in vivo*. One model is associated with dysregulation of the alternative complement pathway due to the missense mutation in the *CFH* gene. The second model is associated with alteration of homeostasis of the RPE extracellular environment due to the polymorphism in the promoter region of *HTRA1* gene.

6.4.1 Complement system model and AMD

The complement system is composed of complex list of enzymes and regulators and provides the innate immune defense mechanism (Figure 6.1). Most of these components are synthesized by the liver. However, local expression has been reported in number of other cells including RPE cells (Chapter 2-4). RPE is monolayer of epithelial cells that separates the retina from the choroid and act as a blood-retina barrier. Secretion of complement components by these cells could be a part of a defense mechanism against potential circulating pathogens. We have shown that RPE secretes both C3 (main activator of the complement system) and its negative regulators CFH and FHL-1. Both CFH and FHL-1 regulate the AP by dissociating C3 convertase and inactivating C3b to protect the host cell, in this case RPE, from inappropriate complement activation[37,271]. The missense mutation in the *CFH* gene was shown to result in a compromised function of the CFH and especially that of the FHL-1[39,40] (Chapter 5). This agrees with our proposed model (Figure 6.2) where RPE cells chronically exposed to age associated stressors (e.g., reactive oxygen species, advanced glycation end products, cytokines and light) will lead to increased secretion of C3. Unchecked, the pathway will lead to uncontrolled C3 activation, increased C3b deposition and membrane attack complex (MAC) formation. This model is supported by an *in vivo* study showing that CFH-deficient mouse

spontaneously develop C3b deposition and drusen like components along the glomerular basement membrane[128] suggesting a protective role of CFH. Indeed, a follow up study further shows that injection of purified CFH to CFH-deficient mice reduced C3b deposition[272]. Increased secretion of C3 by aging RPE cells harboring a missense mutation in the *CFH* gene will also lead to increased formation of C3a and C5a, anaphylatoxin components and inducers of VEGF expression in RPE cells[273,274]. Uncontrolled, this pathway might lead to growth of new blood vessel from adjacent endothelial cells and formation of CNV. In summary, our model shows that missense mutation in the CFH and FHL-1 proteins will result in uncontrolled complement activation in the case of RPE cell injury. To compensate for this deficiency, RPE cells start secreting large amounts of clusterin and vitronectin, extracellular chaperone proteins and also regulators of the complement pathway (Figure 6.1). This unbalanced protein secretion will result in alteration of the extracellular microenvironment of RPE cells and progressive deposition of C3b and accumulation of angiogenic factors. On the other hand, fully functional CFH and FHL-1 will prevent formation of excessive C3b deposition by inactivating C3b and disassociating C3 convertase. This will also balance the secretion of clusterin and vitronectin by RPE cells.

Figure 6.1 Complement pathway and function of CFH

Activation of complement is divided into three pathways: the CP, the LP, and the alternative pathway (AP). The CP is activated by antibody complexes and LP is activated by mannose-binding lectin to mannose groups of pathogen. Both CP and LP utilize C2 and complement component 4 (C4) to generate the C3 convertase (C4bC2a). The AP is constantly activated at low level to guarantee instant response to pathogens, and it uses C3 and BF to generate C3 convertase. It is suggested that the alternative pathway may represent up to 80 % of complement activation[38]. Spontaneous hydrolysis of C3 to C3w (hydrolyzed-C3) induces a conformational change that enables binding to BF and form the initial AP C3 convertase (C3wBb) in fluid phase and C3 is cleaved by this initial AP C3 convertase into C3a and C3b. Covalent binding of C3b to membrane forms C3 convertase (C3bBb) with cleaved BF by factor D and this amplifies the complement system. Accumulation of deposited C3b also leads to the assembly of C5 convertase (C4bC2aC3b for CP and LP and C3bC3bBb for AP) which cleave complement component 5 (C5) into C5a and C5b. C5b initiates the assembly of the MAC[38], a pore that is formed by each molecule of C5b, complement component 6 (C6), complement component 7 (C7), and complement component 8 (C8) and 9 copies of complement component 9 (C9). However, complement system is regulated on host cells. Under normal conditions, complement pathway is tightly controlled by regulators. For example, CFH protein displays a cofactor activity for factor I in the degradation of the C3b and acts as a decay accelerating factor for the C3 convertase (C3bBb) and it is also a competitor for BF binding to C3b. Fibromodulin (FMO) inhibits AP by binding to CFH. Both vitronectin (VTN) and clusterin

(CLU) bind to the C5b-7 complex to prevent the complex from inserting into lipid membrane thus preventing the assembly of the MAC [217,218].

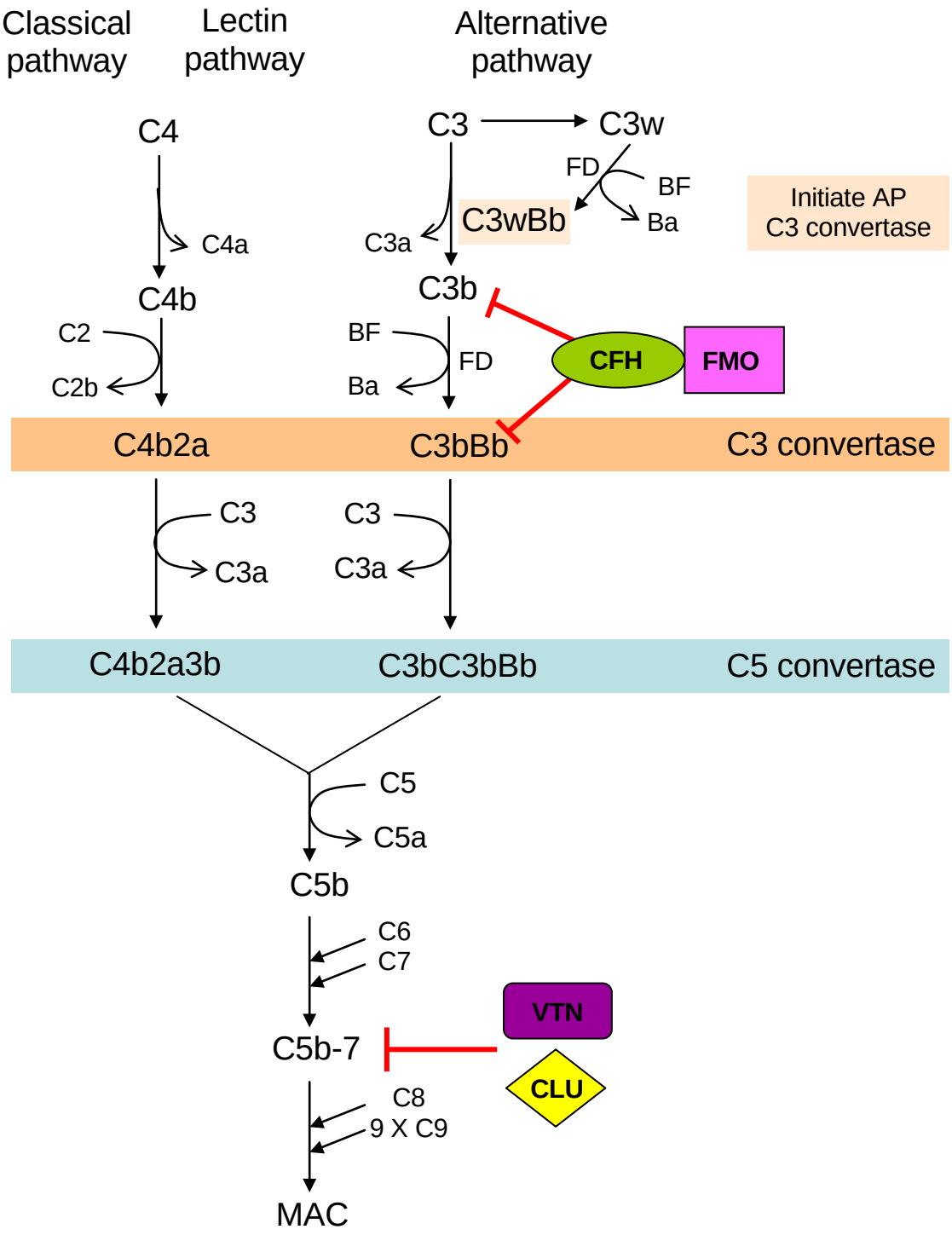
Classical pathway
Lectin pathway
Alternative pathway
C4
C4a
C4b
C2
C2b
C3
C3w
FD
BF
Ba
C3wBb
C3a
Initiate AP C3 convertase
C3b
BF
FD
Ba
CFH
FMO
C4b2a
C3bBb
C3 convertase
C3
C3a
C3
C3a
C4b2a3b
C3bC3bBb
C5 convertase
C5
C5a
C5b
C6
C7
VTN
C5b-7
CLU
C8
9 X C9
MAC

Figure 6.2 Cellular and molecular model for complement system and AMD pathogenesis

Aging RPE cells are exposed to chronic insults such as oxidized proteins from daily phagocytosis of POS, advanced glycation end products (AGEs), oxidative stress and circulating cytokines. These insults may all contribute to increase C3 secretion[180,181,215,275,276] by RPE cells leading to alternative pathway activation. CFH H402 and especially FHL-1 H402 variant fail to control or block the activated pathway (1) leading to increased C3b and C3a formation, deposition of C3b and MAC. To compensate for this activated pathway RPE cells increase their secretion of clusterin and vitronectin, secondary inhibitors of the terminal alternative pathway (pathway 2). Vitronectin and clusterin form complexes with terminal C5b-7 generated from the C3b activation and inhibit its insertion to the plasma membrane and formation of MAC. However, this mechanism might lead to increased formation of clusterin-C5b-7 and vitronectin-C5b-7 complexes leading to their progressive deposition in drusen.

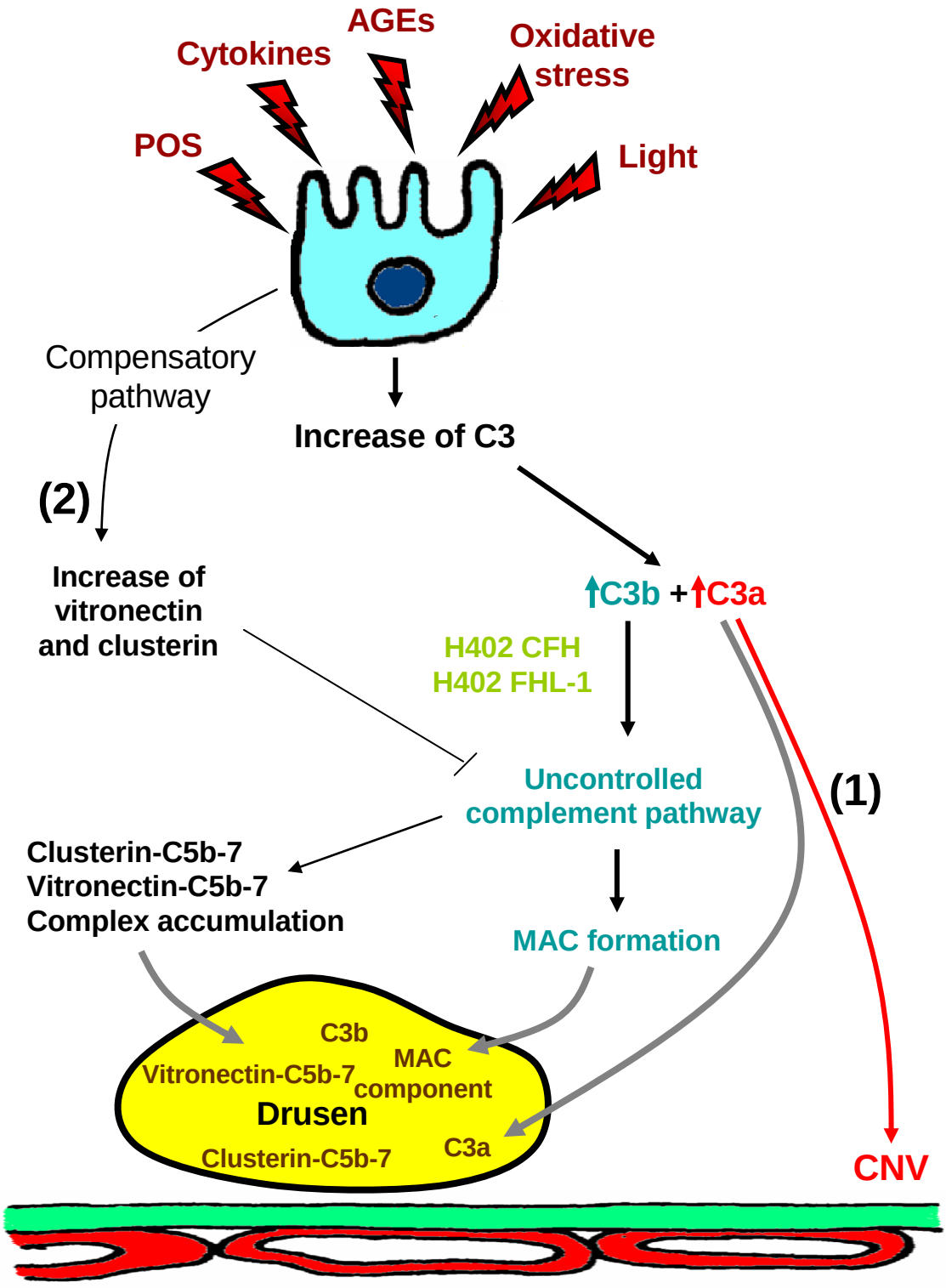
AGEs
Cytokines
Oxidative stress
POS
Light
Compensatory pathway
Increase of C3
(2)
Increase of vitronectin and clusterin
↑C3b +↑C3a
H402 CFH
H402 FHL-1
Uncontrolled complement pathway
(1)
Clusterin-C5b-7
Vitronectin-C5b-7
Complex accumulation
MAC formation
C3b
Vitronectin-C5b-7
MAC component
Drusen
Clusterin-C5b-7
C3a
CNV

6.4.2 HTRA1 model and AMD

Discovery of the second major genetic risk factors (e.g. variants in the promoter region of the *HTRA1* gene and in the *ARMS2* gene) has led to a new hypothesis surrounding AMD pathogenesis. Some suggested that *CFH* variant is primarily associated with the drusen formation and the dry form of AMD, whereas *HTRA1* promoter variant is mainly associated with CNV the hallmark feature of the wet AMD[53,277]. This was later verified by population studies, which show that variants in the *CFH* and *HTRA1/ARMS2* genes contribute equally to both dry and wet form[43,49,52,159,278]. While association of CFH variant with AMD was clear, it has been difficult to define the causal gene in the *HTRA1*/*ARMS2* haplotype because of the high LD between these two variants.

Currently, there is an ongoing debate about the role of *ARMS2* and *HTRA1* polymorphisms in AMD. While original studies showed that *HTRA1* promoter variant result in increased expression of HTRA1 protein and that HTRA1 might have a direct role in AMD pathogenesis[52,53] other studies contrast these finding and suggested that the missense mutation in the *ARMS2* gene is the causal variant[54,55]. Even though the gene encoding for ARMS2 has been cloned into *E. coli* and found to express an 11.3 kDa protein[56], detection and localization of ARMS2 in mammalian cells is still controversial. It has been detected in mitochondria[54], cysosolic[57], or even extracellular localization[58]. We could not detect ARMS2 in our RPE cultures; however, enhanced expression and secretion of HTRA1 protein was detected in RPE with HTRA1 promoter risk genotype (Chapter 4) and this agrees with earlier studies showing elevated expression of HTRA1 in lymphocyte and drusen of AMD donors[52,205,279]. Since we could not detect ARMS2 in our RPE culture, our second model (Figure 6.3) was focused around the role of HTRA1 in AMD. Indeed,

our data in Chapter 4 strongly support this model and suggest two parallel HTRA1 pathways leading to drusen formation, which are presented below and in Figure 6.3.

6.4.2.1 HTRA1 cleaves protein involved in amyloid deposition.

Amyloid is another major component found in drusen. Our secretome studies clearly show that RPE culture express and secrete amyloid precursor protein (APP) in their extracellular milieu. This precursor is processed by either α-secretase ADAM9 to form a protective APP ectodomain or by β-secretase (BACE) and γ-secretase (Presenilin) to form toxic Abeta which forms aggregates (Figure 6.4). Clusterin and Alpha-2-macroglobulin are other amyloid regulators. Alpha 2-mcroglobulin enhances the clearance of amyloid via complex formation with Abeta, which is then internalized by low density lipoprotein receptor (LRP) for further degradation. Clusterin has been suggested to directly bind amyloid and prevent it from depositing[226,227]. Interestingly, our data in Chapter 4 clearly show these amyloid interacting proteins are secreted by RPE cells and are substrate for HTRA1. Thus increased secretion of this protease by RPE cells will favor amyloid deposition.

6.4.2.2 HTRA1 cleaves protein involved in complement pathway regulation.

The second set of proteins that were affected by increased HTRA1 expression is those involved in the complement pathway regulation. These included vitronectin[280], clusterin[217], and fibromodulin[219]. Degradation of these complement pathway regulators by HTRA1 clearly supports a link between HTRA1 and the complement pathway in AMD pathogenesis.

Figure 6.3 Cellular and molecular model for HTRA1 and AMD pathogenesis

RPE cells harboring the risk genotype in the promoter region of *HTRA1* gene have increased secretion of the serine protease HTRA1 in their extracellular milieu. While RPE cells in young individuals might regulate HTRA1 expression via epigenetic mechanisms, RPE cells in aging individuals will fail to regulate this process resulting in progressive accumulation of HTRA1 in the sub RPE extracellulart space. (1) Increased HTRA1 cleaves key proteins involved in the regulation of amyloid deposition leading to progressive amyloid aggregation and drusen formation. (2) Increased HTRA1 cleaves key proteins involved in the negative regulation of the terminal pathway leading to activation of complement pathway and eventual cascade described in the model in figure 6.2. This later pathway links HTRA1 variant to complement pathway.

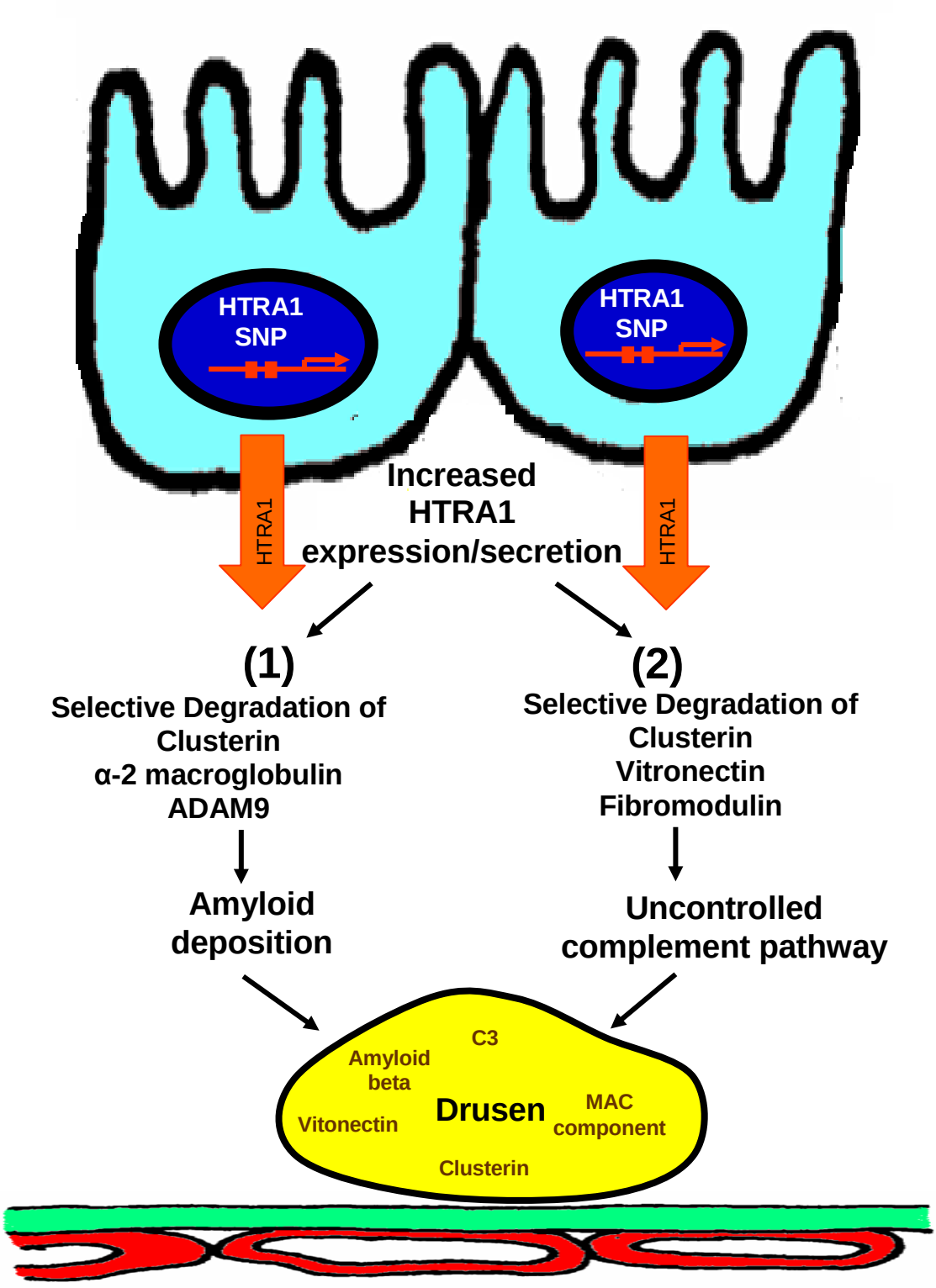
HTRA1
SNP
HTRA1
SNP
HTRA1
HTRA1
Increased
HTRA1
expression/secretion
(1)
Selective Degradation of
Clusterin
α-2 macroglobulin
ADAM9
(2)
Selective Degradation of
Clusterin
Vitronectin
Fibromodulin
Amyloid
deposition
Uncontrolled
complement pathway
C3
Amyloid
beta
Drusen
MAC
component
Vitonectin
Clusterin

6.4.2.3 Regulation of HTRA1 expression

The HTRA1 haplotype rs11200638 SNP is about 500 bp upstream of *HTRA1*, and could either alter binding of transcription factors or alter epigenetic regulation. Previous studies using an *in silico* approach identified a conserved AP2/SRF binding domain in the *HTRA1* promoter region[53]. They suggested that polymorphism in this area might influence binding of these transcription factors leading to increased secretion of HTRA1 in cells harboring the risk genotype. However others were not able to reproduce these data[54] and the regulation of HTRA1 expression by transcription factors remains unclear. Interestingly, the HTRA1 promoter polymorphism was also found to be a cytosine-guanine dinucleotide (CpG) rich region indicating a potential regulation by DNA methylation. We hypothesize that both genotype and aging influence DNA methylation at this locus resulting in differential expression of HTRA1. Indeed, it has been shown that DNA methylation dramatically decreases with age[281,282]. DNA methylation cause chromatin condensation leading to repressed gene expression[283,284]. Thus, as individuals age, decreased DNA methylation will result in enhanced HTRA1 expression. The G>A substitution may further affect this epigenetic regulation leading to uncontrolled expression of HTRA1 (Figure 6.3). HTRA1 predictably accumulates in the sub RPE space leading to progressive degradation of proteins involved in regulation of amyloid deposition and proteins involved in the regulation of complement pathways. This model strongly supports and explains the occurrence of both complement components and amyloid in drusen.

Figure 6.4 Amyloid precursor protein and sites for enzymatic processing

Transmembrane amyloid precursor protein (APP) can be enzymatically processed to either protective peptide or toxic peptide. β-secretase and γ-secretase cleave APP to produce toxic Abeta (blue box) while α-secretase cleaves APP within the Abeta generating protective peptide (blue and white striped box).

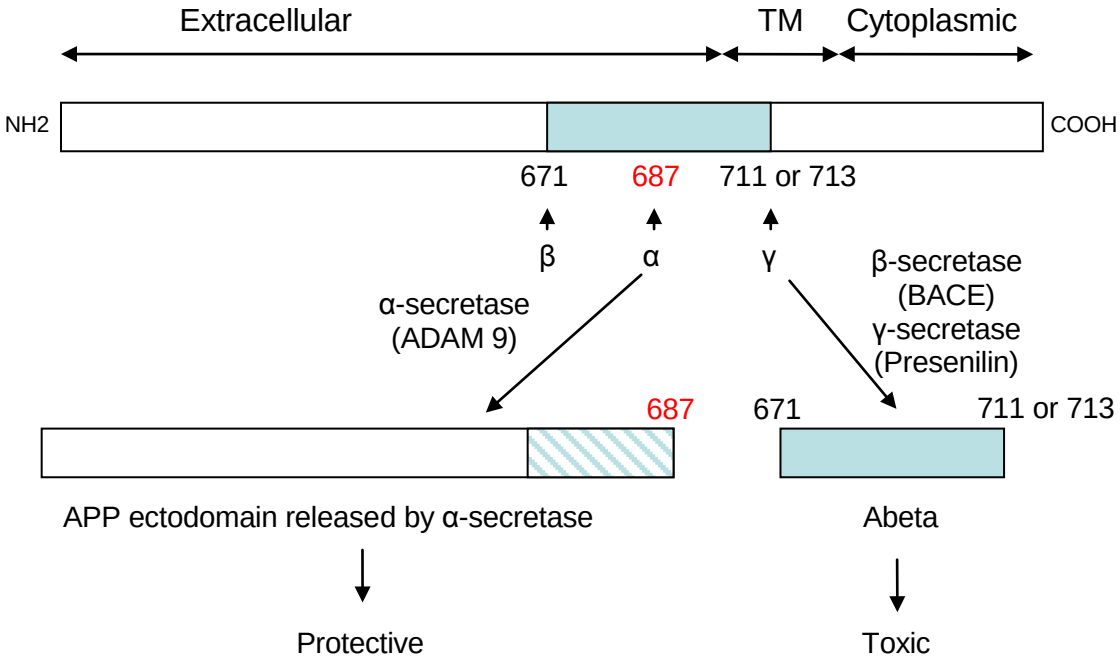
Extracellular
TM
Cytoplasmic
NH2
COOH
671
687
711 or 713
β
α
γ
α-secretase
(ADAM 9)
β-secretase
(BACE)
γ-secretase
(Presenilin)
687
671
711 or 713
APP ectodomain released by α-secretase
Abeta
Protective
Toxic

6.4.3 Joint effects of HTRA1 pathway and complement pathway

So far, we proposed two different models for AMD pathogenesis. One associated with the CFH variant and activation of the complement pathway and one associated with HTRA1 promoter variant leading to both amyloid deposition and indirect activation of the complement pathway. Whether amyloid deposition is specific to individuals with HTRA1 variant versus individuals with CFH variants remain to be examined. However, a recent study by Yang *et al*. (2006) shows that CFH variant and HTRA1/ARMS2 variant have additive risk factors[52] (Figure 6.5). An individual with both genetic risk factors has a 75 % chance of developing AMD. Among our established RPE cultures, one of the donors harbored both risk genotype and effectively had clinically documented AMD. In the context of our models above, this could be explained by a hyper-activation of complement pathway due to the contribution of both CFH/FHL-1 variant deficiency and the cleavage of the complement negative regulators by HTRA1 as well as excessive amyloid deposition due to cleavage of amyloid deposition regulators. Additionally, Abeta alters function of factor I, a complement inhibitor[285] and its increased formation was shown to upregulate BF and complement activator[286]. This further links HTRA1 polymorphism to CFH polymorphism and further explains the synergetic effect of these two variants in AMD.

6.5 Conclusions

The use of an integrated genomic and proteomics approach and the use of primary RPE cells from human autopsy eyes harboring authentic AMD risk genotypes lead to discovery of key pathways that start shedding light on drusen and CNV formation which are hallmark features of AMD pathogenesis. Although these are *in vitro* models and still

need *in vivo* validation, these key pathways could be used as therapeutic targets to treat or slowdown the progression of the disease. This is an area where personalized medicine could be implemented for successful treatments. For example, individuals with HTRA1 risk genotype could greatly benefit from anti amyloid deposition treatment[221,287] while individuals with CFH risk variant could benefit from local inhibition of complement pathway[38,288]. Individuals harboring both risk genotypes could benefit using a combination of both treatments.

Figure 6.5 Synergy between complement pathway and protease

While individual with both homozygote wild type alleles for both CFH and HTRA1 has an odds ratio 1 to develop AMD, odds ratio is tremendously increased when individual has homozygote risk alleles for both genes. Also, persons with heterozygote alleles in the promoter region of HTRA1 have greater odds than persons with heterozygote alleles in CFH [52]. This graph was generated with data from Yang *et al*.[52].

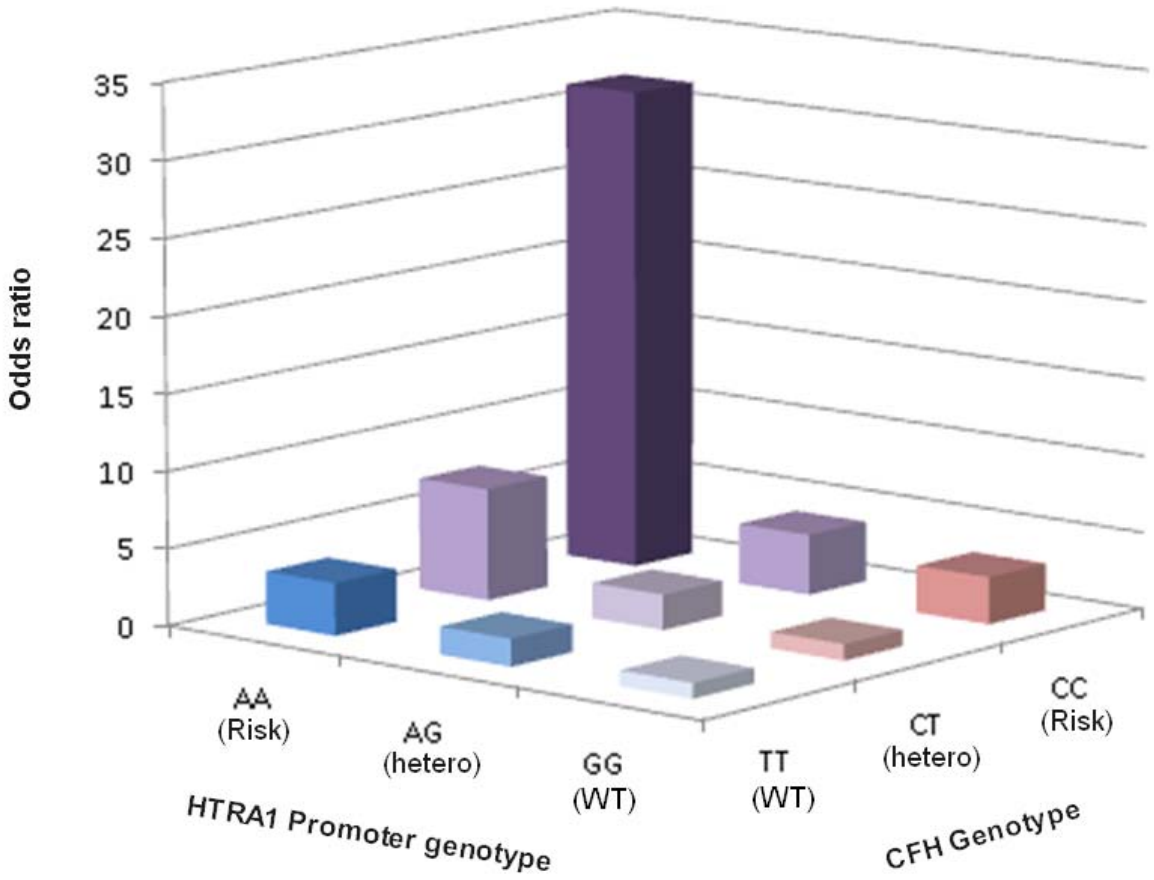
Odds ratio
35
30
25
20
15
10
5
0
AA
(Risk)
AG
(hetero)
GG
(WT)
HTRA1 Promoter genotype
TT
(WT)
CT
(hetero)
CC
(Risk)
CFH Genotype

6.6 Future directions

Even with some limitations with our *in vitro* model system, our findings strongly support the overarching hypothesis that RPE secreted proteins are involved in AMD pathogenesis. AMD assosicated genetic risk factors alter the homeostasis of RPE extracellular environment. We also suggested that two different genes / proteins; CFH and HTRA1 converge to the same downstream pathway leading to drusen formation.

1. Although these are *ex vitro* studies, the generated data could be used to select important proteins and follow their occurrence and activity *in vivo* using immunohistochemistry on cross sectional tissue prepared from freshly obtained autopsy eyes and in primate animal model.

2. We have demonstrated that RPE cells secrete both CFH and FHL-1. While their quantities were not affected by polymorphism in *CFH*, their functions remain to be fully characterized. One can test whether Y402 and H402 CFH and FHL-1 are functionally different in the context of RPE cells.

3. Clusterin, a regulator of complement pathway and a major component in drusen was found to be highly expressed in individual with CFH at risk genotype. Additionally clusterin was found to be selectively cleaved by HTRA1. Defining clusterin interacting proteins will bring more insight into the role of this protein in the context of our proposed models (e.g., Complement system model and HTRA1 model).

4. SNP in promoter of *HTRA1* is in high LD with a neighboring polymorphism (G>T; rs10490924; A69S) in a gene encoding for a poorly characterized protein named ARMS2 making it difficult to pinpoint the causal gene [50-53]. Currently, there is an ongoing debate about the role of ARMS2 and HTRA1 polymorphisms in AMD. Detection and

characterization of ARMS2 in the context of RPE cells and ocular tissue will resolve this controversy and refocus our thinking about AMD pathogenesis.

Chapter 7: References

1. Friedman, D.S. et al. Prevalence of age-related macular degeneration in the United States. *Arch Ophthalmol* **122**, 564-72 (2004).

2. Bok, D. New insights and new approaches toward the study of age-related macular degeneration. *Proc Natl Acad Sci U S A* **99**, 14619-21 (2002).

3. Gehrs, K.M., Anderson, D.H., Johnson, L.V. & Hageman, G.S. Age-related macular degeneration--emerging pathogenetic and therapeutic concepts. *Ann Med* **38**, 450-71 (2006).

4. From the Centers for Disease Control and Prevention. Ten great public health achievements--United States, 1900-1999. *Jama* **281**, 1481 (1999).

5. Klein, R., Klein, B.E. & Linton, K.L. Prevalence of age-related maculopathy. The Beaver Dam Eye Study. *Ophthalmology* **99**, 933-43 (1992).

6. Mitchell, P., Smith, W., Attebo, K. & Wang, J.J. Prevalence of age-related maculopathy in Australia. The Blue Mountains Eye Study. *Ophthalmology* **102**, 1450-60 (1995).

7. Evans, J.R. Risk factors for age-related macular degeneration. *Prog Retin Eye Res* **20**, 227-53 (2001).

8. Kennedy, C.J., Rakoczy, P.E. & Constable, I.J. Lipofuscin of the retinal pigment epithelium: a review. *Eye* **9 (Pt 6)**, 763-71 (1995).

9. Bonnel, S., Mohand-Said, S. & Sahel, J.A. The aging of the retina. *Exp Gerontol* **38**, 825-31 (2003).

10. Ivy, G.O. et al. Lipofuscin-like substances accumulate rapidly in brain, retina and internal organs with cysteine protease inhibition. *Adv Exp Med Biol* **266**, 31-45; discussion 45-7 (1989).

11. Brunk, U.T. & Terman, A. Lipofuscin: mechanisms of age-related accumulation and influence on cell function. *Free Radic Biol Med* **33**, 611-9 (2002).

12. Finnemann, S.C., Leung, L.W. & Rodriguez-Boulan, E. The lipofuscin component A2E selectively inhibits phagolysosomal degradation of photoreceptor phospholipid by the retinal pigment epithelium. *Proc Natl Acad Sci U S A* **99**, 3842-7 (2002).

13. Katz, M.L. Potential role of retinal pigment epithelial lipofuscin accumulation in age-related macular degeneration. *Arch Gerontol Geriatr* **34**, 359-70 (2002).

14. Wolf, G. Lipofuscin and macular degeneration. *Nutr Rev* **61**, 342-6 (2003).

15. Zhou, J., Jang, Y.P., Kim, S.R. & Sparrow, J.R. Complement activation by photooxidation products of A2E, a lipofuscin constituent of the retinal pigment epithelium. *Proc Natl Acad Sci U S A* **103**, 16182-7 (2006).

16. Glenn, J.V. et al. Advanced glycation end product (AGE) accumulation on Bruch's membrane: links to age-related RPE dysfunction. *Invest Ophthalmol Vis Sci* **50**, 441-51 (2009).

17. Gugliucci, A. & Bendayan, M. Renal fate of circulating advanced glycated end products (AGE): evidence for reabsorption and catabolism of AGE-peptides by renal proximal tubular cells. *Diabetologia* **39**, 149-60 (1996).

18. Howes, K.A. et al. Receptor for advanced glycation end products and age-related macular degeneration. *Invest Ophthalmol Vis Sci* **45**, 3713-20 (2004).

19. Glenn, J.V. & Stitt, A.W. The role of advanced glycation end products in retinal ageing and disease. *Biochim Biophys Acta* **1790**, 1109-16 (2009).

20. Hyman, L.G., Lilienfeld, A.M., Ferris, F.L., 3rd & Fine, S.L. Senile macular degeneration: a case-control study. *Am J Epidemiol* **118**, 213-27 (1983).

21. Klein, M.L., Mauldin, W.M. & Stoumbos, V.D. Heredity and age-related macular degeneration. Observations in monozygotic twins. *Arch Ophthalmol* **112**, 932-7 (1994).

22. Meyers, S.M., Greene, T. & Gutman, F.A. A twin study of age-related macular degeneration. *Am J Ophthalmol* **120**, 757-66 (1995).

23. Klein, M.L. et al. Age-related macular degeneration. Clinical features in a large family and linkage to chromosome 1q. *Arch Ophthalmol* **116**, 1082-8 (1998).

24. Weeks, D.E. et al. A full genome scan for age-related maculopathy. *Hum Mol Genet* **9**, 1329-49 (2000).

25. Weeks, D.E. et al. Age-related maculopathy: an expanded genome-wide scan with evidence of susceptibility loci within the 1q31 and 17q25 regions. *Am J Ophthalmol* **132**, 682-92 (2001).

26. Majewski, J. et al. Age-related macular degeneration--a genome scan in extended families. *Am J Hum Genet* **73**, 540-50 (2003).

27. Schick, J.H. et al. A whole-genome screen of a quantitative trait of age-related maculopathy in sibships from the Beaver Dam Eye Study. *Am J Hum Genet* **72**, 1412-24 (2003).

28. Seddon, J.M., Santangelo, S.L., Book, K., Chong, S. & Cote, J. A genomewide scan for age-related macular degeneration provides evidence for linkage to several chromosomal regions. *Am J Hum Genet* **73**, 780-90 (2003).

29. Weeks, D.E. et al. Age-related maculopathy: a genomewide scan with continued evidence of susceptibility loci within the 1q31, 10q26, and 17q25 regions. *Am J Hum Genet* **75**, 174-89 (2004).

30. Abecasis, G.R. et al. Age-related macular degeneration: a high-resolution genome scan for susceptibility loci in a population enriched for late-stage disease. *Am J Hum Genet* **74**, 482-94 (2004).

31. Iyengar, S.K. et al. Dissection of genomewide-scan data in extended families reveals a major locus and oligogenic susceptibility for age-related macular degeneration. *Am J Hum Genet* **74**, 20-39 (2004).

32. Fisher, S.A. et al. Meta-analysis of genome scans of age-related macular degeneration. *Hum Mol Genet* **14**, 2257-64 (2005).

33. Klein, R.J. et al. Complement factor H polymorphism in age-related macular degeneration. *Science* **308**, 385-9 (2005).

34. Haines, J.L. et al. Complement factor H variant increases the risk of age-related macular degeneration. *Science* **308**, 419-21 (2005).

35. Hageman, G.S. et al. A common haplotype in the complement regulatory gene factor H (HF1/CFH) predisposes individuals to age-related macular degeneration. *Proc Natl Acad Sci U S A* **102**, 7227-32 (2005).

36. Edwards, A.O. et al. Complement factor H polymorphism and age-related macular degeneration. *Science* **308**, 421-4 (2005).

37. Janeway, C.J., ; Travers, P.; Walport, m,; Shlomchik, MJ. *Immunobiology*, (Garland Publishing, New York, 2001).

38. Ricklin, D. & Lambris, J.D. Complement-targeted therapeutics. *Nat Biotechnol* **25**, 1265-75 (2007).

39. Ormsby, R.J. et al. Functional and structural implications of the complement factor H Y402H polymorphism associated with age-related macular degeneration. *Invest Ophthalmol Vis Sci* **49**, 1763-70 (2008).

40. Yu, J. et al. Biochemical analysis of a common human polymorphism associated with age-related macular degeneration. *Biochemistry* **46**, 8451-61 (2007).

41. Giannakis, E. et al. A common site within factor H SCR 7 responsible for binding heparin, C-reactive protein and streptococcal M protein. *Eur J Immunol* **33**, 962-9 (2003).

42. Gold, B. et al. Variation in factor B (BF) and complement component 2 (C2) genes is associated with age-related macular degeneration. *Nat Genet* **38**, 458-62 (2006).

43. Maller, J. et al. Common variation in three genes, including a noncoding variant in CFH, strongly influences risk of age-related macular degeneration. *Nat Genet* **38**, 1055-9 (2006).

44. Spencer, K.L. et al. Protective effect of complement factor B and complement component 2 variants in age-related macular degeneration. *Hum Mol Genet* **16**, 1986-92 (2007).

45. Spencer, K.L. et al. C3 R102G polymorphism increases risk of age-related macular degeneration. *Hum Mol Genet* **17**, 1821-4 (2008).

46. Jakobsdottir, J., Conley, Y.P., Weeks, D.E., Ferrell, R.E. & Gorin, M.B. C2 and CFB genes in age-related maculopathy and joint action with CFH and LOC387715 genes. *PLoS One* **3**, e2199 (2008).

47. Magnusson, K.P. et al. CFH Y402H confers similar risk of soft drusen and both forms of advanced AMD. *PLoS Med* **3**, e5 (2006).

48. Sepp, T. et al. Complement factor H variant Y402H is a major risk determinant for geographic atrophy and choroidal neovascularization in smokers and nonsmokers. *Invest Ophthalmol Vis Sci* **47**, 536-40 (2006).

49. Despriet, D.D. et al. Complement factor H polymorphism, complement activators, and risk of age-related macular degeneration. *Jama* **296**, 301-9 (2006).

50. Rivera, A. et al. Hypothetical LOC387715 is a second major susceptibility gene for age-related macular degeneration, contributing independently of complement factor H to disease risk. *Hum Mol Genet* **14**, 3227-36 (2005).

51. Jakobsdottir, J. et al. Susceptibility genes for age-related maculopathy on chromosome 10q26. *Am J Hum Genet* **77**, 389-407 (2005).

52. Yang, Z. et al. A variant of the HTRA1 gene increases susceptibility to age-related macular degeneration. *Science* **314**, 992-3 (2006).

53. Dewan, A. et al. HTRA1 promoter polymorphism in wet age-related macular degeneration. *Science* **314**, 989-92 (2006).

54. Kanda, A. et al. A variant of mitochondrial protein LOC387715/ARMS2, not HTRA1, is strongly associated with age-related macular degeneration. *Proc Natl Acad Sci U S A* **104**, 16227-32 (2007).

55. Fritsche, L.G. et al. Age-related macular degeneration is associated with an unstable ARMS2 (LOC387715) mRNA. *Nat Genet* **40**, 892-6 (2008).

56. Chen, D., Langford, M.P., Duggan, C., Madden, B.J. & Edwards, A.O. Expression of recombinant protein encoded by LOC387715 in Escherichia coli. *Protein Expr Purif* **54**, 275-82 (2007).

57. Wang, G. et al. Localization of age-related macular degeneration-associated ARMS2 in cytosol, not mitochondria. *Invest Ophthalmol Vis Sci* **50**, 3084-90 (2009).

58. Kortvely, E. et al. ARMS2 is a constituent of the extracellular matrix providing a link between familial and sporadic age-related macular degenerations. *Invest Ophthalmol Vis Sci* (2009).

59. Lipinska, B., Sharma, S. & Georgopoulos, C. Sequence analysis and regulation of the htrA gene of Escherichia coli: a sigma 32-independent mechanism of heat-inducible transcription. *Nucleic Acids Res* **16**, 10053-67 (1988).

60. Strauch, K.L. & Beckwith, J. An Escherichia coli mutation preventing degradation of abnormal periplasmic proteins. *Proc Natl Acad Sci U S A* **85**, 1576-80 (1988).

61. Baldi, A. et al. The HtrA1 serine protease is down-regulated during human melanoma progression and represses growth of metastatic melanoma cells. *Oncogene* **21**, 6684-8 (2002).

62. Chien, J. et al. A candidate tumor suppressor HtrA1 is downregulated in ovarian cancer. *Oncogene* **23**, 1636-44 (2004).

63. Esposito, V. et al. Analysis of HtrA1 serine protease expression in human lung cancer. *Anticancer Res* **26**, 3455-9 (2006).

64. Grau, S. et al. The role of human HtrA1 in arthritic disease. *J Biol Chem* **281**, 6124-9 (2006).

65. Tsuchiya, A. et al. Expression of mouse HtrA1 serine protease in normal bone and cartilage and its upregulation in joint cartilage damaged by experimental arthritis. *Bone* **37**, 323-36 (2005).

66. Bakay, M., Zhao, P., Chen, J. & Hoffman, E.P. A web-accessible complete transcriptome of normal human and DMD muscle. *Neuromuscul Disord* **12 Suppl 1**, S125-41 (2002).

67. Chien, J., He, X. & Shridhar, V. Identification of tubulins as substrates of serine protease HtrA1 by mixture-based oriented peptide library screening. *J Cell Biochem* **107**, 253-63 (2009).

68. Carresi, C. et al. Montelparo study: risk factors for age-related macular degeneration in a little rural community in Italy. *Clin Ter* **160**, e43-51 (2009).

69. Cho, E. et al. Prospective study of dietary fat and the risk of age-related macular degeneration. *Am J Clin Nutr* **73**, 209-18 (2001).

70. Seddon, J.M. et al. Dietary fat and risk for advanced age-related macular degeneration. *Arch Ophthalmol* **119**, 1191-9 (2001).

71. Thornton, J. et al. Smoking and age-related macular degeneration: a review of association. *Eye* **19**, 935-44 (2005).

72. Schmidt, S. et al. Cigarette smoking strongly modifies the association of LOC387715 and age-related macular degeneration. *Am J Hum Genet* **78**, 852-64 (2006).

73. DeAngelis, M.M. et al. Cigarette smoking, CFH, APOE, ELOVL4, and risk of neovascular age-related macular degeneration. *Arch Ophthalmol* **125**, 49-54 (2007).

74. Klein, R. et al. The Wisconsin age-related maculopathy grading system. *Ophthalmology* **98**, 1128-34 (1991).

75. Bressler, N.M., Bressler, S.B., West, S.K., Fine, S.L. & Taylor, H.R. The grading and prevalence of macular degeneration in Chesapeake Bay watermen. *Arch Ophthalmol* **107**, 847-52 (1989).

76. Klein, R., Meuer, S.M., Moss, S.E. & Klein, B.E. Detection of drusen and early signs of age-related maculopathy using a nonmydriatic camera and a standard fundus camera. *Ophthalmology* **99**, 1686-92 (1992).

77. Vingerling, J.R. et al. The prevalence of age-related maculopathy in the Rotterdam Study. *Ophthalmology* **102**, 205-10 (1995).

78. Hageman, G.S. & Mullins, R.F. Molecular composition of drusen as related to substructural phenotype. *Mol Vis* **5**, 28 (1999).

79. Curcio, C.A. & Millican, C.L. Basal linear deposit and large drusen are specific for early age-related maculopathy. *Arch Ophthalmol* **117**, 329-39 (1999).

80. Mullins, R.F., Russell, S.R., Anderson, D.H. & Hageman, G.S. Drusen associated with aging and age-related macular degeneration contain proteins common to extracellular deposits associated with atherosclerosis, elastosis, amyloidosis, and dense deposit disease. *Faseb J* **14**, 835-46 (2000).

81. Crabb, J.W. et al. Drusen proteome analysis: an approach to the etiology of age-related macular degeneration. *Proc Natl Acad Sci U S A* **99**, 14682-7 (2002).

82. Li, C.M., Clark, M.E., Chimento, M.F. & Curcio, C.A. Apolipoprotein localization in isolated drusen and retinal apolipoprotein gene expression. *Invest Ophthalmol Vis Sci* **47**, 3119-28 (2006).

83. Umeda, S. et al. Molecular composition of drusen and possible involvement of anti-retinal autoimmunity in two different forms of macular degeneration in cynomolgus monkey (Macaca fascicularis). *Faseb J* **19**, 1683-5 (2005).

84. Sakaguchi, H. et al. Clusterin is present in drusen in age-related macular degeneration. *Exp Eye Res* **74**, 547-9 (2002).

85. Haimovici, R., Gantz, D.L., Rumelt, S., Freddo, T.F. & Small, D.M. The lipid composition of drusen, Bruch's membrane, and sclera by hot stage polarizing light microscopy. *Invest Ophthalmol Vis Sci* **42**, 1592-9 (2001).

86. Mullins, R.F. & Hageman, G.S. Human ocular drusen possess novel core domains with a distinct carbohydrate composition. *J Histochem Cytochem* **47**, 1533-40 (1999).

87. Li, C.M., Clark, M.E., Rudolf, M. & Curcio, C.A. Distribution and composition of esterified and unesterified cholesterol in extra-macular drusen. *Exp Eye Res* **85**, 192-201 (2007).

88. Farkas, T.G., Sylvester, V., Archer, D. & Altona, M. The histochemistry of drusen. *Am J Ophthalmol* **71**, 1206-15 (1971).

89. Tanihara, H., Yoshida, M., Matsumoto, M. & Yoshimura, N. Identification of transforming growth factor-beta expressed in cultured human retinal pigment epithelial cells. *Invest Ophthalmol Vis Sci* **34**, 413-9 (1993).

90. Alexander, J.P., Bradley, J.M., Gabourel, J.D. & Acott, T.S. Expression of matrix metalloproteinases and inhibitor by human retinal pigment epithelium. *Invest Ophthalmol Vis Sci* **31**, 2520-8 (1990).

91. Eichler, W., Friedrichs, U., Thies, A., Tratz, C. & Wiedemann, P. Modulation of matrix metalloproteinase and TIMP-1 expression by cytokines in human RPE cells. *Invest Ophthalmol Vis Sci* **43**, 2767-73 (2002).

92. Hageman, G.S., Mullins, R.F., Russell, S.R., Johnson, L.V. & Anderson, D.H. Vitronectin is a constituent of ocular drusen and the vitronectin gene is expressed in human retinal pigmented epithelial cells. *Faseb J* **13**, 477-84 (1999).

93. Hageman, G.S. et al. An integrated hypothesis that considers drusen as biomarkers of immune-mediated processes at the RPE-Bruch's membrane interface in aging and age-related macular degeneration. *Prog Retin Eye Res* **20**, 705-32 (2001).

94. Ishida, B.Y. et al. Regulated expression of apolipoprotein E by human retinal pigment epithelial cells. *J Lipid Res* **45**, 263-71 (2004).

95. Holtkamp, G.M., Kijlstra, A., Peek, R. & de Vos, A.F. Retinal pigment epithelium-immune system interactions: cytokine production and cytokine-induced changes. *Prog Retin Eye Res* **20**, 29-48 (2001).

96. Adamis, A.P. et al. Synthesis and secretion of vascular permeability factor/vascular endothelial growth factor by human retinal pigment epithelial cells. *Biochem Biophys Res Commun* **193**, 631-8 (1993).

97. Murata, T. et al. The relation between expression of vascular endothelial growth factor and breakdown of the blood-retinal barrier in diabetic rat retinas. *Lab Invest* **74**, 819-25 (1996).

98. Freund, K.B., Yannuzzi, L.A. & Sorenson, J.A. Age-related macular degeneration and choroidal neovascularization. *Am J Ophthalmol* **115**, 786-91 (1993).

99. Lonn, E. et al. Effects of long-term vitamin E supplementation on cardiovascular events and cancer: a randomized controlled trial. *Jama* **293**, 1338-47 (2005).

100. The effect of vitamin E and beta carotene on the incidence of lung cancer and other cancers in male smokers. The Alpha-Tocopherol, Beta Carotene Cancer Prevention Study Group. *N Engl J Med* **330**, 1029-35 (1994).

101. Albanes, D. et al. Alpha-Tocopherol and beta-carotene supplements and lung cancer incidence in the alpha-tocopherol, beta-carotene cancer prevention study: effects of base-line characteristics and study compliance. *J Natl Cancer Inst* **88**, 1560-70 (1996).

102. Omenn, G.S. et al. Effects of a combination of beta carotene and vitamin A on lung cancer and cardiovascular disease. *N Engl J Med* **334**, 1150-5 (1996).

103. Johnson, A.R., Munoz, A., Gottlieb, J.L. & Jarrard, D.F. High dose zinc increases hospital admissions due to genitourinary complications. *J Urol* **177**, 639-43 (2007).

104. Hathout, Y. Approaches to the study of the cell secretome. *Expert Rev Proteomics* **4**, 239-48 (2007).

105. Rabilloud, T. Two-dimensional gel electrophoresis in proteomics: old, old fashioned, but it still climbs up the mountains. *Proteomics* **2**, 3-10 (2002).

106. Zwickl, H. et al. A novel technique to specifically analyze the secretome of cells and tissues. *Electrophoresis* **26**, 2779-85 (2005).

107. Thouvenot, E. et al. The proteomic analysis of mouse choroid plexus secretome reveals a high protein secretion capacity of choroidal epithelial cells. *Proteomics* **6**, 5941-52 (2006).

108. Zvonic, S. et al. Secretome of primary cultures of human adipose-derived stem cells: modulation of serpins by adipogenesis. *Mol Cell Proteomics* **6**, 18-28 (2007).

109. Aebersold, R. & Mann, M. Mass spectrometry-based proteomics. *Nature* **422**, 198-207 (2003).

110. Ong, S.E. et al. Stable isotope labeling by amino acids in cell culture, SILAC, as a simple and accurate approach to expression proteomics. *Mol Cell Proteomics* **1**, 376-86 (2002).

111. Yao, X., Freas, A., Ramirez, J., Demirev, P.A. & Fenselau, C. Proteolytic 18O labeling for comparative proteomics: model studies with two serotypes of adenovirus. *Anal Chem* **73**, 2836-42 (2001).

112. Gygi, S.P. et al. Quantitative analysis of complex protein mixtures using isotope-coded affinity tags. *Nat Biotechnol* **17**, 994-9 (1999).

113. Ong, S.E., Foster, L.J. & Mann, M. Mass spectrometric-based approaches in quantitative proteomics. *Methods* **29**, 124-30 (2003).

114. Gehrmann, M.L., Hathout, Y. & Fenselau, C. Evaluation of metabolic labeling for comparative proteomics in breast cancer cells. *J Proteome Res* **3**, 1063-8 (2004).

115. Everley, P.A., Krijgsveld, J., Zetter, B.R. & Gygi, S.P. Quantitative cancer proteomics: stable isotope labeling with amino acids in cell culture (SILAC) as a tool for prostate cancer research. *Mol Cell Proteomics* **3**, 729-35 (2004).

116. Hathout, Y., Flippin, J., Fan, C., Liu, P. & Csaky, K. Metabolic labeling of human primary retinal pigment epithelial cells for accurate comparative proteomics. *J Proteome Res* **4**, 620-7 (2005).

117. Ibarrola, N., Kalume, D.E., Gronborg, M., Iwahori, A. & Pandey, A. A proteomic approach for quantitation of phosphorylation using stable isotope labeling in cell culture. *Anal Chem* **75**, 6043-9 (2003).

118. Gruhler, A., Schulze, W.X., Matthiesen, R., Mann, M. & Jensen, O.N. Stable isotope labeling of Arabidopsis thaliana cells and quantitative proteomics by mass spectrometry. *Mol Cell Proteomics* **4**, 1697-709 (2005).

119. Zhang, G., Spellman, D.S., Skolnik, E.Y. & Neubert, T.A. Quantitative phosphotyrosine proteomics of EphB2 signaling by stable isotope labeling with amino acids in cell culture (SILAC). *J Proteome Res* **5**, 581-8 (2006).

120. Blagoev, B. et al. A proteomics strategy to elucidate functional protein-protein interactions applied to EGF signaling. *Nat Biotechnol* **21**, 315-8 (2003).

121. Foster, L.J. et al. Insulin-dependent interactions of proteins with GLUT4 revealed through stable isotope labeling by amino acids in cell culture (SILAC). *J Proteome Res* **5**, 64-75 (2006).

122. Gronborg, M. et al. Biomarker discovery from pancreatic cancer secretome using a differential proteomic approach. *Mol Cell Proteomics* **5**, 157-71 (2006).

123. Young, R.W. Pathophysiology of age-related macular degeneration. *Surv Ophthalmol* **31**, 291-306 (1987).

124. van der Schaft, T.L., de Bruijn, W.C., Mooy, C.M. & de Jong, P.T. Basal laminar deposit in the aging peripheral human retina. *Graefes Arch Clin Exp Ophthalmol* **231**, 470-5 (1993).

125. Pauleikhoff, D. et al. [Drusen and their significance in age related macular degeneration]. *Fortschr Ophthalmol* **87**, 429-32 (1990).

126. Algvere, P.V. & Seregard, S. Drusen maculopathy: a risk factor for AMD. Can we prevent visual loss? *Acta Ophthalmol Scand* **81**, 427-9 (2003).

127. Boulton, M. & Dayhaw-Barker, P. The role of the retinal pigment epithelium: topographical variation and ageing changes. *Eye* **15**, 384-9 (2001).

128. Alexander, J.J., Pickering, M.C., Haas, M., Osawe, I. & Quigg, R.J. Complement factor h limits immune complex deposition and prevents inflammation and scarring in glomeruli of mice with chronic serum sickness. *J Am Soc Nephrol* **16**, 52-7 (2005).

129. Alge, C.S. et al. Comparative proteome analysis of native differentiated and cultured dedifferentiated human RPE cells. *Invest Ophthalmol Vis Sci* **44**, 3629-41 (2003).

130. Leschey, K.H., Hackett, S.F., Singer, J.H. & Campochiaro, P.A. Growth factor responsiveness of human retinal pigment epithelial cells. *Invest Ophthalmol Vis Sci* **31**, 839-46 (1990).

131. Livak, K.J. Allelic discrimination using fluorogenic probes and the 5' nuclease assay. *Genet Anal* **14**, 143-9 (1999).

132. Halligan, B.D. et al. ZoomQuant: an application for the quantitation of stable isotope labeled peptides. *J Am Soc Mass Spectrom* **16**, 302-6 (2005).

133. Hittel, D.S., Kraus, W.E. & Hoffman, E.P. Skeletal muscle dictates the fibrinolytic state after exercise training in overweight men with characteristics of metabolic syndrome. *J Physiol* **548**, 401-10 (2003).

134. Expression profiling--best practices for data generation and interpretation in clinical trials. *Nat Rev Genet* **5**, 229-37 (2004).

135. Gygi, S.P., Rochon, Y., Franza, B.R. & Aebersold, R. Correlation between protein and mRNA abundance in yeast. *Mol Cell Biol* **19**, 1720-30 (1999).

136. Tian, Q. et al. Integrated genomic and proteomic analyses of gene expression in Mammalian cells. *Mol Cell Proteomics* **3**, 960-9 (2004).

137. Anderson, D.H., Mullins, R.F., Hageman, G.S. & Johnson, L.V. A role for local inflammation in the formation of drusen in the aging eye. *Am J Ophthalmol* **134**, 411-31 (2002).

138. Malek, G., Li, C.M., Guidry, C., Medeiros, N.E. & Curcio, C.A. Apolipoprotein B in cholesterol-containing drusen and basal deposits of human eyes with age-related maculopathy. *Am J Pathol* **162**, 413-25 (2003).

139. Johnson, L.V., Leitner, W.P., Staples, M.K. & Anderson, D.H. Complement activation and inflammatory processes in Drusen formation and age related macular degeneration. *Exp Eye Res* **73**, 887-96 (2001).

140. Bailey, R.W., Dunker, A.K., Brown, C.J., Garner, E.C. & Griswold, M.D. Clusterin, a binding protein with a molten globule-like region. *Biochemistry* **40**, 11828-40 (2001).

141. DeMattos, R.B. et al. Clusterin promotes amyloid plaque formation and is critical for neuritic toxicity in a mouse model of Alzheimer's disease. *Proc Natl Acad Sci U S A* **99**, 10843-8 (2002).

142. Anderson, D.H. et al. Characterization of beta amyloid assemblies in drusen: the deposits associated with aging and age-related macular degeneration. *Exp Eye Res* **78**, 243-56 (2004).

143. Luibl, V. et al. Drusen deposits associated with aging and age-related macular degeneration contain nonfibrillar amyloid oligomers. *J Clin Invest* **116**, 378-85 (2006).

144. Rosenberg, M.E. & Silkensen, J. Clusterin: physiologic and pathophysiologic considerations. *Int J Biochem Cell Biol* **27**, 633-45 (1995).

145. Plantner, J.J., Jiang, C. & Smine, A. Increase in interphotoreceptor matrix gelatinase A (MMP-2) associated with age-related macular degeneration. *Exp Eye Res* **67**, 637-45 (1998).

146. Leu, S.T. et al. Drusen are Cold Spots for Proteolysis: Expression of Matrix Metalloproteinases and Their Tissue Inhibitor Proteins in Age-related Macular Degeneration. *Exp Eye Res* **74**, 141-54 (2002).

147. Lambert, V. et al. MMP-2 and MMP-9 synergize in promoting choroidal neovascularization. *Faseb J* **17**, 2290-2 (2003).

148. Hiscott, P. et al. Pathobiology of epiretinal and subretinal membranes: possible roles for the matricellular proteins thrombospondin 1 and osteonectin (SPARC). *Eye* **16**, 393-403 (2002).

149. Chlenski, A. et al. SPARC is a key Schwannian-derived inhibitor controlling neuroblastoma tumor angiogenesis. *Cancer Res* **62**, 7357-63 (2002).

150. Nozaki, M. et al. Loss of SPARC-mediated VEGFR-1 suppression after injury reveals a novel antiangiogenic activity of VEGF-A. *J Clin Invest* **116**, 422-9 (2006).

151. Sternlicht, M.D. & Werb, Z. How matrix metalloproteinases regulate cell behavior. *Annu Rev Cell Dev Biol* **17**, 463-516 (2001).

152. Sage, E.H. et al. Cleavage of the matricellular protein SPARC by matrix metalloproteinase 3 produces polypeptides that influence angiogenesis. *J Biol Chem* **278**, 37849-57 (2003).

153. Dawson, D.W. et al. Pigment epithelium-derived factor: a potent inhibitor of angiogenesis. *Science* **285**, 245-8 (1999).

154. Martin, G., Schlunck, G., Hansen, L.L. & Agostini, H.T. Differential expression of angioregulatory factors in normal and CNV-derived human retinal pigment epithelium. *Graefes Arch Clin Exp Ophthalmol* **242**, 321-6 (2004).

155. Gao, G. et al. Down-regulation of vascular endothelial growth factor and up-regulation of pigment epithelium-derived factor: a possible mechanism for the anti-angiogenic activity of plasminogen kringle 5. *J Biol Chem* **277**, 9492-7 (2002).

156. Newsome, D.A., Hewitt, A.T., Huh, W., Robey, P.G. & Hassell, J.R. Detection of specific extracellular matrix molecules in drusen, Bruch's membrane, and ciliary body. *Am J Ophthalmol* **104**, 373-81 (1987).

157. Grossniklaus, H.E. et al. Immunohistochemical and histochemical properties of surgically excised subretinal neovascular membranes in age-related macular degeneration. *Am J Ophthalmol* **114**, 464-72 (1992).

158. Sasaki, T., Brakebusch, C., Engel, J. & Timpl, R. Mac-2 binding protein is a cell-adhesive protein of the extracellular matrix which self-assembles into ring-like structures and binds beta1 integrins, collagens and fibronectin. *Embo J* **17**, 1606-13 (1998).

159. Cameron, D.J. et al. HTRA1 variant confers similar risks to geographic atrophy and neovascular age-related macular degeneration. *Cell Cycle* **6**, 1122-5 (2007).

160. Ishibashi, T., Patterson, R., Ohnishi, Y., Inomata, H. & Ryan, S.J. Formation of drusen in the human eye. *Am J Ophthalmol* **101**, 342-53 (1986).

161. An, E. et al. Secreted proteome profiling in human RPE cell cultures derived from donors with age related macular degeneration and age matched healthy donors. *J Proteome Res* **5**, 2599-610 (2006).

162. Marmor, M.W., TJ. *The Retinal Pigment Epithelium*, (Oxford University Press, New York, 1998).

163. Lopez, P.F. et al. Pathologic features of surgically excised subretinal neovascular membranes in age-related macular degeneration. *Am J Ophthalmol* **112**, 647-56 (1991).

164. Elner, S.G. et al. Monocyte chemotactic protein gene expression by cytokine-treated human retinal pigment epithelial cells. *Lab Invest* **64**, 819-25 (1991).

165. Bian, Z.M. et al. IL-4 potentiates IL-1beta- and TNF-alpha-stimulated IL-8 and MCP-1 protein production in human retinal pigment epithelial cells. *Curr Eye Res* **18**, 349-57 (1999).

166. Shi, G. et al. Control of chemokine gradients by the retinal pigment epithelium. *Invest Ophthalmol Vis Sci* **49**, 4620-30 (2008).

167. Stokes, M.P. et al. Profiling of UV-induced ATM/ATR signaling pathways. *Proc Natl Acad Sci U S A* **104**, 19855-60 (2007).

168. Dobreva, I., Fielding, A., Foster, L.J. & Dedhar, S. Mapping the integrin-linked kinase interactome using SILAC. *J Proteome Res* **7**, 1740-9 (2008).

169. Kruger, M. et al. Dissection of the insulin signaling pathway via quantitative phosphoproteomics. *Proc Natl Acad Sci U S A* **105**, 2451-6 (2008).

170. Amanchy, R., Kalume, D.E., Iwahori, A., Zhong, J. & Pandey, A. Phosphoproteome analysis of HeLa cells using stable isotope labeling with amino acids in cell culture (SILAC). *J Proteome Res* **4**, 1661-71 (2005).

171. Gruhler, A. et al. Quantitative phosphoproteomics applied to the yeast pheromone signaling pathway. *Mol Cell Proteomics* **4**, 310-27 (2005).

172. Liu, J. et al. Predominant release of lysosomal enzymes by newborn rat microglia after LPS treatment revealed by proteomic studies. *J Proteome Res* **7**, 2033-49 (2008).

173. Sidak, A. Rectangular confidence regions for the means of multivariate normal distributions. *JASA* **62**, 626-33 (1967).

174. Yang, P., McKay, B.S., Allen, J.B. & Jaffe, G.J. Effect of NF-kappa B inhibition on TNF-alpha-induced apoptosis in human RPE cells. *Invest Ophthalmol Vis Sci* **45**, 2438-46 (2004).

175. Yang, P. et al. Human RPE expression of cell survival factors. *Invest Ophthalmol Vis Sci* **46**, 1755-64 (2005).

176. DiDonato, J.A., Hayakawa, M., Rothwarf, D.M., Zandi, E. & Karin, M. A cytokine-responsive IkappaB kinase that activates the transcription factor NF-kappaB. *Nature* **388**, 548-54 (1997).

177. Jaffe, G.J. et al. Expression of three forms of melanoma growth stimulating activity (MGSA)/gro in human retinal pigment epithelial cells. *Invest Ophthalmol Vis Sci* **34**, 2776-85 (1993).

178. Elner, V.M., Burnstine, M.A., Strieter, R.M., Kunkel, S.L. & Elner, S.G. Cell-associated human retinal pigment epithelium interleukin-8 and monocyte chemotactic protein-1: immunochemical and in-situ hybridization analyses. *Exp Eye Res* **65**, 781-9 (1997).

179. Narayan, S., Prasanna, G., Krishnamoorthy, R.R., Zhang, X. & Yorio, T. Endothelin-1 synthesis and secretion in human retinal pigment epithelial cells (ARPE-19): differential regulation by cholinergics and TNF-alpha. *Invest Ophthalmol Vis Sci* **44**, 4885-94 (2003).

180. Moon, M.R. et al. Complement component C3 production in IL-1beta-stimulated human intestinal epithelial cells is blocked by NF-kappaB inhibitors and by transfection with ser 32/36 mutant IkappaBalpha. *J Surg Res* **82**, 48-55 (1999).

181. Sheerin, N.S., Zhou, W., Adler, S. & Sacks, S.H. TNF-alpha regulation of C3 gene expression and protein biosynthesis in rat glomerular endothelial cells. *Kidney Int* **51**, 703-10 (1997).

182. Woods, A. & Couchman, J.R. Syndecan 4 heparan sulfate proteoglycan is a selectively enriched and widespread focal adhesion component. *Mol Biol Cell* **5**, 183-92 (1994).

183. Zhang, Y., Pasparakis, M., Kollias, G. & Simons, M. Myocyte-dependent regulation of endothelial cell syndecan-4 expression. Role of TNF-alpha. *J Biol Chem* **274**, 14786-90 (1999).

184. Chen, C.C. et al. Cytotoxicity of TNFalpha is regulated by integrin-mediated matrix signaling. *Embo J* **26**, 1257-67 (2007).

185. Kliffen, M. et al. Identification of glycosaminoglycans in age-related macular deposits. *Arch Ophthalmol* **114**, 1009-14 (1996).

186. Russell, S.R., Mullins, R.F., Schneider, B.L. & Hageman, G.S. Location, substructure, and composition of basal laminar drusen compared with drusen associated with aging and age-related macular degeneration. *Am J Ophthalmol* **129**, 205-14 (2000).

187. Chen, Y.Q. et al. Differential mechanisms of plasminogen activator inhibitor-1 gene activation by transforming growth factor-beta and tumor necrosis factor-alpha in endothelial cells. *Thromb Haemost* **86**, 1563-72 (2001).

188. Macfelda, K. et al. Plasminogen activator inhibitor 1 expression is regulated by the inflammatory mediators interleukin-1alpha, tumor necrosis factor-alpha, transforming growth factor-beta and oncostatin M in human cardiac myocytes. *J Mol Cell Cardiol* **34**, 1681-91 (2002).

189. Pandey, M., Loskutoff, D.J. & Samad, F. Molecular mechanisms of tumor necrosis factor-alpha-mediated plasminogen activator inhibitor-1 expression in adipocytes. *Faseb J* **19**, 1317-9 (2005).

190. Takeshita, Y. et al. Tumor necrosis factor-alpha-induced production of plasminogen activator inhibitor 1 and its regulation by pioglitazone and cerivastatin in a nonmalignant human hepatocyte cell line. *Metabolism* **55**, 1464-72 (2006).

191. Liu, R.M. Oxidative stress, plasminogen activator inhibitor 1, and lung fibrosis. *Antioxid Redox Signal* **10**, 303-19 (2008).

192. Siren, V. et al. Retinal pigment epithelial cells secrete urokinase-type plasminogen activator and its inhibitor PAI-1. *Ophthalmic Res* **24**, 203-12 (1992).

193. Bajou, K. et al. Absence of host plasminogen activator inhibitor 1 prevents cancer invasion and vascularization. *Nat Med* **4**, 923-8 (1998).

194. Elner, S.G. Human retinal pigment epithelial lysis of extracellular matrix: functional urokinase plasminogen activator receptor, collagenase, and elastase. *Trans Am Ophthalmol Soc* **100**, 273-99 (2002).

195. Lambert, V. et al. Dose-dependent modulation of choroidal neovascularization by plasminogen activator inhibitor type I: implications for clinical trials. *Invest Ophthalmol Vis Sci* **44**, 2791-7 (2003).

196. Penn, J.S. & Rajaratnam, V.S. Inhibition of retinal neovascularization by intravitreal injection of human rPAI-1 in a rat model of retinopathy of prematurity. *Invest Ophthalmol Vis Sci* **44**, 5423-9 (2003).

197. Wu, K.H. et al. Circulating inflammatory markers and hemostatic factors in age-related maculopathy: a population-based case-control study. *Invest Ophthalmol Vis Sci* **48**, 1983-8 (2007).

198. Thorpe, C. et al. Sulfhydryl oxidases: emerging catalysts of protein disulfide bond formation in eukaryotes. *Arch Biochem Biophys* **405**, 1-12 (2002).

199. Portes, K.F. et al. Tissue distribution of quiescin Q6/sulfhydryl oxidase (QSOX) in developing mouse. *J Mol Histol* **39**, 217-25 (2008).

200. Bradley, J.R., Johnson, D.R. & Pober, J.S. Four different classes of inhibitors of receptor-mediated endocytosis decrease tumor necrosis factor-induced gene expression in human endothelial cells. *J Immunol* **150**, 5544-55 (1993).

201. Higuchi, M. & Aggarwal, B.B. TNF induces internalization of the p60 receptor and shedding of the p80 receptor. *J Immunol* **152**, 3550-8 (1994).

202. Jones, S.J. et al. TNF recruits TRADD to the plasma membrane but not the trans-Golgi network, the principal subcellular location of TNF-R1. *J Immunol* **162**, 1042-8 (1999).

203. Henkind, P. Senile macular degeneration. *Annu Rev Med* **22**, 95-102 (1971).

204. De Luca, A. et al. Distribution of the serine protease HtrA1 in normal human tissues. *J Histochem Cytochem* **51**, 1279-84 (2003).

205. Chan, C.C. et al. Human HtrA1 in the archived eyes with age-related macular degeneration. *Trans Am Ophthalmol Soc* **105**, 92-7; discussion 97-8 (2007).

206. Zumbrunn, J. & Trueb, B. Primary structure of a putative serine protease specific for IGF-binding proteins. *FEBS Lett* **398**, 187-92 (1996).

207. Hu, S.I. et al. Human HtrA, an evolutionarily conserved serine protease identified as a differentially expressed gene product in osteoarthritic cartilage. *J Biol Chem* **273**, 34406-12 (1998).

208. Wu, J. et al. Comparative proteomic characterization of articular cartilage tissue from normal donors and patients with osteoarthritis. *Arthritis Rheum* **56**, 3675-84 (2007).

209. Grau, S. et al. Implications of the serine protease HtrA1 in amyloid precursor protein processing. *Proc Natl Acad Sci U S A* **102**, 6021-6 (2005).

210. Hou, J., Clemmons, D.R. & Smeekens, S. Expression and characterization of a serine protease that preferentially cleaves insulin-like growth factor binding protein-5. *J Cell Biochem* **94**, 470-84 (2005).

211. Chamberland, A. et al. Identification of a novel HTRA1-susceptible cleavage site in human aggrecan: Evidence for the involvement of htra1 in aggrecan proteolysis in vivo. *J Biol Chem* (2009).

212. Engelmann, K. & Valtink, M. RPE cell cultivation. *Graefes Arch Clin Exp Ophthalmol* **242**, 65-7 (2004).

213. McKechnie, N.M., Boulton, M., Robey, H.L., Savage, F.J. & Grierson, I. The cytoskeletal elements of human retinal pigment epithelium: in vitro and in vivo. *J Cell Sci* **91 (Pt 2)**, 303-12 (1988).

214. Pfaffl, M. Relative quantification. in *Real time PCR* (ed. Dorak, T.) 63-82 (Talyor & Francis, 2006).

215. An, E., Gordish-Dressman, H. & Hathout, Y. Effect of TNF-alpha on human ARPE-19-secreted proteins. *Mol Vis* **14**, 2292-303 (2008).

216. Park, S.K., Venable, J.D., Xu, T. & Yates, J.R., 3rd. A quantitative analysis software tool for mass spectrometry-based proteomics. *Nat Methods* **5**, 319-22 (2008).

217. Jenne, D.E. et al. Clusterin (complement lysis inhibitor) forms a high density lipoprotein complex with apolipoprotein A-I in human plasma. *J Biol Chem* **266**, 11030-6 (1991).

218. Podack, E.R. & Muller-Eberhard, H.J. Isolation of human S-protein, an inhibitor of the membrane attack complex of complement. *J Biol Chem* **254**, 9808-14 (1979).

219. Sjoberg, A., Onnerfjord, P., Morgelin, M., Heinegard, D. & Blom, A.M. The extracellular matrix and inflammation: fibromodulin activates the classical pathway of complement by directly binding C1q. *J Biol Chem* **280**, 32301-8 (2005).

220. Sjoberg, A.P. et al. The factor H variant associated with age-related macular degeneration (His-384) and the non-disease-associated form bind differentially to C-reactive protein, fibromodulin, DNA, and necrotic cells. *J Biol Chem* **282**, 10894-900 (2007).

221. Hotoda, N., Koike, H., Sasagawa, N. & Ishiura, S. A secreted form of human ADAM9 has an alpha-secretase activity for APP. *Biochem Biophys Res Commun* **293**, 800-5 (2002).

222. Allinson, T.M., Parkin, E.T., Turner, A.J. & Hooper, N.M. ADAMs family members as amyloid precursor protein alpha-secretases. *J Neurosci Res* **74**, 342-52 (2003).

223. Yerbury, J.J., Kumita, J.R., Meehan, S., Dobson, C.M. & Wilson, M.R. alpha2-Macroglobulin and haptoglobin suppress amyloid formation by interacting with prefibrillar protein species. *J Biol Chem* **284**, 4246-54 (2009).

224. Fabrizi, C., Businaro, R., Lauro, G.M. & Fumagalli, L. Role of alpha2-macroglobulin in regulating amyloid beta-protein neurotoxicity: protective or detrimental factor? *J Neurochem* **78**, 406-12 (2001).

225. Parry, D.A. et al. Loss of the metalloprotease ADAM9 leads to cone-rod dystrophy in humans and retinal degeneration in mice. *Am J Hum Genet* **84**, 683-91 (2009).

226. Boggs, L.N. et al. Clusterin (Apo J) protects against in vitro amyloid-beta (1-40) neurotoxicity. *J Neurochem* **67**, 1324-7 (1996).

227. McHattie, S. & Edington, N. Clusterin prevents aggregation of neuropeptide 106-126 in vitro. *Biochem Biophys Res Commun* **259**, 336-40 (1999).

228. Dentchev, T., Milam, A.H., Lee, V.M., Trojanowski, J.Q. & Dunaief, J.L. Amyloid-beta is found in drusen from some age-related macular degeneration retinas, but not in drusen from normal retinas. *Mol Vis* **9**, 184-90 (2003).

229. Zipfel, P.F., Jokiranta, T.S., Hellwage, J., Koistinen, V. & Meri, S. The factor H protein family. *Immunopharmacology* **42**, 53-60 (1999).

230. Hageman, G.S. et al. Extended haplotypes in the complement factor H (CFH) and CFH-related (CFHR) family of genes protect against age-related macular degeneration: characterization, ethnic distribution and evolutionary implications. *Ann Med* **38**, 592-604 (2006).

231. Ranganathan, S., Male, D.A., Ormsby, R.J., Giannakis, E. & Gordon, D.L. Pinpointing the putative heparin/sialic acid-binding residues in the 'sushi' domain 7 of factor H: a molecular modeling study. *Pac Symp Biocomput*, 155-67 (2000).

232. Wei, X. et al. The Sushi domain of soluble IL-15 receptor alpha is essential for binding IL-15 and inhibiting inflammatory and allogenic responses in vitro and in vivo. *J Immunol* **167**, 277-82 (2001).

233. Kelly, U. et al. Rapid and sensitive method for detection of Y402, H402, I62, and V62 variants of complement factor H in human plasma samples using mass spectrometry. *Invest Ophthalmol Vis Sci* **50**, 1540-5 (2009).

234. Devaney, S. The George Washington University (2009).

235. Kuhn, S., Skerka, C. & Zipfel, P.F. Mapping of the complement regulatory domains in the human factor H-like protein 1 and in factor H1. *J Immunol* **155**, 5663-70 (1995).

236. Kuhn, S. & Zipfel, P.F. Mapping of the domains required for decay acceleration activity of the human factor H-like protein 1 and factor H. *Eur J Immunol* **26**, 2383-7 (1996).

237. Ambati, J. et al. An animal model of age-related macular degeneration in senescent Ccl-2- or Ccr-2-deficient mice. *Nat Med* **9**, 1390-7 (2003).

238. Dithmar, S., Curcio, C.A., Le, N.A., Brown, S. & Grossniklaus, H.E. Ultrastructural changes in Bruch's membrane of apolipoprotein E-deficient mice. *Invest Ophthalmol Vis Sci* **41**, 2035-42 (2000).

239. Dithmar, S. et al. Murine high-fat diet and laser photochemical model of basal deposits in Bruch membrane. *Arch Ophthalmol* **119**, 1643-9 (2001).

240. Espinosa-Heidmann, D.G., Sall, J., Hernandez, E.P. & Cousins, S.W. Basal laminar deposit formation in APO B100 transgenic mice: complex interactions between dietary fat, blue light, and vitamin E. *Invest Ophthalmol Vis Sci* **45**, 260-6 (2004).

241. Gottsch, J.D., Bynoe, L.A., Harlan, J.B., Rencs, E.V. & Green, W.R. Light-induced deposits in Bruch's membrane of protoporphyric mice. *Arch Ophthalmol* **111**, 126-9 (1993).

242. Hahn, P. et al. Immunolocalization and regulation of iron handling proteins ferritin and ferroportin in the retina. *Mol Vis* **10**, 598-607 (2004).

243. Heckenlively, J.R. et al. Mouse model of subretinal neovascularization with choroidal anastomosis. *Retina* **23**, 518-22 (2003).

244. Imamura, Y. et al. Drusen, choroidal neovascularization, and retinal pigment epithelium dysfunction in SOD1-deficient mice: a model of age-related macular degeneration. *Proc Natl Acad Sci U S A* **103**, 11282-7 (2006).

245. Karan, G. et al. Lipofuscin accumulation, abnormal electrophysiology, and photoreceptor degeneration in mutant ELOVL4 transgenic mice: a model for macular degeneration. *Proc Natl Acad Sci U S A* **102**, 4164-9 (2005).

246. Kliffen, M. et al. The APO(*)E3-Leiden mouse as an animal model for basal laminar deposit. *Br J Ophthalmol* **84**, 1415-9 (2000).

247. Majji, A.B. et al. Age-related retinal pigment epithelium and Bruch's membrane degeneration in senescence-accelerated mouse. *Invest Ophthalmol Vis Sci* **41**, 3936-42 (2000).

248. Malek, G. et al. Apolipoprotein E allele-dependent pathogenesis: a model for age-related retinal degeneration. *Proc Natl Acad Sci U S A* **102**, 11900-5 (2005).

249. Rakoczy, P.E. et al. Progressive age-related changes similar to age-related macular degeneration in a transgenic mouse model. *Am J Pathol* **161**, 1515-24 (2002).

250. Rudolf, M. et al. Increased expression of vascular endothelial growth factor associated with accumulation of lipids in Bruch's membrane of LDL receptor knockout mice. *Br J Ophthalmol* **89**, 1627-30 (2005).

251. Schwesinger, C. et al. Intrachoroidal neovascularization in transgenic mice overexpressing vascular endothelial growth factor in the retinal pigment epithelium. *Am J Pathol* **158**, 1161-72 (2001).

252. Spilsbury, K., Garrett, K.L., Shen, W.Y., Constable, I.J. & Rakoczy, P.E. Overexpression of vascular endothelial growth factor (VEGF) in the retinal pigment epithelium leads to the development of choroidal neovascularization. *Am J Pathol* **157**, 135-44 (2000).

253. Tanaka, N., Ikawa, M., Mata, N.L. & Verma, I.M. Choroidal neovascularization in transgenic mice expressing prokineticin 1: an animal model for age-related macular degeneration. *Mol Ther* **13**, 609-16 (2006).

254. Wang, F. et al. AAV-mediated expression of vascular endothelial growth factor induces choroidal neovascularization in rat. *Invest Ophthalmol Vis Sci* **44**, 781-90 (2003).

255. Dobi, E.T., Puliafito, C.A. & Destro, M. A new model of experimental choroidal neovascularization in the rat. *Arch Ophthalmol* **107**, 264-9 (1989).

256. Frank, R.N., Das, A. & Weber, M.L. A model of subretinal neovascularization in the pigmented rat. *Curr Eye Res* **8**, 239-47 (1989).

257. Hope, G.M. et al. A primate model for age related macular drusen. *Br J Ophthalmol* **76**, 11-6 (1992).

258. Umeda, S. et al. Early-onset macular degeneration with drusen in a cynomolgus monkey (Macaca fascicularis) pedigree: exclusion of 13 candidate genes and loci. *Invest Ophthalmol Vis Sci* **46**, 683-91 (2005).

259. Sarks, S., Cherepanoff, S., Killingsworth, M. & Sarks, J. Relationship of Basal laminar deposit and membranous debris to the clinical presentation of early age-related macular degeneration. *Invest Ophthalmol Vis Sci* **48**, 968-77 (2007).

260. Sarks, S.H., Arnold, J.J., Killingsworth, M.C. & Sarks, J.P. Early drusen formation in the normal and aging eye and their relation to age related maculopathy: a clinicopathological study. *Br J Ophthalmol* **83**, 358-68 (1999).

261. Tso, M.O., Albert, D. & Zimmerman, L.E. Organ culture of human retinal pigment epithelium and choroid: a model for the study of cytologic behavior of RPE in vitro. *Invest Ophthalmol* **12**, 554-66 (1973).

262. Valtink, M. et al. Physiological features of primary cultures and subcultures of human retinal pigment epithelial cells before and after cryopreservation for cell transplantation. *Graefes Arch Clin Exp Ophthalmol* **237**, 1001-6 (1999).

263. Gamm, D.M. et al. A novel serum-free method for culturing human prenatal retinal pigment epithelial cells. *Invest Ophthalmol Vis Sci* **49**, 788-99 (2008).

264. Strauss, O. The retinal pigment epithelium in visual function. *Physiol Rev* **85**, 845-81 (2005).

265. Bird, A.C. The Bowman lecture. Towards an understanding of age-related macular disease. *Eye (Lond)* **17**, 457-66 (2003).

266. Chang, T.S., Hay, D. & Courtright, P. Age-related macular degeneration in Chinese-Canadians. *Can J Ophthalmol* **34**, 266-71 (1999).

267. Oshima, Y. et al. Prevalence of age related maculopathy in a representative Japanese population: the Hisayama study. *Br J Ophthalmol* **85**, 1153-7 (2001).

268. Sho, K. et al. Polypoidal choroidal vasculopathy: incidence, demographic features, and clinical characteristics. *Arch Ophthalmol* **121**, 1392-6 (2003).

269. Uyama, M. et al. Idiopathic polypoidal choroidal vasculopathy in Japanese patients. *Arch Ophthalmol* **117**, 1035-42 (1999).

270. Uyama, M. et al. Polypoidal choroidal vasculopathy: natural history. *Am J Ophthalmol* **133**, 639-48 (2002).

271. Jha, P., Bora, P.S. & Bora, N.S. The role of complement system in ocular diseases including uveitis and macular degeneration. *Mol Immunol* **44**, 3901-8 (2007).

272. Paixao-Cavalcante, D., Hanson, S., Botto, M., Cook, H.T. & Pickering, M.C. Factor H facilitates the clearance of GBM bound iC3b by controlling C3 activation in fluid phase. *Mol Immunol* **46**, 1942-50 (2009).

273. Cortright, D.N., Meade, R., Waters, S.M., Chenard, B.L. & Krause, J.E. C5a, but not C3a, increases VEGF secretion in ARPE-19 human retinal pigment epithelial cells. *Curr Eye Res* **34**, 57-61 (2009).

274. Nozaki, M. et al. Drusen complement components C3a and C5a promote choroidal neovascularization. *Proc Natl Acad Sci U S A* **103**, 2328-33 (2006).

275. Collard, C.D., Lekowski, R., Jordan, J.E., Agah, A. & Stahl, G.L. Complement activation following oxidative stress. *Mol Immunol* **36**, 941-8 (1999).

276. Okamoto, T. et al. Angiogenesis induced by advanced glycation end products and its prevention by cerivastatin. *Faseb J* **16**, 1928-30 (2002).

277. Lu, F. et al. HTRA1 variant increases risk to neovascular age-related macular degeneration in Chinese population. *Vision Res* **47**, 3120-3 (2007).

278. Narayanan, R. et al. Complement factor H polymorphism in age-related macular degeneration. *Ophthalmology* **114**, 1327-31 (2007).

279. Tuo, J. et al. The HtrA1 promoter polymorphism, smoking, and age-related macular degeneration in multiple case-control samples. *Ophthalmology* **115**, 1891-8 (2008).

280. Podack, E.R. & Muller-Eberhard, H.J. SC5b-9 complex of complement: formation of the dimeric membrane attack complex by removal of S-protein. *J Immunol* **124**, 1779-83 (1980).

281. Wilson, V.L. & Jones, P.A. DNA methylation decreases in aging but not in immortal cells. *Science* **220**, 1055-7 (1983).

282. Bollati, V. et al. Decline in genomic DNA methylation through aging in a cohort of elderly subjects. *Mech Ageing Dev* **130**, 234-9 (2009).

283. Busslinger, M., Hurst, J. & Flavell, R.A. DNA methylation and the regulation of globin gene expression. *Cell* **34**, 197-206 (1983).

284. Lee, Y.W. et al. Carcinogenic nickel silences gene expression by chromatin condensation and DNA methylation: a new model for epigenetic carcinogens. *Mol Cell Biol* **15**, 2547-57 (1995).

285. Wang, J. et al. Altered function of factor I caused by amyloid beta: implication for pathogenesis of age-related macular degeneration from Drusen. *J Immunol* **181**, 712-20 (2008).

286. Wang, J. et al. Amyloid-beta up-regulates complement factor B in retinal pigment epithelial cells through cytokines released from recruited macrophages/microglia: Another mechanism of complement activation in age-related macular degeneration. *J Cell Physiol* **220**, 119-28 (2009).

287. Vardy, E.R., Catto, A.J. & Hooper, N.M. Proteolytic mechanisms in amyloid-beta metabolism: therapeutic implications for Alzheimer's disease. *Trends Mol Med* **11**, 464-72 (2005).

288. Ricklin, D. & Lambris, J.D. Compstatin: a complement inhibitor on its way to clinical application. *Adv Exp Med Biol* **632**, 273-92 (2008).